

DraftMar13

THE UNIVERSITY OF CHICAGO

SYMMETRIES AND PATTERNS IN SANDPILES

A DISSERTATION SUBMITTED TO
THE FACULTY OF THE DIVISION OF THE PHYSICAL SCIENCES
IN CANDIDACY FOR THE DEGREE OF
DOCTOR OF PHILOSOPHY

DEPARTMENT OF STATISTICS

BY

AHMED BOU-RABEE

CHICAGO, ILLINOIS

JUNE 2022

DraftMar13

Copyright © 2022 by Ahmed Bou-Rabee
All Rights Reserved

TABLE OF CONTENTS

LIST OF FIGURES	vii
LIST OF TABLES	xi
ABSTRACT	xii
1 INTRODUCTION	1
1.1 Overview	1
1.2 Abelian sandpile	1
1.2.1 Origins	1
1.2.2 Definition	2
1.2.3 Discrete sandpile PDE	4
1.2.4 Existence of scaling limits	8
1.2.5 Characterization of scaling limits	13
1.3 Discussion of new results	16
1.3.1 The effect of randomness on sandpile growth	17
1.3.2 Integer superharmonic functions on Euclidean digraphs	23
1.3.3 Dimensional reduction	25
1.4 Common notation and conventions	27
2 CONVERGENCE OF THE RANDOM ABELIAN SANDPILE	29
2.1 Introduction	29
2.1.1 Overview	29
2.1.2 Main result	31
2.1.3 Outline of the chapter	33
2.2 Assumptions	33
2.3 Sandpiles	34
2.4 Method overview	39
2.5 A monotone quantity	40
2.5.1 Definition of the monotone quantity	40
2.5.2 Comparing subsolutions and supersolutions	42
2.5.3 Basic properties of the monotone quantity	43
2.5.4 Convergence of the monotone quantity	49
2.6 The effective equation	52
2.6.1 Finding the effective equation	52
2.6.2 Basic properties of the effective equation	56
2.7 Proof of convergence	57
2.7.1 An upper bound on the odometer function	58
2.7.2 A lower bound on the odometer function	59
2.7.3 A comparison principle in the limit	65
2.7.4 Convergence	67

2.8	Convergence of the random divisible sandpile	70
2.8.1	Description of the divisible sandpile	70
2.8.2	Convergence of the odometer function	71
2.9	Extensions	73
2.9.1	Sandpiles with open boundaries	73
2.9.2	Single-source sandpile on a random background	75
2.9.3	Sandpiles with low density	76
3	A SHAPE THEOREM FOR EXPLODING SANDPILES	78
3.1	Introduction	78
3.1.1	Overview	78
3.1.2	Main results	80
3.1.3	Proof outline	81
3.2	Regularity of explosions	83
3.2.1	Parallel toppling preliminaries	83
3.2.2	Crossing speeds	85
3.2.3	A static renormalization scheme	86
3.2.4	A path-filling property	88
3.3	The last-wave	92
3.3.1	The n -wave process	93
3.3.2	Basic properties of the last-wave	94
3.3.3	Convergence of the last-wave	97
3.4	Proof of convergence	98
3.5	A generalization	104
3.5.1	Sufficient hypotheses	104
3.5.2	Examples satisfying the hypotheses	108
3.6	Failure of convergence	110
3.6.1	Counterexample in dimension two	111
3.6.2	Counterexample in dimensions larger than two	116
3.7	A criteria for exploding	119
3.7.1	Dimensional reduction	120
3.7.2	The measure is recurrent	121
3.7.3	The measure is box-crossing	122
4	INTEGER SUPERHARMONIC MATRICES ON THE F-LATTICE	125
4.1	Introduction	125
4.1.1	Background	126
4.1.2	Main results	127
4.1.3	Kleinian bugs	131
4.2	Proof outline and comparison to previous work	136
4.3	Hyperbola recursion	139
4.3.1	Matrix and lattice parameterization	139
4.3.2	Modified Farey recursion	141
4.3.3	Rotational symmetry reduction	143

4.4	Almost pseudo-square tilings	148
4.5	Zero-one boundary strings	154
4.5.1	A recursion on binary words	154
4.5.2	Basic definitions	158
4.5.3	Even-odd boundary strings	159
4.5.4	A degenerate boundary string	161
4.5.5	Function data	166
4.5.6	Pseudo-square tiles and boundary strings	170
4.5.7	Explicit formulae for zero-one boundary strings	175
4.6	Base cases	178
4.6.1	Base points	182
4.6.2	Staircases	183
4.6.3	Doubled staircases	190
4.6.4	One-sided recurrence	198
4.7	Odometers and tiles	206
4.7.1	Standard tiles	206
4.7.2	Weak standard odometers	217
4.7.3	Alternate tiles	221
4.7.4	Weak alternate odometers	229
4.8	Correcting the recursion	230
4.8.1	Corrected partial tiles	231
4.8.2	Tile odometers	235
4.9	Global odometers	244
5	DYNAMIC DIMENSIONAL REDUCTION IN THE ABELIAN SANDPILE . . .	248
5.1	Introduction	248
5.1.1	Overview	248
5.1.2	Main Result	251
5.1.3	Outline of the proof	255
5.2	Preliminaries	256
5.2.1	Babai-Gorodezky technique	256
5.2.2	Parabolic least action principle	257
5.2.3	Symmetry and fundamental domains	258
5.2.4	Derivative comparison	261
5.2.5	Weak topple control	268
5.3	Explicit solutions for small cubes	269
5.3.1	Side length two	269
5.3.2	Side length four	269
5.4	Odometer regularity in dimension one	273
5.5	Odometer regularity and dimensional reduction	279
5.5.1	Dimensional reduction	280
5.5.2	Odometer regularity in dimensions larger than one	281

DraftMar13

REFERENCES	288
----------------------	-----

LIST OF FIGURES

1.1	Stabilizing a sandpile. The number within each vertex indicates the number of chips. Unstable vertices are colored red.	3
1.2	A sandpile which never stabilizes.	3
1.3	Single-source sandpiles on \mathbb{Z}^2 and \mathbb{Z}^3 respectively. Vertices which have toppled are colored by the number of chips left behind.	4
1.4	The stabilization of $\eta \equiv 4$ and $\eta \equiv 5$ in large squares. Interior vertices are colored by the number of chips left behind.	5
1.5	Surface plots of the odometers of Figure 1.4.	5
1.6	Single-source sandpiles on \mathbb{Z}^2 where the graph Laplacian is given by $\Delta v(x) = -3v(x) + v(x + e_1) + v(x - e_2) + v(x - e_1 + e_2)$ and $\Delta v(x) = -7v(x) + 2v(x + e_1) + 2v(x - e_2) + v(x - e_1) + v(x - e_1 + e_2) + v(x + e_2)$	7
1.7	Sandpiles on \mathbb{Z}^2 with nearest neighbor edges and initial conditions $n\delta_0 + (2d - k)$ for n large. The left is $k = 2$ and the right is $k = 3$	8
1.8	Sandpiles on \mathbb{Z}^3 with nearest neighbor edges and initial conditions $n\delta_0 + (2d - k)$ for n large. From top left to bottom right $k = 2, 3, 4, 5$	9
1.9	Sandpiles on \mathbb{Z}^2 with nearest neighbor edges. In the picture on the left, the initial condition is 4 chips at every site in the indicated rounded cross domain with sink along the boundary of the cross. On the right, the initial condition is the same as the left, but the sink is removed and chips are free to spread.	10
1.10	A few periods of $\partial\Gamma_0(\mathbb{Z}^2)$; the left is a surface plot, the right a contour plot.	15
1.11	Some of the microscopic structure in Figure 1.4. These are all correspond to periodic recurrent sandpiles.	16
1.12	Single-source sandpiles on robust backgrounds $\eta \sim \text{Bernoulli}(-1, 0, 1/2)$ in dimensions 2 then 3.	18
1.13	Snapshots of an exploding sandpile $\{s_t\}$ for initial background $\eta \sim \text{Bernoulli}(2, 3, 0.01)$	18
1.14	Simulations of $\partial\Gamma_\eta(\mathbb{Z}^2)$ for random backgrounds $\eta \sim \text{Bernoulli}(0, 1, 1/2)$, $\eta \sim \text{Bernoulli}(-1, 1, 1/2)$, and $\eta \sim \text{Bernoulli}(-2, 2, 1/2)$ respectively.	19
1.15	Stabilization of 4 chips at every site in a large ball on \mathbb{Z}^2 . Green is 2 chips.	22
1.16	Single-source sandpiles on backgrounds $-\eta \sim \text{Bernoulli}(p)$ for $p = k/10$ for $k = 1, 2, 3, 4$	22
1.17	By column, three circle packings and sandpiles on \mathbb{Z}^2 , the F lattice, and the $F^{(3)}$ lattice. From left to right: the Apollonian band packing from Levine et al. [2017], the overlapping circle packing from Chapter 4, and the first few generations of $\partial\Gamma_0(F^{(3)})$, a (conjectured) Kleinian bug.	24
1.18	Slices of single-source sandpiles on backgrounds $\eta \equiv (2d - k)$ for $k = 3, 2$	26
2.1	For each x in a ball of radius $n = 500, 1000, 2000$, and 3000 , flip a fair coin. If it lands heads, add 3 chips to x , otherwise add 5 chips. Then, stabilize. Sites with 0,1,2, and 3 chips are represented by white, brown, green, and blue respectively.	30
2.2	The single-source sandpile: start with 10^6 chips at the origin and stabilize. Sites with 0,1,2, and 3 chips are represented by white, brown, green, and blue respectively.	32

2.3	Start with an iid Bernoulli(3,5,1/2) sandpile configuration and stabilize with the open boundary condition. Darker reds are closer to 2 while lighter reds are closer to 3. The displays are approximations of the weak-* limits.	74
2.4	Start with 2^{25} chips at the origin in \mathbb{Z}^2 with an iid Bernoulli(0,-1,1/2) background and stabilize. What's displayed is an approximation of the weak-* limit.	75
2.5	A heat map of the odometer function for a Bernoulli(0,4,0.528) initial sandpile started in a circle of radius $6 \cdot 10^3$ with the open boundary condition.	76
3.1	$s_t 1\{v_t > 0\}$ for $\eta \sim \text{Bernoulli}(2, 3, 1/2)$ and $t = 50, 100, 250, 500$. The color white denotes sites which haven't toppled yet, otherwise white, yellow, red, blue, and black correspond to values 0, 1, 2, 3, (≥ 4).	79
3.2	Snapshot of the support of an exploding sandpile $1\{v_t > 0\}$ for $\eta \sim \text{Bernoulli}(2d-2, 2d-1, p)$ the first time it exits a box of side length 500. The top row is $d = 2$ and the bottom $d = 3$. From left to right, $p = 1/4, 1/2, 3/4$	79
3.3	Terminal A -frozen parallel toppling odometer, w_∞ , on \mathbb{Z}^2 for initial conditions $w_0 = 1\{x \in A\}$ and $s_0 = 2$. Red pixels are sites in A and black pixels are sites which eventually topple.	88
3.4	Initial random backgrounds and computed limit shapes. The random backgrounds are built from Bernoulli clouds of the indicated point sets. Blue is 2 chips and red is 3 chips.	108
3.5	The counterexample from Theorem 3.6.1 for $d = 2$ and $d = 3$	111
4.1	A 5×5 section of the F -lattice	126
4.2	A few periods of the bases of cones in $\partial\Gamma_F$	129
4.3	The first three iterations of the hyperbola recursion defined in Section 4.3. The two visible hyperbolas are outlined by dashed lines.	130
4.4	One $L'(2, 5)$ period of $\Delta g_{2,5}$ and $\Delta \hat{g}_{2,5}$. White and black are values of 0 and 1 respectively. These are used to construct the odometers seen in Figure 4.7. . .	132
4.5	The $F^{(k)}$ lattices for $k = 3, 4, 5$ and computed $\partial\Gamma_k$	134
4.6	The seven largest circles in a period of $\partial\Gamma_3$. Periods of the Laplacians of odometers for the indicated circles on the left are displayed on the right, black is -1 and yellow is 0. Note that the four bordering largest circles have Laplacian identically 0 and correspond to harmonic functions built from (4.10).	134
4.7	The Laplacian of two standard tile odometers corresponding to the Farey pair $(13/32, 15/37)$; the left and right displays are the odd and even child respectively. Gray is 0 and black is -1. The Laplacian of the standard odd-even ancestor odometers and alternate odometers are outlined in blue, red, and gray respectively. The even odometer decomposes perfectly into four-two copies of the odd-even standard odometers for the parent Farey pair, $(2/5, 11/27)$. In particular, two copies of the even parent overlap perfectly on a copy of an even grandparent. The odd odometer does not have a perfect decomposition into parents or grandparents; the decomposition requires multiple copies of the standard and alternate odometers of the distant ancestor pair $(2/5, 3/7)$	135

4.8	A surrounding of a pseudo-square tiling and an almost pseudo-square tiling as defined in Proposition 4.4.1 and Lemma 4.4.1 respectively.	149
4.9	Stacked horizontal and vertical boundary strings. The superscripts $+$, $-$ denote the non-reversed and reversed strings respectively and, e.g., $T_p^{+,i}$ refers to T_i^+ and indicates that T_i^+ is type p . Here the tiles are outlined in the dual lattice.	161
4.10	A gap inside a zero-one horizontal stacked boundary string corresponding to the word $qqqp$. Here we are outlining tiles on a square grid where each $x \in \mathbb{Z}[\mathbf{i}]$ is in the center of a square. On the left, points in the stacked string are filled in with either black ($T_{0/1}$) or yellow ($T_{1/1}$). On the right the outlines and annotations are displayed and the labeling is as in Figure 4.9. For brevity, we write 0 and 1 for 0/1 and 1/1 respectively.	163
4.11	As Figure 4.10 but with gap fixed by $T_{1/1}^d$	163
4.12	A vertical stacked zero-one boundary string corresponding to the word $pqpqq$ with the same labeling scheme as Figure 4.10.	164
4.13	Possible overlaps in a stacked almost palindrome zero-one horizontal boundary string with labeling as Figure 4.10. Note that the first $T_{1/1}$ tile may be a $T_{1/1}^d$ tile.	167
4.14	Possible overlaps in a stacked almost palindrome zero-one vertical boundary string with labeling as Figure 4.10.	168
4.15	The boundary of a (w_h, w_v) -pseudo-square tile where w_h is the horizontal word qp^kqp^{k+1} and w_v is the vertical word $p^{2k+1}q$ for $k = 5$. The boundary word is outlined in the dual lattice in black.	170
4.16	From top left to bottom right, $w_h = q^2pq^2p$, reversed $\text{rev}(w_h)$, $w_v = \mathcal{F}(w_h)$, reversed $\text{rev}(w_v)$. The boundary words, $G(w_h, w_v)$ are drawn in black.	173
4.17	A period of the Laplacian of a staircase odometer on the left and its alternate. The string is 22 and the fraction is 3/4. Each tile is outlined in the dual lattice.	183
4.18	The rotated standard and alternate staircase odometers of Figure 4.17. The string is 33 and the fraction is 1/7.	183
4.19	A period of the Laplacian of a doubled staircase odometer on the left and its alternate. The string is 22 and the reduced fraction is 5/7. Each tile is outlined in the dual lattice.	191
4.20	The rotated standard and alternate doubled staircase odometers of Figure 4.19. The string is 33 and the reduced fraction is 1/6.	191
4.21	The two possible orientations for a standard tile pair from Definition 3. The left column is the odd child and the right column is the even child. The first row is the odd-first orientation and the second is the even-first orientation. Only one type of overlap between parents (corresponding to Type 1 children) is displayed - see Figure 4.22 for the other types of overlaps.	207
4.22	All possible overlaps between parents in a standard tile. The left column denotes the odd child and the right column is the even child. The rows from top to bottom correspond to Type 1, 2, then 3 children. The parent tiles are labeled in their centers with notation from Definition 3. The orientation is the even-first orientation.	210
4.23	As Figure 4.22 (even-first) but for alternate tiles with labels from Definition 7. .	224

4.24 As Figure 4.23 but in the odd-first orientation	225
4.25 A visual explanation of the proof of Lemma 4.7.4. On the top is a lower-right surrounding of the shifted tiling and on the bottom is a lower-right surrounding of the non-shifted tiling.	228
4.26 An odd L -correction with labels as in Definition 10 overlaid on its standard tile.	230
4.27 The four possible orientations for an odd L -correction as described in Definition 10. From top left to bottom right, 10, 00, 11 then 01.	236
4.28 The four possible orientations for an even L -correction as described in Definition 11. From top left to bottom right, 10, 00, 11 then 01.	237
4.29 The two possible odd-even overlaps for an even L -correction as described in Definition 11: $s = 1$ on the left (elongated) and $s = 2$ on the right.	238
4.30 Decompositions of the triple $(\hat{T}(p_2)^1, T(q_2), T(p_2)^2)$ in Figure 4.29: $s = 1$ on the left and $s = 2$ on the right.	238
4.31 Double decomposition of $T(p_0)$ in the even-first orientation for recursion words $w = *1$ and $w = *2$ respectively.	239
4.32 Decomposition and then double decomposition of corrected $T(p_0)$ in the even-first orientation. The first row is $w = *13$ and the second is $w = *23$	239
4.33 Double decomposition of $\hat{T}(q_0)$ in the even-first orientation for recursion words $w = *1$ and $w = *2$ respectively.	240
4.34 Decomposition and then double decomposition of corrected $\hat{T}(q_0)$ in the even-first orientation. The first row is $w = *13$ and the second is $w = *23$	240
5.1 $s_t^{(2)}$ for $t = (25)^2, (50)^2, (100)^2, \infty$, where $N = 200$ and $s_0 \equiv 4$. Sites with $0, \dots, 7$ chips are represented by different colors.	249
5.2 $s_t^{(3)}(\cdot, \cdot, \text{offset})$ for offset = 0, 20, 40, 60, where $t = (50)^2$, $N = 200$, and $s_0 \equiv 6$. Sites with $0, \dots, 11$ chips are represented by different colors and ‘offset’ is distance to the center of $\mathcal{C}_N^{(3)}$	249
5.3 On the left, a corner cube of $s_\infty^{(N,3)}$ and on the right the same corner with all cross sections which match $s_\infty^{(N,2)}$ removed. The initial condition is $s_0 \equiv 7$ and $N = 2^{11}$. Sites with $0, \dots, 5$ chips are represented by different colors.	254
5.4 The parallel toppling odometer for $s_0 \equiv 2d + (d - 1)$ when $d = 100$ and $M = 2$. A black pixel in row t and column x indicates that $v_t(x) = v_{t-1}(x) + 1$. The top row is $t = 0$ and t increases from top to bottom. The left column is $x = 1$ and x increases from left to right.	270

LIST OF TABLES

3.1	Computed limited shapes of periodic, checkerboard backgrounds of the indicated box.	109
4.1	Possible pairwise overlaps in a zero-one boundary string with labeling as Figure 4.10.	166
5.1	Center slices of terminal sandpile configurations for $s_0 \equiv 2d + k$ and $N = 64$. Site colors are normalized by column so that in dimension d a site with z chips has the same color as a site with $(z - 2)$ chips in dimension $(d - 1)$	253

ABSTRACT

The Abelian sandpile is a deterministic diffusion process on graphs which produces striking, kaleidoscopic patterns. Why do these patterns appear? Are the patterns robust to noise? Do different graphs generate distinct patterns? This thesis presents some answers to these questions.

Draft Mar 13

CHAPTER 1

INTRODUCTION

1.1 Overview

This thesis is based on some of the author’s published papers on the Abelian sandpile, Bou-Rabee [2021a,b,c, 2022]. The main results contained in the thesis are as follows.

1. Sandpiles with stationary ergodic initial data converge to deterministic limits in the ‘compact’ regime. In the ‘explosive’ regime, convergence occurs under some additional constraints on the initial sandpile.
2. The scaling limit of the sandpile on the F -lattice, a periodic subgraph of \mathbb{Z}^2 , is described by a degenerate, overlapping circle packing, distinct from the \mathbb{Z}^2 case.
3. Certain sandpiles on \mathbb{Z}^d coincide with cross-sectional slices of sandpiles on \mathbb{Z}^{d+1} .

In the rest of this chapter, we survey some past work on the Abelian sandpile and then discuss the contributions of this thesis together with some directions for future work.

1.2 Abelian sandpile

We present a high level description of prior results most relevant to this thesis.

1.2.1 Origins

The Abelian sandpile model is a natural dynamical system and so was rediscovered in many different contexts. The earliest known occurrence of the sandpile is in an educational article Engel [1975]. Engel introduced the so-called *probabilistic abacus* as a pedagogical tool to help fourth graders learn probability. Engel’s abacus exactly determines, in a deterministic

and simple way, hitting probabilities and expected exit times for Markov chains on finite graphs — for more see Propp [2017].

Engel’s abacus was further developed by the combinatorics community where it became known as *chip-firing* Björner et al. [1991]. Researchers have explored connections of chip-firing to arithmetic geometry Lorenzini [1989] and algebraic graph theory Biggs [1997]. The recent books Klivans [2018], Corry and Perkinson [2018] provide a detailed exposition of some work done in this direction.

The sandpile is perhaps most famous for being (independently) introduced by statistical physicists Bak-Tang-Wiesenfeld as a model of ‘self-organized criticality’ Bak et al. [1987]. Dhar later made substantial contributions; he generalized the model to arbitrary graphs and was the first to observe the Abelian property Dhar [1990]. In fact, to the best of our knowledge, the term ‘Abelian sandpile’ first appears in Majumdar and Dhar [1992].

1.2.2 Definition

In its most general formulation, the Abelian sandpile is a deterministic diffusion process on graphs. Let (V, E) be the vertices and edges of a graph which is strongly connected and locally finite. (For simplicity here, we will further assume undirected.)

A *sandpile* is a function $\eta : V \rightarrow \mathbb{Z}$ where $\eta(x)$ is thought of as the number of chips (or a hole of certain depth) at vertex x . A vertex x is *unstable* if it has at least as many chips as its degree, $\eta(x) \geq \deg(x)$, and is otherwise *stable*. Unstable vertices *topple*, giving one chip to each adjacent vertex. If, eventually, every vertex is stable, then the sandpile is *stabilizable*. Otherwise, it never stops toppling and is *explosive*. The process of toppling unstable vertices until every vertex is stable is *stabilizing*. In this case, the order in which unstable vertices topple doesn’t affect the final, stable configuration, $s : V \rightarrow \mathbb{Z}$; the sandpile model is *Abelian*.

The Abelian property is a consequence of the linearity of toppling. In particular, toppling

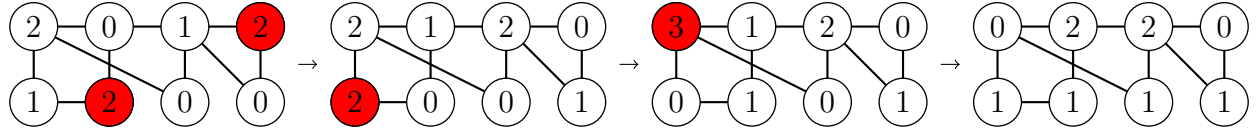


Figure 1.1: Stabilizing a sandpile. The number within each vertex indicates the number of chips. Unstable vertices are colored red.

is *locally confluent*. If two vertices x and y are unstable, then toppling x then y results in the same configuration as toppling y then x . Repeated application of local confluence shows that the final configuration is invariant with respect to the choice of toppling procedure.

One way to ensure sandpiles stabilize is to start with a finite number of chips on an infinite graph. A canonical example is the *single-source sandpile*, start with a large stack of chips at the origin on \mathbb{Z}^d (with nearest neighbor edges) and stabilize — see Figure 1.3. Another common approach is to take a finite graph, say a square $\Omega \subset \mathbb{Z}^2$, and designate all boundary sites as *sinks*. Sinks cannot topple and accumulate chips. Thus, if the initial sandpile η is supported in Ω , all interior vertices will eventually stabilize — see Figure 1.4.

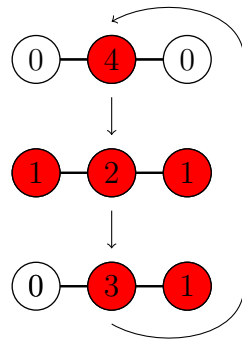


Figure 1.2: A sandpile which never stabilizes.

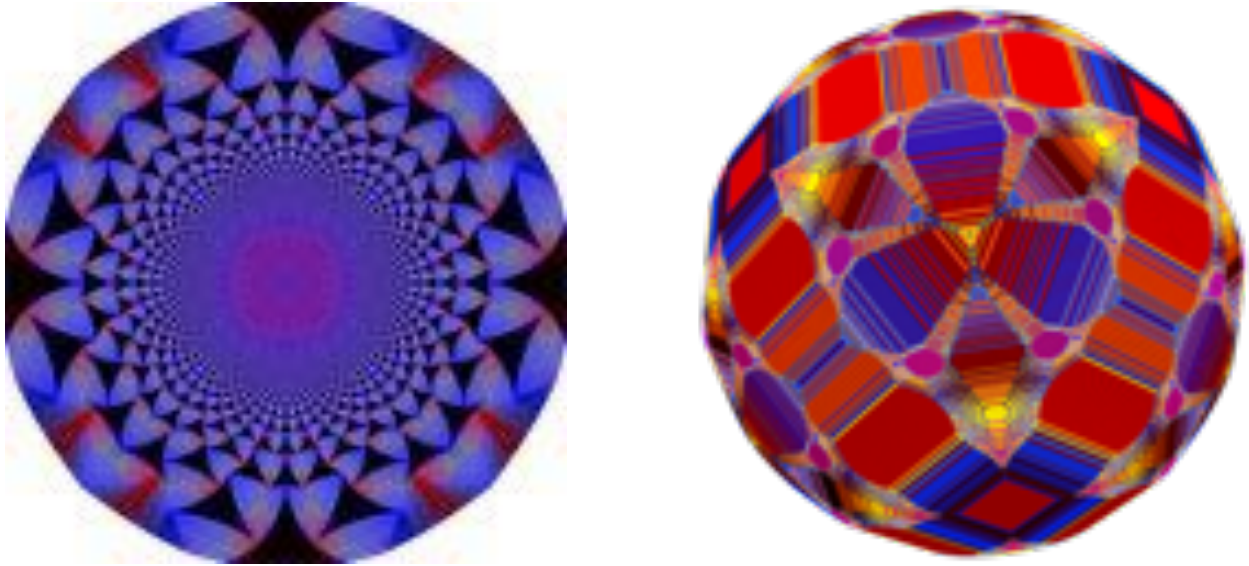


Figure 1.3: Single-source sandpiles on \mathbb{Z}^2 and \mathbb{Z}^3 respectively. Vertices which have toppled are colored by the number of chips left behind.

1.2.3 Discrete sandpile PDE

The process of toppling can be rephrased in terms of the *graph Laplacian*. The graph Laplacian Δ operates on functions $g : V \rightarrow \mathbb{R}$ as

$$\Delta g(x) = \sum_{(y,x) \in E} (g(y) - g(x)), \quad (1.1)$$

where the sum (y, x) is over the outgoing edges of vertex x . The graph Laplacian is also the (normalized) generator of simple random walk on V — see Section 1.5 of Lawler and Limic [2010]. This perspective will be used in part of Chapter 2.

The action of toppling vertex x is equivalent to taking the graph Laplacian of the indicator function: $\eta \rightarrow \eta + \Delta \delta_x$. In fact, stabilizing can be captured by a single function $v : V \rightarrow \mathbb{N}$, the *odometer*, which keeps track of how many times each site toppled:

$$s = \eta + \Delta v. \quad (1.2)$$

DraftMar13

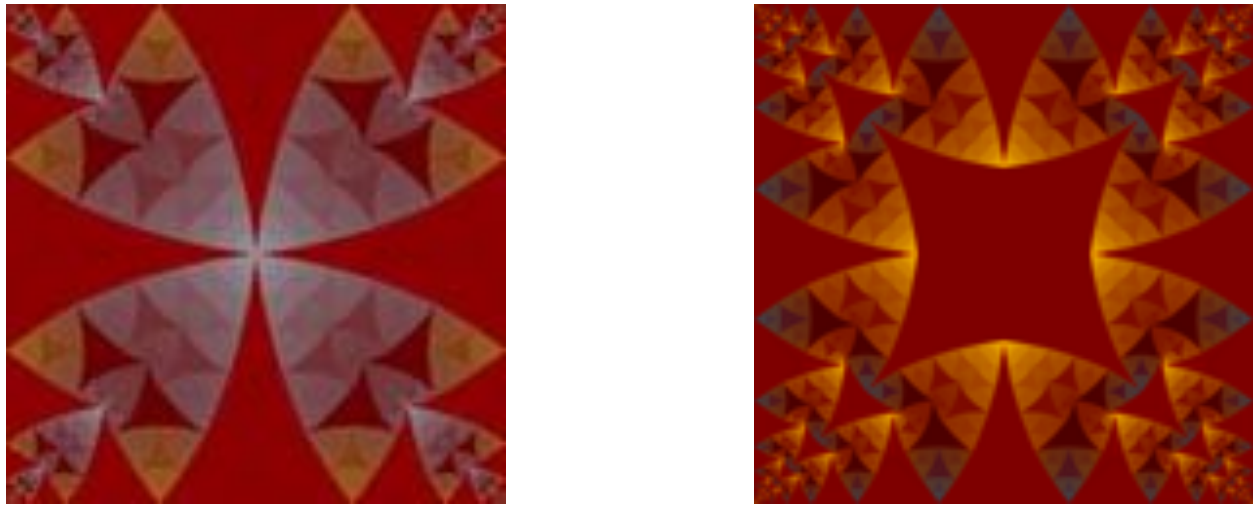


Figure 1.4: The stabilization of $\eta \equiv 4$ and $\eta \equiv 5$ in large squares. Interior vertices are colored by the number of chips left behind.

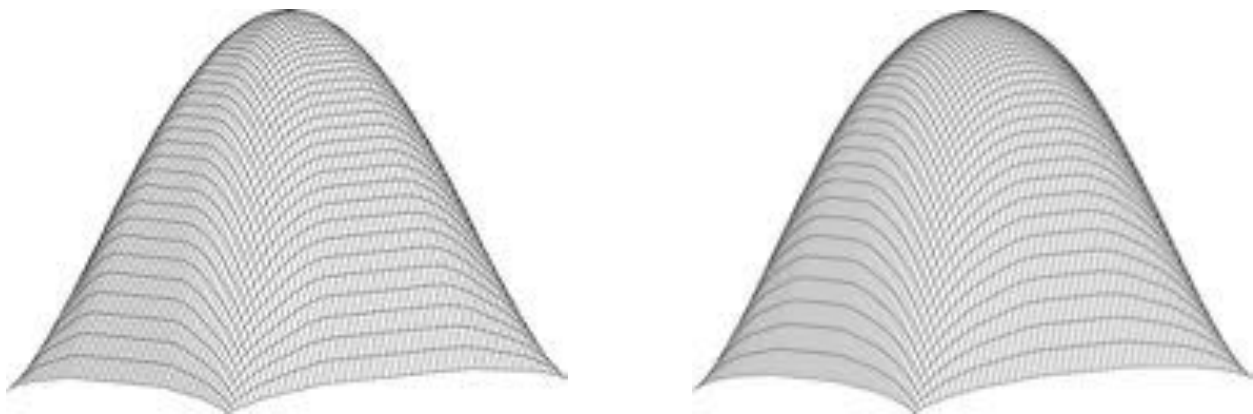


Figure 1.5: Surface plots of the odometers of Figure 1.4.

The odometer provides an entry point into a rigorous understanding of the sandpile. It appears to be a much smoother object than the sandpile which it describes — compare Figures 1.4 and 1.5. In fact, on \mathbb{Z}^d , if the initial sandpile η is bounded then v approximates a differentiable function on \mathbb{R}^d with Hölder continuous derivatives as a consequence of the estimates in Kuo and Trudinger [2005]. (On \mathbb{R}^d functions with bounded Laplacian enjoy this regularity; see, for example, Section 4.5 in Gilbarg et al. [1977].)

Beyond this apparent smoothness, the odometer solves a discrete PDE known as the *least action principle*

$$v = \min\{w : V \rightarrow \mathbb{Z} : \Delta w + \eta \leq \deg - 1\}. \quad (1.3)$$

The least action principle was formulated and proved in Fey et al. [2010]. It can be thought of an efficiency characterization of the sandpile — each vertex topples the least amount of times needed to stabilize. In other words, v is the pointwise least function which stabilizes η , $\Delta v + \eta \leq \deg - 1$.

Notably, the least action principle provides a method to determine whether or not a sandpile stabilizes. If one can construct a single function w with $\Delta w + \eta \leq \deg - 1$, then η is stabilizable and the odometer v exists. Indeed, if such a function w exists, $v \leq w < \infty$ as the graph Laplacian is monotone, $\Delta \min(v, w) \leq \max(\Delta v, \Delta w)$.

In some sense, the least action principle can be thought of as a stronger version of the Abelian property. (Interestingly, one can formulate a so-called parabolic least action principle which can be applied to sandpiles which may not stabilize — see Chapter 5.)

If a sandpile stabilizes on V and its odometer is strictly positive in a subset $\Omega \subset V$, then the restriction of the stable sandpile to Ω is a special sandpile known as a *recurrent sandpile*. (The term recurrent is used because recurrent sandpiles form the recurrent states of a certain Markov chain. If interested, see Dhar et al. [1995] or Holroyd et al. [2008], but we will not employ this perspective.)

A fundamental property of recurrent sandpiles which we will use is the following com-

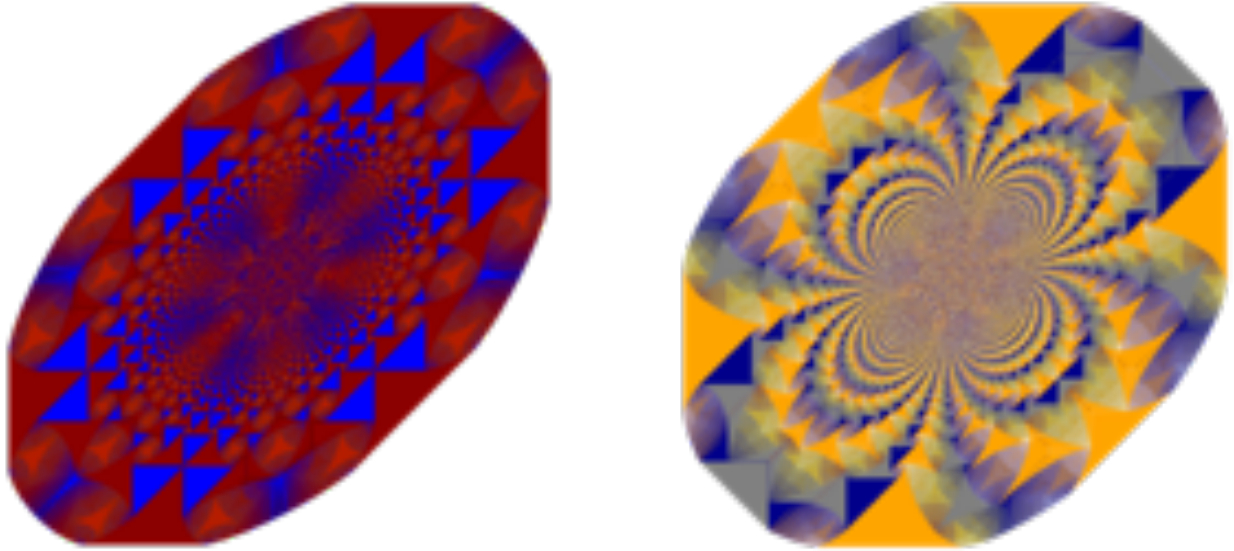


Figure 1.6: Single-source sandpiles on \mathbb{Z}^2 where the graph Laplacian is given by $\Delta v(x) = -3v(x) + v(x + e_1) + v(x - e_2) + v(x - e_1 + e_2)$ and $\Delta v(x) = -7v(x) + 2v(x + e_1) + 2v(x - e_2) + v(x - e_1) + v(x - e_1 + e_2) + v(x + e_2)$.

parison principle. Denote the outer boundary of Ω by

$$\partial\Omega = \{x \in V \setminus \Omega : \text{there exists } (y, x) \in E \text{ with } y \in \Omega\}$$

and let $\bar{\Omega} = \Omega \cup \partial\Omega$. If $s : \Omega \rightarrow \{0, \dots, \deg - 1\}$ is a recurrent sandpile and $s = \Delta v$ for an integer-valued function $v : \bar{\Omega} \rightarrow \mathbb{Z}$ then

$$\sup_{\Omega}(v - w) \leq \sup_{\partial\Omega}(v - w) \tag{1.4}$$

for any $w : \bar{\Omega} \rightarrow \mathbb{Z}$ with $\Delta w \leq \deg - 1$.

Being able to compare two different sandpiles in this way allows one to import tools from elliptic PDE, where such comparison principles play an important role. We will use a slightly stronger version of (1.4) in Chapter 2.

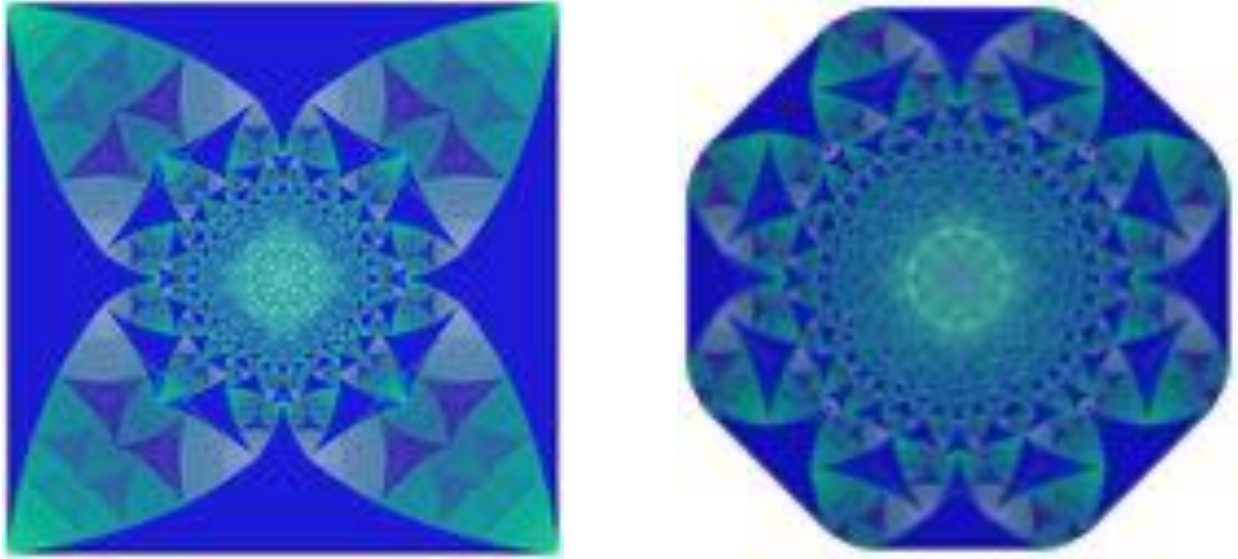


Figure 1.7: Sandpiles on \mathbb{Z}^2 with nearest neighbor edges and initial conditions $n\delta_0 + (2d - k)$ for n large. The left is $k = 2$ and the right is $k = 3$.

1.2.4 Existence of scaling limits

When the initial sandpile has a sufficiently large number of chips and is stabilizable, the stable sandpile usually reveals fascinating fractal structure. Figures 1.3 and 1.4 are two examples on \mathbb{Z}^d , but this phenomena appears to be quite robust to both the choice of graph and initial condition. See Figures 1.6, 1.7, 1.8, and 1.9.

This pattern formation was observed by physicists Liu et al. [1990] and Creutz [1991] soon after the sandpile was introduced. However, a mathematical understanding of why they appear remained elusive for several decades. (Some partial progress was made in Ostojic [2003], Fey-den Boer and Redig [2008], Levine and Peres [2009]. Notably, Paoletti [2013] provided explicit descriptions of some sandpiles on certain graphs.)

In a breakthrough work, Pegden and Smart [2013] proved that the single-source sandpile on \mathbb{Z}^d has a continuum scaling limit as the number of chips goes to infinity. Pegden-Smart used ideas from the theory of viscosity solutions (Crandall [1997]) to show that the discrete least action principle (1.3) has a continuum analogue. They then used this to show that the odometers converge.

DraftMar13

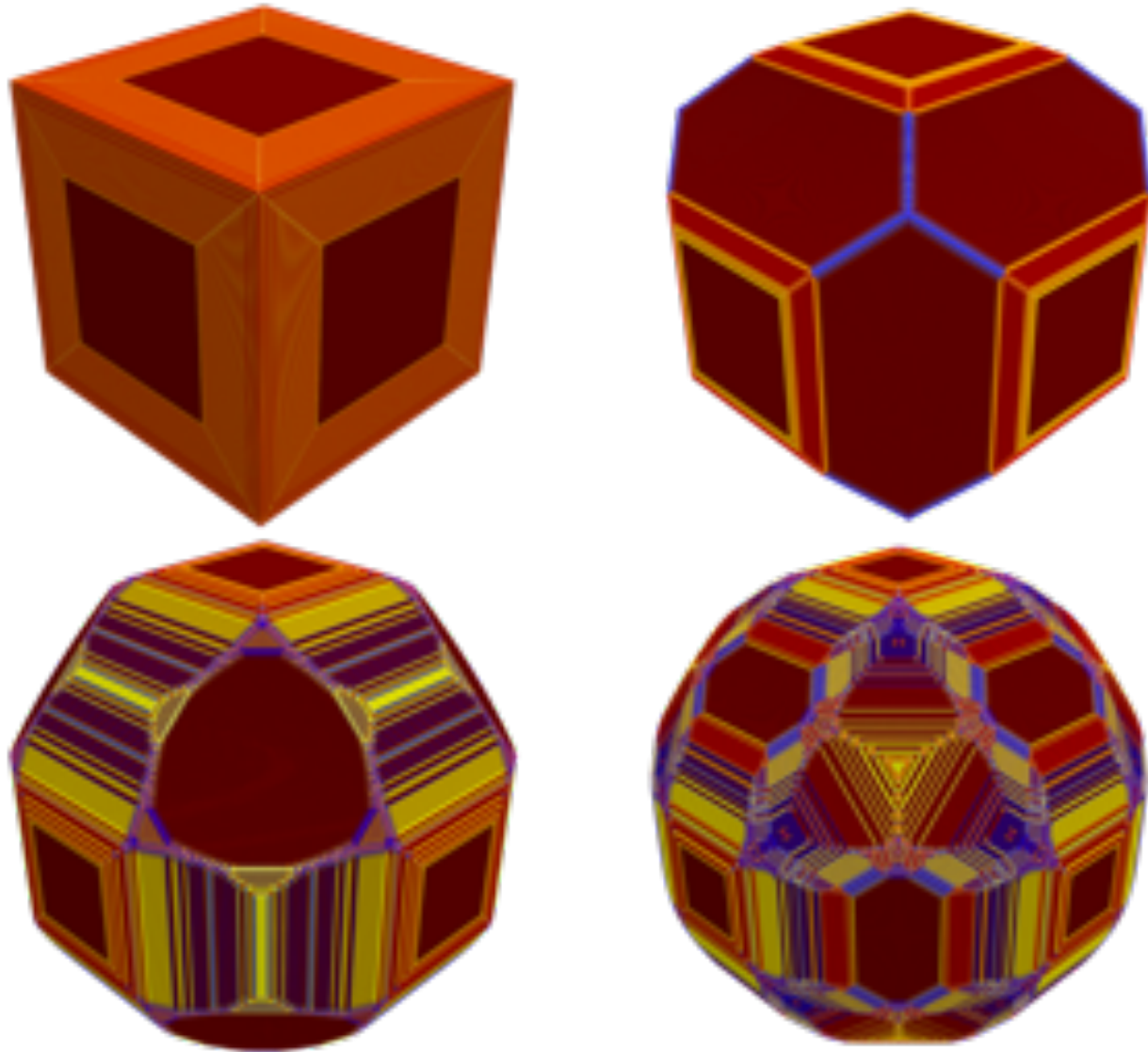


Figure 1.8: Sandpiles on \mathbb{Z}^3 with nearest neighbor edges and initial conditions $n\delta_0 + (2d - k)$ for n large. From top left to bottom right $k = 2, 3, 4, 5$.

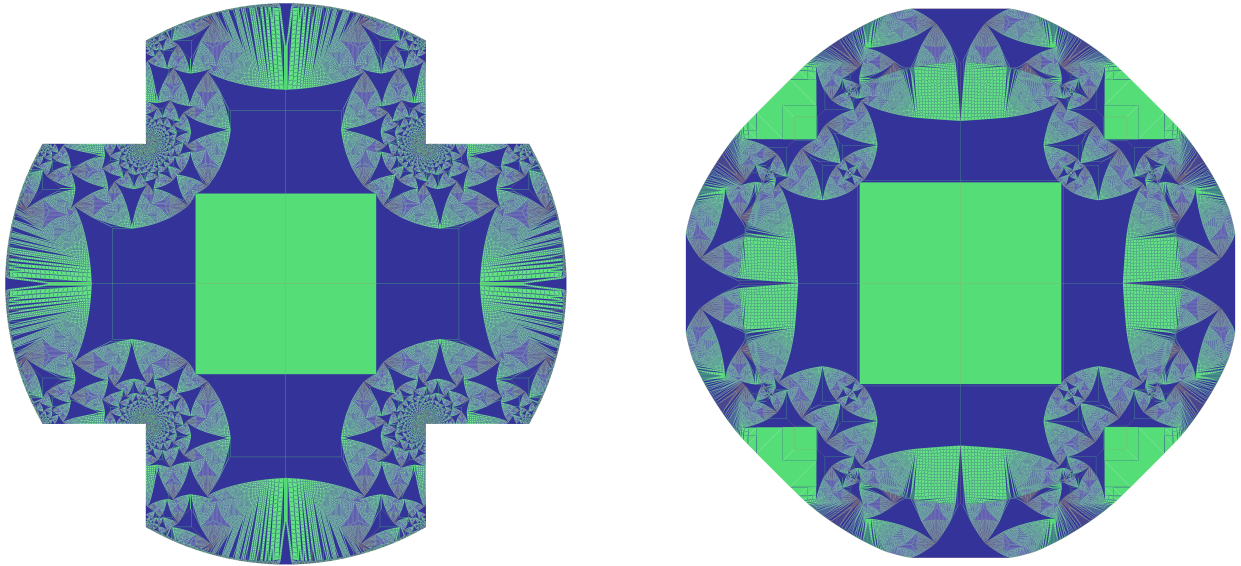


Figure 1.9: Sandpiles on \mathbb{Z}^2 with nearest neighbor edges. In the picture on the left, the initial condition is 4 chips at every site in the indicated rounded cross domain with sink along the boundary of the cross. On the right, the initial condition is the same as the left, but the sink is removed and chips are free to spread.

Specifically, let v_n denote the odometer for initial sandpile $n\delta_0$ on \mathbb{Z}^d with nearest neighbor edges. In other words,

$$v_n = \min\{w : \mathbb{Z}^d \rightarrow \mathbb{N} : \Delta w + n\delta_0 \leq 2d - 1\}, \quad (1.5)$$

where

$$\Delta w(x) = \sum_{i=1}^d (w(x + e_i) + w(x - e_i) - 2w(x)),$$

and e_i are the standard basis vectors of \mathbb{Z}^d . For a domain $\Omega \subset \mathbb{R}^d$, let $C(\Omega)$ be the set of continuous functions on Ω . We will overload notation and write Δ for the continuum Laplacian when the input is in $C(\Omega)$. The notation $[z]$ rounds z to the nearest integer (breaking ties arbitrarily) in \mathbb{Z}^d .

Theorem 1.2.1 (Pegden and Smart [2013]). *The rescaled odometers $\bar{v}_n(x) := n^{-2/d} v_n([n^{1/d} x])$*

converge locally uniformly away from the origin,

$$\bar{v}_n \rightarrow \bar{G} + \bar{u}$$

where $\bar{G} \in C(\mathbb{R}^d \setminus \{0\})$ is the fundamental solution to the Laplacian

$$\Delta \bar{G} = -\delta_0$$

and \bar{u} is the unique viscosity solution to

$$\bar{u} = \inf\{w \in C(\mathbb{R}^d) : w \geq -\bar{G} \text{ and } D^2(w + \bar{G}) \in \Gamma(\mathbb{Z}^d)\}, \quad (1.6)$$

where $\Gamma(\mathbb{Z}^d)$ is a certain set of $d \times d$ symmetric matrices.

Once we know that the odometers v_n converge, discrete integration by parts immediately implies convergence of the sandpiles, $s_n = \Delta v_n + n\delta_0$. That is, the rescaled sandpiles $\bar{s}_n(x) := s_n([n^{1/d}x])$, converge in the L^∞ weakly-* sense,

$$\bar{s}_n \rightarrow \bar{s}. \quad (1.7)$$

and (distributionally), $\Delta \bar{u} = \bar{s}$.

Let us reflect on the form of the continuum least action principle (1.6). The fundamental solution \bar{G} records the initial condition — a stack of chips at the origin — and \bar{u} describes how that stack is redistributed. The odometer is positive, so the discrete condition $v_n \geq 0$ translates to $\bar{u} + \bar{G} \geq 0$. The Hessian constraint is more involved; the discrete version of $D^2(\bar{u} + \bar{G}) \in \Gamma(\mathbb{Z}^d)$ is $\Delta v_n + n\delta_0 \leq 2d - 1$. This suggests that in the continuum least action principle we should instead have $\Delta(\bar{u} + \bar{G}) \leq 2d - 1$.

This is, however, false. If the second order condition were just the Laplacian, then the limit sandpile would be flat, $\bar{s} = (2d - 1)1\{\bar{u} > -\bar{G}\}$. And, by radial symmetry of Δ , the

limit shape would be a ball. This contradicts the appearance of the simulations in Figure 1.3. In fact, the Hessian constraint, the set $\Gamma(\mathbb{Z}^d)$, is the source of all the complexity of the sandpile.

The set $\Gamma(\mathbb{Z}^d)$ is defined as the set of quadratic growths achievable by functions on the lattice \mathbb{Z}^d with bounded Laplacian. To be specific, a $d \times d$ symmetric matrix A is in the set $\Gamma(\mathbb{Z}^d)$ if there exists an integer-valued function $u : \mathbb{Z}^d \rightarrow \mathbb{Z}$ with

$$\Delta u \leq 2d - 1 \quad \text{and} \quad u(x) \geq \frac{1}{2}x^T Ax. \quad (1.8)$$

The proof of convergence in Pegden and Smart [2013] is quite flexible. Although it was presented for the single-source sandpile on \mathbb{Z}^d , the proof shows, with essentially no changes, convergence of the sandpiles shown in Figures 1.4, 1.6, 1.7, 1.8, and 1.9. More generally, their result extends to all periodic sandpiles on lattices where the Laplacian is given by the generator of a random walk on the lattice which satisfies the local central limit theorem (as in Lawler and Limic [2010]).

Here's an explicit example which includes the limits in Figure 1.4. Let \mathbb{L}^d be a *full-rank lattice*, *i.e.*, a discrete additive subgroup of \mathbb{R}^d which can be expressed as the integer span of d linearly independent vectors. Let the initial sandpile $\eta : \mathbb{L}^d \rightarrow \mathbb{Z}$ be a *periodic* function, that is, a function for which there exists a full-rank sub-lattice $\mathbb{S}^d \subset \mathbb{L}^d$ so that $\eta(x) = \eta(x + v)$ for all $v \in \mathbb{S}^d$.

Let $\Gamma_\eta(\mathbb{L}^d)$ be defined as $\Gamma(\mathbb{Z}^d)$ except the integer-valued functions in (1.8) have domain the lattice \mathbb{L}^d and satisfy $\Delta u + \eta \leq \deg - 1$ (so that $\Gamma_0(\mathbb{Z}^d) = \Gamma(\mathbb{Z}^d)$). Let $\Omega \subset \mathbb{R}^d$ be a bounded open set satisfying the exterior sphere condition (this ensures solvability of the classical Dirichlet problem for Laplace's equation in Ω see pages 26-27 of Gilbarg et al. [1977]). Let $v_n : \mathbb{Z}^d \rightarrow \mathbb{N}$ be the pointwise least function that satisfies

$$\Delta v_n + \eta \leq 2d - 1 \quad \text{in } \mathbb{Z}^d \cap n\Omega.$$

Then, the quadratic rescalings, $\bar{v}_n(x) := n^{-2}v_n([nx])$, (here $[nx]$ rounds to the nearest lattice point) converge uniformly as $n \rightarrow \infty$ to

$$\bar{v}_\eta := \inf\{w \in C(\bar{\Omega}) : w \geq 0 \text{ and } D^2w \in \Gamma_\eta(\mathbb{L}^d) \text{ in } \Omega\}. \quad (1.9)$$

Moreover, when η has average density above $2d - 1$ (so that there is a macroscopic number of topplings) \bar{v}_η also solves the Dirichlet problem

$$\begin{cases} D^2\bar{v}_\eta \in \partial\Gamma_\eta(\mathbb{L}^d) & \text{in } \Omega \\ \bar{v}_\eta = 0 & \text{in } \partial\Omega, \end{cases} \quad (1.10)$$

where $\partial\Gamma_\eta(\mathbb{L}^d)$ denotes the topological boundary. In the case of Figure 1.4, the domain is a square, $\Omega = \{x \in \mathbb{R}^2 : \max(|x_1|, |x_2|) \leq 1\}$, the lattice is \mathbb{Z}^d , and the two sandpiles displayed are approximations of $\Delta\bar{v}_\eta$ for $\eta \equiv 4$ and $\eta \equiv 5$ respectively.

The periodicity of the initial sandpile is an important assumption which cannot be relaxed when employing the Pegden-Smart machinery — we will see to what extent periodicity can be generalized in Chapter 2.

1.2.5 Characterization of scaling limits

Although the description of the set $\Gamma_\eta(\mathbb{L}^d)$ is explicit, it doesn't provide an immediate explanation for the appearance of fractals. In a spectacular work, Levine et al. [2016b, 2017] characterized $\Gamma_0(\mathbb{Z}^2)$ via a relation to a recursively generated circle packing. This related the mysterious fractals appearing in the sandpile to another well-studied (but a priori completely unrelated) fractal. We give a precise description of their result.

Start by parameterizing the set of 2×2 symmetric matrices, \mathbf{S}^2 , by $M(a, b, c) : \mathbb{R}^3 \rightarrow \mathbf{S}^2$,

$$M(a, b, c) := \frac{1}{2} \begin{bmatrix} c - a & b \\ b & c + a \end{bmatrix}. \quad (1.11)$$

Notice that $\text{Tr}(M(a, b, c)) = c$. Aside from this, the primary advantage of this parameterization is that the convex cone of positive semi-definite matrices is in fact a geometric cone. Recall that for two matrices $A, B \in \mathbf{S}^2$, $B \leq A$ if $(A - B)$ is positive-semidefinite. Given a matrix $A \in \mathbf{S}^2$, write

$$A^\downarrow := \{B \in \mathbf{S}^2 : B \leq A\}$$

and extend this operator to sets of matrices via unions.

Under the parameterization (1.11), the set A^\downarrow is geometrically a slope-1 downwards cone with apex at A . In particular, as $\Gamma_0(\mathbb{Z}^2)$ is downwards closed (if $A \in \Gamma_0(\mathbb{Z}^2)$, then $A^\downarrow \in \Gamma_0(\mathbb{Z}^2)$), the set $\Gamma_0(\mathbb{Z}^2)$ can be viewed as a volume in \mathbb{Z}^3 and its boundary as a surface. Moreover, the harmonic, integer-valued functions

$$h_1(x) = x_1 x_2 \quad \text{and} \quad h_2(x) = \frac{1}{2}x_1(x_1 + 1) - \frac{1}{2}x_2(x_2 + 1)$$

indicate that $\Gamma_0(\mathbb{Z}^2)$ satisfies a periodicity property.

Indeed, if $A \in \Gamma_0(\mathbb{Z}^2)$, then there is a function $u : \mathbb{Z}^2 \rightarrow \mathbb{Z}$ with $\Delta u \leq 3$ and $u \geq \frac{1}{2}x^T Ax$. Since h_i are integer-valued and harmonic, for all $k_i \in \mathbb{Z}$, $u_k := (u + k_1 h_1 + k_2 h_2)$ is integer-valued and $\Delta u_k \leq 3$. This shows

$$A \in \Gamma_0(\mathbb{Z}^2) \iff A + M(2k_1, 2k_2, 0) \in \Gamma_0(\mathbb{Z}^2)$$

for all $k_i \in \mathbb{Z}$. Therefore, to characterize $\Gamma_0(\mathbb{Z}^2)$, it suffices to specify a period of its boundary; a surface plot and a contour plot can be seen in Figure 1.10.

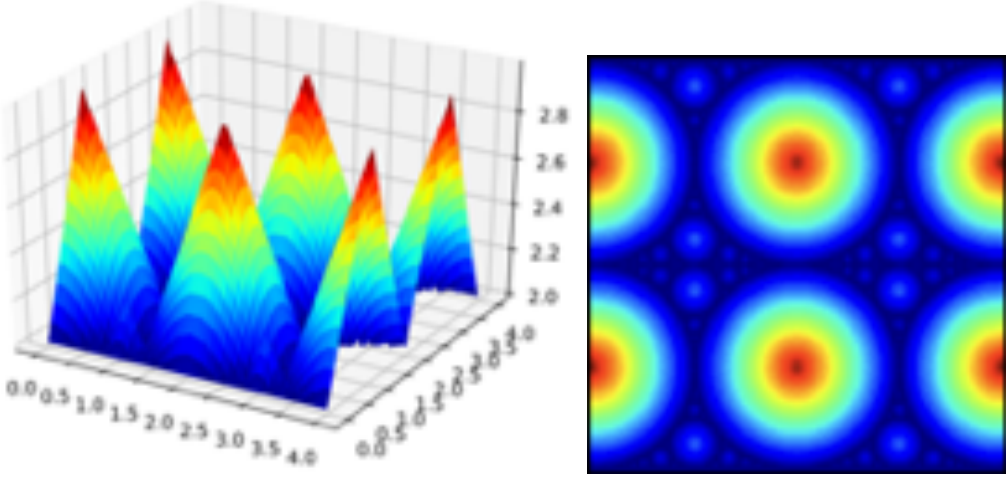


Figure 1.10: A few periods of $\partial\Gamma_0(\mathbb{Z}^2)$; the left is a surface plot, the right a contour plot.

The pictures in Figure 1.10 suggest $\Gamma_0(\mathbb{Z}^2)$ is described by \mathcal{P}^\downarrow for a set of isolated *peak* matrices $\mathcal{P} \subset \partial\Gamma_0(\mathbb{Z}^2)$. Moreover, it seems like the intersection of \mathcal{P}^\downarrow with the trace 2 plane outlines a circle packing. This is exactly what was proved in Levine et al. [2017]. Specifically, Levine-Pegden-Smart showed that $A \in \Gamma_0(\mathbb{Z}^2)$ if and only if $\text{Tr}(A) \leq 2$ or $A \leq P$ for some matrix P corresponding to a circle in an *Apollonian circle packing*.

Apollonian circle packings are recursively generated. In particular, one may construct an Apollonian circle packing by starting with a triple of mutually tangent circles and then recursively filling in *Soddy circles*, the two nonintersecting circles which are tangent to the triple. Levine-Pegden-Smart constructed the set of peak matrices \mathcal{P} following this. They later used the tangency structure of the Apollonian circle packing to construct certain continuum sandpile fractals in Levine et al. [2016b].

The proof that $\mathcal{P} \subset \partial\Gamma_0(\mathbb{Z}^2)$ proceeded by recursively constructing functions $u : \mathbb{Z}^2 \rightarrow \mathbb{Z}$ with Laplacians given by periodic, recurrent sandpiles. Somewhat miraculously, these periodic, recurrent sandpiles appear to describe the microscopic structure of large sandpiles — see Figure 1.11. This phenomena was rigorously proved in Pegden and Smart [2020] where it was shown these periodic patterns actually do appear whenever the limit odometer

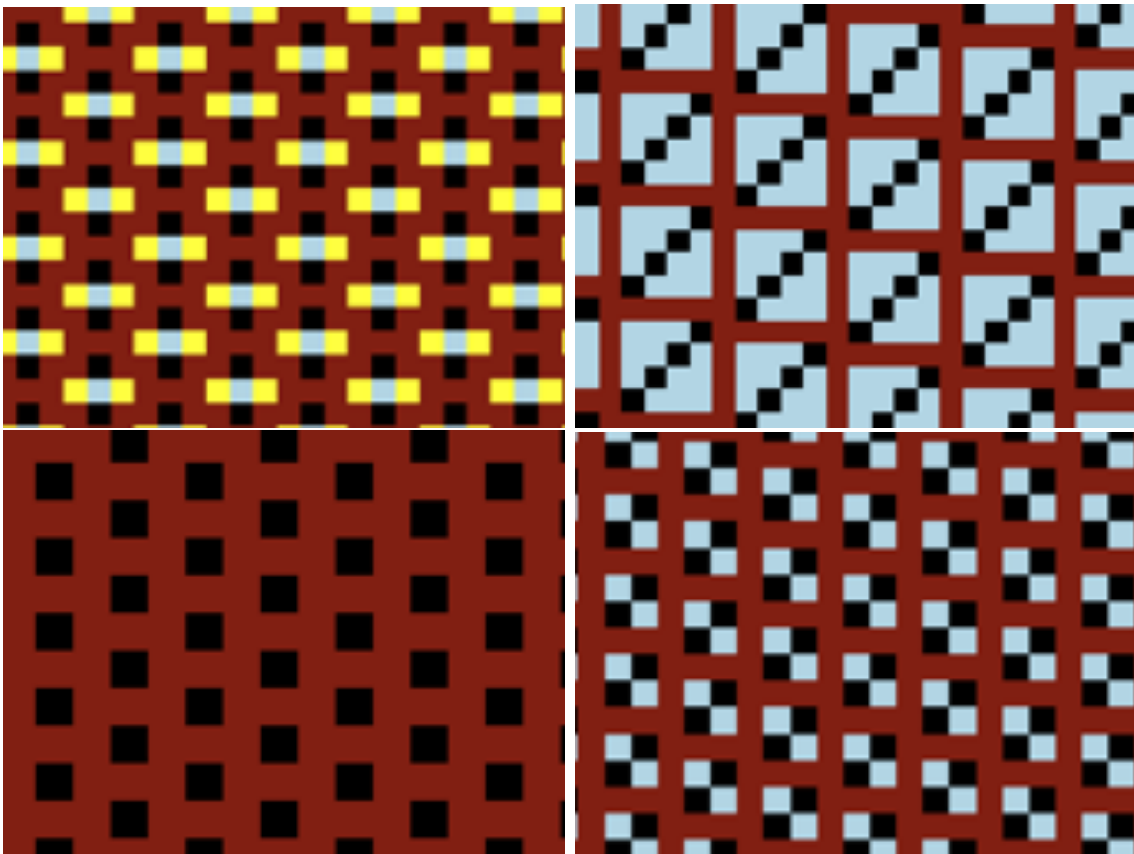


Figure 1.11: Some of the microscopic structure in Figure 1.4. These are all correspond to periodic recurrent sandpiles.

is piecewise quadratic.

The works of Levine-Pegden-Smart completely explain the appearance of sandpiles on \mathbb{Z}^2 and lay the foundation for understanding what happens in general. This thesis can be thought of as a contribution towards their program.

1.3 Discussion of new results

In this section we survey the new results contained in this thesis and also describe some open questions.

1.3.1 The effect of randomness on sandpile growth

The first contribution of this thesis is to extend the convergence theorem of Pegden-Smart to the case where the initial sandpile is not periodic.

Start with a *background* of indistinguishable chips, $\eta : \mathbb{Z}^d \rightarrow \mathbb{Z}$, add n chips at the origin and iterate the following rule:

$$s_{t+1} = s_t + \Delta(1\{s_t \geq 2d\}) \quad (1.12)$$

where $\Delta v(x) = \sum_{i=1}^d (v(x+e_i) + v(x-e_i) - 2v(x))$ is the Laplacian on \mathbb{Z}^d and $s_0 = \eta + n\delta_0$ is the starting sandpile.

If the background is *robust*, then for each n there is a well-defined *stable* sandpile $s_n := s_\infty$, otherwise the sandpile is *explosive* and for some n the infinite sequence $\{s_t\}_{t \geq 0}$ is an *exploding* sandpile. (When the background is robust, by the Abelian property, s_n is just the stabilization of $n\delta_0 + \eta$.)

In each case there is a sequence of growing sandpiles, $\{s_n\}$ or $\{s_t\}$, both of which have been investigated by physicists Dhar and Sadhu [2013]. Simulations suggest some form of convergence is occurring in both the compact and explosive regimes. However, the limits appear to be quite different. In the stable case, hints of the fractal structure appearing in the single-source appear to be retained even when the initial background is random. In the explosive case, the patterns appear to be completely washed out. See Figures 1.12 and 1.13.

Chapters 2 and 3 use techniques from stochastic homogenization to establish convergence of sandpiles for a broad class of deterministic and random initial backgrounds.

Theorem 1.3.1 (Informal statement of results in Chapters 2 and 3). *Each of the following holds on an event of probability 1.*

- If $\eta \leq (2d - 2)$ is stationary and ergodic, then the rescaled, stable sandpiles $\{s_n\}$ converge to the Laplacian of the solution of a certain nonlinear PDE.

DraftMar13

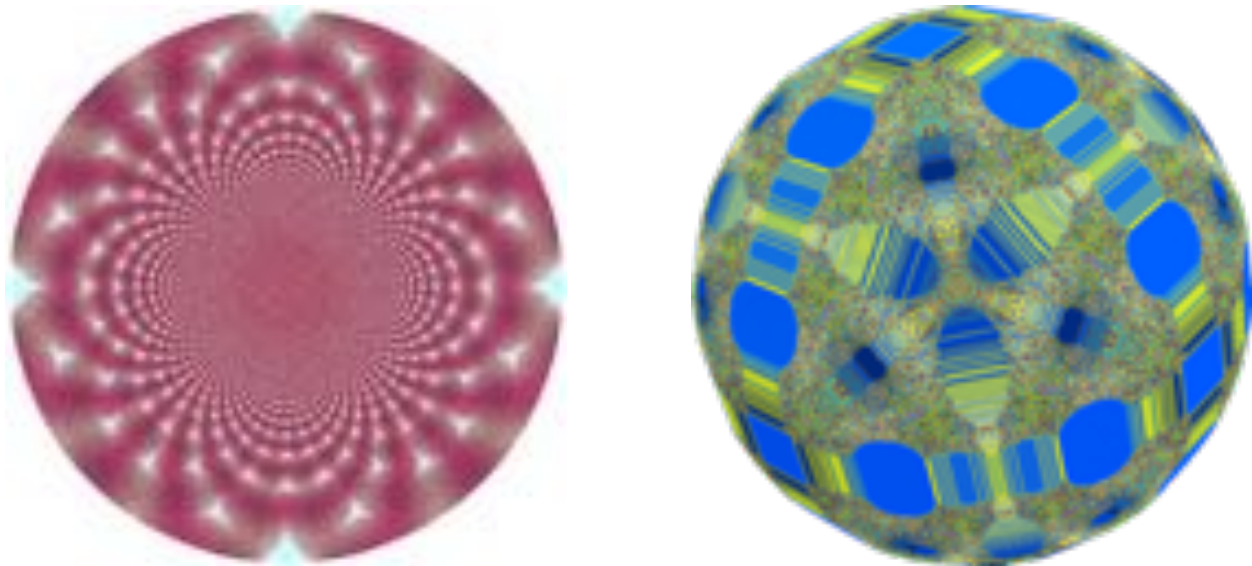


Figure 1.12: Single-source sandpiles on robust backgrounds $\eta \sim \text{Bernoulli}(-1, 0, 1/2)$ in dimensions 2 then 3.

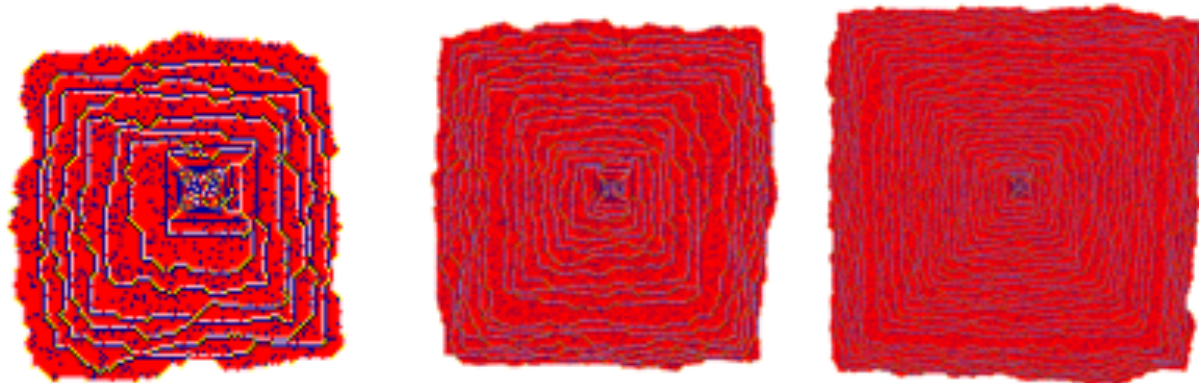


Figure 1.13: Snapshots of an exploding sandpile $\{s_t\}$ for initial background $\eta \sim \text{Bernoulli}(2, 3, 0.01)$

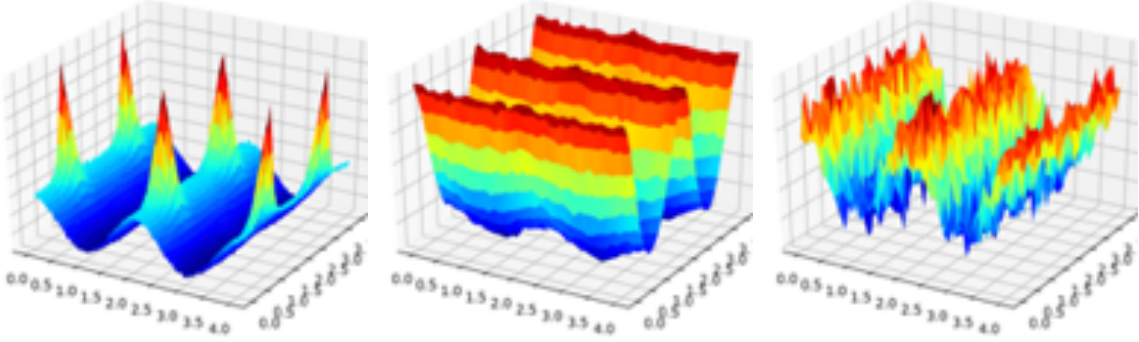


Figure 1.14: Simulations of $\partial\Gamma_\eta(\mathbb{Z}^2)$ for random backgrounds $\eta \sim \text{Bernoulli}(0, 1, 1/2)$, $\eta \sim \text{Bernoulli}(-1, 1, 1/2)$, and $\eta \sim \text{Bernoulli}(-2, 2, 1/2)$ respectively.

- If $\eta \geq (2d-2)$ is stationary with a finite range of dependence and $P(\eta(0) = 2d-1) > 0$, then the rescaled, exploding sandpiles $\{s_t\}$ converge to the level set of a convex function.
- In the intermediate regime ($\eta(x) < (2d-2)$ and $\eta(x') > (2d-2)$ for some x, x') random and deterministic sandpiles may fail to converge.

In the stable case, the sandpiles are rescaled by a factor of $n^{-1/d}$ while in the exploding case the scaling is t^{-1} . The proofs also involve different approaches. In Chapter 2, we use tools from quantitative homogenization of fully nonlinear non-divergence form elliptic PDE Armstrong and Smart [2014a] while in Chapter 3 we combine ideas from bootstrap percolation Schonmann [1992] together with front propagation in random media Xin [2000].

In the explosive regime, it is sometimes possible to explicitly determine the limit shape. For example, in the case $\eta \equiv 2d-1$, the limit shape is a diamond, $\{x \in \mathbb{R}^d : \sum_{i=1}^d |x_i| \leq 1\}$. However, determining the limits in the compact regime appears to be much more difficult.

The proof in the compact case shows that the limit sandpile is given by $\Delta\bar{u}_\eta$ where \bar{u}_η is the unique viscosity solution to

$$\bar{u} = \inf\{w \in C(\mathbb{R}^d) : w \geq -\bar{G} \text{ and } D^2(w + \bar{G}) \in \tilde{\Gamma}_\eta(\mathbb{Z}^d)\}, \quad (1.13)$$

where $\tilde{\Gamma}_\eta(\mathbb{Z}^d)$ is a downwards closed set of $d \times d$ symmetric matrices depending only on the lattice \mathbb{Z}^d and the distribution of the initial background η . However, unlike in the Pegden-Smart proof, the set $\tilde{\Gamma}_\eta(\mathbb{Z}^d)$ is only implicitly identified. (It comes from an application of the subadditive ergodic theorem.) We conjecture that $\tilde{\Gamma}_\eta(\mathbb{Z}^d) = \Gamma_\eta(\mathbb{Z}^d)$. It is not hard to check that $\Gamma_\eta(\mathbb{Z}^d) \subset \tilde{\Gamma}_\eta(\mathbb{Z}^d)$, but the reverse inclusion is currently out of reach.

We believe the reverse inclusion holds because of the output of an algorithm which simulates a closely related set. We now describe the algorithm. Write $q_M(x) = \frac{1}{2}x^T M x$. It is shown in Lemma 3.1 of Levine et al. [2016b] that when η is periodic, $M \in \Gamma_\eta(\mathbb{Z}^d)$ if and only if $\Delta[q_M] + \eta$ is stabilizable (as an infinite-volume sandpile on \mathbb{Z}^d). Levine-Pegden-Smart further observe that when M has rational entries, $\Delta[q_M] + \eta$ is stabilizable on \mathbb{Z}^d if and only if it is stabilizable on a torus whose size depends on the denominators of M and the period size of η . (The proof is given for \mathbb{Z}^2 and $\eta \equiv 0$, but it extends to this case and other lattices.)

This result provides an algorithm for determining, in the periodic case, $\Gamma_\eta(\mathbb{Z}^d)$ up to arbitrary precision. We have no such algorithm in the random case, but we may check that $\Gamma_\eta(\mathbb{Z}^d)$ is the topological closure of

$$\{M \in S_d : \lceil q_M \rceil + \eta \text{ is stabilizable.}\}$$

and S_d is the set of $d \times d$ symmetric matrices.

Here's a quick sketch for the interested reader. If $\Delta[q_M] + \eta$ is stabilizable, then there exists an integer-valued function v satisfying $\Delta v + \Delta[q_M] + \eta \leq 2d - 1$. By conservation of density, Lemma 2.10 in Fey et al. [2009], v is harmonic on large-scales. However, since v is positive and $v(0) < \infty$, this forces $v(x) = o(|x|^2)$. Hence, $w := v + \lceil q_M \rceil$ is integer-valued, has the correct growth, and satisfies $\Delta w + \eta \leq 2d - 1$. Conversely, if such a function w did exist, then $v := w - \lceil q_M \rceil + 1$ is a positive, integer-valued function which stabilizes $\lceil q_M \rceil + \eta$.

We conjecture that $M \in \Gamma_\eta(\mathbb{Z}^d)$ if and only if $\lceil q_M \rceil + \eta$ is stabilizable on all sufficiently

large tori — at least in the case when η is fast mixing. We have computed the latter quantity in Figure 1.14 for some i.i.d. Bernoulli random backgrounds on \mathbb{Z}^2 . The first noticeable feature is that most of the discrete peaks in the non-random case are completely lost — compare with Figure 1.10. The surface also appears to smoothly vary in certain directions. In the case when $\eta \sim \text{Bernoulli}(0, 1, 1/2)$, there do appear to be some isolated peaks. This is in fact provable, and we guess that these peaks correspond to the large curved triangles in Figure 1.12.

To see why these peaks appear, one needs only observe that the function x_1^2 has Laplacian identically equal to 2, and hence $\Delta x_1^2 + \text{Bernoulli}(0, 1, 1/2)$ is a recurrent sandpile. This implies that the quadratic growth of x_1^2 is on $\partial\Gamma_\eta(\mathbb{Z}^2)$. Indeed, one may check directly that $\eta \equiv d$ is recurrent on \mathbb{Z}^d . A sandpile which is stable and pointwise larger than a recurrent sandpile is also recurrent. (See, for example, the proof given in the last section of Chapter 3.)

A similar observation allows us to describe the scaling limits of a family of random and deterministic sandpiles on circle domains.

Take η stationary and ergodic which is pointwise bounded from above and below: $2d \leq \eta \leq 2d + (d - 1)$. Consider the odometer v_n which stabilizes η in $n\Omega$, for $\Omega = \{x \in \mathbb{R}^2 : \|x\|_2 \leq 1\}$, with sink along the boundary. Then the quadratically rescaled odometers converge uniformly in Ω almost surely, $\bar{v}_n(x) \rightarrow \bar{o}(x) := \frac{1-|x|^2}{2}$ — see Figure 1.15. Indeed, the integer-valued function $o(x) = \sum_{i=1}^d -\frac{1}{2}x_i(x_i + 1)$ satisfies $d \leq \Delta o + \eta \leq 2d - 1$ and grows like $q_{D^2\bar{o}}$ at infinity. (And the convergence result for random sandpiles extends to this case.) Another interesting direction is to investigate stability properties of random sandpiles. For example, limit sandpiles appear to vary continuously with respect to bounded noise — see Figure 1.16. To prove this rigorously would require relating the sets $\tilde{\Gamma}_\eta(\mathbb{Z}^d)$ as η varies.

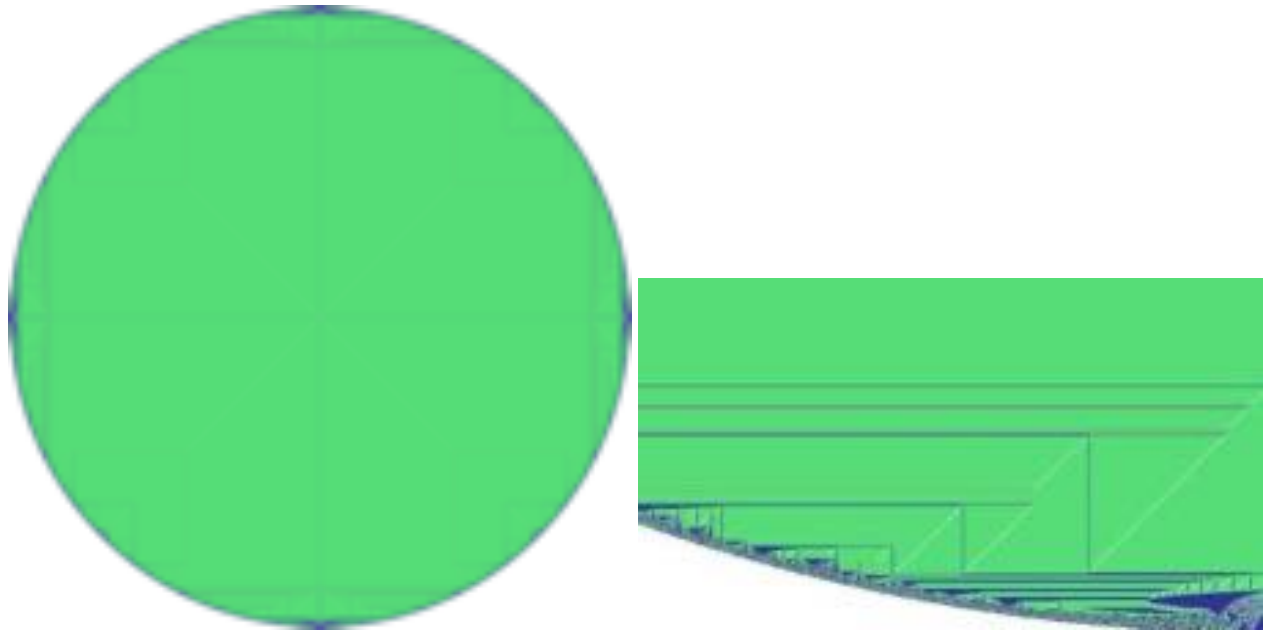


Figure 1.15: Stabilization of 4 chips at every site in a large ball on \mathbb{Z}^2 . Green is 2 chips.

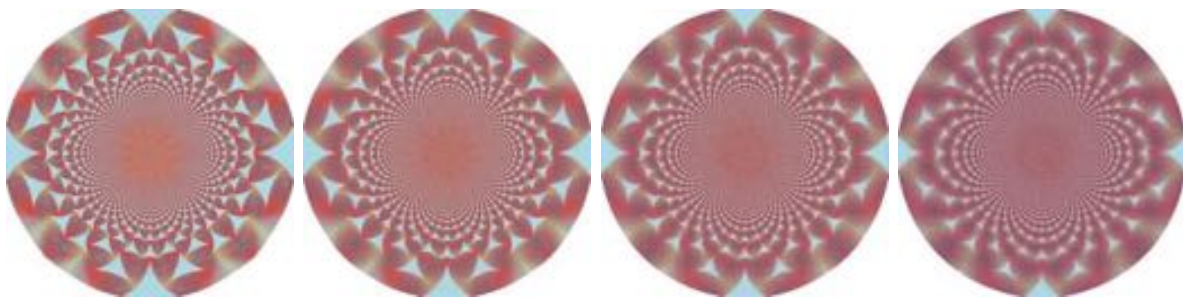


Figure 1.16: Single-source sandpiles on backgrounds $-\eta \sim \text{Bernoulli}(p)$ for $p = k/10$ for $k = 1, 2, 3, 4$.

1.3.2 Integer superharmonic functions on Euclidean digraphs

Our next contribution is an explicit determination of the scaling limit of the sandpile on a particular planar graph. Interestingly, the limit is not a conventional circle packing.

Determining the scaling limit of the sandpile on a lattice is equivalent to understanding the quadratic growths achievable by integer-valued super harmonic functions on the lattice, a direction of independent interest. Indeed, let (V, E) denote a Euclidean digraph. A function $g : V \rightarrow \mathbb{Z}$ is *integer superharmonic* if

$$\Delta g(x) := \sum_{(y,x) \in E} (g(y) - g(x)) \leq 0, \quad (1.14)$$

and has *quadratic growth* A if $g(x) = \frac{1}{2}x^T Ax + o(|x|^2)$. What quadratic growths are achievable by integer superharmonic functions?

The work of Levine-Pegden-Smart answers this question in the case of the square lattice \mathbb{Z}^2 . Indeed, the set $\Gamma_0(\mathbb{Z}^2)$ described in Section 1.2.4 can be translated to this one — given $u : \mathbb{Z}^2 \rightarrow \mathbb{Z}$ with $\Delta u \leq 2d - 1$, an integer superharmonic function may be constructed by subtracting the function $\frac{2d-1}{2}x_1(x_1 + 1)$ which has Laplacian identically equal to $2d - 1$.

In Chapter 4, we characterize such quadratic growths on the F -lattice (defined in (1.15) below for $k = 2$).

Theorem 1.3.2 (Result in Chapter 4). *On the F -lattice, A is integer superharmonic if and only if the difference*

$$\frac{1}{2} \begin{bmatrix} s-t & s+t \\ s+t & t-s \end{bmatrix} - A$$

is positive semi-definite for some $s, t \in \mathbb{Z}$. In particular, taking the matrix parameterization in (1.11), the boundary of the set of integer superharmonic matrices is the union of identical slope-1 cones whose bases are the overlapping circle packing displayed in Figure 1.17.

Theorem 1.3.2 completely determines the scaling limit of the sandpile on the F -lattice.

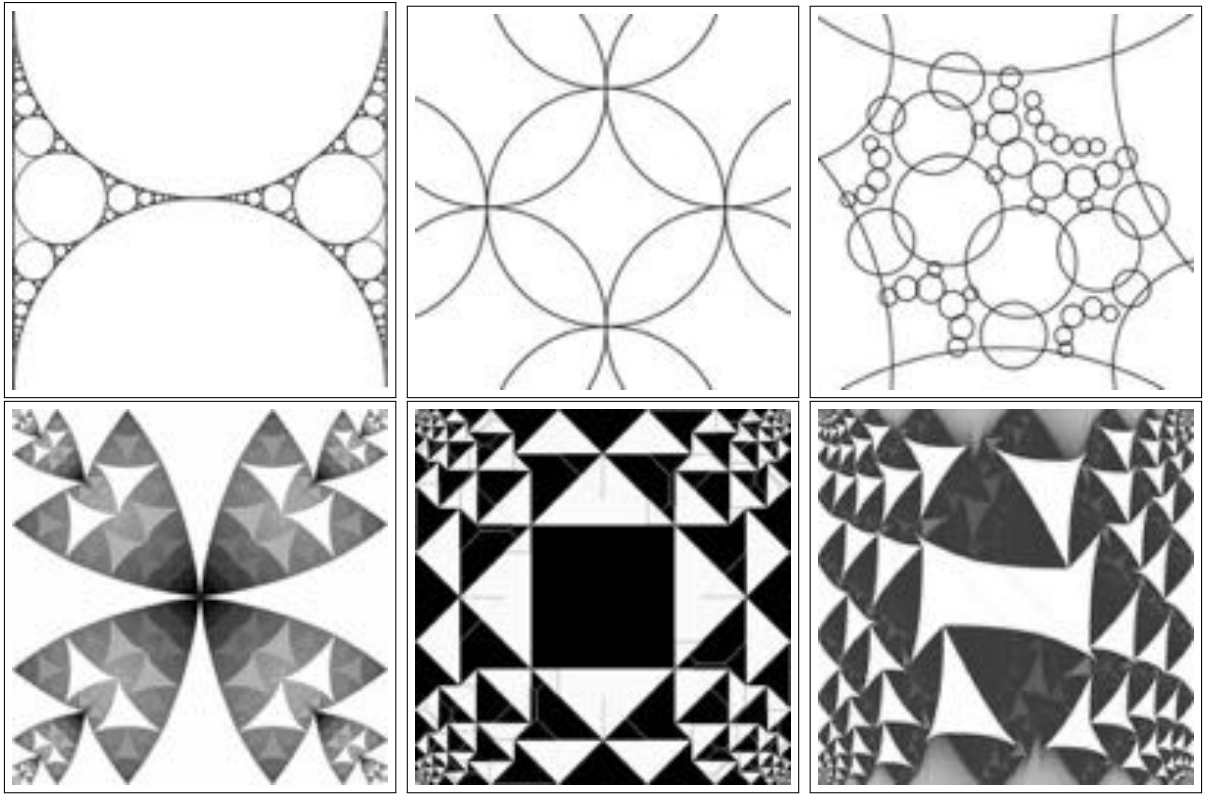


Figure 1.17: By column, three circle packings and sandpiles on \mathbb{Z}^2 , the F lattice, and the $F^{(3)}$ lattice. From left to right: the Apollonian band packing from Levine et al. [2017], the overlapping circle packing from Chapter 4, and the first few generations of $\partial\Gamma_0(F^{(3)})$, a (conjectured) Kleinian bug.

This is the only planar lattice other than \mathbb{Z}^2 for which the scaling limit of the sandpile is characterized — conjectures for other lattices can found in Pegden [2017].

The proof of Theorem 1.3.2 involves recursively constructing integer superharmonic functions for each rational point on a hyperbola. In particular, this shows that while the recursive nature of integer superharmonic functions may persist across different digraphs, the specific recursion is not always Apollonian.

The construction also highlighted several coincidences which occur for the square lattice. For example, the proof of Levine-Pegden-Smart explicitly built one integer superharmonic function for each circle in an Apollonian band packing. Their construction pieced together later functions from earlier ones in a way that mirrored the Soddy-circle generation of Apol-

lonian circle packings. On the F -lattice, the recursion requires building *two distinct* integer superharmonic functions at a time and it sometimes uses parents arbitrarily far up the recursive tree. This latter feature is, in some sense, a sandpile version of the Euclidean algorithm.

The overlapping circle packing appearing in Chapter 4 is an example of an object known as a *Kleinian bug*. Kleinian bugs were recently introduced in Kapovich and Kontorovich [2021] and generalize Apollonian circle packings. An important aspect of Levine et al. [2017] is an analogue of Descartes' rule for integer superharmonic functions — Kleinian bugs share a similar rule.

The symmetry group of the Kleinian bug for the F -lattice is trivial (the difficult aspect of the argument in Chapter 4 is in accounting for the overlaps between circles). However, numerics suggest that integer superharmonic functions on other planar lattices may be described by nontrivial symmetries of Kleinian bugs. One particularly tractable family is the following generalization of the F -lattice: for each $k \geq 2$, the $F^{(k)}$ -lattice is a directed, periodic, planar graph $(\mathbb{Z}^2, E^{(k)})$, where

$$\begin{cases} (x \pm e_1, x) \in E & \text{if } x_1 + x_2 \equiv 0 \pmod{k} \\ (x \pm e_2, x) \in E & \text{otherwise,} \end{cases} \quad (1.15)$$

(the F -lattice is the $F^{(2)}$ lattice). The conjectured Kleinian bug describing the set of integer superharmonic functions on the $F^{(3)}$ lattice is displayed in Figure 1.17.

1.3.3 Dimensional reduction

Our final chapter of this dissertation relates sandpiles across different dimensions.

Start with $2d$ chips in a d -dimensional hypercube of side length m in \mathbb{Z}^d , $s_0 \equiv 2d$, then run parallel toppling (1.12). If a boundary site of the hypercube topples, chips are lost over the edge; thus, for each m there is a well-defined stable sandpile $s_m^{(d)}$.

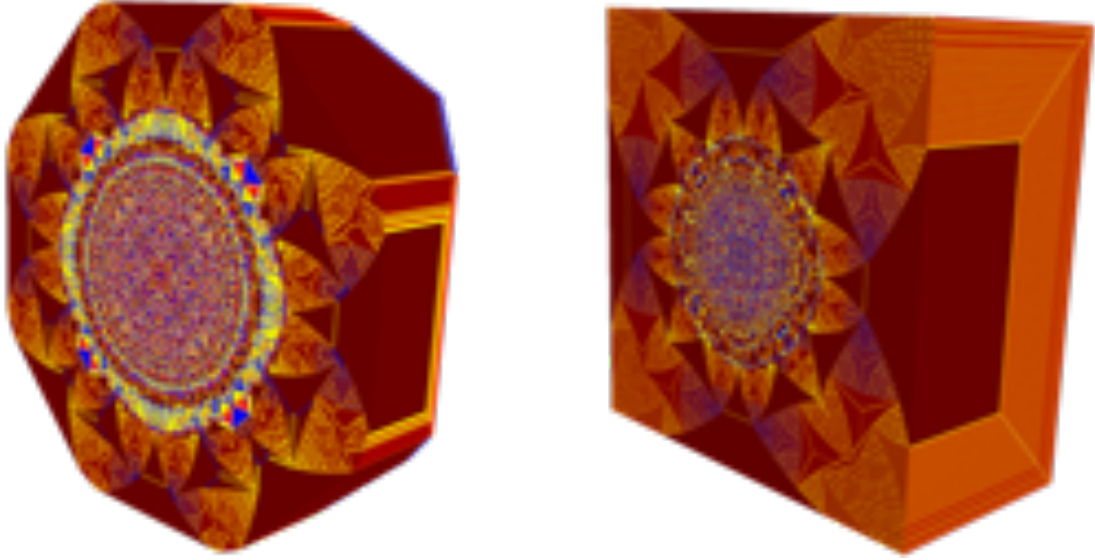


Figure 1.18: Slices of single-source sandpiles on backgrounds $\eta \equiv (2d - k)$ for $k = 3, 2$.

It has been observed empirically since at least Liu et al. [1990] that d -dimensional sandpiles on the hypercube appear embedded in $(d + 1)$ dimensional sandpiles. This *dimensional reduction* also appears to hold for other initial data Levine and Propp [2010], Fey et al. [2010].

In Chapter 5, we prove dimensional reduction when $s_0 \equiv 2d$.

Theorem 1.3.3 (Informal statement of result in Chapter 5). *In all dimensions $d \geq 1$, cross-sections of $(d + 1)$ -dimensional sandpiles are exactly d -dimensional sandpiles:*

$$s_m^{(d+1)}(\lfloor m/2 \rfloor, \cdot) = s_m^{(d)}(\cdot)$$

for all $m \geq 1$.

The key insight is recognizing that dimensional reduction is a consequence of a discrete derivative bound on the *parallel toppling odometers* $v_t^{(d)}$ which encode the number of topples per site over time. In other words, the initial condition and symmetry of the hypercube force the ‘flow’ of parallel toppling to preserve dimensional reduction. In fact, we prove that when

$s_0 \equiv 2d + k$, below a critical dimension, $d \leq d_0 := k + 1$, this bound fails and dimensional reduction does not hold.

We believe that the methods contained in Chapter 5 may be used to establish dimensional reduction in all dimensions $d > d_0$, but have not been able to do so. The technical difficulty lies in formulating and verifying a particular inductive hypothesis in all base dimensions $d_0 \geq 2$. This is relatively straightforward when $d_0 = 1$ and we expect this can be done for any given d_0 , but we do not yet see how to do this simultaneously for all $d_0 \geq 1$.

We also believe that whenever dimensional reduction occurs along cross-sections of the hypercube it extends to the interior. However, tackling this problem seems to require new ideas.

Another interesting question would be to adapt the methods in Chapter 5 to the single-source sandpile; in particular, we conjecture that, away from the origin, slices of $n\delta_0 + (2d - k)$ coincide across dimensions for $d > d_0$. Compare Figures 1.18 and 1.7.

We have made available a GPU-accelerated program which may help in future work on symmetric sandpiles Bou-Rabee. For example, one may check some of the above conjectures up to dimension 12 using it.

1.4 Common notation and conventions

This section describes some common notation and conventions throughout the thesis. We will sometimes use specialized notation in each chapter, in which case, the notation is recalled within the corresponding chapter.

- d will always refer to the dimension of the underlying space.
- Functions on \mathbb{Z}^d are extended via nearest-neighbor interpolation to \mathbb{R}^d and vice-versa.
- e_1, \dots, e_d are the d unit directions in \mathbb{Z}^d .
- $x_i = x \cdot e_i$ is the i th coordinate of vector x and $\mathbf{x}_{d-i} = (x_{i+1}, \dots, x_d)$.

- $|x|$ refers to the Manhattan norm and $|x|_\infty$ the ℓ_∞ norm.
- $y \sim x$ if $|y - x| = 1$.
- Scalar operations on vectors/functions/sets are interpreted pointwise.
- $|\cdot|$ is either the counting measure or Lebesgue measure depending on the input.
- For $A \subset \mathbb{Z}^d$, $A^c := \{x \in \mathbb{Z}^d : x \notin A\}$, $\partial A := \{x \in A^c : \exists y \sim x \in A\}$, and $\bar{A} := A \cup \partial A$.
- C, c , are positive constants which may change from line to line. Dependence is indicated by, for example, C_d .
- The act of *firing* or *toppling* a site, x , removes $2d$ chips from x and adds one chip to each $y \sim x$.
- $\eta \sim \text{Bernoulli}(a, b, p)$ is shorthand for: $\eta : \mathbb{Z}^d \rightarrow \mathbb{Z}$ is drawn from a product measure \mathbf{P} with $\mathbf{P}(\eta(0) = a) = p$ and $\mathbf{P}(\eta(0) = b) = (1 - p)$.
- We denote \mathbf{S}^d as the set of symmetric $d \times d$ matrices with real entries
- If $M \in \mathbf{S}^d$, we write $M \geq 0$ if M has nonnegative eigenvalues; $|M|_2$ will also refer to the largest in magnitude eigenvalue of M .

Code

Code which can be used to compute some of the figures in this thesis is publicly available at https://github.com/nitromannitol/arbitrarydim_sandpiles and <https://github.com/nitromannitol/f-lattice-recursion>.

CHAPTER 2

CONVERGENCE OF THE RANDOM ABELIAN SANDPILE

This chapter is based on the article Bou-Rabee [2021a] which is published in Annals of Probability.

2.1 Introduction

2.1.1 Overview

In this chapter, as a first step towards understanding random sandpiles, we show, using a novel approach, that sandpiles with random initial states have scaling limits. The proof follows the Armstrong-Smart program for stochastic homogenization of non-divergence form elliptic equations.

As a simple example of what's covered by our result, consider the following random sandpile process on \mathbb{Z}^d . Start with $2d - 1$ chips at each site in a ball of radius n . Flip a fair coin for each x in the ball, if the coin lands heads, add two extra chips at x . Once the initial sandpile has been set, stabilize.

If you repeat this experiment for large n and rescale, a non-random pattern emerges. The pattern looks remarkably similar to the scaling limit of the single-source sandpile — compare Figures 2.1 and 2.2. Our main result explains this similarity by proving that the scaling limit of the random sandpile is the Laplacian of the solution to an elliptic obstacle problem with two operators. One operator depends on the distribution of the randomness. The other operator is the exact same one appearing in the scaling limit of the single-source sandpile.

DraftMar13

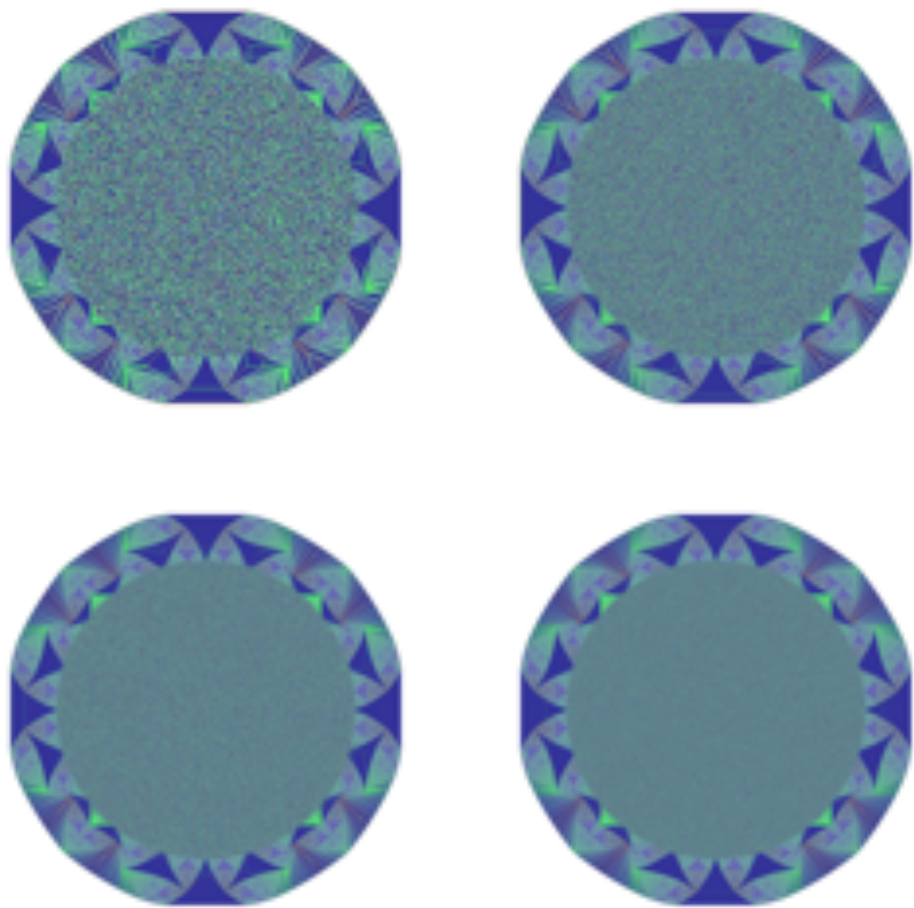


Figure 2.1: For each x in a ball of radius $n = 500, 1000, 2000$, and 3000 , flip a fair coin. If it lands heads, add 3 chips to x , otherwise add 5 chips. Then, stabilize. Sites with 0,1,2, and 3 chips are represented by white, brown, green, and blue respectively.

2.1.2 Main result

Let $\eta : \mathbb{Z}^d \rightarrow \mathbb{Z}$ be stationary, ergodic, bounded, and satisfy $\mathbf{E}(\eta(0)) > 2d - 1$. Let $W \subset \mathbb{R}^d$ be a bounded Lipschitz domain. For each $n \in \mathbb{N}$, let $W_n = \mathbb{Z}^d \cap nW$ denote the finite difference approximation of W . Initialize the sandpile according to η in W_n and set it to be 0 elsewhere. Then, stabilize, counting how many times each site topples with the *odometer function* $v_n : \mathbb{Z}^d \rightarrow \mathbb{N}$. Denote the stable sandpile by $s_n : \mathbb{Z}^d \rightarrow \mathbb{Z}$. Our main result is the following.

Theorem 2.1.1. *Almost surely, as $n \rightarrow \infty$, the rescaled functions $\bar{v}_n(x) := n^{-2}v_n([nx])$ converge uniformly to the unique solution of the elliptic obstacle problem,*

$$\bar{v} := \min\{\bar{v} \in C(\mathbb{R}^d) : \bar{v} \geq 0, \bar{F}_\eta(D^2\bar{v}) \leq 0 \text{ in } W, \text{and } \bar{F}_0(D^2\bar{v}) \leq 0 \text{ in } \mathbb{R}^d\},$$

where \bar{F}_η is a nonrandom, degenerate elliptic operator defined implicitly at the end of Section 2.6.1,

$$\bar{F}_0(M) := \inf\{s \in \mathbb{R} \mid \text{there exists } u : \mathbb{Z}^d \rightarrow \mathbb{Z} \text{ such that for all } y \in \mathbb{Z}^d,$$

$$\Delta_{\mathbb{Z}^d}u(y) \leq 2d - 1, \text{ and } u(y) \geq \frac{1}{2}y^T(M - sI)y\},$$

and the differential inequalities are interpreted in the viscosity sense.

In turn, almost surely, the rescaled sandpiles, $\bar{s}_n(x) := s_n([nx])$ converge weakly-* to a deterministic function $s \in L^\infty(\mathbb{R}^d)$ as $n \rightarrow \infty$. Moreover, the limit satisfies $\int_{\mathbb{R}^d} s = |W| \mathbf{E}(\eta(0))$, $s \leq 2d - 1$, $s = 0$ in $\mathbb{R}^d \setminus B_R(W)$ for some constant $R > 0$ depending on W and $\mathbf{E}(\eta(0))$, and weakly,

$$s = \begin{cases} \Delta\bar{v} + \mathbf{E}(\eta(0)) & \text{in } W \\ \Delta\bar{v} & \text{in } \mathbb{R}^d \setminus W. \end{cases}$$

The main challenge in proving the above theorem is that there is no inherent linear



Figure 2.2: The single-source sandpile: start with 10^6 chips at the origin and stabilize. Sites with 0,1,2, and 3 chips are represented by white, brown, green, and blue respectively.

or subadditive quantity governing the behavior of the sandpile. The Abelian sandpile is nonlocal: one unstable pile can cause a far-reaching avalanche of topplings. This difficulty is the same one faced by those studying stochastic homogenization of fully nonlinear elliptic PDEs. Fortunately, since the sandpile can be expressed as the solution to a nonlinear discrete PDE, we can use those same methods here. To be specific, we import the stochastic homogenization tools introduced by S. Armstrong and C. Smart in Armstrong and Smart [2014a].

The tools, however, don't work out of the box. The sandpile doesn't directly fit into the general framework of fully nonlinear elliptic PDEs; and so appropriate sandpile substitutes must be identified in order to run the program. Further, a main technical hurdle to overcome is the lack of uniform ellipticity. This is done with new arguments which utilize the regularity theory of the discrete Laplace operator as well as a comparison principle hidden in sandpile dynamics.

2.1.3 Outline of the chapter

In Section 2.2, we precisely state the assumptions of our result. Then, in Section 2.3, we recall some necessary properties of the Abelian sandpile. We provide a brief overview of the main ideas of the proof in Section 2.4. Next, in Section 2.5, we define a subadditive quantity, μ , which will implicitly control the random sandpile. Through an appropriate perturbation of μ , we identify \bar{F}_η in Section 2.6. In Section 2.7, we prove the main result by establishing compactness of the odometer and showing that \bar{F}_η has a comparison principle. Then, in Section 2.8 we show a simpler proof of convergence of a related model, the random *divisible* sandpile, introduced by L. Levine and Y. Peres Levine and Peres [2009, 2010]. In stark contrast to the Abelian sandpile, the limit of the random divisible sandpile is exactly the limit of the averaged divisible sandpile. We end with some generalizations and open questions in Section 2.9.

2.2 Assumptions

We consider the sandpile on the integer lattice \mathbb{Z}^d for $d \geq 2$, (although this assumption is not an essential one). Let Ω denote the set of all bounded functions $\eta : \mathbb{Z}^d \rightarrow \mathbb{Z}$. Endow Ω with the σ -algebra \mathcal{F} generated by $\{\eta \rightarrow \eta(x) : x \in \mathbb{Z}^d\}$. We model the randomness by a probability measure \mathbf{P} on (Ω, \mathcal{F}) with the following properties. First, there exists $\eta_{\min}, \eta_{\max} \in \mathbb{Z}$ so that for every $x \in \mathbb{Z}^d$,

$$\text{Uniform Boundedness: } \mathbf{P} [\eta_{\min} \leq \eta(x) \leq \eta_{\max}] = 1. \quad (2.1)$$

Note this may be replaced by an appropriate concentration assumption. We further assume that \mathbf{P} is stationary and ergodic. Denote the action of translation by $T : \mathbb{Z}^d \times \Omega \rightarrow \Omega$,

$$T(y, \eta)(z) = (T_y \eta)(z) := \eta(y + z),$$

and extend this to \mathcal{F} by defining $T_y E := \{T_y \eta : \eta \in E\}$. Stationarity and ergodicity is then

$$\text{Stationarity: for all } E \in \mathcal{F}, y \in \mathbb{Z}^d: \mathbf{P}(T_y E) = \mathbf{P}(E), \quad (2.2)$$

$$\text{Ergodic: } E = \cap_{y \in \mathbb{Z}^d} T_y E \text{ implies that } \mathbf{P}(E) \in \{0, 1\}. \quad (2.3)$$

Lastly, we assume that the density of sand in the initial sandpile is high:

$$\text{High density: } \mathbf{E}(\eta(0)) > 2d - 1. \quad (2.4)$$

High density is a natural, weak assumption which forces interesting behavior to occur. See Section 2.9 for further discussion of this assumption. A concrete example to keep in mind is when $\{\eta(x)\}_{x \in \mathbb{Z}^d}$ are independent and identically distributed with sufficiently large expectation.

2.3 Sandpiles

The results in this section are reformulations of fundamental facts about the Abelian sandpile. Fix a bounded, connected $A \subset \mathbb{Z}^d$ and a starting sandpile $\eta : A \rightarrow \mathbb{Z}$. We call positive integer-valued functions on \bar{A} , *toppling functions*. Recall that a toppling function u is *legal* for η if it can be decomposed into a sequence of topplings so that only sites x where $\eta(x) \geq 2d$ are toppled. More precisely, u is legal for η if we can express for some $n \geq 0$,

$$u = u_0 + u_1 + \cdots + u_n,$$

where $u_0 = 0$ and for $i \geq 1$, $u_i(x) = 0$ for all $x \in A$ except for one $\hat{x}_i \in A$ for which $u_i(\hat{x}_i) = 1$ and

$$(\Delta_{\mathbb{Z}^d}(u_1 + \cdots + u_{i-1}) + \eta)(\hat{x}_i) \geq 2d.$$

When $\eta \leq 2d - 1$, the only legal toppling function is $u = u_0 = 0$. An important observation is that any legal toppling function satisfies $\Delta_{\mathbb{Z}^d} u + \eta \geq \min(0, \eta)$ but this inequality does not imply u is legal. A toppling function v is *stabilizing* for η in A if $\Delta_{\mathbb{Z}^d} v + \eta \leq 2d - 1$ in A .

Denote the set of *locally legal* topplings for η as

$$\begin{aligned} \mathcal{L}(\eta, A) = & \{u : \bar{A} \rightarrow \mathbb{N} : \text{there exists } w : \bar{A} \rightarrow \mathbb{N} \text{ and } \hat{u} : \bar{A} \rightarrow \mathbb{N} \\ & \text{where } u = w + \hat{u}, w(x) = 0 \text{ for } x \in A, \hat{u}(x) = 0 \text{ for } x \in \partial A \\ & \text{and } \hat{u} \text{ is legal for } \Delta_{\mathbb{Z}^d} w + \eta \text{ in } A\} \end{aligned}$$

and the set of stabilizing topplings for η in A as

$$\mathcal{S}(\eta, A) = \{v : \bar{A} \rightarrow \mathbb{N} : \Delta_{\mathbb{Z}^d} v(x) + \eta(x) \leq 2d - 1 \text{ for } x \in A\}.$$

It is important to note that these sets only enforce their constraints in A , they may include arbitrary topplings on ∂A .

The *odometer* function, $v : \mathbb{Z}^d \rightarrow \mathbb{N}$, counts the number of times each site in η topples when stabilizing. Here we distinguish between two common scenarios. In the first scenario, once a grain leaves A , it falls off and disappears. We call this the *open boundary* condition. In this case $v = 0$ on $\mathbb{Z}^d \setminus A$. In the second scenario, grains continue to spread and topplings can occur outside of A . This is the *free boundary* condition. The sandpile we consider in our main theorem has the free boundary condition. However, as we will discuss in Section 2.9, our methods also apply to other sandpiles including those with open boundaries. In this section, we state results for sandpiles with open boundaries.

First, we recall the least-action principle for sandpiles Fey et al. [2010] and rephrase it in a way amenable to the methods of this chapter. We will refer to this as the *discrete sandpile PDE*.

Proposition 2.3.1. *The odometer function v uniquely solves each of the following problems.*

1. *Longest legal toppling,*

$$v = \sup\{w : \bar{A} \rightarrow \mathbb{N} : w \in \mathcal{L}(\eta, A), w = 0 \text{ on } \partial A\}.$$

2. *Shortest stabilizing toppling,*

$$v = \inf\{u : \bar{A} \rightarrow \mathbb{N} : u \in \mathcal{S}(\eta, A), u = 0 \text{ on } \partial A\}.$$

3. *Stabilizing, legal toppling,*

$$v \in \mathcal{L}(\eta, A) \cap \mathcal{S}(\eta, A) \text{ and } v = 0 \text{ on } \partial A.$$

The reader should view locally legal toppling functions as subsolutions and stabilizing toppling functions as supersolutions.

We will also use the following consequence of the Abelian property: any locally legal, stabilizing toppling function can be decomposed into the usual odometer function for η and an odometer function which keeps track of topplings originating from the boundary.

Proposition 2.3.2. *If $v \in \mathcal{L}(\eta, A) \cap \mathcal{S}(\eta, A)$ and $v = f \geq 0$ on ∂A , then v can be decomposed into*

$$v = v_1 + v_2,$$

where

$$\begin{cases} v_1 \in \mathcal{L}(\eta) \cap \mathcal{S}(\eta) & \text{on } A \\ v_1 = 0 & \text{on } \partial A \end{cases}$$

and

$$\begin{cases} v_2 \in \mathcal{L}(\eta + \Delta_{\mathbb{Z}^d} v_1) \cap \mathcal{S}(\eta + \Delta_{\mathbb{Z}^d} v_1) & \text{on } A \\ v_2 = f & \text{on } \partial A \end{cases}$$

A certain class of sandpiles, known as *recurrent* sandpiles will help in the sequel. We say η is recurrent if we can find $s : A \rightarrow \mathbb{N}$ and $u \in \mathcal{L}(s + 2d - 1, A)$ with $u = 0$ on ∂A so that $\eta = 2d - 1 + s + \Delta_{\mathbb{Z}^d} u$ in A . In other words, η is recurrent if we can reach η by starting with $2d - 1$ chips at every site in A , adding chips at some sites in A , and then toppling some sites legally. Also we call η *stable* in A if $\eta \leq 2d - 1$ in A .

A useful consequence of Dhar's burning algorithm Dhar [1990] will aid in controlling topplings in stable, recurrent sandpiles. Recall that the burning algorithm provides a recipe for checking if a stable sandpile is recurrent: topple the boundary of a sandpile once, if the sandpile is recurrent, each inner site will topple exactly once when stabilizing. More generally, topple sites along ∂A and then legally stabilize s in A . If s is a stable sandpile, no site in A will topple more times than a boundary site has toppled. And, if s is a recurrent sandpile, every site in A will topple at least as many times as some boundary site. This leads to both a maximum principle and a comparison principle for the sandpile.

Proposition 2.3.3. *For $f : \partial A \rightarrow \mathbb{N}$, a sandpile $s : A \rightarrow \mathbb{Z}$, let v solve*

$$\begin{cases} v \in \mathcal{L}(s) \cap \mathcal{S}(s) & \text{on } A \\ v = f & \text{on } \partial A \end{cases}$$

If s is stable, then

$$\sup_{x \in A} v(x) \leq \sup_{y \in \partial A} f(y). \quad (2.5)$$

If s is recurrent, then

$$\inf_{x \in A} v(x) \geq \inf_{y \in \partial A} f(y). \quad (2.6)$$

In particular, when s is stable and recurrent, we have the following comparison principle: let u solve

$$\begin{cases} u \in \mathcal{L}(s) \cap \mathcal{S}(s) & \text{on } A \\ u = f' & \text{on } \partial A, \end{cases}$$

for some $f' : \partial A \rightarrow \mathbb{N}$. Then, for any integer-valued harmonic functions $g, h : \bar{A} \rightarrow \mathbb{Z}$ with $\Delta_{\mathbb{Z}^d} g = \Delta_{\mathbb{Z}^d} h = 0$ in A ,

$$\inf_{x \in A} ((u + g) - (v + h))(x) \geq \inf_{y \in \partial A} ((f' + g) - (f + h))(y). \quad (2.7)$$

Proof. The maximum principle, (2.5) and (2.6), follows from the proof of the burning algorithm, see Theorem 2.6.3 in Klivans [2018] or Theorem 7.5 in Corry and Perkins [2018]. We show how these imply (2.7). By definition, $\eta_u := \Delta_{\mathbb{Z}^d} u + s$ and $\eta_v := \Delta_{\mathbb{Z}^d} v + s$ are both stable and recurrent. Let

$$w(x) = ((u + g) - (v + h))(x) - \inf_{y \in \bar{A}} ((u + g) - (v + h))(y),$$

so that $w \geq 0$ and in A ,

$$\Delta_{\mathbb{Z}^d} w + \eta_v = \Delta_{\mathbb{Z}^d} u + s = \eta_u.$$

Let \hat{w} solve

$$\hat{w} \in \mathcal{L}(\eta_v, A) \cap \mathcal{S}(\eta_v, A) \text{ and } \hat{w} = w \text{ on } \partial A.$$

By Propositions 2.3.2, 2.3.1, and then (2.6),

$$\inf_{x \in A} w(x) \geq \inf_{x \in A} \hat{w}(x) \geq \inf_{y \in \partial A} \hat{w}(y) = \inf_{y \in \partial A} w(y).$$

□

We conclude the section by noting a useful alternative characterization of recurrent sand-

piles. If each site in η has toppled at least once, then what remains is recurrent.

Proposition 2.3.4. *Let $A \subset W$ be connected subsets of \mathbb{Z}^d . If $w \in \mathcal{L}(\eta, W)$ with $w \geq 1$ in A , then $\Delta_{\mathbb{Z}^d} w + \eta$ is recurrent in A .*

2.4 Method overview

Let $W \subset \mathbb{R}^d$ be a bounded Lipschitz domain and $\eta : \mathbb{Z}^d \rightarrow \mathbb{Z}$ a uniformly bounded initial sandpile. For every $n \geq 1$ and finite difference approximation $W_n := nW \cap \mathbb{Z}^d$, there is a unique odometer function $v_n : W_n \rightarrow \mathbb{N}$ which determines the stabilization of η in W_n . Uniqueness of v_n comes from the fact that it solves the discrete sandpile PDE for η on W_n and this PDE enjoys a comparison principle, Proposition 2.3.3.

Hence, for each fixed n , v_n is unique. As η is uniformly bounded, the Laplacians of v_n are in turn bounded and $\bar{v}_n(x) := n^{-2}v_n([nx])$ converges along *subsequences* uniformly in W . However, there is no reason to expect the limits to coincide for arbitrary choices of η . We must have, at least, convergence of local averages of η itself. A natural choice is to assume that η is drawn from a stationary and ergodic probability distribution.

If we remove the integer constraint on the sandpile PDE, we can use simple random walk difference estimates (see Section 2.8), to show that the limit *divisible* sandpile coincides with the limit of the averaged divisible sandpile, $\mathbf{E}(\eta(0))$. In this case, the odometers solve a linear PDE in the limit, the Poisson problem, $\Delta \bar{v} + \mathbf{E}(\eta(0)) = 2d - 1$, on W .

The integer constraint imposes a nonlinear structure on the problem which makes it more difficult. Essentially our only available tool is a discrete comparison principle. Our method can be understood as a technique to push the comparison principle for the sandpile from the lattice to the continuum. We show, roughly, that the discrete sandpile PDE converges to a fully nonlinear elliptic PDE with a comparison principle. The limit PDE inherits features from both the lattice \mathbb{Z}^d and the distribution of η . (Interestingly, simulations suggest that the limit PDE is wildly different for different probability distributions, even when they share

the same mean.)

Our proof of Theorem 2.1.1 follows the stochastic homogenization program of Armstrong and Smart [2014a]. The strategy involves comparing the odometer function of the sandpile to the solution of an auxillary Monge-Ampère equation Gutiérrez [2016], Trudinger and Wang [2008] which will control how much the odometer function can ‘bend’. The proof has three steps:

1. Identify the *effective equation* \bar{F}_η describing the limit PDE via the subadditive ergodic theorem applied to an auxiliary Monge-Ampère measure, μ .
2. Show that \bar{F}_η inherits the comparison principle for sandpiles.
3. Conclude by showing every subsequential limit is a viscosity solution to $\bar{F}_\eta(D^2(v)) = 0$.

The most difficult part of this program is to show that \bar{F}_η has a comparison principle, Lemma 2.7.5. In the fully nonlinear elliptic setting, this is done under the assumption of *uniform ellipticity*. The discrete sandpile PDE is not uniformly elliptic (a priori), so our argument for this is completely new. Lack of uniform ellipticity also required us to develop new arguments for the regularity of μ , Lemma 2.6.2 and Lemma 2.6.3.

2.5 A monotone quantity

2.5.1 Definition of the monotone quantity

In this section we introduce μ , a monotone quantity which will control solutions to the discrete sandpile PDE. For a function $v : \mathbb{Z}^d \rightarrow \mathbb{Z}$ and $x \in A \subset \mathbb{Z}^d$ let

$$\partial^+(v, x, A) = \{p \in \mathbb{R}^d : v(x) + p \cdot (y - x) \geq v(y) : \text{for all } y \in \bar{A}\}$$

denote the supergradient set of v at x in A . Similarly,

$$\partial^-(v, x, A) = \{p \in \mathbb{R}^d : v(x) + p \cdot (y - x) \leq v(y) : \text{ for all } y \in \bar{A}\}$$

is the subgradient set at x . For short-hand, we omit the set A when it is clear and write

$$\partial^+(v, A) = \cup_{x \in A} \partial^+(v, x).$$

To completely identify a fully nonlinear elliptic PDE, it suffices to recognize when a parabola is a supersolution or a subsolution. This fundamental observation is due to Caffarelli Caffarelli [1999] and was employed by Caffarelli, Souganidis, and Wang in their obstacle problem argument for stochastic homogenization of fully nonlinear uniformly elliptic equations Caffarelli et al. [2005], Armstrong and Smart [2014c].

Our method is similar: we will perturb solutions by a parabola and then define the effective equation, \bar{F}_η , through these perturbed limits. For $l \in \mathbb{R}$, $M \in \mathbf{S}^d$, and $\eta \in \Omega$, denote the set of perturbed subsolutions as

$$S(A, \eta, l, M) = \{u : \bar{A} \rightarrow \mathbb{N} : u \in \mathcal{L}(\eta, A)\} - (q_l + q_M)$$

and the set of perturbed supersolutions as

$$S^*(A, \eta, l, M) = \{v : \bar{A} \rightarrow \mathbb{N} : v \in \mathcal{S}(\eta, A)\} - (q_l + q_M).$$

The monotone quantity controlling subsolutions is then

$$\mu(A, \eta, l, M) = \sup\{|\partial^+(w, A)| : w \in S(A, \eta, l, M)\},$$

while the monotone quantity which controls supersolutions is

$$\mu^*(A, \eta, l, M) = \sup\{|\partial^-(w, A)| : w \in S^*(A, \eta, l, M)\}.$$

The results in the next two subsections are completely deterministic, so we fix $\eta \in \Omega$.

2.5.2 Comparing subsolutions and supersolutions

We will need to compare legal and stabilizing toppling functions throughout this chapter. However, the discrete sandpile PDE is nonlinear: if v is a stabilizing toppling function for η , then $-v$ is not a legal toppling function for $-\eta$ (unless $v = 0$). This makes it difficult to compare legal and stabilizing toppling functions. However, through μ , we can compare the two using the following lemma, which roughly states that legal, stabilizing toppling functions maximize curvature.

Lemma 2.5.1. *If $u \in \mathcal{L}(\eta, A)$, the solution of*

$$h \in \mathcal{L}(\eta, A) \cap \mathcal{S}(\eta, A) \text{ and } h = u \text{ on } \partial A,$$

satisfies $\partial^+(u, A) \subseteq \partial^+(h, A)$. Similarly, if $v \in \mathcal{S}(\eta, A)$, then the solution of

$$h^* \in \mathcal{L}(\eta, A) \cap \mathcal{S}(\eta, A) \text{ and } h^* = v \text{ on } \partial A,$$

satisfies $\partial^-(v, A) \subseteq \partial^-(h^, A)$.*

Proof. Take $p \in \partial^+(u, x, A)$ and let

$$t = \inf\{c \in \mathbb{R} : u(x) + p \cdot (y - x) + c \geq h(y) \text{ for all } y \in \bar{A}\}$$

By the least action principle and boundary assumption, $h \geq u$, hence $t \geq 0$. Also, as A is

finite, $t < \infty$. Since $h = u$ on ∂A , we must have $y \in A$ for which

$$u(x) + p \cdot (y - x) + t = h(y),$$

which shows $p \in \partial^+(h, y, A)$. The proof for subgradients is similar. \square

2.5.3 Basic properties of the monotone quantity

We now establish control on solutions from above and below which will follow from the proof of the Alexandroff-Bakelman-Pucci (ABP) inequality (Theorem 3.2 in Roberts et al. [1995] and Theorem 1.4.2 in Gutiérrez [2016]).

Lemma 2.5.2. *There exists $C_d > 0$ so that for all $w \in S(B_n, \eta, l, M)$,*

$$\max_{x \in B_n} w(x) \leq \max_{x \in \partial B_n} w(x) + C_d n \mu(B_n, \eta, l, M)^{1/d} \quad (2.8)$$

and for all $w \in S^*(B_n, \eta, l, M)$,

$$\inf_{x \in \partial B_n} w(x) \leq \inf_{x \in B_n} w(x) + C_d n \mu^*(B_n, \eta, l, M)^{1/d}. \quad (2.9)$$

Proof. Let $a = \max_{x \in B_n} w(x) - \max_{x \in \partial B_n} w(x)$. Assume $a > 0$, otherwise the claim is immediate. Choose x_0 so that $\max_{x \in B_n} w(x) = w(x_0)$. Let $p \in \mathbb{R}^d$ satisfy $|p| \leq \text{adiam}(B_n)^{-1} = C_d a/n$. Then, for each $x \in B_n$,

$$\begin{aligned} w(x_0) + p \cdot (x - x_0) &\geq w(x_0) - |p||x - x_0| \\ &> w(x_0) - w(x_0) + \max_{x \in \partial B_n} w(x) \\ &= \max_{x \in \partial B_n} w(x). \end{aligned} \quad (2.10)$$

Now, we shift the hyperplane up just enough so that it lies above w in \bar{B}_n : let

$$t = \inf\{c \in \mathbb{R} : w(x_0) + p \cdot (x - x_0) + c \geq w(x) \text{ for all } x \in \bar{B}_n\}$$

and note that $t \geq 0$ and that there exists $y \in \bar{B}_n$ with

$$w(y) = w(x_0) + p \cdot (y - x_0) + t.$$

If $t > 0$, then (2.10) shows that $y \in B_n$. If $t = 0$, we can choose $y = x_0$. Hence, there is a $y \in B_n$ with $p \in \partial^+(w, y, B_n)$. Since this holds for every $|p| < a/\text{diam}(B_n)$, this implies

$$|\partial^+(w, B_n)| \geq C_d \frac{a^d}{\text{diam}(B_n)^d}.$$

And so rearranging, we get

$$a \leq |\partial^+(w, B_n)|^{1/d} C_d \text{diam}(B_n) \leq C_d n \mu(B_n, \eta, l, M)^{1/d}$$

The proof for μ^* is identical. □

Next we introduce the concave envelope of a subsolution. First, we extend the discrete domain Q_n and its closure to their convex hulls: $\mathcal{Q}_n := \mathbf{conv} Q_n$ and $\bar{\mathcal{Q}}_n := \mathbf{conv} \bar{Q}_n$. Then, define the concave envelope of w by, $\Gamma_w : \bar{\mathcal{Q}}_n \rightarrow \mathbb{R}$,

$$\Gamma_w(x) = \inf_{p \in \mathbb{R}^d} \max_{y \in \bar{Q}_n} (w(y) + p \cdot (x - y)),$$

noting that Γ_w is the pointwise least concave function so that on \bar{Q}_n , $\Gamma_w \geq w$. We recall a useful representation of the concave envelope.

Proposition 2.5.1 (Lemma 4.5 in Imbert and Silvestre [2013]). *We can alternatively represent*

$$\Gamma_w(x) = \sup \left\{ \sum_{i=1}^{d+1} \lambda_i w(x_i) : x_i \in \bar{Q}_n, \sum_{i=1}^{d+1} \lambda_i x_i = x, \lambda_i \in [0, 1], \sum_{i=1}^{d+1} \lambda_i = 1 \right\},$$

and if

$$\Gamma_w(x) = \sum_{i=1}^{d+1} \lambda_i w(x_i),$$

then for each x_i , $\Gamma_w(x_i) = w(x_i)$ and Γ_w is linear in $\text{conv}(x_1, \dots, x_{d+1})$.

The next statement uses this representation to show that the measure of the supergradient set is preserved under the operation of taking the concave envelope. As the concave envelope is defined on \mathbb{R}^d , we first extend the definition of supergradient set to functions $g : Q_n \rightarrow \mathbb{R}$,

$$\partial^+(g, Q_n) = \{p \in \mathbb{R}^d : \exists x \in Q_n : g(x) + p \cdot (y - x) \geq g(y) : \text{ for all } y \in \bar{Q}_n\}. \quad (2.11)$$

Lemma 2.5.3.

$$\begin{aligned} \sum_{x \in Q_n} |\partial^+(w, x, Q_n)| &= |\partial^+(w, Q_n)| \\ &= \sum_{\{x : \Gamma_w(x) = w(x)\}} |\partial^+(\Gamma_w, x, Q_n)| = |\partial^+(\Gamma_w, Q_n)|. \end{aligned}$$

Proof. We split the proof into two steps.

Step 1

We first show that

$$|\partial^+(w, Q_n)| = \sum_{x \in Q_n} |\partial^+(w, x, Q_n)|,$$

which follows from the proof in the continuous setting: since

$$|\partial^+(w, Q_n)| = |\cup_{x \in Q_n} \partial^+(w, x)|,$$

it suffices to show that

$$S = \{p \in \mathbb{R}^d : \text{there exists } x, y \in Q_n, x \neq y \text{ and } p \in \partial^+(w, x) \cap \partial^+(w, y)\}$$

has measure zero. Denote the discrete Legendre transform $w^* : \mathbb{R}^d \rightarrow \mathbb{R}$ by $w^*(p) := \min_{x \in \bar{Q}_n} (x \cdot p - w(x))$. This is a concave, finite function as Q_n is bounded and it is a minimum of affine functions. Further, if $p \in \partial^+(w, x)$, then $w^*(p) = x \cdot p - w(x)$. Hence, if $p \in S$ then $w^*(p) = x_1 \cdot p - w(x_1) = x_2 \cdot p - w(x_2)$ for $x_1 \neq x_2$. This implies that $w^*(p)$ is not differentiable at p . But, since w^* is concave it is differentiable almost everywhere, which implies S has measure zero since it is a subset of a measure zero set. This completes the proof of Step 1.

Step 2

We now show that

$$|\partial^+(w, Q_n)| = |\partial^+(\Gamma_w, Q_n)| = \sum_{\{x : \Gamma_w(x) = w(x)\}} |\partial^+(\Gamma_w, x, Q_n)|.$$

First consider $p \in \partial^+(w, x)$ and the affine function $L(y) = w(x) + p \cdot (y - x)$ for $y \in Q_n$. By definition of the concave envelope, for any $y \in Q_n$,

$$\Gamma_w(x) + p \cdot (y - x) \geq w(x) + p \cdot (y - x) = L(y) \geq \Gamma_w(y),$$

and so $p \in \partial^+(\Gamma_w, Q_n)$.

Next, take $p \in \partial^+(\Gamma_w, x)$ for $x \in Q_n$ and use Proposition 2.5.1 to express

$$\Gamma_w(x) = \sum_{i=1}^k \lambda_i w(x_i),$$

for $\lambda_i > 0$, $x_i \in \bar{Q}_n$, and some $k \geq 1$. This implies that $p \in \partial^+(\Gamma_w, x_i)$ for some $x_i \in \bar{Q}_n$. If $k = 1$ and $x_i = x \in Q_n$, we are done as $\Gamma_w(x_i) = w(x_i)$, so suppose not. Then, we can find some $x_i \neq x$ and $p \in \partial^+(\Gamma_w, x) \cap \partial^+(\Gamma_w, x_i)$. However, the argument in Step 1 implies that such p have measure zero. This also implies the third equality.

□

The arithmetic-geometric mean inequality and the lower bound on the Laplacian of sub-solutions imply an upper bound on μ .

Lemma 2.5.4. *There is $C := C_{\eta_{\max}, l, M, d}$ and $C^* := C_{\eta_{\min}, l, M, d}^*$ for which*

$$\mu(Q_n, \eta, l, M) < C|Q_n|,$$

$$\mu^*(Q_n, \eta, l, M) < C^*|Q_n|.$$

For $l \leq -\eta_{\max} - \text{Tr}(M)$

$$\mu(Q_n, \eta, l, M) = 0$$

and for $l \geq (2d - 1) - \eta_{\min} - \text{Tr}(M)$

$$\mu^*(Q_n, \eta, l, M) = 0.$$

Proof. Let $w := u - q_l - q_M \in S(A, \eta, l, M)$. Since u is legal, $\Delta_{\mathbb{Z}^d} u \geq \min(-\eta_{\max}, 0)$ in Q_n . Using $\Delta_{\mathbb{Z}^d} q_M = \text{Tr}(M)$, we get $\Delta_{\mathbb{Z}^d} w \geq -l - \text{Tr}(M) - \eta_{\max}$.

Choose $x \in Q_n$ so that $|\partial^+(w, x)| > 0$. As the supergradient set is preserved under affine transformations, we may suppose $w(x) = 0$ and $0 \in \partial^+(w, x)$. This implies $w(y) \leq 0$ for all

$y \in \bar{A}$. Then, by definition, for $p \in \partial^+(w, x)$,

$$p \cdot (x + e_i - x) \geq w(x + e_i),$$

and

$$p \cdot (x - e_i - x) \geq w(x - e_i).$$

Putting these two inequalities together, we get for each direction $i = 1, \dots, d$,

$$w(x + e_i) \leq p_i \leq -w(x - e_i). \quad (2.12)$$

And so,

$$|\partial^+(w, x)| \leq \prod_{i=1}^d (-w(x - e_i) - w(x + e_i)) = \prod_{i=1}^d (-\Delta_i w).$$

Our affine transformation of w ensures that $-\Delta_i w \geq 0$, and so an application of the arithmetic geometric mean inequality yields

$$-\Delta_{\mathbb{Z}^d} w = \sum_{i=1}^d (-\Delta_i w) \geq d \left(\prod_{i=1}^d (-\Delta_i w) \right)^{1/d}.$$

And so

$$|\partial^+(w, x)| \leq d^{-d} (-\Delta_{\mathbb{Z}^d} w)^d \leq d^{-d} (\eta_{\max} + \text{Tr}(M) + l)^d, \quad (2.13)$$

which implies the claim by Lemma 2.5.3. The other direction is similar. □

We state the following consequence of the discrete Harnack inequality Lawler and Limic [2010] which we will later use to regulate the growth of the concave envelope in balls around contact points.

Proposition 2.5.2 (Lemma 2.17 in Levine and Peres [2010]). *Fix $0 < \beta < 1$. For any*

$f : \mathbb{Z}^d \rightarrow \mathbb{R}$ nonnegative, with $f(0) = 0$ and $|\Delta_{\mathbb{Z}^d} f| \leq \lambda$ in B_R there is a constant $C_{\beta, \lambda}$ so that

$$f(x) \leq C_{\beta, \lambda} |x|^2 \quad (2.14)$$

for $x \in B_{\beta R}$.

2.5.4 Convergence of the monotone quantity

We next use the multiparameter subadditive ergodic theorem of Akcoglu and Krengel [1981] as modified by Dal Maso and Modica [1985] to show almost sure convergence of μ . For the reader's convenience, we restate the theorem, following the exposition in Armstrong and Smart [2014b].

Let \mathcal{U}_0 be the family of bounded subsets of \mathbb{Z}^d and \mathcal{L} the set of bounded Lipschitz domains in \mathbb{R}^d . A function $f : \mathcal{U}_0 \rightarrow \mathbb{R}$ is *subadditive* if

$$f(A) \leq \sum_{j=1}^k f(A_j),$$

whenever $k \in \mathbb{N}$ and $A, A_1, \dots, A_k \in \mathcal{U}_0$ are such that A_1, \dots, A_k are pairwise disjoint and $A = \cup_{j=1}^k A_j$. For a fixed constant C , let \mathcal{M}_C be the collection of subadditive functions $f : \mathcal{U}_0 \rightarrow \mathbb{R}$ which satisfy

$$0 \leq f(A) \leq C|A| \quad \text{for every } A \in \mathcal{U}_0.$$

A *subadditive process* is a function $f : \Omega \rightarrow \mathcal{M}_C$. Overload notation and write $f(A, \eta) = f(\eta)(A)$ for $A \in \mathcal{U}_0$ and $\eta \in \Omega$. Recall that we have assumed the probability measure is stationary and ergodic.

Proposition 2.5.3 (Multiparameter subadditive ergodic theorem). *Let $f : \Omega \rightarrow \mathcal{M}_C$ be a subadditive process. There exists an event Ω_0 of full probability and a constant $0 \leq a \leq C$*

so that for every $\eta \in \Omega_0$ and $W \in \mathcal{L}$,

$$\lim_{n \rightarrow \infty} \frac{f(nW \cap \mathbb{Z}^d, \eta)}{|nW \cap \mathbb{Z}^d|} = a. \quad (2.15)$$

The next lemma is an easy consequence.

Lemma 2.5.5. *For each $M \in \mathbf{S}^d$ and $l \in \mathbb{R}$, there exists an event, $\Omega_{l,M}$, of full probability so that for every $\eta \in \Omega_{l,M}$ and $W \in \mathcal{L}$,*

$$\mu(l, M) := \lim_{n \rightarrow \infty} \frac{\mu(nW \cap \mathbb{Z}^d, \eta, l, M)}{|nW \cap \mathbb{Z}^d|}$$

and

$$\mu^*(l, M) := \lim_{n \rightarrow \infty} \frac{\mu^*(nW \cap \mathbb{Z}^d, \eta, l, M)}{|nW \cap \mathbb{Z}^d|}.$$

Moreover, there exist constants $C := C_{\eta_{\max}, l, M, d}$ and $C^* := C_{\eta_{\min}, l, M, d}^*$ so that

$$0 \leq \mu(l, M) \leq C$$

and

$$0 \leq \mu(l, M)^* \leq C^*.$$

Proof. Fix M and l and let $W_n = nW \cap \mathbb{Z}^d$ for given $W \in \mathcal{L}$. We apply Proposition 2.5.3 to

$$f(W_n, \eta) = \sup\{| \partial^+(w, W_n) | : w \in S(W_n, \eta, l, M)\}.$$

Let $\Omega_{l,M}$ be given by Proposition 2.5.3 and take $\eta \in \Omega_{l,M}$. By Lemma 2.5.4, $0 \leq f(W_n, \eta) \leq C|W_n|$. It remains to check subadditivity for subsets of \mathbb{Z}^d . Let $A \in \mathcal{U}_0$ and let A_1, \dots, A_k be pairwise disjoint subsets of A which satisfy $\cup_{j=1}^k A_j = A$.

Let u be a locally legal toppling function for η in A . For each A_i , we can decompose u into illegal topplings on ∂A_i followed by locally legal topplings in A_i . Hence $u - q_l - q_M \in$

$S(A_i, \eta, l, M)$ for all A_i . Moreover, the definition of supergradient shows that for each $x \in A$ there is an A_i so that

$$\partial^+(u - q_l - q_M, x, A) \subset \partial^+(u - q_l - q_M, x, A_i),$$

hence by Lemma 2.5.3 and disjointness of the A_i ,

$$\begin{aligned} |\partial^+(u - q_l - q_M, A)| &= \sum_{x \in A} |\partial^+(u - q_l - q_M, x, A)| \\ &\leq \sum_{i=1}^k \sum_{x \in A_i} |\partial^+(u - q_l - q_M, A_i, x)| \\ &= \sum_{i=1}^k |\partial^+(u - q_l - q_M, A_i)|. \end{aligned}$$

Since this holds for any locally legal toppling of η in A , taking the supremum of both sides implies that

$$f(A, \eta) \leq \sum_{i=1}^k f(A_i, \eta),$$

which completes the proof. The exact same argument, using the fact that any stabilizing toppling for A is also stabilizing in A_i , shows convergence of μ^* . \square

In light of Proposition 2.5.2, if both $\mu(l, M)$ and $\mu^*(l, M)$ are 0, we have a comparison principle in the limit. This will allow us to identify the effective equation; and hence is what we carry out in the next section.

2.6 The effective equation

2.6.1 Finding the effective equation

We will identify, for each parabola M , the largest real number l_M , so that in the limit $\mu(l_M, M) = \mu^*(l_M, M) = 0$. This then defines the effective equation \bar{F}_η . To show that such a number exists, since μ is bounded, it suffices to show that μ is Lipschitz continuous in the limit. In the continuum, this is done with an argument that utilizes a certain regularity of concave envelopes of subsolutions which we do not have. This difficulty is circumvented by a consequence of the stationarity of η , Lemma 2.6.2. We first prove the easier direction of continuity, monotonicity of the curvature.

Lemma 2.6.1. *For $s \geq 0$,*

$$\mu(B_n, \eta, l + s, M) \geq \mu(B_n, \eta, l, M).$$

and

$$\mu^*(B_n, \eta, l - s, M) \geq \mu^*(B_n, \eta, l, M).$$

Proof. Let $w \in S(B_n, \eta, l, M)$. By Lemma 2.5.3, it suffices to show

$$|\partial^+(w, x, B_n)| \leq |\partial^+(w - q_s, x, B_n)|,$$

for each $x \in B_n$. Choose $p \in \partial^+(w, x)$, if this is not possible, we are done. Then, for each

$$y \in \bar{B}_n,$$

$$\begin{aligned} w(x) + (p - sx) \cdot (y - x) + \frac{1}{2}s(|y|^2 - |x|^2) &= w(x) + p \cdot (y - x) - sxy \\ &\quad + s|x|^2 + \frac{1}{2}s|y|^2 - \frac{1}{2}s|x|^2 \\ &\geq w(y) + \frac{1}{2}s|x - y|^2 \\ &\geq w(y). \end{aligned}$$

And so rearranging, we get

$$w(x) - q_s(x) + (p - sx) \cdot (y - x) \geq w(y) - q_s(y),$$

meaning $p - sx \in \partial^+(w - q_s, x, B_n)$. Since this holds for all $p \in \partial^+(w, x, B_n)$, this implies

$$|\partial^+(w, x, B_n)| \leq |\partial^+(w - q_s, x, B_n)|.$$

The proof for μ^* is identical. \square

In the next lemma, we show that if μ is strictly positive in the limit, then a subsolution must curve downwards in every direction.

Lemma 2.6.2. *Suppose that $\alpha := \mu(l_M, M) > 0$. There exists a constant*

$$C := C_{\eta_{\min}, \eta_{\max}, l, M, d}$$

so that for each η in a set $\Omega_{l, M}$ of full probability and $0 < \beta < 1$ the following holds. There is an $n_0 \in \mathbb{N}$ so that for all $n \geq n_0$, there exists $w_n \in S(B_n, \eta, l, M)$ so that for each $x_0 \in \{\Gamma_{w_n} = w_n\} \cap B_{\beta n}$ and $p_0 \in \partial^+(w_n, x_0, B_n)$

$$w_n(y) \leq w_n(x_0) + p_0 \cdot (y - x) - C\alpha n^2$$

for all $y \in \partial B_n$. An analogous result holds for μ^* with a sign change.

Proof. As $\alpha > 0$, by Lemma 2.5.5, we can choose a set of full probability $\Omega_{l,M}$, so that for every $\eta \in \Omega_{l,M}$ there exists n_0 so that for all $n \geq n_0$, there is $w_n \in S(B_n, \eta, l, M)$ with

$$\frac{\alpha}{2} \leq \frac{|\partial^+(\Gamma_{w_n}, B_{\beta n})|}{|B_{\beta n}|} \leq \frac{\mu(B_n, l, M)}{|B_n|} \leq 2\alpha \quad (2.16)$$

In light of Lemma 2.5.1, we can assume

$$w_n \in S(B_n, \eta, l, M) \cap S^*(B_n, \eta, l, M).$$

As $|\partial^+(w_n, B_{\beta n})| > 0$, we can find $x_0 \in B_{\beta n}$ with $w_n(x_0) = \Gamma_{w_n}(x_0)$ and $|\partial^+(w_n, x_0)| > 0$. Take $p_0 \in \partial^+(w_n, x_0)$. By a translation and affine transformation, we can suppose $\Gamma_{w_n}(x_0) = 0$, $p_0 = 0$, and $x_0 = 0$. Take $1 > \delta > \beta$. By rescaling and subadditivity, it suffices to show

$$\Gamma_{w_n}(y) \leq -\alpha Cn^2 \quad (2.17)$$

for $y \in \partial B_{\delta n}$. Let $\bar{\phi}_n : B_\delta \rightarrow \mathbb{R}$ be a scaling of the interior of the concave envelope,

$$\bar{\phi}_n := \frac{1}{n^2} \Gamma_{w_n}([nx]), \text{ for } x \in B_\delta.$$

As $w_n \in S(B_n, \eta, l, M) \cap S^*(B_n, \eta, l, M)$, we have $|\Delta_{\mathbb{Z}^d} w_n| \leq C$. Hence, by Proposition 2.5.2 and the definition of Γ_{w_n} , $0 \geq \bar{\phi}_n \geq -C$.

Moreover, as the ball is strictly convex, $\bar{\phi}_n$ is uniformly Lipschitz in B_δ and hence contains a subsequence which converges uniformly to a concave, continuous function $\bar{\phi}$ (Lemma 1.6.1 in Gutiérrez [2016]). By taking a further subsequence, $\bar{w}_n := \frac{1}{n^2} w_n([nx])$ also converges uniformly to a limit \bar{w} . As $\bar{\phi}$ is the concave envelope of \bar{w} , it is differentiable with Lipschitz gradient and $|D^2 \bar{\phi}| \leq C$ almost everywhere (Lemma 3.3 and Lemma 3.5 in Roberts et al. [1995]). By Lemma 2.5.5 and weak convergence of Monge-Ampère measures (Lemma 1.6.1

in Gutiérrez [2016]) the subsequential limit, $\bar{\phi}$, must solve a Monge-Ampère equation with constant right-hand side $-\alpha$. Hence, $\det D^2\bar{\phi} = -\alpha$ and in turn $D^2\bar{\phi} \leq -C\alpha$ almost everywhere. Taking n_0 larger if necessary and undoing the scaling, we have (2.17). \square

We next use Lemma 2.6.2 to show Lipschitz continuity of μ .

Lemma 2.6.3. *There is a constant $C_{\eta_{\min}, \eta_{\max}, l, M, d}$ so that for all $0 < s < 1$,*

$$\mu(l, M) \leq \mu(l - s, M) + sC$$

and

$$\mu^*(l, M) \geq \mu^*(l + s, M) + sC.$$

Proof. Let $0 < s < 1$ be given. Take $\beta = (1 - s)$ and let $C, \eta \in \Omega_{l, M}$, and $n \geq n_0$ be given by Lemma 2.6.2. Assume $\mu(l, M) > sC$. We will show that after removing a shell of volume proportional to s , the set of slopes remaining must be in $\partial^+(w_n + q_s, B_n)$ for all w_n close to achieving the supremum in $\mu(B_n, \eta, l, M)$.

By Lemma 2.6.2, there is $w_n \in S(B_n, \eta, l, M)$ so that for every $x \in B_{(1-s)n}$ with $\Gamma_{w_n}(x) = w_n(x)$ and $p \in \partial^+(w_n, x)$

$$w_n(x) + p \cdot (y - x) \geq w_n(y) + q_s C(y), \quad (2.18)$$

for all $y \in \partial B_n$. Hence, the argument in the proof of Lemma 2.5.2 shows that $p \in \partial^+(w_n + q_s C, B_n)$ and since this applies for all such p ,

$$\partial^+(w_n, B_{(1-s)n}) \subseteq \partial^+(w_n + q_s C, B_n)$$

Further, using Lemma 2.5.4,

$$|\partial^+(w_n, B_n \setminus B_{(1-s)n})| \leq sC|B_n|,$$

which completes the proof after taking limits. \square

The above results show Lipschitz continuity of μ for each fixed $l \in \mathbb{R}$. Repeating this for every rational l in the interval specified by Lemma 2.5.4 and using the intermediate value theorem, we can choose the largest $l_M \in \mathbb{R}$ so that in the limit,

$$\mu(l_M, M) = \mu^*(l_M, M),$$

then define the *effective equation* uniquely as

$$\bar{F}_\eta(M) = l_M.$$

2.6.2 Basic properties of the effective equation

Here we show that the effective equation is bounded, degenerate elliptic, and Lipschitz continuous. This together with the fact any legal stabilizing toppling function has bounded Laplacian will be used in Section 2.7.4 to establish a comparison principle for solutions to the effective equation.

Lemma 2.6.4. *For every $M, N \in \mathbf{S}^d$, the following hold.*

1. *Degenerate elliptic:* If $M \leq N$, $\bar{F}_\eta(M) \geq \bar{F}_\eta(N)$.
2. *Lipschitz continuous:* $|\bar{F}_\eta(M) - \bar{F}_\eta(N)| \leq C|M - N|_2$.
3. *Bounded:* $|\bar{F}_\eta(M)| < \infty$.

Proof. We show the first inequality. Suppose $N = M + A$ with $A \geq 0$. The proof of Lemma 2.6.1, using $q_A \geq 0$ in place of $q_s \geq 0$, shows that $\mu(l_M, M + A) \geq \mu(l_M, M)$ and $\mu^*(l_M, M + A) \leq \mu(l_M, M)$. By Lemma 2.6.1, $f(s) := \mu(l_M + s, M + A) - \mu^*(l_M + s, M + A)$, is nondecreasing in s and we have just showed $f(0) \geq 0$. Hence, $l_{M+A} \leq l_M$ and so $\bar{F}_\eta(M + A) \leq \bar{F}_\eta(M)$.

For the second inequality, first rewrite,

$$\mu(l_M, M) = \mu(l_M, N + (M - N)) = \mu(l_M - |M - N|_2, N + (M - N) + |M - N|_2 I),$$

then observe that $(M - N) + |M - N|_2 I \geq 0$. Hence, by the argument in the first paragraph, $\mu(l_M, M) \geq \mu(l_M - |M - N|_2, N)$ and so

$$\mu^*(l_M - |M - N|_2, N) \geq \mu^*(l_M, M) = \mu(l_M, M) \geq \mu(l_M - |M - N|_2, N).$$

and hence

$$\bar{F}_\eta(N) \geq \bar{F}_\eta(M) - |M - N|_2.$$

Swapping the roles of M and N then show

$$|\bar{F}_\eta(M) - \bar{F}_\eta(N)| \leq |M - N|_2.$$

The third claim follows by construction and Lemma 2.5.4.

□

2.7 Proof of convergence

For each $n \in \mathbb{N}$, recall that

$$v_n = \min\{v : \mathbb{Z}^d \rightarrow \mathbb{N} : \Delta_{\mathbb{Z}^d} v_n + \eta I(\cdot \in W_n) \leq 2d - 1\},$$

is the odometer function for η on W_n with the *free* boundary condition and $\bar{v}_n = n^{-2}v_n([nx])$ is its rescaled linear interpolation. We start by showing that \bar{v}_n is equicontinuous and bounded. Then, we show that the high density assumption, $\mathbf{E}(\eta(0)) > 2d - 1$, implies $v_n \geq 1$ in $W_{n-o(n)}$, enabling an essential tool in the proof of Lemma 2.7.5, (Dhar's burning algorithm, Lemma 2.3.3). We then conclude by showing that every scaled subsequence converges to the same limit.

2.7.1 An upper bound on the odometer function

We establish an upper bound on \bar{v}_n by constructing a toppling function which stabilizes η_{\max} and hence η . Since η_{\max} is constant, we can stabilize by toppling ‘one dimension at a time’, a trick from Fey et al. [2010], and restated below for the reader. (Note one could also compare to the divisible sandpile as in Levine and Peres [2009] to get a tighter bound).

Lemma 2.7.1 (Lemma 3.3 in Fey et al. [2010]). *Let $\ell \in \mathbb{N}$ be given. Pick $k \in \mathbb{N}$ so that $R_k := \eta_{\max} - (2d - k) = 2r$ for some $r \in \mathbb{N}$. Then, there exists $g : \mathbb{Z} \rightarrow \mathbb{N}$ so that*

$$\Delta_{\mathbb{Z}^d} g = f,$$

where $f : \mathbb{Z} \rightarrow \mathbb{Z}$ is given by

$$f(x) = \begin{cases} -R_k & \text{for } |x| \leq \ell \\ 2 & \text{for } \ell < |x| \leq \ell(r+1) \\ 1 & \text{for } \ell(r+1) < |x| \leq \ell(r+1) + r \\ 0 & \text{for } \ell(r+1) + r < |x| \end{cases}$$

Moreover, g is supported in $I = \{x \in \mathbb{Z} : |x| < \ell(r+1) + r\}$ and there exists $C := C_r$ for

which

$$g(x) \leq Cx^2. \quad (2.19)$$

We use this technique together with the universal bound on the Laplacian to show compactness of \bar{v}_n .

Lemma 2.7.2. *For every subsequence $n_k \rightarrow \infty$ there is a subsequence n_{k_j} and a function $\bar{v} \in C(\mathbb{R}^d)$ so that $\bar{v}_{n_{k_j}} \rightarrow \bar{v}$ uniformly as $j \rightarrow \infty$.*

Proof. Cover W_n with a box of side length $C_{d,W}n$ for some $C_{d,W} \in \mathbb{N}$. Choose g from Lemma 2.7.1 with $\ell = C_{d,W}n$ and for $x = (x_1, \dots, x_d) \in \mathbb{Z}^d$, define

$$u_i(x) = g(x_i),$$

and observe that by definition of g , $\Delta_{\mathbb{Z}^d} u_i + \eta_{\max} \leq 2d - 1$. Hence, by the least action principle, as $\min(u_1, \dots, u_d)$ is also stabilizing,

$$v_n(x) \leq \min(u_1(x), \dots, u_d(x)) \leq C_d|x|^2.$$

Hence, $\bar{v}_n \leq C_d$ and is supported in $Q_{C_{d,W}}$. We have equicontinuity since $|\Delta_{\mathbb{Z}^d} v_n| \leq C_{d,\eta_{\min},\eta_{\max}}$ (Kuo and Trudinger [2005]). The Arzela-Ascoli theorem now implies the claim. \square

2.7.2 A lower bound on the odometer function

In this subsection, we use a comparison principle argument to show that on an event of probability 1, $v_n \geq 1$ in $W_{n-o(n)}$. As a corollary, this argument gives a quantitative proof of the (now classical) fact that if $\mathbf{E}(\eta(0)) > 2d - 1$ then η is almost surely *exploding*, (see Fey et al. [2009]). The technique takes inspiration from Theorem 4.1 in Levine and Peres [2009]. In essence, the proof is a comparison of v_n with the odometer function for the random

divisible sandpile with threshold $2d - 1$. See Section 2.8 for more on the random divisible sandpile, including a proof of convergence which uses Lemma 2.7.3.

We start by briefly recalling the Green's function for simple random walk on \mathbb{Z}^d stopped when exiting the ball . Let $S_n^{(x)}$ be simple random walk started at a site x in \mathbb{Z}^d and let $\tau_n = \min\{t \geq 0 : S_t \notin B_n\}$. Let

$$g_n(x, y) = \frac{1}{2d} \mathbf{E} \sum_{n=0}^{\tau_n-1} \mathbf{1}\{S_n^{(x)} = y\},$$

Fix $\delta > 0$ and $x \in B_n$. From Lawler and Limic [2010], we have the following exit time estimates,

$$\begin{aligned} \sum_{y \in B_n} g_n(x, y) &= O(n^2) \\ \sum_{z \in B_{\delta n}} g_n(x, x + z) &= \delta O(n^2) \end{aligned} \tag{2.20}$$

and the following difference estimates, for $\max(|x|, |y|) < (1 - \delta)n^2$,

$$|g_n(x, y) - g_n(x, y + e_i)| = O(|x - y|^{1-d}) + O_\delta(n^{2-2d}). \tag{2.21}$$

Next, define for each n

$$r_n(x) := \sum_{y \in B_n} g_n(x, y) \eta(y),$$

$$d_n(x) := \sum_{y \in B_n} g_n(x, y) \mathbf{E}(\eta(0)).$$

so that $\Delta r_n(x) = -\eta(x)$, $\Delta d_n(x) = -\mathbf{E}(\eta(0))$, and $r_n(y) = d_n(y) = 0$ on ∂B_n . The next lemma uses these estimates together with the ergodic theorem to show that r_n and d_n are identical in the scaling limit.

Lemma 2.7.3. *For each $\eta \in \tilde{\Omega}_0$, an event of probability 1, there is a constant $C := C_{d, \eta}$ so*

that the following holds. For each $\epsilon > 0$, there exists $n_0 \in \mathbb{N}$ so that for all $n \geq n_0$,

$$\sup_{x \in B_n} |r_n(x) - d_n(x)| \leq \epsilon Cn^2 \quad (2.22)$$

Proof. Let $1 > \epsilon > 0$ be given. Fix dyadic rational $\epsilon > \beta > 0$ small. By Proposition 2.5.5 there is an event of full probability, $\tilde{\Omega}_0$, so that for each $\eta \in \tilde{\Omega}_0$, for all $n \geq n_0$,

$$(\mathbf{E}(\eta(0)) - \epsilon) \leq \frac{1}{|A_{\beta n}(z_i)|} \sum_{y \in A_{\beta n}(z)} \eta(y) \leq (\mathbf{E}(\eta(0)) + \epsilon), \quad (2.23)$$

for all $A_{\beta n}(z_i) \subset B_n$ which are defined in the following way. Take a dyadic partition of disjoint cubes of radius β which cover Q_1 in \mathbb{R}^d , remove cubes which do not overlap B_1 , and delete parts of the cubes which are outside B_1 . Label each cube by an interior point $z_i \in B_n$ and enumerate them as $\{A_\beta(z_i)\}$. For each z_i , let its finite difference approximation be $A_{\beta n}(z_i) = nA_\beta(z_i) \cap B_n$ (delete overlapping boundaries if needed).

Rewrite,

$$r_n(x) - d_n(x) = \sum_{A_{\beta n}(z_i) \subset B_n} \sum_{y \in A_{\beta n}(z_i)} g_n(x, y)(\eta(y) - \mathbf{E}(\eta(0))). \quad (2.24)$$

The rest of the argument is roughly the following. Imagine a non-random sandpile, η_{avg} , in which $\eta_{avg} := \mathbf{E}(\eta(0))$ divisible grains are at each coordinate in B_n . In each subcube, $A_{\beta n}(z_i) \subset B_n$, we try to rearrange the grains in the random sandpile, η , to match the deterministic sandpile η_{avg} . It's possible that there aren't enough grains to do this, so we add just enough for it to match η_{avg} . By (2.23), we need to add at most $\epsilon|A_{\beta n}(z_i)|$ grains to each subcube. Hence, by the exit time estimate, the total cost associated with adding grains is of order $\epsilon O(n^2)$, by the difference estimate, the total cost of rearranging grains within each subcube is of order $o(n^2)$, leading to (2.22).

Here are the details. If $x \in B_n \setminus B_{(1-\beta)n}$, by comparing to a quadratic, $\max(r_n, d_n)(x) \leq$

$C\beta n^2$. Hence, we may suppose $x \in B_{(1-\beta)n}$. First, we add ϵ grains to every site in the cube, this incurs an error which we can bound using (2.20),

$$\mathcal{E}_1(x) = \sum_{y \in B_n} \epsilon g_n(x, y) \leq \epsilon C_d n^2. \quad (2.25)$$

Then, we start rearranging. First, we remove a constant number of cubes near x ,

$$\mathcal{A}_x = \{A_{\beta n}(z_i) : \inf_{y \in A_{\beta n}(z_i)} |y - x| < \beta n\}, \quad (2.26)$$

by adding $\eta_{avg} - \eta_{min}$ grains to each site in the subcubes,

$$\mathcal{E}_2(x) = \sum_{A_{\beta n}(z_i) \in \mathcal{A}_x} \sum_{y \in A_{\beta n}(z_i)} (\eta_{avg} - \eta_{min}) g_n(x, y) \leq C\beta n^2, \quad (2.27)$$

using (2.20).

Now, we rearrange the random assortment of grains in all other subcubes $A_{\beta n}(z_i)$ so that the number of grains at every site is η_{avg} . We start by pooling every grain at sites $y \in A_{\beta n}(z_i)$ to z_i , this incurs an error of

$$\mathcal{E}_3(x, y) = (\eta(x) + \epsilon)(g_n(x, y) - g_n(x, z_i)). \quad (2.28)$$

Then, we move η_{avg} grains from z_i back to y , with error

$$\mathcal{E}_4(x, y) = \eta_{avg}(g_n(x, z_i) - g_n(x, y)). \quad (2.29)$$

We can iterate (2.21) to see that

$$\sup_{x, y} |\max(\mathcal{E}_3(x, y), \mathcal{E}_4(x, y))| \leq C_d \beta n \sup_{z \in A_{\beta n}(z_i)} |x - z|^{1-d}, \quad (2.30)$$

And, by an integral approximation,

$$C_d \beta n \sum_{z_i \notin \mathcal{A}_x} \sup_{z \in A_{\beta n}(z_i)} |x - z|^{1-d} \leq C_d \beta^{-1} n = o(n^2). \quad (2.31)$$

For each $y \in B_n$, write,

$$\begin{aligned} g_n(x, y)\eta(y) &= -g_n(x, y)\epsilon \\ &\quad + (\eta(y) + \epsilon)(g_n(x, y) - g_n(x, z_i)) \\ &\quad + (\eta(y) + \epsilon)g_n(x, z_i) \\ &\quad + \eta_{avg}(g_n(x, z_i) - g_n(x, y)) \\ &\quad - \eta_{avg}(g_n(x, z_i) - g_n(x, y)). \end{aligned}$$

Putting this together,

$$\begin{aligned} &\sum_{A_{\beta n}(z_i) \subset B_n} \sum_{y \in A_{\beta n}(z_i)} g_n(x, y)\eta(y) \\ &\geq \sum_{A_{\beta n}(z_i) \subset B_n} \sum_{y \in A_{\beta n}(z_i)} g_n(x, y)\eta_{avg} \\ &\quad + (-\epsilon C n^2) \\ &\quad + \sum_{\{A_{\beta n}(z_i) \subset B_n\} \setminus \mathcal{A}_x} g_n(x, z_i) \left(\sum_{y \in A_{\beta n}(z_i)} (\eta(y) + \epsilon - \eta_{avg}) \right) \\ &\geq -\epsilon C n^2 + \sum_{A_{\beta n}(z_i) \subset B_n} \sum_{y \in A_{\beta n}(z_i)} g_n(x, y)\eta_{avg} \end{aligned}$$

Where we used the fact $\inf_{\{x, y\} \in B_n} g_n(x, y) \geq 0$. The other direction follows by swapping the roles of η and η_{avg} .

□

We next use this to provide the desired lower bound on v_n .

Lemma 2.7.4. *For each $\eta \in \tilde{\Omega}_0$, an event of probability 1, and each $\epsilon > 0$, there exists n_0 so that for all $n \geq n_0$,*

$$w_n \geq 1 \text{ for all } x \in B_{(1-\epsilon)n},$$

where

$$w_n \in \mathcal{L}(\eta, B_n) \cap \mathcal{S}(\eta, B_n) \text{ and } w_n = 0 \text{ on } \partial B_n.$$

Proof. Let $\epsilon > 0$ be given and

$$\delta := (\mathbf{E}(\eta(0)) - 2d - 1) > 0.$$

Choose $\eta \in \tilde{\Omega}_0$, C , and $n \geq n_0$ from Lemma 2.7.3 with $\epsilon' > 0$ small to be chosen below. As $w_n - r_n - q_{2d-1}$ is superharmonic in B_n , for $x \in B_n$,

$$\begin{aligned} w_n(x) - r_n(x) - q_{2d-1}(x) &\geq \min_{y \in \partial B_n} (w_n(y) - r_n(y) - q_{2d-1}(y)) \\ &= \min_{y \in \partial B_n} -q_{2d-1}(y), \end{aligned}$$

using $w_n = r_n = 0$ on ∂B_n . Hence, Lemma 2.7.3 then shows

$$w_n(x) \geq d_n(x) - (2d - 1) \frac{1}{2} (n^2 - |x|^2) - \epsilon' C n^2$$

By assumption, $d_n + q_{2d-1+\delta}$ is superharmonic in B_n and so

$$d_n(x) + q_{2d-1+\delta}(x) \geq \min_{y \in \partial B_n} (d_n(y) + q_{2d-1+\delta}(y)).$$

Using again $d_n(y) = 0$ on ∂B_n ,

$$w_n(x) \geq \delta/2(n^2 - |x|^2) - \epsilon' Cn^2.$$

In particular, we can choose ϵ' small and n_0 large so that

$$w_n(x) \geq 1$$

for $x \in B_{(1-\epsilon)n}$. □

2.7.3 A comparison principle in the limit

In order to compare subsequential limits of the odometer for different η we must show that $\mu(l_M, M) = \mu^*(l_M, M) = 0$. The argument is roughly this: if both μ and μ^* are strictly positive in the limit, then there is a subsolution and supersolution whose difference bends upwards in every direction. However, when there are enough topples, this difference obeys a comparison principle on the microscopic scale, due to Proposition 2.3.3, and so this cannot happen.

Lemma 2.7.5. $\mu(l_M, M) = \mu^*(l_M, M) = 0$

Proof. By definition, $\mu(l_M, M) = \mu^*(l_M, M) \geq 0$. We will show that it is impossible for both $\mu(l_M, M)$ and $\mu^*(l_M, M)$ to be strictly positive. Suppose for sake of contradiction that $\mu(l_M, M) = \mu^*(l_M, M) = \alpha > 0$.

As $\alpha > 0$ we can invoke Lemma 2.6.2 for both μ and μ^* . Take $0 < \beta < 1$ small. Using the fact μ converges evenly over the unit ball, (see Lemma 3.2 in Armstrong and Smart [2014c]), we may select $v, u \in \mathcal{L}(B_n, \eta) \cap \mathcal{S}(B_n, \eta)$ with $|\partial^-(v, B_{\beta n}, B_n)| > 0$ and $|\partial^+(u, B_{\beta n}, B_n)| > 0$ for which the claims in Lemma 2.6.2 apply. (Note we used Lemma 2.5.1 to pick locally legal *and* stabilizing toppling functions.)

Moreover, as μ and μ^* are invariant under affine transformations, we can then choose affine functions L_u and L_v so that

$$\inf_{x \in B_n} -(u - q_M + L_u)(x) = (u - q_M + L_u)(x_0) = 0 \quad (2.32)$$

$$\inf_{x \in B_n} (v - q_M + L_v)(x) = (v - q_M + L_v)(x_0^*) = 0,$$

for some $x_0, x_0^* \in B_{\beta n}$ and

$$-(u - q_M + L_u) \geq Cn^2 \text{ on } \partial B_n \quad (2.33)$$

$$(v - q_M + L_v) \geq Cn^2 \text{ on } \partial B_n.$$

Now, use the Abelian property, Proposition 2.3.2, to decompose u and v into the initial toppling of η and then topplings originating from the boundary, $u = u_1 + w$ and $v = v_1 + w$. By Lemma 2.7.4 and Proposition 2.3.4, (moving the boundary of the ball inwards if necessary and accumulating an $o(n^2)$ error), $\Delta_{\mathbb{Z}^d} w + \eta$ is recurrent in B_n . Now, approximate $L_v(x) = p \cdot x + r$ by

$$\tilde{L}_v(x) = [p] \cdot x + [r],$$

an integer-valued function, (this approximation also incurs an $o(n^2)$ error). Repeat for L_u with \tilde{L}_u . Hence, by Proposition 2.3.3 and (2.33)

$$\begin{aligned} & \left((v + \tilde{L}_v - q_M) - (u + \tilde{L}_u - q_M) \right) (0) \\ &= \left((v_1 + \tilde{L}_v) - (u_1 + \tilde{L}_u) \right) (0) \\ &\geq \inf_{y \in \partial B_n} \left((v_1 + \tilde{L}_v) - (u_1 + \tilde{L}_u) \right) (y) \\ &= \inf_{y \in \partial B_n} ((v + L_v - q_M) - (u + L_u - q_M)) (y) - o(n^2) \\ &\geq Cn^2. \end{aligned}$$

However, this contradicts the Harnack inequality for n large and β small. Indeed, due to (2.32) and

$$\max(|\Delta_{\mathbb{Z}^d}(v - q_M + L_v)|, |\Delta_{\mathbb{Z}^d}(u - q_M + L_u)|) \leq C,$$

we can apply the Harnack inequality, Lemma 2.5.2, to see

$$((v + L_v - q_M) - (u + L_u - q_M))(0) \leq C\beta n^2 \quad (2.34)$$

as $x_0, x_0^* \in B_{\beta n}$.

□

2.7.4 Convergence

Choose Ω_0 to be the intersection of $\Omega_{l,M}$ in Lemma 2.5.5 over all $l \in \mathbb{R}$ and $M \in \mathbf{S}^d$ with rational entries and $\tilde{\Omega}_0$ from Lemma 2.7.4. Pick $\eta, \eta' \in \Omega_0$ and choose subsequences of scaled odometers \bar{v}_n and \bar{v}'_n corresponding to η and η' with *free boundaries* which converge uniformly to v and v' . Suppose for sake of contradiction that $v \neq v'$. Since $v = v' = 0$ outside B_R for some $R > 0$, we may assume without loss of generality that

$$\sup_{B_R}(v - v') > 0 = \sup_{\partial B_R}(v - v')$$

We restate for the reader results contained in Pegden and Smart [2013].

Lemma 2.7.6. *Pegden and Smart [2013]*

1. *There exists $a \in \mathbb{R}^d$ either in W or outside the closure of W so that $v(a) > v'(a)$, both v and v' are twice differentiable at a and $D^2(v - v')(a) < -\delta I$ for some $\delta > 0$.*
2. *For each $\epsilon > 0$, if a is outside the closure of W , we may select $u : \mathbb{Z}^d \rightarrow \mathbb{Z}$ such that*

$$\Delta_{\mathbb{Z}^d} u(x) \leq 2d - 1 \text{ and } u(x) \geq \frac{1}{2}x^T(D^2v(a) - \epsilon I)x \text{ for all } x \in \mathbb{Z}^d.$$

3. For each $\epsilon > 0$, if a is in W , we may select $u : \mathbb{Z}^d \rightarrow \mathbb{Z}$ such that

$$\Delta_{\mathbb{Z}^d} u(x) \leq 2d - 1 \text{ and } u(x) \geq \frac{1}{2}x^T(D^2v(a) - \epsilon I)x + o(|x|^2) \text{ for all } x \in \mathbb{Z}^d.$$

Proof. The first and second statements are Proposition 2.5 and Lemma 4.1 in Pegden and Smart [2013]. We sketch the third. For each $\epsilon > 0$, the proof of Lemma 4.1 in Pegden and Smart [2013] gives a function

$$u : \mathbb{Z}^d \rightarrow \mathbb{Z}$$

with

$$u(x) \geq \frac{1}{2}x^T(D^2v(x_0) - \epsilon I)x.$$

and

$$\Delta_{\mathbb{Z}^d} u + \tilde{\eta} \leq 2d - 1$$

where $\tilde{\eta}$ is a periodic tiling of η in B_{rn} for some $r > 0$ and $n \in \mathbb{N}$ large. Due to Lemma 2.5.5, picking n larger if necessary, we have

$$\frac{1}{B_{rn}} \sum_{x \in B_{rn}} \eta(x) \geq 2d - 1$$

Hence, by Rossin's observation Rossin [2000] (see Fact 3.5 in Levine et al. [2016b]), as a sandpile configuration on \mathbb{Z}^d , $\Delta_{\mathbb{Z}^d} u$ is stabilizable, and so by toppling it, we find a subquadratic, finite $w : \mathbb{Z}^d \rightarrow \mathbb{N}$ so that

$$\Delta_{\mathbb{Z}^d}(u + w) \leq 2d - 1,$$

and $(u + w)(x) = q_{D^2v(a) - \epsilon}(x) + o(|x|^2)$.

□

Now, let $a \in \mathbb{R}^d \setminus \partial W$ be a given point satisfying the properties in part 1 of Lemma 2.7.6. If a is outside the closure of W , the argument in the proof of Theorem 4.2 in Pegden and

Smart [2013] which uses part 2 of Lemma 2.7.6 leads to a contradiction. So, it suffices to suppose $a \in W$. In this case, we cannot use the same argument to compare v and v' as they stabilize (possibly) different random sandpiles. Instead, we use μ to compare the two.

Since v' is twice differentiable at a , by Taylor's theorem,

$$v'(x) = \phi(x) + o(|x - a|^2)$$

where

$$q_M + L_\phi := \phi(x) := v'(a) + Dv'(a) \cdot (x - a) + \frac{1}{2}(x - a)^T D^2 v'(a)(x - a)$$

Pick the unique $l := \bar{F}_\eta(D^2 v'(a)) \in \mathbb{R}$ so that

$$\mu(l, D^2 v'(a)) = \mu^*(l, D^2 v'(a)) = 0.$$

By approximation, (using Lemma 2.6.4), we can assume M and l are rational. Then, by Lemma 2.5.2, (recalling that μ is invariant under affine transformations), for all small $r > 0$ and $n \in \mathbb{N}$ large,

$$\begin{aligned} \inf_{x \in B_{rn}(a)} (v_n - q_M - nL_\phi - q_l)(x) &\geq \inf_{y \in \partial B_{rn}(a)} (v_n - q_M - nL_\phi - q_l)(y) \\ &\quad - C_d n \mu^*(B_{rn}, \eta, 0, M)^{1/d}. \end{aligned}$$

And so, after rescaling,

$$\begin{aligned} \inf_{x \in n^{-1} B_{rn}(a)} (\bar{v}_n - \phi - q_l)(x) &\geq \inf_{y \in \partial n^{-1} B_{rn}(a)} (\bar{v}_n - \phi - q_l)(y) \\ &\quad - \left(\frac{C_d n \mu^*(B_{rn}, \eta, 0, M)^{1/d}}{n^2} \right) \end{aligned}$$

which implies by uniform convergence of $\bar{v}_n \rightarrow v$ and Lemma 2.5.5,

$$\inf_{x \in B_r(a)} (v - \phi - q_l)(x) \geq \inf_{y \in \partial B_r(a)} (v - \phi - q_l)(y).$$

In particular,

$$\begin{aligned} (v - v' - q_l)(a) &= (v - \phi - q_l)(a) \\ &\geq \inf_{y \in \partial B_r(a)} (v - \phi - q_l)(y) \\ &= \inf_{y \in \partial B_r(a)} (v - v' - q_l)(y) - o(r^2) \end{aligned} \tag{2.35}$$

If $l \leq 0$, sending $r \rightarrow 0$ in (2.35) contradicts $D^2(v - v')(a) < -\delta I$. Hence $l > 0$. However, the same argument, applying Lemma 2.5.5 to μ and v' shows,

$$(v' - \phi - q_l)(a) \geq \inf_{y \in \partial B_r(a)} (v' - \phi - q_l)(y)$$

which contradicts Taylor's theorem for r small as v' and q_l are twice differentiable at a .

2.8 Convergence of the random divisible sandpile

One of the challenges involved in the Abelian sandpile model is the integrality constraint on the odometer function. In the *divisible sandpile* model, this constraint is relaxed and sites are allowed to topple a fractional number of times. This relaxation enables the use of simple random walk estimates which leads to a more direct proof of convergence.

2.8.1 Description of the divisible sandpile

We briefly describe the divisible sandpile, referring the interested reader to Levine and Peres [2010], Levine et al. [2016a] for more details. Begin with some, possibly fractional, distribu-

tion of sand and holes, on a domain $V \in \mathbb{Z}^d$, $\eta : V \rightarrow \mathbb{R}$. A site $x \in V$ is unstable whenever $\eta(x) > 1$, in which case the *excess mass*, $1 - \eta(x)$, is equally distributed among the neighbors of x until every site is stable. The odometer function, v , then counts the total mass emitted by each site. Here, the starting point is also a discrete PDE: the *least action principle for the divisible sandpile*.

Proposition 2.8.1 (Proposition 2.5 in Levine et al. [2016a]).

$$v = \min\{f : \bar{V} \rightarrow \mathbb{R}^+ : \Delta_{\mathbb{Z}^d} f + \eta \leq 1\}$$

2.8.2 Convergence of the odometer function

As in Section 2, we consider a stationary, ergodic, probability space $(\Omega, \mathcal{F}, \mathbf{P})$, with Ω the set of all bounded backgrounds,

$$\eta : \mathbb{Z}^d \rightarrow \mathbb{R}$$

for which

$$\sup_{x \in \mathbb{Z}^d} \eta(x) < \infty.$$

In this case, we do not require η to be high density, but we do assume for simplicity uniform boundedness: there exists $\eta_{\min}, \eta_{\max} \in \mathbb{R}$ so that for every $x \in \mathbb{Z}^d$,

$$\mathbf{P} [\eta_{\min} \leq \eta(x) \leq \eta_{\max}] = 1. \quad (2.36)$$

Let $W \subset \mathbb{R}^d$ be a bounded Lipschitz domain. For each $n \in \mathbb{N}$, let $W_n = \mathbb{Z}^d \cap nW$ denote the discrete approximation of W . Initialize the sandpile according to $\eta(x)$ in W_n and let v_n be its odometer function (defined via Proposition 2.8.1). Next, consider the averaged initial sandpile,

$$\eta_{avg} := \mathbf{E} \eta(0),$$

and the corresponding odometer function, v_{avg_n} for η_{avg} in W_n . For the reader's convenience, we restate the form of Lemma 2.7.3 we use. Let $g_n(x, y)$ be the Green's function for simple random walk started at x stopped when exiting W_n , and

$$r_n(x) := \sum_{y \in W_n} g_n(x, y)\eta(y),$$

$$d_n(x) := \sum_{y \in W_n} g_n(x, y)\eta_{avg}.$$

Lemma 2.8.1. *There exists a constant $C := C_d$ so that on an event of full probability, for each $\epsilon > 0$, there exist $n_0 \in \mathbb{N}$ so that for all $n \geq n_0$,*

$$\sup_{x \in W_n} |r_n(x) - d_n(x)| \leq \epsilon C_d n^2 \quad (2.37)$$

Levine and Peres showed in Levine and Peres [2010] that \bar{v}_{avg_n} converges uniformly to the solution of a linear PDE. So, in order to show that \bar{v}_n has a scaling limit, it suffices to show that it stays close to \bar{v}_{avg_n} for all large n . Most of the work for this proof is done in Lemma 2.8.1, all that's left is a use of the least action principle for the divisible sandpile.

Theorem 2.8.2. *On an event of full probability, as $n \rightarrow \infty$, the rescaled functions $\bar{v}_n := n^{-2}v_n([nx])$ and $\bar{v}_{avg_n} := n^{-2}v_{avg_n}([nx])$ converge uniformly together,*

$$\sup_{x \in n^{-1}\bar{W}_n} |\bar{v}_n(x) - \bar{v}_{avg_n}(x)| \rightarrow 0.$$

Proof. By definition,

$$\Delta_{\mathbb{Z}^d} v_n + \eta \leq 1,$$

in W_n , which can be rewritten as

$$\Delta_{\mathbb{Z}^d}(v_n - (r_n - d_n)) + \eta_{avg} \leq 1.$$

Let $\epsilon > 0$ be given. For n large, Lemma 2.8.1 implies $-(r_n - d_n) + \epsilon Cn^2$ is positive in W_n . Hence, by the least action principle in W_n ,

$$v_n - (r_n - d_n) + \epsilon Cn^2 \geq v_{avg_n}$$

and so,

$$v_n - v_{avg_n} \geq (r_n - d_n) - \epsilon Cn^2.$$

Scale and invoke Lemma 2.8.1 again to see that

$$\bar{v}_n - \bar{v}_{avg_n} \geq -\epsilon C.$$

The other direction is identical. □

2.9 Extensions

We conclude with some straightforward extensions of our results.

2.9.1 Sandpiles with open boundaries

The exact same argument given in this chapter also works for sandpiles with the open boundary condition.

Theorem 2.9.1. *Let W be a bounded Lipschitz domain and let v_n be the odometer function for the sandpile $W_n := \mathbb{Z}^d \cap nW$ with the open boundary condition:*

$$v_n \in \mathcal{L}(\eta, W_n) \cap \mathcal{S}(\eta, W_n) \text{ and } v_n = 0 \text{ on } \partial W_n.$$

Almost surely, as $n \rightarrow \infty$, the rescaled functions $\bar{v}_n := n^{-2}v_n([nx])$ converge uniformly to

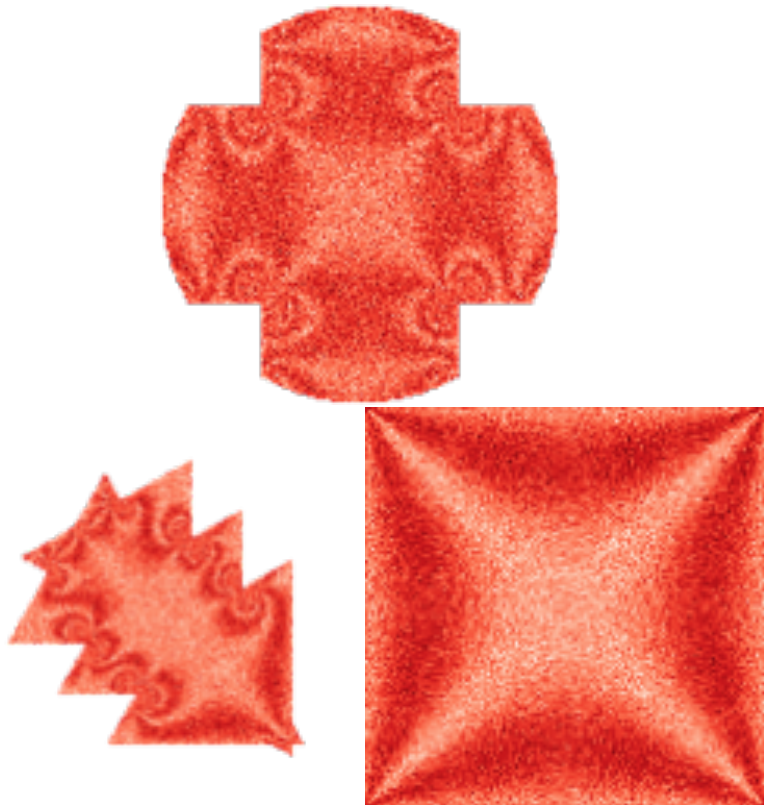


Figure 2.3: Start with an iid Bernoulli(3,5,1/2) sandpile configuration and stabilize with the open boundary condition. Darker reds are closer to 2 while lighter reds are closer to 3. The displays are approximations of the weak-* limits.

the unique viscosity solution $\bar{v} \in C(\mathbb{R}^d)$ of the deterministic equation

$$\begin{cases} \bar{F}_\eta(D^2\bar{v}) = 0 & \text{in } W \\ \bar{v} = 0 & \text{on } \partial W, \end{cases}$$

where \bar{F}_η is a unique degenerate elliptic operator.

Note that \bar{F}_η is the *same* operator appearing in the limit of the free boundary sandpile. For example, if the background is the product Bernoulli measure, simulations reveal interesting pictures. These may help characterize \bar{F}_η - see Figure 2.3.



Figure 2.4: Start with 2^{25} chips at the origin in \mathbb{Z}^2 with an iid Bernoulli(0,-1,1/2) background and stabilize. What's displayed is an approximation of the weak-* limit.

2.9.2 Single-source sandpile on a random background

Straightforward modifications of the arguments appearing above and in Pegden and Smart [2013] show that single-source sandpiles on random backgrounds also have scaling limits. See Figure 2.4 for an example.

Theorem 2.9.2. *Let v_n be the odometer function for the sandpile with n chips at the origin on a stationary, ergodic, random background $\eta_{\min} \leq \eta \leq \eta_{\max} = 2d - 2$,*

$$v_n \in \mathcal{L}(\eta + n\delta_0, \mathbb{Z}^d) \cap \mathcal{S}(\eta + n\delta_0, \mathbb{Z}^d).$$

Almost surely, as $n \rightarrow \infty$, the rescaled functions $\bar{v}_n := n^{-2/d} v_n([n^{1/d} x])$ converge locally uniformly away from the origin to $\bar{v} + G$, where G is the fundamental solution of the Laplacian in \mathbb{R}^d and $\bar{v} \in C(\mathbb{R}^d)$ is the unique viscosity solution of the obstacle problem,

$$\bar{v} := \inf\{\bar{v} \in C(\mathbb{R}^d) | \bar{v} \geq -G \text{ and } \bar{F}_\eta(D^2(\bar{v} + G)) \leq 0\}.$$

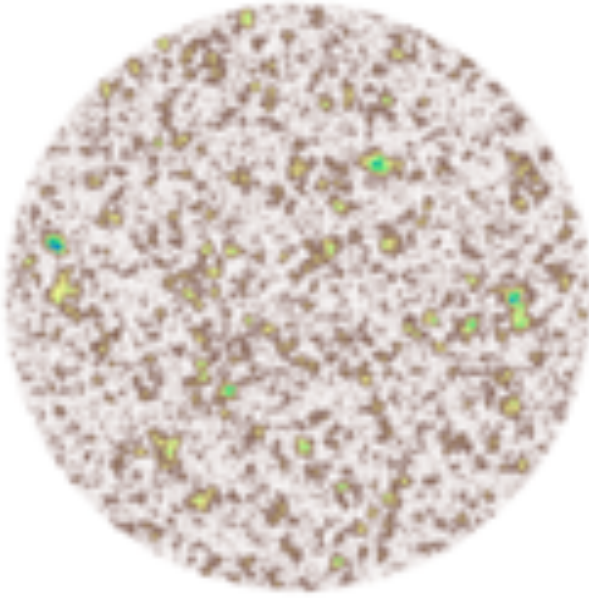


Figure 2.5: A heat map of the odometer function for a $\text{Bernoulli}(0,4,0.528)$ initial sandpile started in a circle of radius $6 \cdot 10^3$ with the open boundary condition.

We would like to emphasize that essentially *any* well-posed PDE involving the operator \bar{F}_η can be realized as the scaling limit of sandpiles with the arguments in this chapter.

2.9.3 Sandpiles with low density

The high density assumption, $\mathbf{E}(\eta(0)) > 2d - 1$, was used in two places in the chapter. The first was to ensure that after stabilizing η in a sufficiently large initial domain what is left is close to a recurrent configuration. The second was to show that solutions to $\bar{F}_\eta(D^2\bar{v}) \leq 0$ also satisfy $\bar{F}_0(D^2\bar{v}) \leq 0$.

For the first usage, we can replace the assumption on $\mathbf{E}(\eta(0))$ by assuming that after stabilizing in all large enough nested volumes and removing an $o(n^2)$ portion of the boundary, what remains is recurrent. For example, for each $p \in [0, 1]$, the following random sandpile

on \mathbb{Z}^2 has a scaling limit by our argument as it is always recurrent,

$$\eta(x) = \begin{cases} 2 & \text{with probability } p \\ 4 & \text{with probability } 1 - p. \end{cases}$$

For the second usage, it suffices to use the weaker bound $\mathbf{E}(\eta(0)) \geq d$. And in fact, if $\mathbf{E}(\eta(0)) < d$, the sandpile is almost surely *stabilizable*, Fey et al. [2009]. This implies, by conservation of density, (Lemma 2.10 in Fey et al. [2009], Lemma 3.2 in Levine et al. [2016a]), that the stable sandpiles converge weakly* to $\mathbf{E}(\eta(0))$ and so $\bar{v}_n \rightarrow 0$.

This still leaves unaddressed sandpiles with $\mathbf{E}(\eta(0)) \in [d, 2d-1]$ which are not stabilizable, but also not close to a recurrent configuration. We believe, but cannot prove, that all such sandpiles have odometer functions with subquadratic growth. See Figure 2.5 for an example of what could be such a sandpile.

CHAPTER 3

A SHAPE THEOREM FOR EXPLODING SANDPILES

This chapter is based on the submitted article Bou-Rabee [2021b].

3.1 Introduction

3.1.1 Overview

In this chapter, we study scaling limits of exploding Abelian sandpiles using ideas from percolation and front propagation in random media. We establish sufficient conditions under which a limit shape exists and show via a family of counterexamples that convergence may not occur in general. A corollary of our proof is a simple criteria for determining if a sandpile is explosive; this strengthens a result of Fey et al. [2010].

Start with a *background* of indistinguishable chips, $\eta : \mathbb{Z}^d \rightarrow \mathbb{Z}$, add n chips at the origin, and attempt to *stabilize* via *parallel toppling*:

$$\begin{aligned} v_{t+1} &= v_t + 1\{s_t \geq 2d\} \\ s_{t+1} &= s_t + \Delta(v_{t+1} - v_t), \end{aligned} \tag{3.1}$$

where $\Delta v(x) = \sum_{y \sim x} (v(y) - v(x))$ is the Laplacian on \mathbb{Z}^d , $v_0 = 0$ is the initial *odometer*, and $s_0 = \eta + n\delta_0$ is the starting sandpile. We say s_0 is *stabilizable* if there is $T < \infty$ so that $v_t = v_T$ for all $t \geq T$. A background is *robust* if $\eta + n\delta_0$ is stabilizable for all $n \geq 1$, and otherwise is *explosive*. When $s_0 = \eta + n\delta_0$ is not stabilizable, it is explosive and the infinite sequence $\{s_t\}_{t \geq 0}$ is an *exploding* sandpile. See Figures 3.1 and 3.2.

Fey-Levine-Peres coined these notions in Fey et al. [2010] (see also Fey and Redig [2005]) and provided sufficient conditions for determining if a background is explosive or robust: backgrounds $\eta \leq (2d - 2)$ are always robust, but otherwise can be robust or explosive,

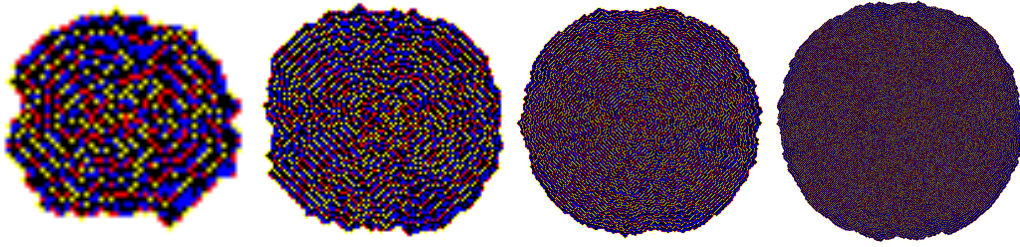


Figure 3.1: $s_t \{v_t > 0\}$ for $\eta \sim \text{Bernoulli}(2, 3, 1/2)$ and $t = 50, 100, 250, 500$. The color white denotes sites which haven't toppled yet, otherwise white, yellow, red, blue, and black correspond to values 0, 1, 2, 3, (≥ 4).



Figure 3.2: Snapshot of the support of an exploding sandpile $1\{v_t > 0\}$ for $\eta \sim \text{Bernoulli}(2d-2, 2d-1, p)$ the first time it exits a box of side length 500. The top row is $d = 2$ and the bottom $d = 3$. From left to right, $p = 1/4, 1/2, 3/4$.

depending on the arrangement of sites with $(2d - 1)$ chips. In fact, they showed that if $\eta \leq (2d - 2)$, not only is the background robust, but if n chips are added to the origin of such η , the diameter of the set of sites which topple grows like $n^{1/d}$.

This bound was used by Pegden-Smart to show convergence of the the terminal odometer for $n\delta_0$ in Pegden and Smart [2013]. In Chapter 2, this bound is used to extend convergence to all initial backgrounds which are stationary, ergodic, and bounded from above by $(2d - 2)$.

These results explain the phenomena of *scale-invariance* in sandpiles which have a *compact*, $n^{1/d}$, growth rate — large, compact-growth sandpiles look like high-resolution versions of smaller sandpiles. Simple models of growth are of interest to the mathematics and physics

communities - see, for example, Dhar and Sadhu [2013], Diaconis and Fulton [1991], Gravner and Griffeath [1998], Packard and Wolfram [1985] and the references therein.

In this chapter, we study limit shapes of sandpiles in the explosive regime. The techniques used differ fundamentally from the existing compact-growth theory. Indeed, as we will demonstrate, some explosive sandpiles (both random and deterministic) do not converge. On the other hand, compact-growth sandpiles essentially always have limits — the argument there is ‘soft’ and applies in wide generality. Our proof below is quantitative and involves establishing specific, finite-scale estimates. We identify sufficient conditions under which exploding sandpiles converge to the level set of an asymmetric norm — much like in first-passage percolation Cox and Durrett [1981] and threshold growth Willson [1978], Gravner and Griffeath [1993].

3.1.2 Main results

For expositional clarity, we consider one family of random, explosive backgrounds with limit shapes. The reader interested in generalizations may consult Section 3.5. Suppose $\eta : \mathbb{Z}^d \rightarrow \mathbb{Z}$ is drawn from a product measure \mathbf{P} with

$$\begin{cases} \mathbf{P}(\eta(0) = (2d-2)) = 1-p \\ \mathbf{P}(\eta(0) = (2d-1)) = p. \end{cases} \quad (3.2)$$

Fey-Levine-Peres showed the following.

Theorem 3.1.1 (Proposition 1.4 in Fey et al. [2010]). *In all dimensions $d \geq 1$, if $p > 0$, η is explosive with probability 1.*

Fix $p > 0$ and denote the (almost surely finite) *explosion threshold* by

$$M_\eta := \min\{n \geq 1 : \eta + n\delta_0 \text{ is not stabilizable}\}. \quad (3.3)$$

We prove that the support of the infinite sequence of parallel toppling odometers, $\{v_t\}_{t \geq 1}$, for the explosive sandpile $s_0 = \eta + M_\eta \delta_0$ converges in the Hausdorff topology.

Theorem 3.1.2. *There exists a convex domain $\mathcal{B}(p) \subset \mathbb{R}^d$ so that on an event of probability 1,*

$$|\{\bar{v}_t > 0\} \Delta \mathcal{B}(p)| \rightarrow 0,$$

where $\bar{v}_t(x) := v_t([tx])$.

In fact, we prove something stronger. Not only does the support of the explosion converge, but the rate at which the explosion spreads also converges.

Theorem 3.1.3. *Let $T_\eta(x) := \min\{t \geq 1 : v_t(x) > 0\}$. On an event of probability 1, the rescaled arrival times $\bar{T}_\eta(x) := n^{-1} T_\eta([nx])$ converge locally uniformly to \mathcal{N}_p , a continuous, convex, one-homogeneous function on \mathbb{R}^d .*

During our proof of Theorem 3.1.3, we introduce a quantitative criteria for determining if a sandpile is explosive. The criteria asserts, roughly, that if a sandpile explodes quickly on a finite box, then it must do so on the entire lattice. We use this and a coupling with bootstrap percolation to extend the aforementioned Theorem 3.1.1.

Theorem 3.1.4. *Suppose $\beta : \mathbb{Z}^d \rightarrow \mathbb{Z}$ is drawn from a product measure \mathbf{P} . If $\beta \geq d$ and $\mathbf{P}(\beta(0) = (2d - 1)) > 0$, then β is explosive with probability 1.*

3.1.3 Proof outline

An exploding sandpile may be thought of as a heterogeneous, discrete reaction-diffusion equation. This perspective leads us to the literature for stochastic homogenization of reaction-diffusion equations Zhang and Zlatos [2020], Feldman [2019], Lin and Zlatoš [2019], Armstrong and Cardaliaguet [2018], Caffarelli and Monneau [2014], Gravner and Griffeath [2006], Ishii et al. [1999], Barles and Souganidis [1998], Gravner and Griffeath [1996, 1993], Willson

[1978]. These works suggest two methods of proof. The first, which we do not pursue, is *half-space propagation* — a limit shape can be completely described by those starting with a half-space initial condition — an early example of this technique appears in Willson [1978]. Another method is to identify a subadditive quantity similar to the first-passage time, Cox and Durrett [1981], which (directly or indirectly) describes the limit shape, then apply the subadditive ergodic theorem.

Our proof of Theorem 3.1.3 follows the second outline, however, there are several hurdles to overcome. A fundamental one is the nonlinear diffusion of the sandpile. This nonlinearity can cause explosions to propagate irregularly. In fact, an arbitrary exploding sandpile may spread quickly in certain cells, but slowly in others, causing convergence to fail. We demonstrate an explicit family of counterexamples to that effect in Section 3.6. A major part of our argument is showing that this irregularity cannot happen if $\eta \geq (2d - 2)$ and there are ‘enough’ sites with $(2d - 1)$ chips.

From now until Section 3.5, take η as in the statement of Theorem 3.1.3 and fix $p > 0$. We begin in Section 3.2 by showing that explosions on η spread quickly. This is done by establishing a high-probability bound on the ‘crossing-speed’ of η in a finite, but large cube and passing to a coarsened lattice. On the coarsened lattice, there is an infinite cluster of ‘good cubes’ upon which explosions are guaranteed to spread quickly. We use this together with large-deviations for the chemical distance of supercritical Bernoulli percolation to get uniform, linear bounds on the arrival times. (This portion of the proof shares some similarities with Schonmann’s argument for bootstrap percolation Schonmann [1992].)

At this stage, if the arrival times, T_η , were subadditive, we could apply the subadditive ergodic theorem and conclude. However, T_η is not, in general, subadditive: roughly, when an explosion started at the origin reaches some site x for the first time, it mixes up the background and so cannot be compared directly to the explosion originating from x .

We overcome this lack of subadditivity by shifting our focus to a related, but simpler

process, the *last-wave* — an exploding sandpile where the origin is constrained to topple a fixed number of times. In Section 3.3, we use the established regularity of explosions to show that the last-wave can be approximated by a quantity which is exactly subadditive, and hence converges. This can also be viewed as a shape theorem for a bootstrap percolation type process.

The proof of Theorem 3.1.3 is completed in Section 3.4 where we show that the last-wave is an approximation to the expanding front of an exploding sandpile. The argument for this is a deterministic comparison which requires $\eta \geq (2d - 2)$. Then, in Section 3.5, we generalize Theorem 3.1.3 by presenting sufficient hypotheses under which a limit shape exists. We demonstrate some need of these hypotheses by constructing a family of (random and deterministic) exploding sandpiles which fail to have a limit shape in Section 3.6. We conclude in Section 3.7 with a proof of Theorem 3.1.4. There we indicate explicit criteria for determining if a sandpile is explosive.

3.2 Regularity of explosions

We use $\eta \geq (2d - 2)$ together with the i.i.d. assumption to establish almost sure regularity of explosions. The main result of this section is a quantification of Fey et al. [2010]’s Theorem 3.1.1 recalled above. The method is a static renormalization (see Chapter 7 in Grimmett [2013]) inspired by Schonmann’s proof for bootstrap percolation Schonmann [1992].

3.2.1 Parallel toppling preliminaries

Before proceeding, we mention some basic properties of parallel toppling which we use below. Recall that $\{v_t\}_{t \geq 1}$ and $\{s_t\}_{t \geq 1}$ are the infinite sequence of parallel toppling odometers and sandpiles for initial conditions $v_0 = 0$ and $s_0 = \eta + M_\eta \delta_0$. An induction argument ((4.4) in

Babai and Gorodezky [2007]) shows

$$\begin{aligned} v_{t+1}(x) &= \min\left\{\left\lfloor \frac{s_0(x) + \sum_{y \sim x} v_t(y)}{2d} \right\rfloor, v_t(x) + 1\right\} \\ s_{t+1}(x) &= s_0(x) + \Delta v_{t+1}(x). \end{aligned} \tag{3.4}$$

Another induction shows that when $s_0 \leq 2(2d) - 1$, the minimum in (3.4) is unnecessary.

In the sequel we also consider a version of parallel toppling where the odometer on some set, \mathcal{S} , (the complement of a cube, the origin) is ‘frozen’ at the initial value w_0 but the initial sandpile $s'_0 = s_0$ is the same,

$$\begin{aligned} w_{t+1}(x) &= \begin{cases} w_t(x) + 1\{s'_t(x) \geq 2d\} & \text{if } x \notin \mathcal{S} \\ w_0(x) & \text{if } x \in \mathcal{S} \end{cases} \\ s'_{t+1} &= s'_t + \Delta(w_{t+1} - w_t). \end{aligned} \tag{3.5}$$

We call this \mathcal{S} -frozen parallel toppling. (Recently, and after this chapter was written, Goles et al. [2021] was posted - therein so-called ‘freezing sandpiles’ are studied in the context of computational complexity.) If $s_0 + \Delta w_0 \leq 2(2d) - 1$ on \mathcal{S}^c , then as above:

$$\begin{aligned} w_{t+1}(x) &= \left\lfloor \frac{s_0(x) + \sum_{y \sim x} w_t(y)}{2d} \right\rfloor && \text{for } x \notin \mathcal{S} \\ s'_{t+1}(x) &= s_0(x) + \Delta w_{t+1}(x). \end{aligned} \tag{3.6}$$

Also, if $s_0 \leq (2d - 1)$, then $w_t \leq \max_{x \in \mathcal{S}} w_0(x)$. The definitions allow us to compare the two versions of parallel toppling,

$$\begin{aligned} v_{t+t_0} &\geq w_t && \text{where } t_0 := \min\{t \geq 0 : v_t \geq w_0\} \\ w_t &\geq v_t && \text{if } w_0 \geq v_0 \text{ and } w_0(\mathcal{S}) \geq \sup_t v_t(\mathcal{S}). \end{aligned} \tag{3.7}$$

3.2.2 Crossing speeds

To provide a global upper bound on the arrival times, $\mathcal{T}_\eta(x)$, we show a local upper bound.

In particular we study the following ‘cell problem’, a term from homogenization denoting a simple problem which describes the local behavior of a more complicated one.

We consider sandpile dynamics on a box of side length k , $Q_k := \{x \in \mathbb{Z}^d : 1 \leq x \leq k\}$.

For a point $z \in \bar{Q}_k$ and direction $1 \leq i \leq d$, denote the line passing from one side of the box to the other

$$\mathcal{L}_k^{(i,z)} := \bigcup_{j=1,\dots,k} (z_1, \dots, z_{i-1}, j, z_{i+1}, \dots, z_d). \quad (3.8)$$

Let w_t be the parallel toppling odometer for $\{Q_k^c \cup \mathcal{L}_k^{(i,z)}\}$ -frozen parallel toppling (defined in (3.5)) with initial conditions $w_0(x) = 1\{x \in \mathcal{L}_k^{(i,z)}\}$, $s'_0 = \eta$. Denote the *crossing time*,

$$\mathfrak{C}_k^{(i,z)} := \min\{t \geq 1 : w_t(Q_k) = 1\}, \quad (3.9)$$

where the right-hand side is ∞ if $w_\infty(Q_k) \neq 1$. We show that if k is sufficiently large, the crossing time is bounded with high probability.

Proposition 3.2.1. *For every $\delta > 0$, there is a k so that*

$$\max_{i,z} \mathfrak{C}_k^{(i,z)} \leq k^d \quad (3.10)$$

with probability at least $(1 - \delta)$.

Proof. For each $k \geq 1$, we construct an event for which (3.10) occurs with probability approaching 1 in k . By Harris’ inequality and symmetry, it suffices to show (3.10) for lines in one direction, say $i = 1$. Let $z \in \bar{Q}_k$ be given.

Write $\mathfrak{C}_k = \mathfrak{C}_k^{(1,z)}$. We show that if all lines, $\mathcal{L}_k^{(1,y)}$, $y \in Q_k$, contain at least one site with $(2d - 1)$ chips, then every site in the cube eventually topples. Denote the event upon

which this happens by,

$$\Omega' := \bigcap_{y \in Q_k} \Omega_y := \bigcap_{y \in Q_k} \{\eta : \mathbb{Z}^d \rightarrow \mathbb{Z} : \eta(x) = (2d - 1) \text{ for some } x \in \mathcal{L}_k^{(1,y)}\}. \quad (3.11)$$

Recall $p > 0$ is the probability of a site having $(2d - 1)$ chips. Fix $0 < \epsilon < p$, and note, by Hoeffding's inequality, for each $y \in Q_k$,

$$\mathbf{P}\left(\sum_{x \in \mathcal{L}_k^{(1,y)}} 1(\eta(x) = 2d - 1) \leq (p - \epsilon)k\right) \leq \exp(-2\epsilon^2 k).$$

Therefore, by the union bound, (deleting duplicates),

$$\mathbf{P}(\Omega'^c) \leq k^{d-1} \mathbf{P}(\Omega_1'^c) \leq k^{d-1} \exp(-2\epsilon^2 k),$$

and so for every $\delta > 0$, there is k sufficiently large so that $P(\Omega') \geq 1 - \delta$.

It remains to check that for $\eta \in \Omega'$, $\mathfrak{C}_k \leq k^d$. We do so by constructing a toppling procedure which is dominated by w_t . After firing $\mathcal{L}_k^{(1,z)}$, all sites in neighboring lines, $\mathcal{L}_k^{(1,y)}$, $\mathbf{y}_{d-1} \sim \mathbf{z}_{d-1}$ have at least $(2d - 1)$ chips. In fact, since $\eta \in \Omega'$, at least one site in each neighbor $\mathcal{L}_k^{(1,y)} \subset Q_k$ has $2d$ chips, causing all sites in the line to topple. Iterating shows this procedure will terminate with every site in Q_k toppling in at most k^d steps.

□

3.2.3 A static renormalization scheme

We exhibit a coarsening of the lattice upon which explosions are guaranteed to spread quickly. A cube, Q_k , is *good* if $\max_{i,z} \mathfrak{C}_k^{(i,z)} \leq k^d$. For each $i \in \mathbb{Z}^d$, let

$$Q_k(i) := Q_k + ik. \quad (3.12)$$

The cubes $\{Q_k(i)\}_{i \in \mathbb{Z}^d}$ define a *macroscopic lattice* with edge set $\{(Q_k(i), Q_k(j)), |j-i|=1\}$. For k sufficiently large, Proposition 3.2.1 implies that the set of good cubes is dominated by a supercritical site percolation process on the macroscopic lattice. This together with large deviations bounds for supercritical percolation Antal and Pisztora [1996], Garet and Marchand [2007] imply the following. (See, for example, Section 5 in Mathieu [2008] for an explicit proof.)

Proposition 3.2.2. *For fixed k large enough, there are constants c, C so that the following hold on an event of probability 1.*

1. *There is an infinite cluster \mathcal{C}_∞ of good cubes on the macroscopic lattice $\{Q_k(i)\}_{i \in \mathbb{Z}^d}$.*
2. *There is n_0 so that for $n \geq n_0$, any connected component of \mathcal{C}_∞^c that intersects $[-n, n]^d$ has volume smaller than $(\log n)^{5/2}$.*
3. *There is n_0 so that for $n \geq n_0$, for any $x, y \in \mathcal{C}_\infty$ with $|x| \leq n$ and $|x - y| \geq (\log n)^2$,*

$$c|x - y| \leq d(x, y) \leq C|x - y|,$$

where d is the chemical (graph) distance on \mathcal{C}_∞ .

The definition of \mathcal{C}_∞ ensures that once $Q_k(i) \in \mathcal{C}_\infty$ is *overlapped* by the support of the odometer - $Q_k(i) \cap \{v_t > 0\}$ contains a straight line - an explosion will occur. This together with Proposition 3.2.2 controls the speed at which the explosion propagates. We show next that the explosion spreading in \mathcal{C}_∞ also quickly fills holes in the cluster.



Figure 3.3: Terminal A -frozen parallel toppling odometer, w_∞ , on \mathbb{Z}^2 for initial conditions $w_0 = 1\{x \in A\}$ and $s_0 = 2$. Red pixels are sites in A and black pixels are sites which eventually topple.

3.2.4 A path-filling property

For a set of points $A \subset \mathbb{Z}^d$, let $m_i := \min_{z \in A} z_i$ and $M_i := \max_{z \in A} z_i$ for $i = 1, \dots, d$.

Denote the bounding rectangle of A as

$$\mathbf{br}(A) := \{z \in \mathbb{Z}^d : m \leq z \leq M\}. \quad (3.13)$$

We show, using $\eta \geq (2d - 2)$, that any path of points touched by the odometer eventually fills its bounding rectangle. Essentially, if it doesn't fill its bounding rectangle, then the support of the odometer must have a corner, *i.e.*, an untoppled site with two neighbors which have toppled, a contradiction. Our proof uses this idea together with a slightly technical induction (which, it seems, we cannot avoid as the claim is needed in all dimensions). See Figure 3.3 for an illustration of this result.

Lemma 3.2.1. *Let $A := \{z^{(i)}\}$ be a finite path $z^{(i)} \sim z^{(i+1)}$. Let w_t denote A -frozen parallel toppling with initial conditions $w_0(A) = 1$, $s'_0 = \eta$. Then, $w_t(\mathbf{br}(A)) = 1$, for all $t \geq |\mathbf{br}(A)|$.*

Proof. By monotonicity of parallel toppling, we may take $\eta = (2d - 2)$. Moreover, it suffices to show that every site in $\mathbf{br}(A)$ eventually topples, as if no site topples at time t , then no site topples at time $(t + 1)$.

We say A contains a $(\pm i, \pm j)$ turn if $z^{(m)} = z^{(m-1)} \pm e_i$ and $z^{(m+1)} = z^{(m)} \pm e_j$ for

some $i \neq j$ where $z^{(m-1)} \sim z^{(m)} \sim z^{(m+1)}$ are in A . If A does not contain a turn, then $\mathbf{br}(A) = A$. Hence, we may suppose it contains at least one turn.

Case 1 - one-turn path

By shifting coordinates, we may suppose A contains only a $(1, 2)$ turn and that

$$A = \{0, e_1, \dots, k_1 e_1, k_1 e_1 + e_2, \dots, k_1 e_1 + k_2 e_2\} \quad (3.14)$$

for $k_1 \geq k_2$. We induct on k_2 . If $k_2 = 1$, then after firing every site in A , all sites in $A + e_2$ get one chip, while the corner site, $((k_1 - 1)e_1 + e_2)$ gets 2 chips. Since $\eta = (2d - 2)$, that corner becomes unstable and fires, causing all of its neighbors to the left, $((k_1 - 2)e_1 + e_2) \sim ((k_1 - 3)e_1 + e_2) \sim \dots \sim e_2$ to fire. Continuing the induction shows that every site in $\mathbf{br}(A) = \{x \in \mathbb{Z}^d : 0 \leq x \leq (k_1 e_1 + k_2 e_2)\}$ eventually fires.

Case 2 - cubic path

We call A a *cubic* path if, after an isometry,

$$A = \{0, e_1, \dots, k_1 e_1, k_1 e_1 + e_2, \dots, \sum_{i=1}^d k_i e_i\} \quad (3.15)$$

for $k_1 \geq \dots \geq k_d \geq 0$. Let $d_0 := \max\{i \leq d : k_i > 0\}$. We induct on d_0 , the base case $d_0 = 2$ established in Case 1. For notational convenience, suppose the claim holds for $d_0 = (d - 1)$ and we verify it for $d_0 = d$.

Consider the $(d - 1)$ -turn subpaths,

$$\begin{aligned}\mathcal{P}_1 &:= \{0, e_1, \dots, \sum_{i=1}^{d-1} k_i e_i\} \\ \mathcal{P}_2 &:= \{k_1 e_1, k_1 e_1 + e_2, \dots, \sum_{i=1}^d k_i e_i\}.\end{aligned}\tag{3.16}$$

By the inductive hypothesis, after \mathcal{P}_i fire, both $(d - 1)$ -dimensional faces,

$$\begin{aligned}\mathcal{F}_1 &:= \{x \in \mathbb{Z}^d : 0 \leq x \leq \sum_{i=1}^{d-1} k_i e_i\} \\ \mathcal{F}_2 &:= \{x \in \mathbb{Z}^d : k_1 e_1 \leq x \leq \sum_{i=1}^d k_i e_i\}\end{aligned}\tag{3.17}$$

fire. We then ‘fill in’ the cube by identifying newly fired $(d - 1)$ -turn paths:

$$\begin{aligned}\mathcal{P}'_j &:= \{je_2, je_2 + e_1, \dots, je_2 + k_1 e_1, \\ &\quad je_2 + k_1 e_1 + e_3, \dots, je_2 + k_1 e_1 + k_3 e_3, \\ &\quad \dots \\ &\quad je_2 + \sum_{i \neq 2} k_i e_i\}\end{aligned}\tag{3.18}$$

which are in $\mathcal{F}_1 \cup \mathcal{F}_2$ for $j = 0, \dots, k_2$. By the inductive hypothesis, the firing of each \mathcal{P}'_j makes every $(d - 1)$ -dimensional layer,

$$\mathcal{L}_j := \{x \in \mathbb{Z}^d : je_2 \leq x \leq je_2 + \sum_{i \neq 2} k_i e_i\},$$

fire and $\mathbf{br}(A) = \bigcup_{j=0}^{k_2} \mathcal{L}_j$.

Case 3 - general path

It suffices to show that if there is a path of firings between any two distinct points x, y , then $\mathbf{br}(\{x, y\})$ eventually fires. Before showing this, we suppose it were true and demonstrate sufficiency. Take $q \in \mathbf{br}(A)$ and observe by definition there are points

$$(z^{(1)}, Z^{(1)}), \dots, (z^{(d)}, Z^{(d)})$$

in A with $z_i^{(i)} \leq q_i \leq Z_i^{(i)}$. Then,

$$q^{(1)} := (q_1, \mathbf{q}'_{d-1}) \in \mathbf{br}(\{z^{(1)}, Z^{(1)}\})$$

for some $(d-1)$ -vector \mathbf{q}'_{d-1} . Continue and let

$$q^{(2)} := \begin{cases} (q_1, q_2, \mathbf{q}''_{d-2}) \in \mathbf{br}(\{q^{(1)}, z^{(2)}\}) & \text{if } q_2^{(1)} \geq q_2 \\ (q_1, q_2, \mathbf{q}'''_{d-2}) \in \mathbf{br}(\{q^{(1)}, Z^{(2)}\}) & \text{otherwise} \end{cases}$$

for some $(d-2)$ -vectors $\mathbf{q}''_{d-2}, \mathbf{q}'''_{d-2}$. After iterating, we find $q^{(d)} = q$, which shows that eventually q will fire.

Now fix two points $x, y \in A$ and decompose a path between them into a sequence of cubic paths

$$\mathcal{P}^{(1)} := \bigcup_{i=1}^m \mathcal{P}_i^{(1)},$$

where $\mathcal{P}_i^{(1)} := \{p_{i-1}, \dots, p_i\}$ is cubic and $p_0 := x$ and $p_m := y$. (This can be done by, for example, starting at x and exploring the path but cutting whenever the cubic condition is violated.) Case 2 shows that eventually every site in $\mathcal{A}^{(1)} := \bigcup_{i=1}^m \mathbf{br}(\mathcal{P}_i^{(1)})$ will fire. If $m = 1$, we are done, otherwise we construct a new cubic path from p_0 to p_2 passing through $\mathcal{A}^{(1)}$. Once we have shown this, we iterate to conclude.

Suppose $p_0 = 0$, $p_1 = \sum_{j=1}^d k_j e_j$, and

$$p_2 = \sum_{j=1}^{d_1} (k_j - k'_j) e_j + \sum_{j=(d_1+1)}^{d_2} (k_j - k'_j) e_j + \sum_{j=(d_2+1)}^d (k_j + k'_j) e_j,$$

for some $1 \leq d_1 \leq d_2 \leq d$ and $k_j, k'_j \geq 1$ where $(k_j - k'_j) < 0$ for $j \leq d_1$ and $(k_j - k'_j) \geq 0$ for $(d_1 + 1) \leq j \leq d_2$. After this coordinate change, it suffices to exhibit a path from p_0 to p_2 with differences constrained to be $-e_j$ for $j = 1, \dots, d_1$ and $+e_j$ for $j = (d_1 + 1), \dots, d$.

There is a cubic path (only positive moves) from p_0 to

$$w_1 := \sum_{j=(d_1+1)}^{d_2} (k_j - k'_j) e_j + \sum_{j=(d_2+1)}^d (k_j) e_j$$

contained within $\mathbf{br}(\{p_0, p_1\})$ as $p_0 = 0 \leq w_1 \leq p_1$. Then, since $w_1 \in \mathbf{br}(\{p_1, p_2\})$ there is a cubic path (only positive moves) from w_1 to

$$w_2 := w_1 + \sum_{j=(d_2+1)}^d k'_j e_j$$

contained in $\mathbf{br}(\{p_1, p_2\})$ and similarly there is a cubic path (only negative moves) from w_2 to

$$p_2 = w_2 + \sum_{j=1}^{d_1} (k_j - k'_j) e_j.$$

Our new cubic path is the concatenation of these three paths: $p_0 \rightarrow w_1 \rightarrow w_2 \rightarrow p_2$. \square

3.3 The last-wave

In this section we study a simplified parallel toppling procedure closely related to bootstrap percolation (see Section 3.7 for an explicit connection, we do not utilize the coupling here). This simplified process has an inherent subadditive structure which allows us to prove

convergence using the subadditive ergodic theorem. In the next section we show that this process is a good approximation to an exploding sandpile.

3.3.1 The n -wave process

Fix $n \geq 1$, $z \in \mathbb{Z}^d$, and consider the following modified parallel toppling process

$$\begin{aligned} u_0^{(z)} &:= n\delta_z \\ u_{t+1}^{(z)}(x) &:= \lfloor \frac{\sum_{y \sim x} u_t^{(z)}(y) + \eta(x)}{2d} \rfloor \text{ for } x \neq z. \end{aligned} \tag{3.19}$$

This is a $\{z\}$ -frozen parallel toppling process (see (3.5)) which we call the n -wave for η starting at z . Overloading terminology, the n -wave is *stabilizable* if there is $T < \infty$ so that $u_t^{(z)} = u_T^{(z)}$ for all $t \geq T$. Let

$$\hat{M}_\eta(z) := \min\{n \geq 1 : \text{the } n\text{-wave for } \eta \text{ starting at } z \text{ is not stabilizable}\}. \tag{3.20}$$

We write $u_t^{(z)}$ for the $\hat{M}_\eta(z)$ -wave starting at z and call this the *last-wave*. We also consider the *penultimate-wave* starting at z as the terminal odometer for the $(\hat{M}_\eta(z) - 1)$ -wave, $\tilde{u}^{(z)}$. The set of sites touched by the penultimate wave is its *penultimate-cluster*,

$$\mathcal{P}(z) := \{z\} \cup \{x \in \mathbb{Z}^d : \text{there is } y \sim x \text{ with } \tilde{u}^{(z)}(y) > 0\} \tag{3.21}$$

(we included the point, $\{z\}$, as $\hat{M}_\eta(z)$ may be 1). When z is the origin, we omit the superscripts.

The *arrival time* for the last-wave starting at site s to site x is

$$\hat{T}(s, x) := \min\{t \geq 1 : u_t^{(s)}(x) > 0\} \tag{3.22}$$

and the *penultimate-cluster arrival time* is

$$\tilde{T}(s, x) := \min\{t \geq 1 : u_t^{(s)}(\mathcal{P}(x)) > 0\}. \quad (3.23)$$

We write $\hat{T}(x) := \hat{T}(0, x)$ and $\tilde{T}(x) := \tilde{T}(0, x)$ (choice of the same letter T for all arrival times was intentional - we will see they are asymptotically close).

3.3.2 Basic properties of the last-wave

We derive some basic properties of the last-wave. Throughout this section and the next, let η be drawn from the event of probability 1 in Proposition 3.2.2 and let k be the (deterministic but large) side length of a good cube. The following is a consequence of Theorem 4.1 in Fey-den Boer and Redig [2008].

Lemma 3.3.1. *There is a constant $C := C_d$ so that for all $R \geq 1$, the support of the (CR^d) -wave contains $[-R, R]^d$.*

Proof. From Theorem 4.1 in Fey-den Boer and Redig [2008], we know that if n chips are placed at the origin on a background of $(2d - 2)$, then the support of the terminal odometer, \tilde{v} , contains a cube of radius $r_n \geq (n^{1/d} - 3)/2$. Moreover, $\tilde{v}(0) \leq Cn^d$. This implies, by (3.7) that a (Cn^d) -wave contains $[-r_n, r_n]^d$. \square

Lemma 3.3.2. *The last-wave is well-defined, $\hat{M}_\eta(0) < \infty$.*

Proof. By Lemma 3.3.1 and Proposition 3.2.2, if the origin is fired a sufficient number of times, the support of the odometer contains a good cube, $Q_k \subset \mathcal{C}_\infty$. \square

Lemma 3.3.3. *The last wave is bounded by one outside the interior of the penultimate-cluster, for all $t \geq 1$ and $x, z \in \mathbb{Z}^d$,*

$$u_t^{(z)}(x) \leq (1 + \tilde{u}^{(z)}(x)).$$

Proof. To reduce clutter, we take $z = 0$. We prove this by induction on t . The base case $t = 0$ follows by definition. For all $t \geq 1$, the definition also ensures it holds at the origin. So, we may take $x \neq 0$ and check:

$$\begin{aligned} u_{t+1}(x) &= \lfloor \frac{\sum_{y \sim x} u_t(y) + \eta(x)}{2d} \rfloor \\ &\leq \lfloor \frac{\sum_{y \sim x} (1 + \tilde{u}(y)) + \eta(x)}{2d} \rfloor \\ &= 1 + \tilde{u}(x) + \lfloor \frac{\sum_{y \sim x} (\tilde{u}(y) - \tilde{u}(x)) + \eta(x)}{2d} \rfloor \\ &= 1 + \tilde{u}(x) \end{aligned}$$

as $\Delta \tilde{u}(x) + \eta(x) \leq (2d - 1)$ for $x \neq 0$.

□

Lemma 3.3.4. *The penultimate-cluster arrival times are subadditive: for all $a, b, c \in \mathbb{Z}^d$,*

$$\tilde{T}(a, c) \leq \tilde{T}(a, b) + \tilde{T}(b, c).$$

Proof. Suppose $\mathcal{P}(c) \not\subseteq \mathcal{P}(b)$, otherwise the claim is immediate. It suffices to check

$$w_t(x) := u_{\tilde{T}(a,b)+t}^{(a)}(x) \geq u_t^{(b)}(x) \quad \text{for all } t \geq 1 \text{ and } x \in \mathcal{P}(b)^c, \quad (3.24)$$

which we do by induction. By Lemma 3.3.3, $u_t^{(b)}(x) \leq 1$ if $\tilde{u}^{(b)}(x) = 0$. In particular, for all $t \geq 1$ and $x \in \partial^\circ \mathcal{P}(b)$, $u_t^{(b)}(x) \leq 1 \leq w_t(x)$ (where the interior boundary of a set $S \subset \mathbb{Z}^d$ is $\partial^\circ S := \{x \in S : \text{there is } y \sim x \text{ in } S^c\}$). Using this and the inductive hypothesis,

if $x \in \mathcal{P}(b)^c \cap \{a\}^c$,

$$\begin{aligned} w_{t+1}(x) &= \lfloor \frac{\sum_{y \sim x} w_t(y) + \eta(x)}{2d} \rfloor \\ &\geq \lfloor \frac{\sum_{y \sim x} u_t^{(b)}(y) + \eta(x)}{2d} \rfloor \\ &= u_{t+1}^{(b)}(x). \end{aligned}$$

If $x \in \mathcal{P}(b)^c \cap \{a\}$, then $w_t(x) \geq 1 \geq u_t^{(b)}(x)$ as $\hat{M}_\eta(a) \geq 1$.

□

Lemma 3.3.5. *There is a constant $\gamma > 0$ so that for all n sufficiently large and $|x| \leq n$,*

$$\mathcal{P}(x) \subset [-r_n, r_n]^d,$$

where $r_n \leq (\log n)^\gamma$.

Proof. By Lemma 3.2.1, $1\{\tilde{u}^{(x)} > 0\}$ is a rectangle, therefore it suffices to bound the maximal side length. By Proposition 3.2.2, if any side length of the rectangle exceeds $(2k \log n)^{5/2}$ then it must overlap a good cube, contradicting stability. □

Lemma 3.3.6. *There are constants γ and C so that on an event of probability 1, for all n sufficiently large and $|x| \leq n$,*

$$\hat{T}(x) \leq C|x| + (\log n)^\gamma.$$

Proof. Let $x \in \mathbb{Z}^d$ be given. Since the sandpile is exploding, at some constant time C the support of the odometer will overlap the infinite cluster at a good cube near the origin, $Q_k(z)$ for some $z \in \mathbb{Z}^d$. Once this occurs the arrival time to any site is at most a constant times the chemical distance in the infinite cluster. Let $Q_k(y)$ for $y \in \mathbb{Z}^d$ be one of the nearest cubes in \mathcal{C}_∞ to x . There are now two cases to consider.

Case 1: $|z - y| < (\log n)^2$

Choose nearby points $M_i \in \mathcal{C}_\infty$ so that $(\log n)^c \leq d(z, M_i) \leq (\log n)^C$ and $x, y \in \mathbf{br}(\{M_i\})$.

Case 2: $|z - y| \geq (\log n)^2$

By the chemical distance bound and the definition of \mathcal{C}_∞ , within at most $C|z - y| \leq C(|z| + |y|)$ steps, $Q_k(y)$ will topple. Once this happens, $\mathcal{P}(x)$ is surrounded in at most $(\log n)^C$ more steps and $\mathcal{P}(x)$ will fire in at most $|\mathcal{P}(x)|$ additional steps.

□

3.3.3 Convergence of the last-wave

We show that the arrival time for the last-wave converges.

Lemma 3.3.7. *There exists a constant $\gamma > 0$ so that on an event of probability 1, for all n sufficiently large and $|x| \leq n$,*

$$\hat{T}(x) \leq \tilde{T}(x) \leq \hat{T}(x) + (\log n)^\gamma.$$

Proof. The first inequality is immediate. For the second, suppose $v_t(x) > 0$ for $\min(t, |x|) > C$. We must show that there is a nearby good cube $Q_k(y) \subset \mathcal{C}_\infty$ which has already fired. Once we have shown this, the same argument as in Lemma 3.3.6 allows us to conclude. This is, however, a consequence of Lemma 3.2.1 and Proposition 3.2.2. Any path of topplings of length at least $(2k \log n)^{5/2}$ must overlap a good cube. □

Proposition 3.3.1. *On an event of probability 1, the rescaled last-wave arrival times*

$$n^{-1}\hat{T}_\eta([nx])$$

converge locally uniformly to \mathcal{N}_p , a continuous, convex, one-homogeneous function on \mathbb{R}^d .

Proof. In light of Lemma 3.3.7 it suffices to prove the result for \tilde{T} . Convergence in integer directions follows from the subadditive ergodic theorem. Everywhere convergence then

follows from continuity and approximation. The properties of \mathcal{N}_p are immediate from the scaling and microscopic subadditivity. \square

Remark 1. *Convergence of the last wave may be viewed as a sort of bootstrap percolation shape theorem. Sites are initially randomly assigned two thresholds, 1 or 2. A site with threshold l becomes infected when at least l of its neighbors are infected. Infected sites remain infected. The above shows that if you start off with a large enough cluster of infected sites at the origin, every site will eventually become infected and the speed at which the infection spreads converges.*

For more on the relationship between sandpiles and bootstrap percolation, see Section 3.7 below. Similar shape theorems include Garet and Marchand [2012], Kesten and Sidoravicius [2008], Alves et al. [2002], Cox and Durrett [1981] and especially Willson [1978], Gravner and Griffeath [1993], Fey and Liu [2011].

3.4 Proof of convergence

Let η be drawn from the event of full probability in Proposition 3.3.1. It suffices to show that the last-wave is a good approximation of the original process.

Proposition 3.4.1. *On an event of probability 1, there are constants C_1, C_2 so that for all $x \in \mathbb{Z}^d$,*

$$T(x) \leq \hat{T}(x) + C_1 \quad (3.25)$$

and

$$\hat{T}(x) \leq T(x) + C_2, \quad (3.26)$$

where the last-wave arrival time \hat{T} is defined in (3.22) and $T(x) := \min\{t \geq 0 : v_t(x) > 0\}$.

Proof. Recall that v_t is the parallel toppling odometer for $\eta + M_\eta \delta_0$ and u_t from Section 3.3.1. We first observe that (3.25) follows immediately from (3.7): since $\hat{M}_\eta(0) < \infty$, and $\eta + M_\eta \delta_0$ is not stabilizable, for $t \geq C_\eta$, $v_t(0) \geq \hat{M}_\eta(0) = u_0(0)$.

We now verify (3.26). We first consider the special case where only one firing at the origin is needed to have an infinite last-wave.

Step 1: Special case, $\hat{M}_\eta(0) = 1$

Denote the reachable sets up to time t for the last wave and exploding sandpile as

$$\begin{aligned}\mathcal{R}_t &:= \{x \in \mathbb{Z}^d : v_t(x) > 0\} \\ \hat{\mathcal{R}}_t &:= \{x \in \mathbb{Z}^d : u_t(x) > 0\}.\end{aligned}\tag{3.27}$$

Note, by minimality, if $\hat{M}_\eta(0) = 1$, then $\eta(0) + M_\eta(0) = 2d$. This together with $\eta \geq (2d - 2)$, implies a strong regularity. Specifically, we show by induction that for all $t \geq 1$,

$$\mathcal{R}_t \subseteq \hat{\mathcal{R}}_t\tag{3.28}$$

and

$$\begin{aligned}|v_t(x \pm e_i \pm e_j) - v_t(x))| &\leq 1 && \text{for all } x \in \mathbb{Z}^d \text{ and } e_i \neq e_j \\ |v_t(x \pm e_i) - v_t(x))| &\leq 1 && \text{for all } x \in \mathbb{Z}^d \text{ and } e_i\end{aligned}\tag{3.29}$$

and

$$v_t(0) \geq \max_{x \in \mathbb{Z}^d} v_t(x).\tag{3.30}$$

The base case is immediate, so suppose (3.28), (3.29), and (3.30) hold at t and we check $(t + 1)$.

Inductive step for (3.30)

(3.4) and (3.30) at time t imply if $x \neq 0$,

$$\begin{aligned} v_{t+1}(x) &\leq \left\lfloor \frac{2dv_t(0) + \eta(x)}{2d} \right\rfloor \\ &= v_t(0) + \left\lfloor \frac{\eta(x)}{2d} \right\rfloor \\ &= v_t(0) \\ &\leq v_{t+1}(0), \end{aligned}$$

as $\eta \leq (2d - 1)$.

Inductive step for (3.29)

We first check the origin. By (3.30), if $v_t(y) = v_t(0) - 1$ for some $y \sim 0$, then $\Delta v_t(0) + 2d \leq (2d - 1)$. Otherwise, suppose $v_t(e_i + e_j) = v_t(0) - 1$ for some $e_i \neq e_j$ and the origin is unstable. Then, $v_t(e_i) = v_t(0)$ and $v_t(e_j) = v_t(0)$. This implies, by (3.29) applied to e_i and e_j , that all other neighbors $y \sim (e_i + e_j)$ have a lower bound, $v_t(y) \geq v_t(0) - 1$. Hence, $\Delta v_t(x + e_i + e_j) \geq 2$, which implies that $(x + e_i + e_j)$ is unstable using $\eta \geq (2d - 2)$.

Now, take $x \neq 0$ and suppose for sake of contradiction

$$\Delta v_t(x) + \eta(x) \geq 2d \tag{3.31}$$

but for some adjacent neighbor $(x + e_j)$,

$$v_t(x + e_j) = v_t(x) - 1 \quad \text{and} \quad \Delta v_t(x + e_j) + \eta(x + e_j) \leq 2d - 1. \tag{3.32}$$

At least two other adjacent neighbors, $y' \sim x$ must satisfy $v_t(y') = v_t(x) + 1$. Indeed, otherwise by (3.32) and (3.29), $\Delta v_t(x) \leq 0$, violating our assumption (3.31). However, one

of those neighbors must be $y' = x \pm e_i$ for some $e_i \neq e_j$. This contradicts (3.29) at time t since

$$v_t(x + e_i) = v_t(x + e_i + (-e_i + e_j)) + 2.$$

Next, take a diagonal neighbor, $(x+e_i+e_j)$ for $i \neq j$, and suppose for sake of contradiction (3.31) but

$$v_t(x + e_i + e_j) = v_t(x) - 1 \quad \text{and} \quad \Delta v_t(x + e_i + e_j) + \eta(x + e_i + e_j) \leq (2d - 1). \quad (3.33)$$

By (3.31) there must be at least one adjacent neighbor $y \sim x$ with $v_t(y) = v_t(x) + 1$. This neighbor cannot be $(x+e_i)$ or $(x+e_j)$ as it would contradict (3.29) for $(x+e_i+e_j)$. Possibly $y = (x \pm e_{i'})$ for $i' \notin \{i, j\}$, $y = x - e_i$, or $y = x - e_j$. In these cases,

$$v_t(x + e_i) = v_t(x + e_j) = v_t(x) = v_t(x + e_i + e_j) + 1. \quad (3.34)$$

Indeed, if not, then, say, $v_t(x + e_i) = v_t(x) - 1$, and so there must be an additional neighbor, $y' \sim x$, $y' \neq y$, with $v_t(y') = v_t(x) + 1$. But, either y' or y is diagonal to $(x + e_i)$, which contradicts (3.29).

Assuming (3.34), the same argument implies $v_t(y) \geq v_t(x+e_i+e_j)$ for all $y \sim (x+e_i+e_j)$. This together with (3.34) shows $\Delta v_t(x + e_i + e_j) \geq 2$, which contradicts (3.33).

Inductive step for (3.28)

It suffices to check this for $x \neq 0$ as $u_t(0) = 1$. Suppose for sake of contradiction there is some site x with

$$\Delta v_t(x) + \eta(x) \geq 2d \quad (3.35)$$

but

$$\Delta u_t(x) + \eta(x) \leq (2d - 1) \quad (3.36)$$

and $u_t(x) = 0$. By (3.28), $u_t(x) = v_t(x) = 0$ and hence

$$v_t(y) \leq 1 \quad \text{for all } y \sim x, \quad (3.37)$$

by (3.29). However, (3.28) and (3.37) imply that $\Delta v_t(x) + \eta(x) = \Delta u_t(x) + \eta(x) \leq (2d - 1)$, contradicting (3.35).

Step 2: General case

In the general case, we introduce a pair of approximations to which we can apply the arguments of the special case. Let \tilde{v} be the terminal (unfrozen) odometer for $\eta + (M_\eta(0) - 1)\delta_0$ and let

$$\tilde{\mathcal{P}} := \{0\} \cup \{x \in \mathbb{Z}^d : \text{there is } y \sim x \text{ with } \tilde{v}(y) > 0\}. \quad (3.38)$$

Let \tilde{w}_t be the $\tilde{\mathcal{P}}$ -frozen parallel toppling odometer with initial conditions

$$\begin{aligned} \tilde{w}_0(x) &= 1\{x \in \tilde{\mathcal{P}}\} \\ s'_0 &= \eta. \end{aligned} \quad (3.39)$$

Let w_t be the parallel toppling odometer for $s : \mathbb{Z}^d \rightarrow \mathbb{Z}$ where

$$s(x) := \begin{cases} \eta(x) & \text{if } x \notin \tilde{\mathcal{P}} \\ (2d - 1) + \delta_0 & \text{otherwise.} \end{cases} \quad (3.40)$$

Denote the reachable sets for these processes by

$$\begin{aligned} \mathcal{R}_t &:= \{x \in \mathbb{Z}^d : w_t(x) > 0\} \\ \tilde{\mathcal{R}}_t &:= \{x \in \mathbb{Z}^d : \tilde{w}_t(x) > 0\}. \end{aligned} \quad (3.41)$$

Draft Mar 13

The same argument as in Step 1 shows that

$$\mathcal{R}_t \subseteq \tilde{\mathcal{R}}_t. \quad (3.42)$$

We claim that we can conclude after proving the following inequalities,

$$\tilde{w}_t \leq u_{t+c} \quad (3.43)$$

$$v_t \leq (w_t + \tilde{v}). \quad (3.44)$$

Indeed, if $v_t(x) > 0$, then (3.44) implies $\tilde{v}(x) > 0$ or $w_t(x) > 0$. In both cases, using either (3.42) or (3.39), $\tilde{w}_t(x) > 0$ and so by (3.43) $u_{t+c}(x) > 0$.

Proof of (3.43)

We know that $|\tilde{\mathcal{P}}| = C < \infty$. Hence, at some finite time $u_c(\tilde{\mathcal{P}}) \geq 1$. Monotonicity implies $\tilde{w}_t \leq u_{t+c}$.

Proof of (3.44)

This is true at $t = 0$, we use (3.4) and induct,

$$\begin{aligned} v_{t+1}(x) &\leq \lfloor \frac{\sum_{y \sim x} v_t(y) + \eta(x) + M_\eta \delta_0}{2d} \rfloor \\ &\leq \lfloor \frac{\sum_{y \sim x} (w_t(y) + \tilde{v}(y)) + \eta(x) + M_\eta \delta_0}{2d} \rfloor \\ &= \tilde{v}(x) + \lfloor \frac{\sum_{y \sim x} w_t(y) + \sum_{y \sim x} (\tilde{v}(y) - \tilde{v}(x)) + \eta(x) + M_\eta \delta_0}{2d} \rfloor \\ &\leq \tilde{v}(x) + \lfloor \frac{\sum_{y \sim x} w_t(y) + s(x)}{2d} \rfloor \\ &= \tilde{v}(x) + w_{t+1}(x). \end{aligned}$$

The third inequality used $\Delta\tilde{v}(x) + (M_\eta - 1)\delta_0 + \eta \leq (2d - 1)$.

□

Remark 2. Some qualitative features of the limit shape are immediate. For example, the origin is an interior point and the limit is invariant with respect to symmetries of the lattice (symmetry may fail in the periodic case introduced in Section 3.5). Also, a coupling with oriented percolation as in Durrett and Liggett [1981], Marchand [2002] can be used to establish a ‘flat-edge’ for p sufficiently close to one in all dimensions. We omit the details since it is routine - see, for example, the proof of Theorem 1.2 in Alves et al. [2002] or Theorem 6.3 in Garet and Marchand [2004].

3.5 A generalization

3.5.1 Sufficient hypotheses

We present sufficient hypotheses on η under which the arguments above go through seamlessly. Fix $\eta_{\min} \in \mathbb{Z}$ and let Ω denote the set of all bounded functions $\eta : \mathbb{Z}^d \rightarrow \mathbb{Z}$, $\eta_{\min} \leq \eta \leq (2d - 1)$. Endow Ω with the σ -algebra \mathcal{F} generated by $\{\eta \rightarrow \eta(x) : x \in \mathbb{Z}^d\}$. Denote the action of integer translation by $T : \mathbb{Z}^d \times \Omega \rightarrow \Omega$,

$$T(y, \eta)(z) = (T_y\eta)(z) := \eta(y + z),$$

and extend this to \mathcal{F} by defining $T_y E := \{T_y \eta : \eta \in E\}$. Let $\mathcal{L} \subseteq \mathbb{Z}^d$ be a sublattice, a finite index subgroup of \mathbb{Z}^d . Let \mathbf{P} be a stationary and ergodic probability measure on (Ω, \mathcal{F}) with respect to \mathcal{L} ,

$$\text{Stationary: for all } E \in \mathcal{F}, y \in \mathcal{L}: \mathbf{P}(T_y E) = \mathbf{P}(E), \quad (3.45)$$

$$\text{Ergodic: } E = \bigcap_{y \in \mathcal{L}} T_y E \text{ implies that } \mathbf{P}(E) \in \{0, 1\}. \quad (3.46)$$

We refer to the probability measure \mathbf{P} as *explosive* if $\mathbf{P}(\eta \text{ is explosive}) = 1$.

Stationarity and ergodicity are the weakest hypotheses under which a convergence result is proved - straightforward counterexamples can be constructed. However, we do not expect exploding sandpiles to have a limit shape without an additional independence hypothesis. At the very least, our proof will not work, as domination by a coarsened product measure was essential. Our first hypothesis is hence a quantification of ergodicity.

Hypothesis 1 (Finite range of dependence). *There exists a constant $K < \infty$ so that for all $x, y \in \mathbb{Z}^d$, $\eta(x)$ and $\eta(y)$ are independent if $|x - y| > K$.*

Next, fix a finite (rectangular) box with side length $k > 0$, $\mathcal{B}_k := \{x \in \mathbb{Z}^d : 1 \leq x_i \leq k_i\}$.

The $2d$ external faces of \mathcal{B}_k are

$$\begin{aligned}\mathcal{F}_i &:= \{x \in \bar{\mathcal{B}}_k : x_i = 0\}, \\ \mathcal{F}_{d+i} &:= \{x \in \bar{\mathcal{B}}_k : x_i = k_i + 1\}.\end{aligned}$$

Take a face, \mathcal{F}_i , and let $w_t : \bar{\mathcal{B}}_k \rightarrow \mathbb{N}$ be the sequence of \mathcal{B}_k^c -frozen parallel toppling odometers with initial conditions $w_0 = 1\{x \in \mathcal{F}_i\}$ and $s'_0 = \eta$. We say that $\mathcal{B}_k(\eta)$ can be *crossed* in direction i if $w_t(x) \geq 1\{x \in \mathcal{B}_k\}$ for $t \geq |\mathcal{B}_k|$.

Hypothesis 2 (Box-crossing). *For each $\delta > 0$, there is k so that*

$$\min_{j \in \mathbb{Z}^d} \mathbf{P}(\mathcal{B}_k^{(j)}(\eta) \text{ can be crossed in each direction}) > 1 - \delta,$$

where

$$\bigcup_{j \in \mathbb{Z}^d} \mathcal{B}_k^{(j)} := \bigcup_{j \in \mathbb{Z}^d} (\mathcal{B}_k + jk) = \mathbb{Z}^d$$

is a tiling of the lattice by \mathcal{B}_k .

If η were recurrent, Hypothesis 2 would imply η explodes with probability 1. In particular, no holes would develop in the support of the odometer. (If unfamiliar, see Section 3.7 below

for the definition of recurrence, although this is not used here.) Our next hypothesis ensures this and more: any sufficiently long path of topplings fills its bounding rectangle.

Hypothesis 3 (Path-filling). *There exists a constant $\gamma > 0$ so that on an event of probability 1, for all $n \geq n_0$, and every path of distinct points, $[-n, n]^d \supset L_m := \{z_1, \dots, z_m\}$, $z_{i+1} \sim z_i$, of length $m \geq (\log n)^\gamma$ the following holds. The L_m -frozen parallel toppling odometer with initial conditions $w_0 = 1\{x \in L_m\}$ and $s'_0 = \eta$ quickly exceeds 1 on the bounding rectangle of L_m :*

$$w_t \geq 1\{\mathbf{br}(L_m)\} \quad \text{for } t \geq m^d.$$

In order for η to have a limit shape in dimensions $d \geq 3$, we need to strengthen Hypothesis 2. The next assumption prevents low-dimensional tendrils from burrowing through good cubes (for a counterexample in three-dimensions take a large cube filled with 4 and connect each of the faces with disjoint tunnels of 5). For a point $z \in \bar{\mathcal{B}}_k$ and direction $1 \leq i \leq d$, consider, as before, a line passing from one side of the box to the other

$$\mathcal{L}_k^{(i,z)} := \bigcup_{j=1, \dots, k_i} (z_1, \dots, z_{i-1}, j, z_{i+1}, \dots, z_d). \quad (3.47)$$

We say $\mathcal{B}_k(\eta)$ is *strongly box-crossing* if, for all $1 \leq i \leq d$ and $z \in \bar{\mathcal{B}}_k$, $w_{|k|} \geq 1\{x \in \mathcal{B}_k\}$, where w_t is the odometer for $\{\mathcal{B}_k^c \cup \mathcal{L}_k^{(i,z)}\}$ -frozen parallel toppling with initial conditions $w_0(x) = 1\{x \in \mathcal{L}_k^{(i,z)}\}$, $s'_0 = \eta$.

Hypothesis 4 (Strongly box-crossing). *For each $\delta > 0$, there is k so that, using the same notation as Hypothesis 2,*

$$\min_{j \in \mathbb{Z}^d} \mathbf{P}(\mathcal{B}_k^{(j)}(\eta) \text{ is strongly box-crossing}) > 1 - \delta.$$

We now have made enough assumptions to prove convergence of the last-wave as in Section 3.3.

Proposition 3.5.1 (Convergence of the last-wave). *Under Hypotheses 1, 3, and 4, on an event of probability 1, η is explosive and the rescaled last-wave arrival times, $n^{-1}\hat{T}_\eta([nx]) := n^{-1} \min\{t > 0 : u_t([nx]) > 0\}$ converge locally uniformly to \mathcal{N}_η , a continuous, convex, one-homogeneous function on \mathbb{R}^d .*

Proof. For $\delta > 0$ small, pick side length k from Hypotheses 4. For $j \in \mathbb{Z}^d$, let

$$X_j := \mathbf{1}\{\mathcal{B}_k^{(j)} \text{ is strongly box-crossing}\}.$$

By Theorem 0.0 in Liggett et al. [1997], $\{X_j\}_{j \in \mathbb{Z}^d}$ stochastically dominates a sequence of Bernoulli independent random variables $\{Y_j\}_{j \in \mathbb{Z}^d}$ with $P(Y_j = 1) \geq (1 - \pi(\delta))$ for $\pi : [0, 1] \rightarrow [0, 1]$ satisfying $\pi(\delta) \rightarrow 0$ as $\delta \rightarrow 0$. Therefore, for $\delta > 0$ sufficiently small, on an event of probability 1, $\{X_j\}_{j \in \mathbb{Z}^d}$ contains an infinite supercritical percolation cluster \mathcal{C}_∞ .

The rest of the argument follows almost exactly the proof in Section 3.3. The only minor change is in the proof of Lemma 3.3.1. We use $\eta \geq \eta_{\min}$ rather than $\eta \geq (2d - 2)$ and invoke Theorem 4.1 in Levine and Peres [2009] to get that the support of a (CR^d) -wave contains $[-R, R]^d$ (where the constant C is larger than before). \square

If additionally $\eta \geq (2d - 2)$, then the argument given in Section 3.4 implies that the exploding sandpile is close to the last-wave and hence converges. Simulations indicate $\eta \geq (2d - 2)$ is not necessary, however, we have not found an alternative condition and are forced to assume this:

Hypothesis 5 (Wave-approximation). *Suppose η is explosive, let u_t denote the last-wave, v_t the parallel toppling odometer for $\eta + M_\eta \delta_0$, and \hat{T}_η, T_η the respective arrival times. On an event of probability 1,*

$$\sup_{x \in [-n, n]^d} |\hat{T}_\eta(x) - T_\eta(x)| = o(n).$$

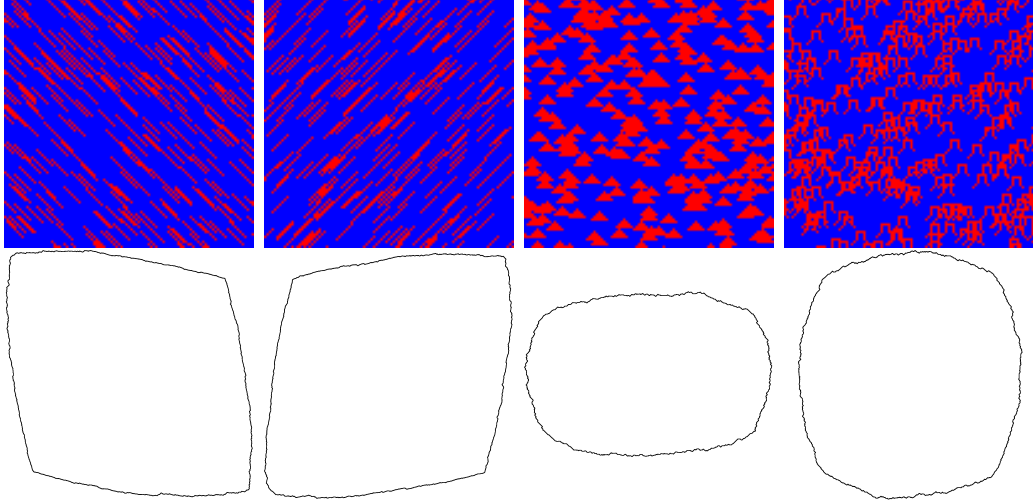


Figure 3.4: Initial random backgrounds and computed limit shapes. The random backgrounds are built from Bernoulli clouds of the indicated point sets. Blue is 2 chips and red is 3 chips.

Theorem 3.5.1 (Convergence of the exploding sandpile). *Under the assumptions in Proposition 3.5.1 and Hypothesis 5, on an event of probability 1, η is explosive and the rescaled arrival times, $n^{-1}T_\eta([nx]) := n^{-1} \min\{t > 0 : v_t([nx]) > 0\}$ converge locally uniformly to \mathcal{N}_η , a continuous, convex, one-homogeneous function on \mathbb{R}^d .*

Proof. Immediate from Hypothesis 5 and Proposition 3.5.1. \square

Remark 3. *Box-crossing with probability 1 implies η is recurrent (see Section 3.7 if unfamiliar). However, not every recurrent sandpile is explosive - take $\eta = (2d - 2)$ and use Fey et al. [2010] - and not every exploding sandpile has a recurrent initial condition - see Section 3.6.*

3.5.2 Examples satisfying the hypotheses

The simplest way to ensure Hypotheses 3 and 5 is to take $\eta \geq (2d - 2)$. A random background can be built which satisfies the rest of the hypotheses using a *Bernoulli cloud*, see Figure 3.4. Take $p > 0$, fix a finite set of points, $\mathcal{S} \subset \mathbb{Z}^d$ (say a triangle, circle, or a line), and independently sample a uniform random variable at each site on the lattice, $\{U_j\}_{j \in \mathbb{Z}^d}$. Then,

Draft Mar 13

let

$$\eta(x) := \begin{cases} (2d-1) & \text{if there exists } j \in \mathbb{Z}^d \text{ such that } U_j < p \text{ and } x \in \{\mathcal{S} + j\} \\ (2d-2) & \text{otherwise.} \end{cases} \quad (3.48)$$

Hypothesis 1 is satisfied as $|\mathcal{S}| < \infty$ and Hypothesis 4 as $p > 0$.

Another family of examples is the *random checkerboard*. Fix a box \mathcal{B} which tiles the lattice, $\mathbb{Z}^d = \bigcup_{j \in \mathbb{Z}^d} \mathcal{B}_j$. Take functions ζ_1, \dots, ζ_m , defined on the box, $\zeta_i : \mathcal{B} \rightarrow \{(2d-2), (2d-1)\}$. Suppose further that $\mathcal{B}(\zeta_1)$ contains at least one site with $(2d-1)$ chips along every straight line. Let $\{Y_j\}_{j \in \mathbb{Z}^d}$ be a field of i.i.d. random variables, where $P(Y_j = i) = p_i$, for $i = 1, \dots, m$. Then, let

$$\eta(x) := \zeta_i(z(x)) \quad \text{if } Y_{j(x)} = i, \quad (3.49)$$

where $z(x) \in \mathcal{B}$ is the position of x in its tiled box, $\mathcal{B}_{j(x)}$. Finite range of dependence is immediate by construction. If we further assume $p_1 > 0$, then Hypothesis 4 is satisfied by the assumption on $\mathcal{B}(\zeta_1)$.

The random checkerboard includes the degenerate case $p_1 = 1$, where η is a periodic copy

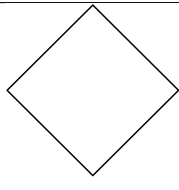
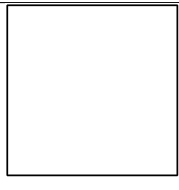
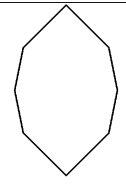
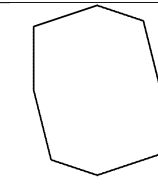
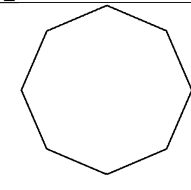
$[3]$	$\begin{bmatrix} 2 & 3 \\ 3 & 2 \end{bmatrix}$	$\begin{bmatrix} 3 & 2 & 3 \\ 2 & 3 & 3 \\ 3 & 2 & 3 \end{bmatrix}$	$\begin{bmatrix} 2 & 2 & 3 & 3 \\ 3 & 2 & 3 & 2 \\ 2 & 3 & 2 & 2 \\ 2 & 2 & 3 & 2 \end{bmatrix}$	$\begin{bmatrix} 3 & 2 & 3 & 3 & 3 \\ 2 & 2 & 3 & 3 & 3 \\ 2 & 2 & 3 & 2 & 2 \\ 3 & 3 & 2 & 2 & 2 \\ 3 & 3 & 3 & 2 & 3 \end{bmatrix}$
				

Table 3.1: Computed limited shapes of periodic, checkerboard backgrounds of the indicated box.

of ζ_1 . See Table 3.1 for pictures. In this case, if $\eta \geq (2d - 2)$ but is not box-crossing, then the background is not explosive by Theorem 4.2 in Fey et al. [2010]. However, it is possible to build random (and periodic) checkerboard, exploding sandpiles with $\eta \not\geq (2d - 2)$. One could then proceed in an adhoc manner to check the hypotheses. However, we have not found a general recipe in this case. The counterexample in Section 3.6 uses $\eta \not\geq (2d - 2)$.

3.6 Failure of convergence

In this section we construct a family of exploding sandpiles which fail to have a limit shape. As the construction indicates, the counterexample is stable: it can be random or periodic.

Theorem 3.6.1. *For each $d \geq 2$, there are explosive backgrounds $\eta \not\geq (2d - 2)$ which fail to have a limit shape; the first arrival times $\mathcal{T}(n) := \min\{t > 0 : v_t(ne_1) > 0\}$ do not converge,*

$$\limsup_{n \rightarrow \infty} n^{-1} \mathcal{T}(n) \geq 3/2 \quad (3.50)$$

and

$$\liminf_{n \rightarrow \infty} n^{-1} \mathcal{T}(n) = 1. \quad (3.51)$$

We explicitly demonstrate a family of checkerboard backgrounds which are explosive but do not have a limit shape. Our counterexample is essentially a two-dimensional one. After constructing it in two dimensions, we embed it into higher-dimensions and show failure of convergence by comparison with the two-dimensional counterexample.

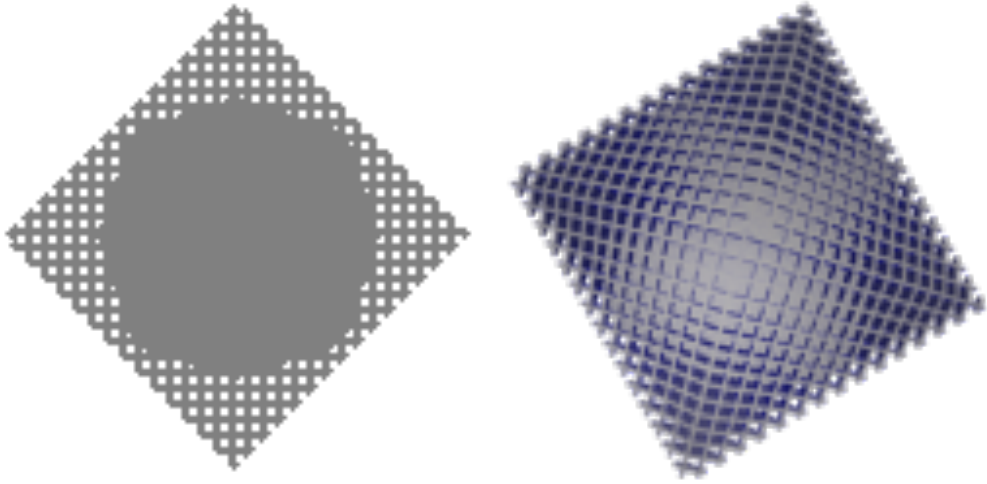


Figure 3.5: The counterexample from Theorem 3.6.1 for $d = 2$ and $d = 3$.

3.6.1 Counterexample in dimension two

We use the notation of Section 3.5. Let $\mathcal{B} := \{x \in \mathbb{Z}^2 : 0 \leq x \leq 3\}$ denote a box of side length 4 and take $\zeta_1, \zeta_2 : \mathcal{B} \rightarrow \{1, 3\}$ as

$$\zeta_1 := \begin{bmatrix} 1 & 3 & 3 & 1 \\ 3 & 3 & 3 & 3 \\ 3 & 3 & 3 & 3 \\ 1 & 3 & 3 & 1 \end{bmatrix} \quad \zeta_2 := \begin{bmatrix} 1 & 3 & 3 & 1 \\ 3 & 2 & 3 & 3 \\ 3 & 3 & 3 & 3 \\ 1 & 3 & 3 & 1 \end{bmatrix},$$

where the lower-left corner of the box is $(0, 0)$ and left-to-right and down-to-up are increasing. Let η be an arbitrary tiling of ζ_1, ζ_2 ; for example, η could be a sample from the random checkerboard measure. Fix coordinates so that

$$\eta(x_1, x_2) = \zeta_i(x_1 \bmod 4, x_2 \bmod 4).$$

Let v_t be the sequence of parallel toppling odometers for $s_0 = \eta + 3\delta_0$. We first verify (3.51).

Step 1: Proof of (3.51)

We show for all $n \geq 0$

$$(4n + 1) \leq \mathcal{T}(4n + 1) \leq 4n + 4. \quad (3.52)$$

By inspection, $v_1(0) = 1$ and $v_2(e_1) = v_2(e_2) = 1$. Now, take $n \geq 1$ and observe that there is a line of 3s connecting e_2 to $(e_2 + (4n + 1)e_1)$. Thus, $v_{4n+3}(e_2 + (4n + 1)e_1) = 1$ and $v_{4n+4}((4n + 1)e_1) = 1$. The lower bound is immediate from $\eta \leq (2d - 1)$ - a site can fire only if a neighbor has fired previously.

Step 2: η is explosive

We construct a toppling procedure dominated by v_t which transforms η into a configuration η' which is not stabilizable. We may topple the origin, every 3, then 2, and then the 2×2 box of 1s containing the origin,

$$\eta' := \eta + \Delta(\{1\{\eta \geq 2\} + \delta_0 + \delta_{-e_1} + \delta_{-e_2} + \delta_{-e_1-e_2}\}).$$

The resulting configuration is (away from the origin) a tiling of $\zeta'_1, \zeta'_2 : \mathcal{B} \rightarrow \{2, 3\}$,

$$\zeta'_1 := \begin{bmatrix} 3 & 2 & 2 & 3 \\ 2 & 3 & 3 & 2 \\ 2 & 3 & 3 & 2 \\ 3 & 2 & 2 & 3 \end{bmatrix} \quad \zeta'_2 := \begin{bmatrix} 3 & 2 & 2 & 3 \\ 2 & 2 & 3 & 2 \\ 2 & 3 & 3 & 2 \\ 3 & 2 & 2 & 3 \end{bmatrix}. \quad (3.53)$$

Remark 4. *The reason why convergence fails for this counterexample is that the limit shape of the explosive background η' is not a diamond. See Figure 3.5. When $d = 2$ the limit shape is a regular octagon with boundary $\max(|x - y/3|, |x + y/3|, |x/3 - y|, |x/3 + y|)$, but we will not prove this.*

Both ζ'_1 and ζ'_2 are box-crossing, so we just check that we can construct a sequence of firings to the outer face of a box away from the origin dominated by v_t . The box containing the origin is at least

$$\eta'(0 : 3, 0 : 3) \geq \begin{bmatrix} 3 & 2 & 2 & 3 \\ 2 & 2 & 3 & 2 \\ 3 & 3 & 3 & 2 \\ 1 & 3 & 2 & 3 \end{bmatrix}.$$

From this we see that $3\delta_0 + \eta'$ is not stabilizable - in a finite number of steps every site in $(0 : 3, 0 : 3)$ will fire.

Step 3: Reductions

Before proving (3.50), we make several reductions. We seek to lower bound \mathcal{T} , therefore, we are free to add to η as this will only decrease the arrival time. First, we may suppose all of the boxes are ζ_1 rather than ζ_2 .

We then increment the background so as to reduce to a sandpile on a cylinder, $\mathcal{C} := \{x \in \mathbb{Z}^2 : x_1 \geq 0, 3 \geq x_2 \geq 0\}$. Specifically, let $\zeta : \mathcal{C} \rightarrow \{1, 3, 4\}$,

$$\zeta := \begin{bmatrix} 1 & 3 & 3 & 1 \\ 3 & 3 & 3 & 3 \\ 3 & 3 & 3 & 3 \\ 4 & 3 & 3 & 1 \end{bmatrix} \zeta_1 \quad \dots$$

with the origin, $(0, 0)$, on the bottom left with left-to-right, down-to-up increasing. To periodically tile by ζ : set for $x_1 \geq 0$,

$$\hat{\eta}(x_1, x_2) := \zeta(x_1, x_2 \bmod 4)$$

and for $x_1 < 0$,

$$\hat{\eta}(x_1, x_2) := \hat{\eta}(-(x_1 + 1), x_2).$$

Note that $\hat{\eta} \geq \eta$.

The structure of $\hat{\eta}$ allows us to reduce to a symmetrized Laplacian on the cylinder \mathcal{C} (see for example Lemma 2.3 in Bou-Rabee [2022]) with reflecting boundaries at $x_1 = 0$: $v_t(-1, x_2) = v_t(0, x_2)$ and torus boundary conditions for $x_2 \in \{0, 3\}$: $v_t(x_1, -1) = v_t(x_1, 3)$ and $v_t(x_1, 4) = v_t(x_1, 0)$. This defines the *symmetrized* Laplacian Δ and nearest neighbors $y \sim x$ on \mathcal{C} .

Let $\tilde{u}(x) : \mathcal{C} \rightarrow \{0, 1\}$ be $\tilde{u}(x) := 1\{\hat{\eta}(x) \geq 3\}$. Then,

$$\Delta \tilde{u} + \zeta = \begin{bmatrix} 4 & 2 & 2 & 3 \\ 2 & 3 & 3 & 2 \\ 3 & 3 & 3 & 2 \\ 3 & 3 & 2 & 3 \end{bmatrix} \zeta'_1 \quad \zeta'_1 \quad \cdots =: \zeta'.$$

Let $v_t : \mathcal{C} \rightarrow \mathbb{N}$ be the symmetrized parallel toppling odometer for ζ and $w_t : \mathcal{C} \rightarrow \mathbb{N}$ the same for $\hat{\eta}'$ (defined with ζ' as $\hat{\eta}$ was with ζ). We claim that

$$\mathcal{T}'(3 + 8n) \leq \mathcal{T}(3 + 8n), \tag{3.54}$$

where $\mathcal{T}'(n) := \min\{t > 0 : w_t(ne_1) > 0\}$. In fact, we claim

$$v_t \leq w_t + \tilde{u} \tag{3.55}$$

for all $t \geq 0$. This includes (3.54) as $\tilde{u}((3 + 8n)e_1) = 0$. We observe (3.55) is a consequence

of induction: the base case $t = 0$ is automatic and the inductive step is,

$$\begin{aligned} v_{t+1}(x) &= \lfloor \frac{\sum_{y \sim x} v_t(y) + \zeta(x)}{4} \rfloor \\ &\leq \lfloor \frac{\sum_{y \sim x} (w_t(y) + \tilde{u}(y)) + \zeta(x)}{4} \rfloor \\ &= \tilde{u}(x) + \lfloor \frac{\sum_{y \sim x} w_t(y) + \Delta\tilde{u}(x) + \zeta(x)}{4} \rfloor \\ &= \tilde{u}(x) + w_{t+1}(x). \end{aligned}$$

Step 4: Proof of (3.50)

We show for all $n \geq 1$,

$$\mathcal{T}'(3 + 8n) \geq 12n. \quad (3.56)$$

We do so by building a ‘pulsating front’ for w_t in the horizontal direction. (Readers interested in pulsating fronts in periodic media on \mathbb{R}^d may see Section 2.2 of Xin [2009].)

We first reduce to the last-wave for w_t , \hat{w}_t , with initial conditions $\hat{w}_0 = \delta_{(0,3)}$ and $\hat{s}_0 = \zeta' + \Delta\hat{w}_0$. The justification is identical to Step 1 of the proof of Proposition 3.4.1 and so is omitted. Using $\hat{w}_t \leq 1$, we make another reduction to initial condition $\hat{w}_0 : \mathcal{C} \rightarrow \{0, 1\}$,

$$\hat{w}_0 = \begin{bmatrix} 1 & 1 & 1 & 1 \\ 1 & 1 & 1 & 0 \\ 1 & 1 & 1 & 0 \\ 1 & 1 & 1 & 1 \end{bmatrix} \quad \mathbf{0} \quad \mathbf{0} \quad \dots.$$

We now show, by manual computation, that the configuration of the odometer at the front, the rightmost 4×4 box in \mathcal{C} containing a site which has toppled, is 12-periodic in time. For

Draft Mar 13

notational ease, we denote sites which have toppled by *,

$$\begin{aligned}
\hat{s}_0 &= \left[\begin{array}{ccccccccc} * & * & * & * & 4 & 2 & 2 & 3 & 3 & 2 & 2 & 3 \\ * & * & * & 4 & 2 & 3 & 3 & 2 & 2 & 3 & 3 & 2 \\ * & * & * & 4 & 2 & 3 & 3 & 2 & 2 & 3 & 3 & 2 \\ * & * & * & * & 4 & 2 & 2 & 3 & 3 & 2 & 2 & 3 \end{array} \dots \right] & \hat{s}_7 &= \left[\begin{array}{ccccccccc} * & * & * & * & * & * & * & * & * & 3 & 2 & 3 \\ * & * & * & * & * & * & * & * & * & 4 & 3 & 3 & 2 \\ * & * & * & * & * & * & * & * & * & 3 & 2 & 3 \\ * & * & * & * & * & * & * & * & * & 3 & 2 & 3 \end{array} \dots \right] \\
\hat{s}_1 &= \left[\begin{array}{ccccccccc} * & * & * & * & 3 & 2 & 3 & 3 & 2 & 2 & 3 \\ * & * & * & * & 4 & 3 & 3 & 2 & 2 & 3 & 3 & 2 \\ * & * & * & * & 4 & 3 & 3 & 2 & 2 & 3 & 3 & 2 \\ * & * & * & * & * & 3 & 2 & 3 & 3 & 2 & 2 & 3 \end{array} \dots \right] & \hat{s}_8 &= \left[\begin{array}{ccccccccc} * & * & * & * & * & * & * & * & * & 3 & 2 & 3 \\ * & * & * & * & * & * & * & * & * & 4 & 3 & 2 \\ * & * & * & * & * & * & * & * & * & 4 & 3 & 2 \\ * & * & * & * & * & * & * & * & * & 3 & 2 & 3 \end{array} \dots \right] \\
\hat{s}_2 &= \left[\begin{array}{ccccccccc} * & * & * & * & 3 & 2 & 3 & 3 & 2 & 2 & 3 \\ * & * & * & * & 4 & 3 & 2 & 2 & 3 & 3 & 2 \\ * & * & * & * & 4 & 3 & 2 & 2 & 3 & 3 & 2 \\ * & * & * & * & * & 3 & 2 & 3 & 3 & 2 & 2 & 3 \end{array} \dots \right] & \hat{s}_9 &= \left[\begin{array}{ccccccccc} * & * & * & * & * & * & * & * & * & 4 & 2 & 3 \\ * & * & * & * & * & * & * & * & * & 4 & 2 \\ * & * & * & * & * & * & * & * & * & 4 & 2 \\ * & * & * & * & * & * & * & * & * & 4 & 2 & 3 \end{array} \dots \right] \\
\hat{s}_3 &= \left[\begin{array}{ccccccccc} * & * & * & * & 4 & 2 & 3 & 3 & 2 & 2 & 3 \\ * & * & * & * & * & 4 & 2 & 2 & 3 & 3 & 2 \\ * & * & * & * & * & 4 & 2 & 2 & 3 & 3 & 2 \\ * & * & * & * & * & 4 & 2 & 3 & 3 & 2 & 2 & 3 \end{array} \dots \right] & \hat{s}_{10} &= \left[\begin{array}{ccccccccc} * & * & * & * & * & * & * & * & * & 4 & 3 \\ * & * & * & * & * & * & * & * & * & 3 \\ * & * & * & * & * & * & * & * & * & 3 \\ * & * & * & * & * & * & * & * & * & 4 & 3 \end{array} \dots \right] \\
\hat{s}_4 &= \left[\begin{array}{ccccccccc} * & * & * & * & * & 4 & 3 & 3 & 2 & 2 & 3 \\ * & * & * & * & * & * & 3 & 2 & 3 & 3 & 2 \\ * & * & * & * & * & * & 3 & 2 & 3 & 3 & 2 \\ * & * & * & * & * & * & 4 & 3 & 3 & 2 & 2 & 3 \end{array} \dots \right] & \hat{s}_{11} &= \left[\begin{array}{ccccccccc} * & * & * & * & * & * & * & * & * & 4 \\ * & * & * & * & * & * & * & * & * & 3 \\ * & * & * & * & * & * & * & * & * & 3 \\ * & * & * & * & * & * & * & * & * & 4 \end{array} \dots \right] \\
\hat{s}_5 &= \left[\begin{array}{ccccccccc} * & * & * & * & * & * & 4 & 3 & 2 & 2 & 3 \\ * & * & * & * & * & * & 3 & 2 & 3 & 3 & 2 \\ * & * & * & * & * & * & 3 & 2 & 3 & 3 & 2 \\ * & * & * & * & * & * & 4 & 3 & 2 & 2 & 3 \end{array} \dots \right] & \hat{s}_{12} &= \left[\begin{array}{ccccccccc} * & * & * & * & * & * & * & * & * & * \\ * & * & * & * & * & * & * & * & * & 4 \\ * & * & * & * & * & * & * & * & * & 4 \\ * & * & * & * & * & * & * & * & * & * \end{array} \dots \right]. \end{aligned}$$

This shows that

$$\hat{w}_{12} = \begin{bmatrix} 1 & 1 & 1 & 1 & 1 & 1 & 1 & 1 & 1 & 1 & 1 & 1 \\ 1 & 1 & 1 & 1 & 1 & 1 & 1 & 1 & 1 & 1 & 1 & 0 \\ 1 & 1 & 1 & 1 & 1 & 1 & 1 & 1 & 1 & 1 & 1 & 0 \\ 1 & 1 & 1 & 1 & 1 & 1 & 1 & 1 & 1 & 1 & 1 & 1 \end{bmatrix} \mathbf{0} \quad \mathbf{0} \quad \dots,$$

so the odometer at the front is identical to what it was at the start and the process ‘resets’.

Hence, by induction on n ,

$$\hat{T}(3 + 8n) = 12n, \quad (3.57)$$

where $\hat{T}(n) := \min\{t > 0 : \hat{w}_t(ne_1) > 0\}$. This implies (3.56), completing the proof by (3.54).

3.6.2 Counterexample in dimensions larger than two

Let $\eta^{(2D)} : \mathbb{Z}^2 \rightarrow \{1, 2, 3\}$ be the random background defined in Section 3.6.1 and let $d \geq 3$ be given. Our higher-dimensional counterexample $\eta : \mathbb{Z}^d \rightarrow \{2d - 3, 2d - 2, 2d - 1\}$ is built

by stacking the two-dimensional one,

$$\eta(x_1, x_2, \dots, x_d) = 2(d-2) + \eta^{(2D)}(x_1, x_2) \text{ for all } x \in \mathbb{Z}^d. \quad (3.58)$$

Step 1: Proof of (3.51)

The argument is identical to $d = 2$.

Step 2: η is explosive

Let $\eta'^{(2D)}$ be the tiling of ζ'_1, ζ'_2 , defined in (3.53). The higher-dimensional analogue, $\eta' : \mathbb{Z}^d \rightarrow \{2d-3, 2d-2, 2d-1\}$ is also stacked,

$$\eta'(x_1, x_2, \dots, x_d) := \eta'^{(2D)}(x_1, x_2) + 2(d-2). \quad (3.59)$$

The argument is as before: we construct a toppling procedure dominated by v_t , the parallel toppling odometer for η , that transforms η into η' . Since $3\delta_0 + \eta' \geq (2d-2)$ is box-crossing, it is not stabilizable.

Topple the origin, all sites with $(2d-1)$ chips, then all sites with $(2d-2)$, then the column of $(2d-3)$ near the origin. Let \tilde{u} denote the odometer for this and $\tilde{u}^{(2D)}$ the two-dimensional

version and observe that $\tilde{u}(x_1, x_2, \dots, x_d) = \tilde{u}^{(2D)}(x_1, x_2)$. This implies,

$$\begin{aligned}
& \sum_{i=1}^d (\tilde{u}(x - e_i) + \tilde{u}(x + e_i) - 2\tilde{u}(x)) + \eta \\
&= \sum_{i=1}^2 (\tilde{u}^{(2D)}(x - e_i) + \tilde{u}^{(2D)}(x + e_i) - 2\tilde{u}^{(2D)}(x)) + \eta \\
&= \sum_{i=1}^2 (\tilde{u}^{(2D)}(x - e_i) + \tilde{u}^{(2D)}(x + e_i) - 2\tilde{u}^{(2D)}(x)) + \eta^{(2D)} + 2(d-2) \\
&= \eta'^{(2D)} + 2(d-2) \\
&= \eta'.
\end{aligned}$$

We conclude by observing η' is box-crossing as $3\delta_0 + \eta' \geq (2d-2)$ and every layer in the box $\mathbf{B}^{(d)} := \{x \in \mathbb{Z}^d : 0 \leq x \leq 3\}$, contains at least one site with $(2d-1)$ chips. Indeed, for all $(3, 3, \mathbf{x}_{d-2}) \in \mathbf{B}^{(d)}$,

$$\eta'(3, 3, \mathbf{x}_{d-2}) = \eta'^{(2D)}(3, 3) + 2(d-2) = (2d-1),$$

and every layer in $\eta'^{(2D)}$ has at least one site with 3 chips.

Step 3: Proof of (3.50)

Let $v_t^{(2D)}$ be the parallel toppling odometer for $\eta^{(2D)}$. By (3.56) it suffices to show that

$$v_t(x_1, x_2, \dots, x_d) \leq v_t^{(2D)}(x_1, x_2). \quad (3.60)$$

This is a consequence of the parabolic least action principle (Lemma 2.3 in Bou-Rabee [2022]) but we provide a self-contained proof here:

Suppose (3.60) holds at time t and we want to show it holds at $(t+1)$. Let x be given.

If $v_t(x) < v_t^{(2D)}(x_1, x_2)$ we are done. Hence, we may suppose $v_t(x) = v_t^{(2D)}(x_1, x_2)$ and

$$\Delta v_t(x) + \eta = \sum_{i=1}^d (v_t(x + e_i) + v_t(x - e_i) - 2v_t(x)) + \eta \geq 2d.$$

By (3.60) at time t , this implies

$$\sum_{i=1}^2 (v_t^{(2D)}((x_1, x_2) + e_i) + v_t^{(2D)}((x_1, x_2) - e_i) - 2v_t^{(2D)}(x_1, x_2)) + \eta \geq 2d,$$

and by (3.58),

$$\Delta v_t^{(2D)}(x_1, x_2) + \eta^{(2D)}(x_1, x_2) \geq 2d - 2 \cdot (d - 2) = 4,$$

completing the proof.

3.7 A criteria for exploding

Let $(\Omega, \mathcal{F}, \mathbf{P})$ be a probability space of sandpile backgrounds defined in Section 3.5. For a finite domain $V \subset \mathbb{Z}^d$, we say $\eta : V \rightarrow \mathbb{Z}$ is *recurrent* if the firing of ∂V causes every site in V to eventually topple. Specifically, the V^c -frozen parallel toppling odometer for initial conditions $w_0 = 1\{x \in \partial V\}$, $s'_0 = \eta$, is eventually 1 on V : $w_t(V) = 1$ for $t \geq |V|$. We say $\eta : \mathbb{Z}^d \rightarrow \mathbb{Z}$ is recurrent if its restriction to V is recurrent for every finite $V \subset \mathbb{Z}^d$. The measure \mathbf{P} is recurrent if $\mathbf{P}(\eta \text{ is recurrent}) = 1$. The arguments in Section 3.5 imply the following criteria.

Proposition 3.7.1. *If Hypotheses 1 and 2 are satisfied and \mathbf{P} is recurrent then \mathbf{P} is explosive.*

In this section, we use Proposition 3.7.1 to prove Theorem 3.1.4. Let \mathbf{P} denote a product measure with $\mathbf{P}(\eta \geq d) = 1$ and $\mathbf{P}(\eta = 2d - 1) > 0$. We show that \mathbf{P} is recurrent and box-crossing. Both arguments require a form of dimensional reduction, which we record in

Draft Mar 13

the first subsection. Also, by monotonicity, we may assume $\eta \rightarrow \{d, 2d - 1\}$.

3.7.1 Dimensional reduction

Let $Q_n^{(d)} := \{x \in \mathbb{Z}^d : 1 \leq x \leq n\}$ and denote each of the (internal) $2d$ faces of $Q_n^{(d)}$ as

$$\begin{aligned}\mathcal{F}_i(Q_n^{(d)}) &:= \{x \in Q_n^{(d)} : x_i = 1\} \\ \mathcal{F}_{d+i}(Q_n^{(d)}) &:= \{x \in Q_n^{(d)} : x_i = n\}.\end{aligned}\tag{3.61}$$

We show that after firing the outer boundary of $\mathcal{F}_i(Q_n^{(d)})$, the sandpile dynamics on $\mathcal{F}_i(Q_n^{(d)})$ can be coupled with $(d-1)$ -dimensional sandpile dynamics on $Q_n^{(d-1)}$.

Specifically, fix $i = 1$, and for each $x \in \mathcal{F}_1(Q_n^{(d)})$ write $x = (1, \mathbf{x}_{d-1})$. Let the initial d -dimensional background be given, $\eta^{(d)} : Q_n^{(d)} \rightarrow \mathbb{Z}$. Let $s_t^{(d-1)}, u_t^{(d-1)}$, and $s_t^{(d)}, u_t^{(d)}$ be the sequence of $(Q_n^{(d)})^c, (Q_n^{(d-1)})^c$ frozen toppling processes with initial conditions,

$$\begin{aligned}u_0^{(d)}(0, \mathbf{x}_{d-1}) &= 1 \\ u_0^{(d-1)}(\mathbf{x}_{d-1}) &= u_0^{(d)}(1, \mathbf{x}_{d-1}) \\ s_0^{(d)}(1, \mathbf{x}_{d-1}) &= \Delta u_0^{(d)}(1, \mathbf{x}_{d-1}) + \eta^{(d)}(1, \mathbf{x}_{d-1}) \\ s_0^{(d-1)}(\mathbf{x}_{d-1}) &= \eta^{(d)}(\mathbf{x}_{d-1}) - 1 := \eta^{(d-1)}(\mathbf{x}_{d-1})\end{aligned}\tag{3.62}$$

and constraints,

$$\begin{aligned}u_t^{(d)}(x_1, \mathbf{x}_{d-1}) &= 0 \quad \text{for all } x_1 > 1 \\ u_t^{(d)}(1, \mathbf{x}_{d-1}) &\leq 1 \\ u_t^{(d-1)}(\mathbf{x}_{d-1}) &\leq 1,\end{aligned}\tag{3.63}$$

for all $t \geq 0$. We prove the following by an induction on time. Note that a symmetric result holds for every face.

Proposition 3.7.2. For all $t \geq 0$ and $(1, \mathbf{x}_{d-1}) \in \mathcal{F}_1(Q_n^{(d)})$,

$$u_t^{(d)}(1, \mathbf{x}_{d-1}) = u_t^{(d-1)}(\mathbf{x}_{d-1}) \quad (3.64)$$

and

$$s_t^{(d)}(1, \mathbf{x}_{d-1}) = s_t^{(d-1)}(\mathbf{x}_{d-1}) + 2 \quad \text{if } u_t^{(d)}(1, \mathbf{x}_{d-1}) = 0. \quad (3.65)$$

Proof. For all $t \geq 0$, if $u_t^{(d)}(1, \mathbf{x}_{d-1}) = 0$ and $u_t^{(d)}(1, \mathbf{y}_{d-1}) = u_t^{(d-1)}(\mathbf{y}_{d-1})$ for all \mathbf{y}_{d-1} ,

$$\begin{aligned} & s_t^{(d)}(1, \mathbf{x}_{d-1}) \\ &= \eta^{(d)}(1, \mathbf{x}_{d-1}) \\ &+ \left(-2u_t^{(d)}(1, \mathbf{x}_{d-1}) + u_t^{(d)}(0, \mathbf{x}_{d-1}) + u_t^{(d)}(2, \mathbf{x}_{d-1}) \right) \\ &+ \sum_{i=2}^d \left(u_t^{(d)}((1, \mathbf{x}_{d-1}) + e_i) + u_t^{(d)}((1, \mathbf{x}_{d-1}) - e_i) - 2u_t^{(d)}(1, \mathbf{x}_{d-1}) \right) \\ &= \eta^{(d-1)}(\mathbf{x}_{d-1}) + 2 \\ &+ \sum_{i=1}^{d-1} \left(u_t^{(d-1)}(\mathbf{x}_{d-1} + e_i) + u_t^{(d-1)}(\mathbf{x}_{d-1} - e_i) - 2u_t^{(d-1)}(\mathbf{x}_{d-1}) \right) \\ &= s_t^{(d-1)}(\mathbf{x}_{d-1}) + 2. \end{aligned}$$

Therefore, we may begin the induction and suppose (3.64) and (3.65) hold at time t . If $s_t^{(d-1)}(\mathbf{x}_{d-1}) \geq 2(d-1) = (2d-2)$, then $s_t^{(d)}(1, \mathbf{x}_{d-1}) = 2d$. The other direction is identical, showing $u_{t+1}^{(d)}(1, \mathbf{x}_{d-1}) = u_{t+1}^{(d-1)}(\mathbf{x}_{d-1}) = 1$ in this case.

□

3.7.2 The measure is recurrent

By monotonicity of recurrence, it suffices to prove the following.

Proposition 3.7.3. For every $d \geq 1$, $\eta : \mathbb{Z}^d \rightarrow \{d\}$ is recurrent.

Proof. By consistency of recurrence, it suffices to show this for domains which are cubes (see for example Remark 3.2.1 in Redig [2005]). Write $Q_n^{(d)}$ for a cube of side length n in \mathbb{Z}^d . We induct on dimension, then cube side length. The base case for dimension $d = 1$ is immediate. Moreover, the base case $n = 2$ is also immediate for every dimension. It remains to check $\eta : Q_n^{(d)} \rightarrow \{d\}$ is recurrent given $\eta : Q_{n-2}^{(d)} \rightarrow \{d\}$ is recurrent.

We decompose the cube into its faces and an inner cube,

$$Q_n^{(d)} = Q_{n-2}^{(d)} \cup \bigcup_{i=1}^{2d} \mathcal{F}_i(Q_n^{(d)}). \quad (3.66)$$

By the inductive hypotheses on n , once every external face of $Q_{n-2}^{(d)}$ is toppled, every site in $Q_{n-2}^{(d)}$ eventually fires. Therefore, by (3.66), it suffices to check that every site in $\mathcal{F}_i(Q_n^{(d)})$ fires after the boundary of $Q_n^{(d)}$ fires. This, however, is a consequence of the inductive hypothesis on dimension and Proposition 3.7.2, any site in $\mathcal{F}_i(Q_n^{(d)})$ which topples for the $(d - 1)$ -dimensional process also topples in d -dimensions.

□

Remark 5. *The argument given here is similar to the proof of Lemma 3.1 in Schonmann [1992].*

3.7.3 The measure is box-crossing

A coupling between the sandpile and bootstrap percolation has been observed before Fey et al. [2010]. Bootstrap percolation is a cellular automata on \mathbb{Z}^d with a random initial state and a deterministic update rule. Every site $x \in \mathbb{Z}^d$ starts off as *infected* independently at random with probability p . Infected sites remain infected and if an uninfected site contains at least d neighbors which are infected, it becomes infected.

These dynamics exactly match parallel toppling for a background $\eta' : \mathbb{Z}^d \rightarrow \{d, 2d\}$ where sites are constrained to topple at most once. Infected sites are those which have toppled,

and sites with $2d$ chips start as infected. Indeed, any site beginning with d chips topples if and only if it has at least d neighbors which have toppled.

Our proof that \mathbf{P} is box-crossing uses this coupling together with a large deviation result of Schonmann. Borrowing the terminology of Schonmann, we say a cube $Q_n^{(d)} \subset \mathbb{Z}^d$ is η' -internally spanned if the $(Q_n^{(d)})^c$ -frozen parallel toppling procedure with $u_0 = 0$, $s'_0 = \eta'$, and sites constrained to topple at most once, concludes with every site in $Q_n^{(d)}$ toppling.

Proposition 3.7.4 (Schonmann [1992]). *Let*

$$\eta'(x) := \begin{cases} 2d & \text{with probability } p \\ d & \text{otherwise.} \end{cases}$$

There are constants c, C depending only on dimension and $p > 0$ so that

$$P(Q_n^{(d)} \text{ is } \eta'\text{-internally spanned}) \geq 1 - c \exp(-Cn). \quad (3.67)$$

We use Proposition 3.7.4 to show \mathbf{P} is box-crossing.

Proposition 3.7.5. *In all dimensions, \mathbf{P} is box-crossing*

Proof. The claim is immediate in dimension one. Let $(d+1) \geq 2$ be given. For $n \geq 1$, decompose the box into layers

$$Q_n^{(d+1)} = \bigcup_{i=1}^n \mathcal{L}_i,$$

where $\mathcal{L}_i := \{x \in Q_n^{(d+1)} : x = (i, \mathbf{x}_d)\}$. The projection of each layer to a d -dimensional box is $\mathcal{L}_i^{(d)}$. Let

$$\Omega'_i := \{\eta : \mathcal{L}_i^{(d)} \text{ is } \eta'\text{-internally spanned where } \eta'(\mathbf{x}_d) := \eta(i, \mathbf{x}_d) - 1\}$$

and let

$$\Omega' := \cap_{i=1}^n \Omega_i.$$

By definition of being internally spanned and Proposition 3.7.2, if $\eta \in \Omega'$, then $Q_n^{(d+1)}(\eta)$ can be crossed in direction e_1 . We conclude by symmetry and Proposition 3.7.4.

□

DraftMar13

CHAPTER 4

INTEGER SUPERHARMONIC MATRICES ON THE F-LATTICE

This chapter is based on the submitted article Bou-Rabee [2021c].

4.1 Introduction

The F -lattice is a directed periodic planar graph (\mathbb{Z}^2, E) , where

$$\begin{cases} (x \pm e_1, x) \in E & \text{if } x_1 + x_2 \equiv 0 \pmod{2} \\ (x \pm e_2, x) \in E & \text{otherwise,} \end{cases}$$

and e_1, e_2 are the standard basis vectors in \mathbb{Z}^2 . A function $g : \mathbb{Z}^2 \rightarrow \mathbb{Z}$ is *integer superharmonic* if

$$\Delta g(x) := \sum_{(y,x) \in E} (g(y) - g(x)) \leq 0, \quad (4.1)$$

for all $x \in \mathbb{Z}^2$. The *quadratic growth* of g is specified by a 2×2 symmetric matrix $A \in \mathbf{S}^2$,

$$g(x) = \frac{1}{2}x^T Ax + o(|x|^2). \quad (4.2)$$

When g is integer superharmonic and has quadratic growth A , we say that it is an *integer superharmonic representative* of A and A is an *integer superharmonic matrix*. Moreover, g is *recurrent* if whenever $f : \mathbb{Z}^2 \rightarrow \mathbb{Z}$ is integer superharmonic and $X \subset \mathbb{Z}^2$ is finite and strongly connected (with respect to E),

$$\sup_X (g - f) \leq \sup_{\partial X} (g - f), \quad (4.3)$$

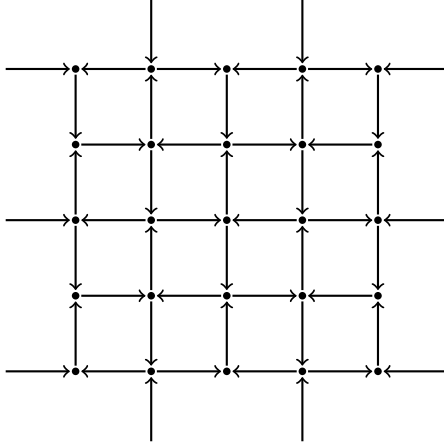


Figure 4.1: A 5×5 section of the F -lattice

where $\partial X = \{y \in \mathbb{Z}^2 : \text{there is } x \in X \text{ with } (y, x) \in E\}$. We call an integer superharmonic representative of A which is recurrent an *odometer* for A .

In this chapter we demonstrate an explicit characterization of integer superharmonic matrices on the F -lattice via a recursive construction of their odometers.

4.1.1 Background

Any periodic Euclidean directed graph, (V, E) , defines a set of integer superharmonic matrices. The scaling limit of deterministic sandpiles on (V, E) is characterized by the set of integer superharmonic matrices; in particular, the fractal structure of large sandpiles is dependent on the graph upon which the sandpile is run. In a tour de force, Levine, Pegden, and Smart showed that the set of integer superharmonic matrices on the square lattice, \mathbb{Z}^2 with nearest neighbor edges, is the downwards closure of an Apollonian circle packing Levine et al. [2017]. This led to an understanding of the fractal patterns appearing in sandpile experiments, Levine et al. [2016b], Pegden and Smart [2020], something which had evaded physicists and mathematicians for decades Liu et al. [1990], Le Borgne and Rossin [2002], Ostojic [2003].

Levine-Pegden-Smart's proof in Levine et al. [2017] involved explicitly constructing an

odometer for each circle in an Apollonian band packing. Their construction mirrored the Soddy recursive generation of Apollonian circle packings — it pieced together later odometers from earlier ones. In this chapter, we also recursively construct odometers, but the recursion follows rational points on a hyperbola rather than curvatures in an Apollonian packing. Our choice of lattice also highlights several other coincidences which occur for \mathbb{Z}^2 and forces us to develop new proof techniques which may generalize. We discuss these possible generalizations in Section 4.1.3 and provide a detailed proof overview in Section 4.2.

The patterns which appear in s_n on the F -lattice have also been investigated by mathematical physicists with notable contributions made by Caracciolo, Paoletti, Sportiello Caracciolo et al. [2008], Paoletti [2013] and Dhar, Sadhu, Chandra Dhar et al. [2009], Dhar and Sadhu [2013, 2010], Sadhu and Dhar [2011]. This chapter provides a new perspective on their results. For example, the patterns which appear in their experiments correspond empirically to the Laplacians of our constructed odometers. In fact, an immediate consequence of Theorems 4.1.1 and 4.1.2 is that the weak-* limit of the sandpile identity on ellipsoidal domains is constant Melchionna [2020]. We leave open, but expect that these results can also be used to construct more elaborate sandpile fractals as in Levine et al. [2016b]. Moreover, it is a difficult open problem to construct the weak-* limit of the single-source sandpile on the square lattice. It would be interesting to see if the relatively simple structure of the sandpile PDE here can be used to make progress on this for the F -lattice.

4.1.2 Main results

Our primary result is that the set of integer superharmonic matrices on the F -lattice is the downwards closure of an overlapping circle packing.

Theorem 4.1.1. $A \in \mathbf{S}^2$ is integer superharmonic if and only if the difference

$$\frac{1}{2} \begin{bmatrix} s-t & s+t \\ s+t & t-s \end{bmatrix} - A$$

is positive semidefinite for some $s, t \in \mathbb{Z}$.

We explain the connection to circles. Denote the set of integer superharmonic matrices on the F -lattice by Γ_F . The boundary of Γ_F may be viewed as a surface by taking the parameterization $M : \mathbb{R}^3 \rightarrow \mathbf{S}^2$,

$$M(a, b, c) := \frac{1}{2} \begin{bmatrix} c+a & b \\ b & c-a \end{bmatrix}.$$

In particular, Theorem 4.1.1 may be restated as

$$\partial\Gamma_F = \{M(a, b, \gamma_F(a, b)) : (a, b) \in \mathbb{R}^2\},$$

where

$$\gamma_F(x) := \max_{s, t \in \mathbb{Z}} -|x - (s-t, s+t)|. \quad (4.4)$$

Viewed from above, $\partial\Gamma_F$ is the union of identical slope-1 cones whose bases are the overlapping circle packing displayed in Figure 4.2.

One may check that the matrices, $M(s-t, s+t, 0)$ lie on $\partial\Gamma_F$ for all $s, t \in \mathbb{Z}$ (see Section 4.1.3 for the data to do so in a more general setting). This together with the downwards closure of Γ_F reduces the proof of Theorem 4.1.1 to verifying that the intersection curve of each pair of overlapping cones is in $\partial\Gamma_F$. Moreover, by symmetry, it suffices to check only one such hyperbola. Smart made these observations in Smart [2013] and then conjectured the following, which we prove.

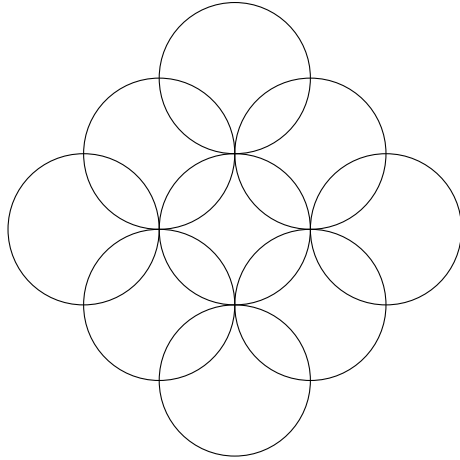


Figure 4.2: A few periods of the bases of cones in $\partial\Gamma_F$.

Theorem 4.1.2. *For each $0 \leq t \leq 1$, $M(t, 1-t, -\sqrt{t^2 + (1-t)^2})$ lies on the boundary of Γ_F .*

The set Γ_F is closed (Lemma 3.4 in Levine et al. [2017]), therefore, it suffices to prove Theorem 4.1.2 for all rational $0 \leq t \leq 1$ along the bottom branch of the hyperbola $\mathcal{H} := \{(t, c) \in \mathbb{R} \times \mathbb{R}^- : t^2 + (1-t)^2 = c^2\}$. We do this recursively. We start with explicit formulae for the odometers for $(0, -1)$ and $(1, -1)$ and then use those to construct odometers for all other rational points in between. Surprisingly, the recursion requires building not just one odometer for each such rational t , but *two* distinct odometers. This is a significant difference between the square lattice case which builds one odometer at a time; the square lattice odometers were also later shown to have a strong uniqueness property Pegden and Smart [2020].

Another new challenge is in identifying the correct recursive structure. There is a well-known secant line sweep algorithm which produces (and parameterizes) the rational points on \mathcal{H} given a single rational point on \mathcal{H} (and generally any elliptic curve - see *e.g.*, Tan [1996]). For example, since $(0, -1) \in \mathcal{H}$, all other rational points can be enumerated by varying the rational slope of a secant line between $(0, -1)$ and \mathcal{H} . Unfortunately, the odometers lying on \mathcal{H} under this labeling do not have an apparent recursive structure.

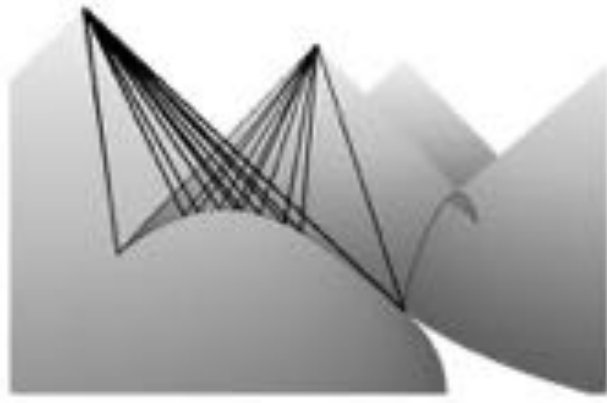


Figure 4.3: The first three iterations of the hyperbola recursion defined in Section 4.3. The two visible hyperbolas are outlined by dashed lines.

The parameterization which we adopt in this chapter utilizes the geometry of two adjacent cones. Each rational point on \mathcal{H} is an intersection of two unique lines of rational slope starting at the apexes of the cones. These intersections are dense in \mathcal{H} so we may identify each such point by its rational slope. See Figure 4.3.

Specifically, each point in $\mathbb{Q}^2 \cap \mathcal{H}$ may be labeled by a reduced fraction $0 \leq n/d \leq 1$ with corresponding matrix

$$M(n, d) := \frac{1}{(d^2 + 2dn - n^2)} \begin{bmatrix} -n^2 & dn \\ dn & -d^2 \end{bmatrix}. \quad (4.5)$$

We construct odometers for each $M(n, d)$ which grow along the lattice of the matrix,

$$L(n, d) = \{x \in \mathbb{Z}^2 : M(n, d)x \in \mathbb{Z}^2\}, \quad (4.6)$$

and which have periodic Laplacians. However, the F -lattice is not transitive. In particular, if $h : \mathbb{Z}^2 \rightarrow \mathbb{Z}$ is $L(n, d)$ periodic, then Δh may not be $L(n, d)$ periodic unless its period is even. To circumvent this, we must pass to a sub-lattice by doubling along the kernel of

$M(n, d)$. We show in Section 4.3 that $L(n, d)$ is equal to the integer span of

$$v_{n/d,1} := \begin{bmatrix} d \\ n \end{bmatrix} \quad v_{n/d,2} := \begin{bmatrix} n-d \\ n+d \end{bmatrix}, \quad (4.7)$$

and $v_{n/d,1}$ generates the kernel of $M(n, d)$. Our modified lattice is

$$L'(n, d) = \begin{cases} L(n, d) & \text{if } (n+d) \text{ is even} \\ 2\mathbb{Z}v_{n/d,1} + \mathbb{Z}v_{n/d,2} & \text{if } (n+d) \text{ is odd.} \end{cases} \quad (4.8)$$

We then derive Theorem 4.1.2 from the following.

Theorem 4.1.3. *For each reduced fraction $0 < n/d < 1$ there exists two distinct odometers $g_{n,d}, \hat{g}_{n,d}$ both of which satisfy the periodicity condition*

$$g(x+v) = g(x) + x^T M(n, d)x + c_v \quad (4.9)$$

for all $v \in L'(n, d)$ where c_v is a constant depending on v .

As in Levine et al. [2017], the periodicity condition (4.9) implies that $g_{n,d}$ and $\hat{g}_{n,d}$ are each integer superharmonic representatives for $M(n, d)$. Moreover, integer superharmonic matrices with odometers are on $\partial\Gamma_F$. Indeed, if g were recurrent but not on the boundary of Γ_F there would exist an integer superharmonic $f \geq g + \delta|x|^2$ for some $\delta > 0$. However, on the boundary of a lattice ball of radius n , B_n , $\sup_{\partial B_n}(g - f) \leq -n\delta$ for all n sufficiently large, contradicting the definition of recurrent as $\sup_{B_n}(g - f) \geq g(0) - f(0)$, a constant.

4.1.3 Kleinian bugs

We briefly mention a connection and possible extensions. The overlapping circle packing in Figure 4.2 is an object known as a *Kleinian bug* Kapovich and Kontorovich [2021].

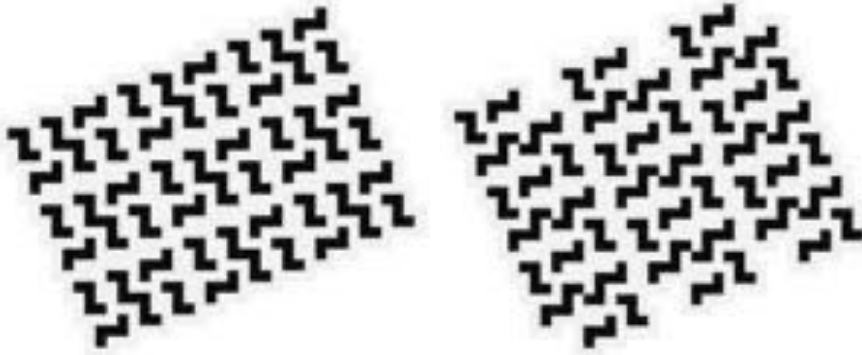


Figure 4.4: One $L'(2, 5)$ period of $\Delta g_{2,5}$ and $\Delta \hat{g}_{2,5}$. White and black are values of 0 and 1 respectively. These are used to construct the odometers seen in Figure 4.7.

Kleinian bugs were recently introduced by Kapovich-Kontorovich [2021] and generalize Apollonian circle packings. An important aspect of Levine et al. [2017] is an analogue of Descartes' rule Graham et al. [2005], Stange [2016] for integer superharmonic functions — Kleinian bugs share a similar rule.

The symmetry group of the Kleinian bug for the F -lattice is trivial (the difficult aspect of the argument in this manuscript is in accounting for the intersections between adjacent cones). However, numerical evidence suggests that the set of integer superharmonic matrices on other planar lattices may also be described by nontrivial symmetries of Kleinian bugs.

Levine-Pegden-Smart have derived a numerical algorithm which can determine the set of integer superharmonic matrices on periodic graphs up to arbitrary precision Levine et al. [2016b] (see Pegden [2017] for some high resolution outputs of this algorithm). We ran the Levine-Pegden-Smart algorithm on a family of lattices which generalize the F -lattice, what we call the $F^{(k)}$ lattices. For each $k \geq 2$, the $F^{(k)}$ -lattice is a directed, periodic, planar graph $(\mathbb{Z}^2, E^{(k)})$, where

$$\begin{cases} (x \pm e_1, x) \in E & \text{if } x_1 + x_2 \equiv 0 \pmod{k} \\ (x \pm e_2, x) \in E & \text{otherwise.} \end{cases}$$

Computed sets of $\partial\Gamma_k$, the boundary of the set of integer superharmonic matrices for the the $F^{(k)}$ lattice, are in Figure 4.5.

Some basic structure of these sets for all $k \geq 2$ may be understood after verifying that

$$\begin{aligned}\Delta r_1(x, y) &= 1\{(x_1 + x_2) \not\equiv 0 \pmod{k}\} \quad \text{for} \quad r_1(x_1, x_2) = \frac{x_2(x_2 + 1)}{2} \\ \Delta r_2 &= \Delta r_1 \quad \text{for} \quad r_2(x_1, x_2) = q_k(x_1 + x_2) \\ \Delta r_3 &= 1 \quad \text{for} \quad r_3(x_1, x_2) = \frac{x_1(x_1 + 1) + x_2(x_2 + 1)}{2}\end{aligned}\tag{4.10}$$

where

$$q_k(n) = \frac{(k-1)}{2k}(n^2 - s^2) + \frac{s(s-1)}{2} \quad \text{where } s \equiv n \pmod{k},$$

(note the Laplacian is that of the $F^{(k)}$ lattice). In particular, $h_1 := r_1 - r_2$ is integer valued and harmonic, $\Delta h_1 = 0$. The function $h_2(x_1, x_2) := x_1 x_2$ is also harmonic. This together with (4.10) and the standard argument in Lemma 4.6.1 below can be used to show that $r_i + sh_1 + th_2 - r_3$ are odometers for all $s, t \in \mathbb{Z}$ and $i \in \{1, 2\}$. These odometers lie on the hyperbolas between the largest cones in Figure 4.5 and the harmonic functions explain the apparent periodicity of Γ_k .

Remark 6. *Interestingly, the function $q_k(n)$ also counts the number of edges in a k -partite Turan graph of order n . We note that $q_k(n)$ has a simple closed form when k is small,*

$$q_k(n) = \left\lfloor \frac{(k-1)}{2k} n^2 \right\rfloor \quad \text{only for } k \leq 7,$$

but this is false for $k \geq 8$.

The general characterization of Γ_k seems to require both a recursive construction of the odometers for all circles in a Kleinian bug as in Levine et al. [2017] and all rational points on an infinite family of inequivalent hyperbolas. For example, we have explicitly computed in Figure 4.6 odometers for some of the largest circles appearing in $\partial\Gamma_3$. Each pair of

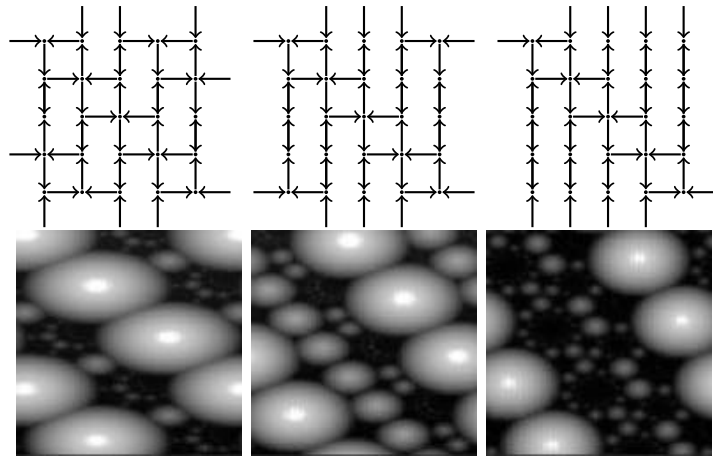


Figure 4.5: The $F^{(k)}$ lattices for $k = 3, 4, 5$ and computed $\partial\Gamma_k$.

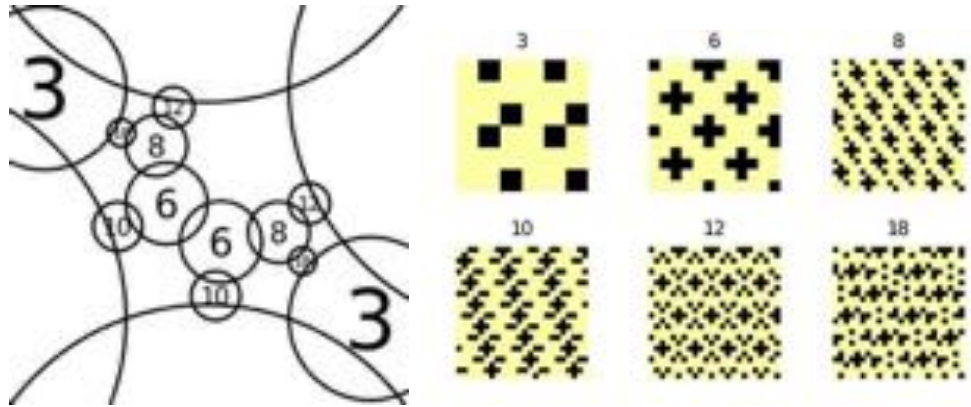


Figure 4.6: The seven largest circles in a period of $\partial\Gamma_3$. Periods of the Laplacians of odometers for the indicated circles on the left are displayed on the right, black is -1 and yellow is 0. Note that the four bordering largest circles have Laplacian identically 0 and correspond to harmonic functions built from (4.10).

overlapping circles generates a new hyperbola which we must check contains a dense family of odometers.

We leave the possibility of more detailed investigations of Γ_k for future work. From here onwards, we focus solely on Γ_2 and revert to writing Γ_F .

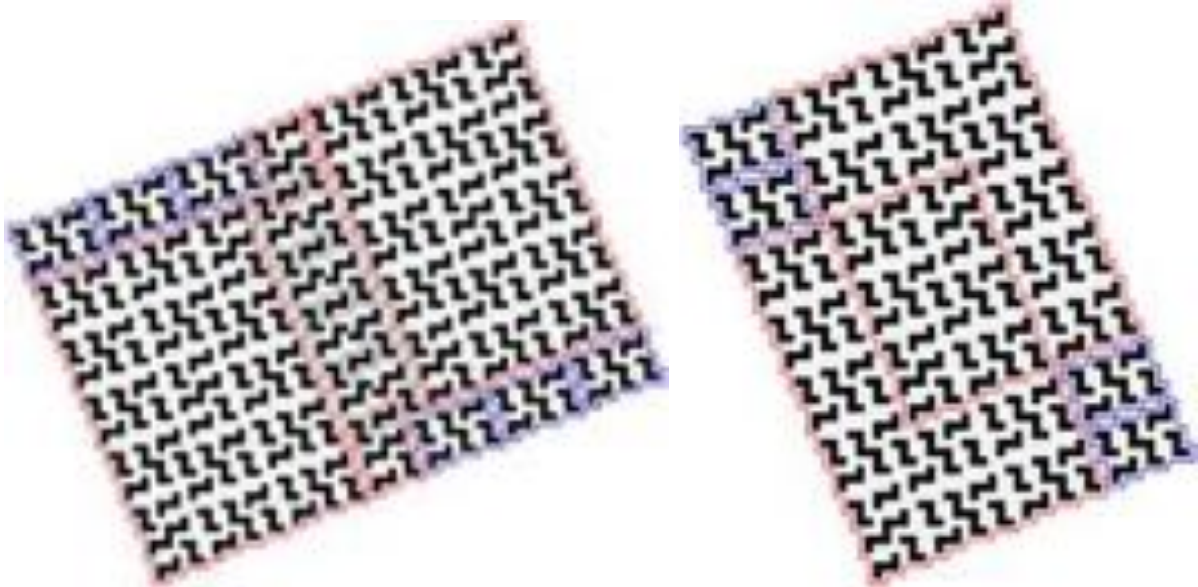


Figure 4.7: The Laplacian of two standard tile odometers corresponding to the Farey pair $(13/32, 15/37)$; the left and right displays are the odd and even child respectively. Gray is 0 and black is -1. The Laplacian of the standard odd-even ancestor odometers and alternate odometers are outlined in blue, red, and gray respectively. The even odometer decomposes perfectly into four-two copies of the odd-even standard odometers for the parent Farey pair, $(2/5, 11/27)$. In particular, two copies of the even parent overlap perfectly on a copy of an even grandparent. The odd odometer does not have a perfect decomposition into parents or grandparents; the decomposition requires multiple copies of the standard and alternate odometers of the distant ancestor pair $(2/5, 3/7)$.

4.2 Proof outline and comparison to previous work

Our method at a high level follows the program of Levine et al. [2017]: the proof recursively constructs odometers which then identify Γ_F . The implementation of this program, however, requires several new ideas, the most significant being the recursive algorithm itself. Moreover, our techniques - in particular the zero-one boundary string construction - may extend to other lattices.

In order to make the comparison, we briefly recall Levine-Pegden-Smart's construction in Levine et al. [2017]. On the square lattice, odometers were built by first specifying a *tile odometer*, a function with a finite domain, and then extending that function via a periodicity condition like (4.9) above. Levine-Pegden-Smart's construction associates tile odometers to circles in an Apollonian band packing. Recall that Apollonian packings can be drawn by starting with a triple of mutually tangent circles and then recursively filling in Soddy circles Graham et al. [2005]. Each circle in a packing is then part of a *Descartes quadruple* of pair-wise mutually tangent circles - thus every circle (other than the initial three) has a unique triple of parent circles. Levine-Pegden-Smart build tile odometers following this - the recursion starts with a simple formula for the largest circles in a band packing and then builds each child odometer by gluing together two copies each of the three parent odometers in a specified way.

In our setting, the Apollonian band packing is replaced by reduced rationals $0 \leq t \leq 1$ lying on a hyperbola $\mathcal{H} = \{(t, c) \in \mathbb{R} \times \mathbb{R}^+ : t^2 + (1-t)^2 = c^2\}$. The rational recursion is Farey-like but parity aware. That is, all *odd* and *even* reduced rationals - those whose numerator and denominator sum to an odd and even integer respectively - are grouped together into unique odd-even *Farey pairs*. The initial Farey pair is $(0/1, 1/1)$ and subsequent pairs are produced via a modification of the mediant operation and parent-child rotation; the rational recursion produces a ternary tree of unique *Farey quadruples*, a grouping of child and parent Farey pairs. We use this tree structure to recursively produce tile odometers.

A major difference beyond this is that we build for each reduced rational in a Farey pair not one but *two* distinct odometers. If the recursive algorithm attempted to use only one of the two odometers, it would get stuck - see Figure 4.7. (This can be thought of as coupling one odometer to each of the two intersecting downwards paths in Figure 4.3.) The construction also requires ancestor odometers which are arbitrarily far up the recursive tree. Moreover, although the function domains, the *tiles*, constructed are 180-degree symmetric, the tile odometers are not even centrally symmetric, leading to a blow-up in the number of cases the algorithm must consider.

For these reasons and more, proving correctness of the recursive algorithm presents new technical challenges. A notable one being distant ancestor dependence precludes a finite step inductive proof. We address this by augmenting the recursion and associating a binary *boundary string* to each odometer. These strings encapsulate certain compatibility properties across the recursive tree and show it is possible to glue distinct tile odometers together in a well-defined way. These strings allow us to run, in some sense, an analogue of the Euclidean algorithm.

Our proof that the functions which we construct are recurrent also differs from the corresponding proof on the square lattice. There, the odometers were shown to be *maximal*, a property strictly stronger than recurrent. Roughly, an integer superharmonic function is maximal if no other integer superharmonic function grows faster than it. Levine-Pegden-Smart showed that their constructed odometers were maximal using the fact that their Laplacians have a ‘web of 0s’, an infinite connected subgraph of 0s. In our case, there is no such web (which uses F -lattice edges) and no hyperbola odometer is maximal. Another technical difference is that the tiles which we construct do not tile \mathbb{Z}^2 - they ‘almost’ do but this is fortunately sufficient for our arguments.

To summarize, our proof proceeds as follows.

1. Identify a Farey-like recursion on reduced fractions $t = n/d$ which is dense on a hyper-

bola and tracks the parity of $(n + d)$.

2. Pair each reduced fraction with a binary word which records how it was generated.
3. Associate to each such word a *boundary string* which carries additional function and domain data.
4. Augment the rational recursion to produce two distinct tile odometers, a standard and an alternate by piecing together combinations of earlier standard and alternate odometers.
5. Show the recursion is well-defined by reducing every interface into a pair of boundary strings.
6. Prove that the functions constructed are recurrent and have the correct growth.

We start in Section 4.3 by precisely defining the modified Farey recursion on the hyperbola. We then prove a technical ‘almost’ tiling lemma in Section 4.4; this is later used to show that tile odometers extend periodically to cover space. Then in Section 4.5, we introduce and analyze a recursion on binary words which supplements the hyperbola recursion. There we also associate degenerate function and tile data, boundary strings, to each such word.

Then, in Section 4.6 we prove Theorem 4.1.3 for a special family of reduced fractions. In particular, this family is simple enough that we are able to provide explicit formulae for the tile odometers. This forms the base case for the general recursion. In Section 4.7 we then introduce a weak form of the recursion which essentially builds only the boundary of tile odometers. We show that these boundaries consist of exactly the boundary strings from Section 4.5. The full recursion is completed in Section 4.8 where we show the interior of tile odometers can be filled in either by immediate parents or by a chain of distant ancestors. We conclude in Section 4.9 by showing that both standard and alternate tile odometers can be extended in a way that give the desired growth and recurrence.

4.3 Hyperbola recursion

We specify a modified Farey recursion for rational matrices lying on the hyperbola $\mathcal{H} := \{(t, c) \in [0, 1] \times \mathbb{R}^- : t^2 + (1-t)^2 = c^2\}$. We also prove that the recursion is invariant with respect to a certain rotation of matrix space. As is later shown, this rotational invariance is maintained in the general recursion and can be leveraged to simplify the proofs of correctness.

4.3.1 Matrix and lattice parameterization

Recall the map $M : \mathbf{S}^2 \rightarrow \mathbb{R}^3$

$$M(a, b, c) = \frac{1}{2} \begin{bmatrix} c+a & b \\ b & c-a \end{bmatrix} \quad (4.11)$$

and the hyperbola matrices in the statement of Theorem 4.1.2, $M(t, 1-t, -\sqrt{t^2 + (1-t)^2})$. By solving for the intersection point of rank 1 perturbations of two adjacent cones and then subtracting a harmonic matrix, we can label $(t, c) \in \mathbb{Q} \cap \mathcal{H}$ by

$$f(n, d) := \frac{1}{T(n, d)}((d^2 - n^2), -(d^2 + n^2)), \quad (4.12)$$

which has corresponding matrix

$$M(n, d) := \frac{1}{T(n, d)} \begin{bmatrix} -n^2 & dn \\ dn & -d^2 \end{bmatrix},$$

where $T(n, d) := (d^2 + 2dn - n^2)$. Another computation shows that $(n, d) \rightarrow (d - n, n + d)$ is a rotation of \mathbf{S}^2 by: $(a, b) \rightarrow (b, a)$. We return to these rotations in Section 4.3.3 once we have defined the rational recursion.

As indicated in the introduction, we consider the lattice

$$L'(n, d) = \begin{cases} \mathbb{Z}v_{n/d,1} + \mathbb{Z}v_{n/d,2} & \text{if } (n+d) \text{ is even} \\ 2\mathbb{Z}v_{n/d,1} + \mathbb{Z}v_{n/d,2} & \text{if } (n+d) \text{ is odd.} \end{cases} \quad (4.13)$$

where

$$v_{n/d,1} := \begin{bmatrix} d \\ n \end{bmatrix} \quad v_{n/d,2} := \begin{bmatrix} n-d \\ n+d \end{bmatrix}. \quad (4.14)$$

Setting $a_i := M(n, d)v_i$, we note

$$a_1 := \begin{bmatrix} 0 \\ 0 \end{bmatrix} \quad a_2 := \begin{bmatrix} n \\ -d \end{bmatrix}. \quad (4.15)$$

We first observe that $v_{n/d,1}$ and $v_{n/d,2}$ generate the lattice of the matrix $M(n, d)$.

Lemma 4.3.1. *For each reduced fraction $t = n/d$,*

$$L(n, d) := \{v \in \mathbb{Z}^2 : M(n, d)v \in \mathbb{Z}^2\} = \mathbb{Z}v_{n/d,1} + \mathbb{Z}v_{n/d,2}.$$

Proof. Suppose $M(n, d)x = y$ for $x, y \in \mathbb{Z}^2$. For convenience, write $v_{n/d,i} =: v_i$. Since $\mathbb{R}^2 = \mathbb{R}v_1 + \mathbb{R}v_2$, we may write

$$x = cv_1 + c'v_2$$

for $c, c' \in \mathbb{Q}$. We show that c, c' must be in \mathbb{Z} , starting with c' . By (4.15),

$$M(n, d)x = cM(n, d)v_1 + c'M(n, d)v_2 = c'a_2$$

where by supposition

$$c'a_2 := \begin{bmatrix} z_1 \\ z_2 \end{bmatrix},$$

for integers z_1, z_2 . Since $\gcd(n, -d) = 1$, by Bezout's identity, there exists $w_1, w_2 \in \mathbb{Z}$ so that

$$w_1n - w_2d = 1.$$

Multiplying the above expression by c' ,

$$w_1z_1 + w_2z_2 = c',$$

in particular, since the left-hand side is integer-valued, $c' \in \mathbb{Z}$. The exact same argument then shows that $c \in \mathbb{Z}$ once we observe $cv_1 = x - c'v_2$ is integer valued.

□

We then check that the map in (4.12) is indeed dense in \mathcal{H} by noting it is dense in the first output.

Lemma 4.3.2. $\frac{d^2 - n^2}{d^2 + 2dn - n^2}$ is dense in $[0, 1]$ for reduced fractions $0 \leq n/d \leq 1$.

Proof. Suppose $0 < n/d < 1$ and rewrite

$$\frac{d^2 - n^2}{d^2 + 2dn - n^2} = 1 - \frac{1}{1 + \frac{1}{2}(\frac{d}{n} - \frac{n}{d})}.$$

Conclude after observing that $\frac{d}{n} - \frac{n}{d}$ is dense in $[0, \infty)$. □

4.3.2 Modified Farey recursion

As evident from (4.13), the recursion which we specify must be parity-aware. To that end, we say a reduced fraction p_n/p_d is *even* if $p_n + p_d$ is even and otherwise is *odd*. We exhibit a modified Farey recursion which generates all rationals in $[0, 1]$ and associates to each rational a unique set of odd-even parents and a sibling of the opposite parity.

An odd reduced fraction $p = o_n/o_d$ and an even reduced fraction $q = e_n/e_d$ produce an odd-even child pair by

$$\mathcal{C}(p, q) := \left(\frac{e_n + o_n}{e_d + o_d}, \frac{2o_n + e_n}{2o_d + e_d} \right). \quad (4.16)$$

A quadruple of reduced rationals, (p_1, q_1, p_2, q_2) is a *Farey quadruple* if $p_1, q_1 = \mathcal{C}(p_2, q_2)$, p_2 is odd, and q_2 is even. Each odd-even pair in a Farey quadruple is a *Farey pair*, the second pair are the *Farey parents* of each child in the first pair. A Farey quadruple (p_1, q_1, p_2, q_2) produces three children

$$\begin{aligned} \text{Type 1: } & \mathcal{C}_1 & (\mathcal{C}(p_1, q_1), p_1, q_1) \\ \text{Type 2: } & \mathcal{C}_2 & (\mathcal{C}(p_1, q_2), p_1, q_2) \\ \text{Type 3: } & \mathcal{C}_3 & (\mathcal{C}(p_2, q_1), p_2, q_1). \end{aligned} \quad (4.17)$$

The *modified Farey recursion* begins with the base quadruple

$$\mathbf{q}_{()} = \left(\frac{1}{2}, \frac{1}{3}, \frac{0}{1}, \frac{1}{1} \right) \quad (4.18)$$

and generates descendants which are labeled by *recursion words* in the free monoid F_3^* generated by $\{1, 2, 3\}$. The empty word $\{\}$ corresponds to the base quadruple. Each letter in a recursion word corresponds to the type of the child chosen in each step. For example $\mathbf{q}_{(12)}$ refers to the resulting quadruple after taking the Type 1 child of the root, then the Type 2 child of that child.

We will also use regex notation: $w = *w'$ for $w' \in F_3^*$ refers to any recursion word $w \in F_3^*$ which ends in w' . The notation s^k refers to $s \in F_3^*$ concatenated k times, *e.g.*, $3^2 = 3 * 3$.

Here is the connection to the usual, vanilla Farey recursion. Recall that the vanilla Farey sequence of order n consists of all reduced fractions of denominator at most n between 0 and 1. If a/b and c/d are neighboring terms in a vanilla Farey sequence of order n , then the first term which appears between them in a later sequence of order $m > n$ is the mediant, $p = \frac{a+c}{b+d}$. We refer to $(a/b, c/d)$ as the *vanilla Farey parents* of p while p is the *vanilla Farey*

child of vanilla Farey neighbors $(a/b, c/d)$. We then observe that (4.16) is simply two steps of the vanilla Farey recursion.

Lemma 4.3.3. *The modified Farey recursion generates unique Farey quadruples in reduced form*

$$\mathbf{q} = (p_1, q_1, p_2, q_2) = \left(\frac{e_n + o_n}{e_d + o_d}, \frac{2o_n + e_n}{2o_d + e_d}, \frac{o_n}{o_d}, \frac{e_n}{e_d} \right),$$

in particular, p_1, p_2 are odd, q_1, q_2 are even and \mathbf{q} is a Farey quadruple.

Proof. This follows once we inductively check that (p_2, q_2) are vanilla Farey neighbors with vanilla Farey child p_1 and (p_1, p_2) are vanilla Farey neighbors with vanilla Farey child q_1 . That is, by induction, (p_1, q_1) , (p_1, q_2) , and (p_2, q_1) are each pairs of neighbors in some vanilla Farey sequence and thus each child has a unique set of Farey parents. \square

Lemma 4.3.3 shows that the recursion defines a ternary tree of Farey quadruples. Each node in the tree has 3 outgoing edges corresponding to the three types of children. For later reference let \mathcal{T}_n denote the set of all Farey quadruples associated to words of length exactly n and denote the full tree by

$$\mathcal{T} = \bigcup \mathcal{T}_n. \quad (4.19)$$

4.3.3 Rotational symmetry reduction

As noted previously in Section 4.3.1, the following operator

$$\mathcal{R}(n, d) = (d - n, n + d) \quad (4.20)$$

rotates $\partial\Gamma_F$. The goal of this section is to show that an extension of \mathcal{R} to Farey quadruples preserves the depth of the modified Farey recursion. We start by observing a parity flipping property of \mathcal{R} .

Lemma 4.3.4. *If $0 \leq n/d \leq 1$ is an even reduced fraction then $\gcd((d-n)/2, (n+d)/2) = 1$, otherwise $\gcd(d-n, n+d) = 1$. Therefore, in the even case, the reduction of $\frac{d-n}{n+d}$ is odd and vice versa.*

Proof. We split the proof into two steps.

Step 1. We check the first claim. By the Euclidean algorithm,

$$\gcd(n, d) = \gcd(d - n, n) = 1,$$

and,

$$\begin{aligned} \gcd(n + d, d - n) &= \gcd((n + d) - (d - n), d - n) \\ &= \gcd(2n, d - n). \end{aligned}$$

If $(n + d)$ is even or odd, then $(d - n)$ is respectively even or odd. By Bezout's identity, there exist integers a_i, b_i so that

$$a_1(d - n) + b_12 = c$$

$$a_2(d - n) + b_2n = 1$$

where c is 1 if $(d - n)$ is odd and 2 otherwise. Multiplying the above two expressions together shows

$$a'(d - n) + b'(2n) = c,$$

for integers a', b' . If $c = 1$, this implies $\gcd(d - n, 2n) = 1$. Otherwise, since both $(d - n)$ and $2n$ are even, $\gcd(n + d, d - n) = \gcd(d - n, 2n) = 2$, concluding this step.

Step 2. If $(n + d)$ is odd, then Step 1 shows $\frac{d-n}{d+n}$ is in reduced form and therefore is even. Otherwise, reduce $\frac{d-n}{d+n} = \frac{(d-n)/2}{(d+n)/2}$ and note $(d - n + d + n)/2 = d$. Since $(n + d)$ is even and $\gcd(n, d) = 1$, both n and d must be odd, concluding the proof. \square

In light of Lemma 4.3.4, we extend \mathcal{R} to act on reduced fractions n/d by:

$$\mathcal{R}(n, d) = \begin{cases} (d - n, d + n) & \text{if } n + d \text{ is odd} \\ (\frac{d-n}{2}, \frac{n+d}{2}) & \text{otherwise.} \end{cases} \quad (4.21)$$

In an abuse of notation, we sometimes write $\mathcal{R}(n/d) = n'/d'$ instead. We extend \mathcal{R} to Farey pairs by $\mathcal{R}(p, q) = (\mathcal{R}(q), \mathcal{R}(p))$ and then component-wise to Farey quadruples. Our next two lemmas verify that this is well-defined.

Lemma 4.3.5. *If (p, q) is a Farey pair, $\mathcal{R}(\mathcal{C}(p, q)) = \mathcal{C}(\mathcal{R}(p, q))$.*

Proof. This is a direct computation. \square

We then show $\mathcal{R}(p)$ is a parent preserving bijection of the recursive tree \mathcal{T}_n .

Lemma 4.3.6. *The following holds for each word of length $n \geq 0$, $\mathbf{q}_{(w)} = (p_1, q_1, p_2, q_2) \in \mathcal{T}_n$.*

1. *Rotations flip Type 2 and Type 3 children and preserve Type 1 children,*

$$\mathcal{R}(\mathbf{q}_{(w1)}) = \mathcal{R}(\mathbf{q}_{(w)})_{(1)} \quad \mathcal{R}(\mathbf{q}_{(w2)}) = \mathcal{R}(\mathbf{q}_{(w)})_{(3)} \quad \mathcal{R}(\mathbf{q}_{(w3)}) = \mathcal{R}(\mathbf{q}_{(w)})_{(2)}.$$

In particular,

$$\mathcal{R} \circ \mathcal{C}_1 = \mathcal{C}_1 \circ \mathcal{R} \quad \mathcal{R} \circ \mathcal{C}_2 = \mathcal{C}_3 \circ \mathcal{R} \quad \mathcal{R} \circ \mathcal{C}_3 = \mathcal{C}_2 \circ \mathcal{R}.$$

2. *The rotation preserves depth $\mathcal{R}(\mathcal{T}_n) = \mathcal{T}_n$.*

Proof. We prove the claims by induction on n , the depth of the tree; the base case $n = 0$ can be checked directly.

Proof of (1). By definition

$$\mathbf{q}_{(w1)} = (\mathcal{C}(p_1, q_1), p_1, q_1)$$

$$\mathbf{q}_{(w2)} = (\mathcal{C}(p_1, q_2), p_1, q_2)$$

$$\mathbf{q}_{(w3)} = (\mathcal{C}(p_2, q_1), p_2, q_1).$$

By Lemma 4.3.5,

$$\begin{aligned}\mathcal{R}(\mathbf{q}_{(w)})_{(1)} &= (\mathcal{C} \circ \mathcal{R}(p_1, q_1), \mathcal{R}(p_1, q_1)) \\ &= (\mathcal{R} \circ \mathcal{C}(p_1, q_1), \mathcal{R}(p_1, q_1)) \\ &= \mathcal{R}(\mathbf{q}_{(w1)}).\end{aligned}$$

For the other cases, we also use the induction hypothesis. Recall

$$\mathcal{R}(\mathbf{q}_{(w)}) = (\mathcal{R}(q_1), \mathcal{R}(p_1), \mathcal{R}(q_2), \mathcal{R}(p_2)),$$

hence

$$\begin{aligned}\mathcal{R}(\mathbf{q}_{(w)})_{(2)} &= (\mathcal{C}(\mathcal{R}(q_1), \mathcal{R}(p_2)), \mathcal{R}(q_1), \mathcal{R}(p_2)) \\ &= (\mathcal{C} \circ \mathcal{R}(p_2, q_1), \mathcal{R}(p_2, q_1)) \\ &= (\mathcal{R} \circ \mathcal{C}(p_2, q_1), \mathcal{R}(p_2, q_1)) \\ &= \mathcal{R}(\mathbf{q}_{(w3)}).\end{aligned}$$

The other case is symmetric.

Proof of (2). By the inductive hypothesis, $\mathcal{R}(T_{n-1}) = T_{n-1}$ and by definition, $T_n =$

$\bigcup_{i=1}^3 \mathcal{C}_i \circ T_{n-1}$. Hence, by part (1),

$$\mathcal{R} \circ T_n = \bigcup_{i=1}^3 \mathcal{R} \circ \mathcal{C}_i \circ T_{n-1} = \bigcup_{i=1}^3 \mathcal{C}_i \circ \mathcal{R} \circ T_{n-1} = \bigcup_{i=1}^3 \mathcal{C}_i \circ T_{n-1} = T_n,$$

concluding the proof. \square

We conclude the section by observing that \mathcal{R} is also a rotation of the lattice vectors given by (4.14) and (4.15). By identifying \mathbb{Z}^2 with $\mathbb{Z}[\mathbf{i}]$ we may write

$$v_{n/d,1} = d + n\mathbf{i} \quad v_{n/d,2} = (n-d) + (n+d)\mathbf{i} \quad (4.22)$$

and

$$a_{n/d,1} = 0 \quad a_{n/d,2} = n - d\mathbf{i} \quad (4.23)$$

Lemma 4.3.7. *For even p and odd q ,*

$$v_{\mathcal{R}(p),1} = -\mathbf{i}v_{p,2} \quad v_{\mathcal{R}(p),2} = \mathbf{i}2v_{p,1} \quad (4.24)$$

and

$$2v_{\mathcal{R}(q),1} = -\mathbf{i}v_{q,2} \quad v_{\mathcal{R}(q),2} = \mathbf{i}v_{q,1} \quad (4.25)$$

Proof. Note that if n/d is odd, then

$$\begin{aligned} v_{\mathcal{R}(n/d),1} &= (n+d) + (d-n)\mathbf{i} \\ &= -\mathbf{i}v_{n/d,2} \end{aligned}$$

and

$$\begin{aligned}
v_{\mathcal{R}(n/d),2} &= (d-n) - (n+d) + (d-n+n+d)\mathbf{i} \\
&= 2(-n+d\mathbf{i}) \\
&= \mathbf{i}2v_{n/d,1}.
\end{aligned}$$

The equation for n/d even follows once we recall \mathcal{R} is an involution, $\mathcal{R} \circ \mathcal{R}(q) = q$ \square

For the remainder of the chapter write

$$v_{n/d,1} = \begin{cases} 2v_{n/d,1} & \text{if } n/d \text{ is odd} \\ v_{n/d,1} & \text{otherwise.} \end{cases} \quad (4.26)$$

4.4 Almost pseudo-square tilings

In this section we prove a technical tiling lemma which will allow us to show that the tiles which we define in the subsequent sections cover \mathbb{Z}^2 periodically.

We identify \mathbb{Z}^2 with $\mathbb{Z}[\mathbf{i}]$. A *cell* is a unit square $s_x = \{x, x+1, x+\mathbf{i}, x+1+\mathbf{i}\} \subset \mathbb{Z}[\mathbf{i}]$ and a *tile* is a simply connected union of cells whose boundary is a simple closed curve. The *vertices* of a tile are the Gaussian integers on its boundary. Let $(F_2, *)$ be the free group generated by $\{1, \mathbf{i}\}$. For $w \in F_2$, let \hat{w} denote its involution, *i.e.*, $\hat{w} * w = \{\}$. Let $\mathbf{rev}(w)$ denote the reversal of $w \in F_2$, $w[j]$ the j -th letter of w , and $|w|$ the number of letters in w . The *boundary word* of a tile is a word $w \in F_2$ which represents a vertex walk around the boundary of the tile. In particular, $\sum w = 0$ and $\sum w' \neq 0$ for any non-empty sub-word w' of w , where \sum denotes the abelianization of F_2 .

A *tiling* of the plane is an infinite set of translations of a tile T where every cell is contained in exactly one copy of T . A tiling of T is (v_1, v_2) -*regular* if every tile T' in the tiling can be expressed as $T + kv_1 + k'v_2$ for $k, k' \in \mathbb{Z}$ and $v_1, v_2 \in \mathbb{Z}[\mathbf{i}]$. That is, the translations of T by

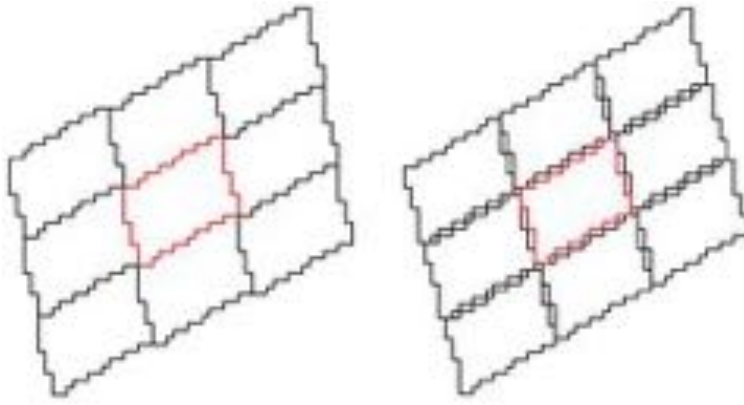


Figure 4.8: A surrounding of a pseudo-square tiling and an almost pseudo-square tiling as defined in Proposition 4.4.1 and Lemma 4.4.1 respectively.

(v_1, v_2) generate the tiling.

Beauquier-Nivat Beauquier and Nivat [1991] have a simple criteria for determining if a tile generates a regular tiling. Their criteria is expressed in terms of the boundary words of a tile, but can be interpreted geometrically as: a tile generates a regular tiling if it can be perfectly surrounded by copies of itself. We refer to a tiling satisfying the conditions in Proposition 4.4.1 as a *pseudo-square tiling*.

Proposition 4.4.1 (Beauquier and Nivat [1991]). *If the boundary word of a tile, $w \in F_2$, can be expressed as*

$$w = w_1 * w_2 * \hat{w}_1 * \hat{w}_2,$$

then the tile generates a $(\sum w_1, \sum w_2)$ -regular tiling.

In our main argument, we require a technical modification of the notion of tiling in which bounded gaps are allowed. That is, we cannot use Proposition 4.4.1 and are thus forced to modify it. An *almost* tiling \mathcal{T} , is an infinite set of translations of a tile T where every cell is contained in at most one tile and every $x \in \mathbb{Z}^2$ is a vertex of a cell in \mathcal{T} , i.e., there is $s_y \in \mathcal{T}$ with $x \in s_y$. The notion of regular with respect to a lattice is also extended to almost tilings.

We now give a sufficient condition for generating almost tilings. Roughly, this condition allows for slight gaps between cells in the surrounding of a tile. We will refer to the almost

tiling from Lemma 4.4.1 as an *almost pseudo-square tiling*. See Figure 4.8 for an illustration of this.

Lemma 4.4.1. Suppose $w = w_1 * w_2 * \widehat{\text{rev}}(w_1) * \widehat{\text{rev}}(w_2)$ is the boundary word of a tile T .

Further suppose the following conditions on $w \in \{w_1, -\mathbf{i}w_2\}$.

1. Monotonicity: $\{-1, -\mathbf{i}\} \notin w$ and $w[1] = w[|w|] = 1$
2. At least one of the following three cases concerning the form of w and its reversal is satisfied:
 - (a) w is a palindrome, $w = \text{rev}(w)$
 - (b) $w = (1 * 1 * \mathbf{i}) * \tilde{w} * 1$, where \tilde{w} is a palindrome. Moreover, every \mathbf{i} in w is followed by at least one 1.
 - (c) $w = 1 * \tilde{w} * (1 * 1 * 1)$ where \tilde{w} is a palindrome. Moreover, every \mathbf{i} in w is followed by at least three 1s.

Then, T generates a $(\sum w_1 + \mathbf{i}, \sum w_2 - 1)$ -regular almost tiling. Moreover, the only tiles in the tiling which share edges with T are $T \pm (\sum w_1 + \mathbf{i})$ and $T \pm (\sum w_2 - 1)$.

Proof. Let $(v_1, v_2) = (\sum w_1, \sum w_2)$. To show that T generates a $(v_1 + \mathbf{i}, v_2 - 1)$ -regular almost tiling, by periodicity, it suffices to analyze one surrounding of T ,

$$S := \bigcup_{|k_1| \leq 1, |k_2| \leq 1} \{T + k_1(v_1 + \mathbf{i}) + k_2(v_2 - 1)\},$$

see Figure 4.8. Specifically we show that the closure,

$$\bar{S} = \{s_x : x \in S \cap \mathbb{Z}^2\}.$$

is simply connected and no two cells in the decomposition of S overlap.

Observe that the boundary word of T implies it is 180-degree symmetric. Hence, S is 180-degree symmetric and we may reduce to analyzing the interfaces between T and its lower, right, and lower-right neighbors,

$$T_h := T + v_1 + \mathbf{i}$$

$$T_v := T - v_2 + 1$$

$$T_d := T + v_1 - v_2 + 1 + \mathbf{i}.$$

We show that the conditions imply no two pairs of edges cross and that every gap in the interface borders a cell of T .

Step 1: The bottom interface

We start with the bottom interface, T and T_v . Designate the origin as the lower-left vertex of T so that cells along the bottom of T can be labeled by a w_1 walk. By the definition and translation offsets, vertices along the top edge of T_v can then be labeled by $\text{rev}(w_1) + 1$. For $j \leq |w_1|$, let $x_j = \sum w_1[1:j]$ and $y_j = 1 + \sum(\text{rev}(w_1)[1:j])$, where $w[1:j]$ represents the first j letters of w . In particular, $x_0 = 0$ and $y_0 = 1$.

We now split the argument into three cases depending on the form of w_1 as dictated by condition (2).

Case (a): $w_1 = \text{rev}(w_1)$

In this case, $y_j = 1 + \sum w_1[1:j]$ and so

$$x_j = y_j - 1. \tag{4.27}$$

Therefore, any vertex y_j along the top edge of T_v is distance at most one from x_j , the lower left-corner of a cell in T .

To see that the top edge of T_v does not cross above the bottom edge of T , we use

monotonicity. Suppose for sake of contradiction a crossing occurs. Since $w_1 = 1$, $x_1 = y_0$ and therefore there is a first $j, j' \geq 1$ at which $y_j = x_{j'}$ and $y_{j+1} = x_{j'} + \mathbf{i}$. By (4.27), $y_j = x_j + 1$ and so by monotonicity, $j' = (j + 1)$. However, by (4.27) $y_{j+1} = x_{j+1} + 1 \neq x_{j+1} + \mathbf{i}$, a contradiction.

Case (b):

In this case

$$\begin{aligned} w_1 &= (1 * 1 * \mathbf{i}) * \tilde{w} * 1 \\ \mathbf{rev}(w_1) &= 1 * \tilde{w} * (\mathbf{i} * 1 * 1) \end{aligned}$$

for a palindrome $\tilde{w} \in F_2$. Therefore, (after remembering the offset of T_v)

$$\begin{aligned} x_0 &= 0 & x_1 &= 1 & x_2 &= 2 & x_3 &= 2 + \mathbf{i} \\ y_0 &= 1 & y_1 &= 2 & y_2 &= 2 + \tilde{w}[1] & y_3 &= 2 + \tilde{w}[1] + \tilde{w}[2] \end{aligned}$$

and

$$\begin{aligned} x_{3+|\tilde{w}|} &= (2 + \mathbf{i}) + \sum \tilde{w} & x_{4+|\tilde{w}|} &= (3 + \mathbf{i}) + \sum \tilde{w} \\ y_{1+|\tilde{w}|} &= (2) + \sum \tilde{w} & y_{2+|\tilde{w}|} &= (2 + \mathbf{i}) + \sum \tilde{w} \\ y_{3+|\tilde{w}|} &= (3 + \mathbf{i}) + \sum \tilde{w} & y_{4+|\tilde{w}|} &= (4 + \mathbf{i}) + \sum \tilde{w}. \end{aligned}$$

Thus, it suffices to consider $1 \leq j \leq 1 + |\tilde{w}|$ for which the above computations show

$$x_{j+2} = y_j + \mathbf{i}. \quad (4.28)$$

It remains to show this implies there are no crossings. Suppose for contradiction $y_j = x_{j'}$ and $y_{j+1} = y_j + \mathbf{i}$ but $x_{j'+1} = x_{j'} + 1$. for some $1 \leq j \leq 1 + |\tilde{w}|$. By (4.28), $y_{j+1} = x_{j+2} = x_{j'} + \mathbf{i}$.

By monotonicity, $j' = j + 1$ and so $x_{j'+1} = x_{j'} + \mathbf{i}$, a contradiction.

Case (c):

In this case,

$$w_1 = 1 * \tilde{w} * (1 * 1 * 1)$$

$$\mathbf{rev}(w_1) = (1 * 1 * 1) * \tilde{w} * 1$$

for a palindrome $\tilde{w} \in F_2$. Thus,

$$x_0 = 0 \quad x_1 = 1 \quad x_2 = 1 + \tilde{w}[1]$$

$$y_0 = 1 \quad y_1 = 2 \quad y_2 = 3 \quad y_3 = 4$$

and

$$\begin{aligned} x_{1+|\tilde{w}|} &= 1 + \sum \tilde{w} & x_{1+|\tilde{w}|+z} &= (1+z) + \sum \tilde{w} \quad \text{for } z \leq 3 \\ y_{3+|\tilde{w}|} &= 4 + \sum \tilde{w} & y_{4+|\tilde{w}|} &= 5 + \sum \tilde{w}. \end{aligned}$$

We note that for all $2 \leq j \leq |\tilde{w}| + 3$,

$$y_j = x_{j-2} + 3. \tag{4.29}$$

Indeed, $x_{1+z} = 1 + \sum \tilde{w}[1 : z]$ and $y_{3+z} = 4 + \tilde{w}[1 : z]$ for $z \leq |\tilde{w}|$.

We claim that this together with the moreover clause implies no gaps of size larger than 1. Indeed, if $y_j = x_{j-2} + 3$, then $x_j = x_{j-2} + 1 + (1 \text{ or } i)$. In the first case, we are done. In the second case, $x_{j+2} = x_{j-2} + 1 + \mathbf{i} + 2$.

The relation (4.29) also implies no crossings. Indeed, suppose for contradiction $y_j = x_{j'}$ and $y_{j+1} = y_j + \mathbf{i}$ but $x_{j'+1} = x_{j'} + 1$. for some $2 \leq j \leq 2 + |\tilde{w}|$. By (4.29), $y_j = x_{j-2} + 3$

and $y_{j+1} = x_{j-1} + 3$. This implies $x_{j-1} = x_{j-2} + \mathbf{i}$ and hence the moreover clause implies

$$x_{j+2} = x_{j-1} + 3 = x_{j-2} + 3 + \mathbf{i} = y_j + \mathbf{i} = y_{j+1}.$$

Monotonicity then implies $x_{j+1} = x_{j'} = y_j$, but this then contradicts $x_{j'+1} = x_{j'} + 1$.

Step 2: Conclude

After rotating, the arguments in Step 1 apply to the interface between T and T_h . We then check T and T_d . Let $z_0 = \sum w_1$ and note that the top left vertex of T_d is $z_0 + 1 + \mathbf{i}$. By the assumption on the first and last letter of w_2 , the next vertices on the top and left edges of T_d are $z_0 + 2 + \mathbf{i}$ and $z_0 + 1$ respectively while the next vertex on the right edge of T is $z_0 + \mathbf{i}$. This implies that no cell of T overlaps a cell of T_d and that the gap between the two tiles is of unit size.

Finally, by monotonicity, for any other pair of cells in S to overlap, there must first be a crossing on the horizontal or vertical edges which we have just shown to be impossible.

□

Remark 7. *Our usage of Lemma 4.4.1 is not strictly necessary and may be replaced by an appropriate application of Lemma 4.5.4 below. We included it as we believe it makes the overall proof easier to follow. It may also be of independent interest.*

4.5 Zero-one boundary strings

In this section we begin to associate additional data to the hyperbola recursion.

4.5.1 A recursion on binary words

We associate to each reduced fraction in the modified Farey recursion a binary word and expose some basic properties. Specifically, given any initial Farey pair (p, q) we associate

each descendant to a *binary word*, a word in the alphabet generated by the two letters, $\{p, q\} \in F_2^*$, by augmenting the recursion.

Given a recursion word $w \in F_3^*$ and two binary words $p_t, q_t \in F_2^*$ we extend the child operator in (4.16) to pairs of binary words by

$$\mathcal{C}_{(w)}(p_t, q_t) = \begin{cases} (q_t q_t p_t, q_t p_t) & \text{if } \sum 1\{w_j = 1\} \text{ is even} \\ (p_t q_t q_t, p_t q_t) & \text{otherwise.} \end{cases} \quad (4.30)$$

Let $w_0 \in F_3^*$ describe the Farey pair (p, q) and $\mathbf{Q}_{(w_0)} = (\mathcal{C}_{w_0}(p, q), p, q)$ be the initial binary word quadruple with each term in F_2^* . Then, recursively, given $w \in F_3^*$ and $\mathbf{Q}_{(w)} = (p_{t+1}, q_{t+1}, p_t, q_t)$, each child binary word quadruple is defined by

$$\begin{aligned} \mathbf{Q}_{(w*1)} &= \left(\mathcal{C}_{(w*1)}(p_{t+1}, q_{t+1}), p_{t+1}, q_{t+1} \right) \\ \mathbf{Q}_{(w*2)} &= \left(\mathcal{C}_{(w*2)}(p_{t+1}, q_t), p_{t+1}, q_t \right) \\ \mathbf{Q}_{(w*3)} &= \left(\mathcal{C}_{(w*3)}(p_t, q_{t+1}), p_t, q_{t+1} \right). \end{aligned} \quad (4.31)$$

Recall that a palindrome $\tilde{w} \in F_2^*$ is a word that is equal to its reversal, $\tilde{w} = \mathbf{rev}(\tilde{w})$. An *almost palindrome* is a word $w = s_1 * \tilde{w} * \mathbf{S}^2$, where $s_1, s_2 \in \{p, q\}$ are two letters and \tilde{w} is a palindrome. Write $w[a : b]$ for the subword starting at the a -th letter of w and ending at the b -th letter.

Lemma 4.5.1. *The following hold for every subsequent pair of binary words (p_t, q_t) produced by (4.31).*

1. Both p_t and q_t are almost palindromes
2. If $\sum 1\{w_{0j} = 1\}$ is even then all subsequent binary words begin with q and end with p and otherwise begin with p and end with q .

3. Let $n = \min(|p_t|, |q_t|)$ and $m = \min(|p_t|, 2|q_t|)$. Then,

$$p_t[2:n] = \mathbf{rev}(q_t)[2:n] \quad p_t[2:m] = \mathbf{rev}(q_t q_t)[2:m].$$

Proof. We may suppose without loss of generality that $\sum 1\{w_{0j} = 1\}$ is even, otherwise, reverse the subsequent statements.

Let $\mathbf{Q}_{(w)} = (p_{t+1}, q_{t+1}, p_t, q_t)$ be given and we will verify claims (1) and (2) for the child Farey pair and claim (3) for the parent Farey pair in the quadruple

$$\mathbf{Q}_{(w')} = (p_{t+2}, q_{t+2}, p'_{t+1}, q'_{t+1})$$

defined by (4.31). To do so, we must eliminate the degenerate cases $p'_{t+1} = p$ or $q'_{t+1} = q$. Fortunately, these can only occur if $w' = 3^k$ or $w' = 2^k$ for $k \geq 0$ respectively. An induction shows that

$$\begin{aligned} \mathbf{Q}_{(3^k)} &= (qp^k qp^{k+1}, qp^{k+1}, p, qp^k) \\ \mathbf{Q}_{(2^k)} &= (q^{2(k+1)} p, q^{2k+1} p, q^{2k} p, q), \end{aligned} \tag{4.32}$$

and we can verify the claim directly in these cases by inspection. We can then use (4.32) to also handle the cases $w' = 3^k * \{1 \text{ or } 2\}$ or $w' = 2^k * \{1 \text{ or } 3\}$.

Hence, we may assume none of $p_t, q_t, p_{t+1}, q_{t+1}$ are singletons, that is the induction hypotheses hold for each of them. We also suppose $\sum 1\{w_j = 1\}$ is even. By the induction hypotheses

$$p_t = qw^1 p \quad q_t = qw^2 p$$

for palindromes w^1 and w^2 and so

$$\begin{aligned} p_{t+1} &= qw^2 p q w^2 p q w^1 p \\ q_{t+1} &= qw^2 p q w^1 p. \end{aligned} \tag{4.33}$$

Since p_{t+1} and q_{t+1} are almost palindromes and $w^i = \mathbf{rev}(w^i)$ we have the reversal relations

$$\begin{aligned} w^2 p q w^1 &= w^1 q p w^2 \\ w^2 p q w^2 p q w^1 &= w^1 q p w^2 q p w^2. \end{aligned} \tag{4.34}$$

This implies claim (3),

$$\begin{aligned} \mathbf{rev}(q_{t+1}) &= p w^1 q p w^2 q \\ p_{t+1} &= q w^1 q p w^2 q p w^2 p \\ \mathbf{rev}(q_{t+1} q_{t+1}) &= p w^1 q p w^2 q p w^2 p q w^1 q. \end{aligned}$$

For claims (1) and (2), the possible decompositions of (p_{t+2}, q_{t+2}) are

$$\begin{aligned} (p_{t+1} q_{t+1} q_{t+1}, p_{t+1} q_{t+1}) &\quad \text{Type 1} \\ (q_t q_t p_{t+1}, q_t p_{t+1}) &\quad \text{Type 2} \\ (q_{t+1} q_{t+1} p_t, q_{t+1} p_t) &\quad \text{Type 3.} \end{aligned}$$

The reversal relations (4.34) together with (4.33) show that each of the decompositions are almost palindromes. We show only the odd Type 1 case as the rest are similar. First, write using (4.33)

$$p_{t+1} q_{t+1} q_{t+1} = q w^2 p q w^2 p q w^1 p q w^2 p q w^1 p q w^2 p q w^1 p,$$

and then use (4.34) to check

$$\begin{aligned} \mathbf{rev}(w^2 p q w^2 p q w^1 p q w^2 p q w^1 p q w^2 p q w^1) &= [w^1 q p w^2] q p [w^1 q p w^2] q p [w^1 q p w^2 q p w^2] \\ &= [w^2 p q (w^1) q p (w^2) p q (w^1 q p (w^2) p q w^2 p q w^1)] \\ &= w^2 p q (w^2 p q w^1) p q (w^2 p q w^1) p q w^2 p q w^1. \end{aligned}$$

□

4.5.2 Basic definitions

We next associate tile and function data to the binary word recursion. But in order to do so, we must recall and modify some definitions from Levine et al. [2017]. A *tile* T is now, depending on the context, either a finite subset of \mathbb{Z}^2 or a finite union of simply connected cells. Let $c(T)$ denote the coordinate-wise minimum of T - geometrically the lower-left vertex. A *partial odometer* is a function $h : T \rightarrow \mathbb{Z}$. The domain of h is $T(h)$ and $s(h) \in \mathbb{C}$ is the *slope* of T , the average of

$$\begin{aligned} & \frac{1}{2} (h(x+1) - h(x) + h(x+1+\mathbf{i}) - h(x+\mathbf{i})) + \\ & \frac{\mathbf{i}}{2} (h(x+\mathbf{i}) - h(x) + h(x+1+\mathbf{i}) - h(x+1)) \end{aligned} \tag{4.35}$$

for $x \in T$. Two partial odometers o_1 and o_2 are *translations* of one another if

$$T(o_1) = T(o_2) + v \quad \text{and} \quad o_1(x) = o_2(x+v) + a^T x + b \tag{4.36}$$

for some $v, a \in \mathbb{Z}^2$ and $b \in \mathbb{Z}$.

Partial odometers o_1 and o_2 are *compatible* if $o_1 - o_2 = c$ on $T(o_1) \cap T(o_2)$ for some *offset constant* $c \in \mathbb{Z}$. As in Levine et al. [2017], if the offset constant is 0 or the tiles do not overlap then $o_1 \cup o_2$ is the common extension to $T(o_1) \cup T(o_2)$. We recall for later reference the following lemma which will allow us to construct global odometers from pairwise compatible partial odometers.

Lemma 4.5.2 (Lemma 9.2 in Levine et al. [2017]). *If $\mathcal{S} = \{o_i\}$ is a collection of pairwise compatible partial odometers such that $\{T(o_i)\}$ forms an almost pseudo-square tiling then there is a function $g : \mathbb{Z}^2 \rightarrow \mathbb{Z}$ unique up to adding a constant that is compatible with every $o_i \in \mathcal{S}$.*

4.5.3 Even-odd boundary strings

We now associate additional data to each binary word constructed in the first subsection. The result in this subsection will form a key tool in verifying correctness of the subsequent tile and odometer recursion.

We first adapt the notion of *boundary string* from Levine et al. [2017] to our setting. Suppose T_p and T_q are tiles which generate $(v_{p,1}, v_{p,2})$ and $(v_{q,1}, v_{q,2})$ regular almost pseudo-square tilings respectively. A q - p *boundary string* is a collection of tiles $T_i \in \{T_q, T_p\}$ such that

$$c(T_i) - c(T_{i-1}) = \begin{cases} v_{p,j} & \text{if } T_{i-1} = T_p \\ v_{q,j} & \text{if } T_{i-1} = T_q, \end{cases} \quad (4.37)$$

for fixed $j \in \{1, 2\}$. A q - p *reversed boundary-string* is also a collection of tiles $T_i \in \{T_q, T_p\}$ but with different offsets:

$$c(T_i) - c(T_{i-1}) = \begin{cases} v_{p,j} + (v_{p,j'} - v_{q,j'}) & \text{if } pq \\ v_{p,j} & \text{if } pp \\ v_{q,j} + (v_{q,j'} - v_{p,j'}) & \text{if } qp \\ v_{q,j} & \text{if } qq, \end{cases} \quad (4.38)$$

where $(j, j') \in \{(1, 2), (2, 1)\}$ is fixed and the right column denotes the tile tuple, *e.g.*, the first row is $(T_{i-1}, T_i) = (T_p, T_q)$. When $j = 1$, a boundary string is *horizontal* and otherwise is *vertical*. We label a boundary string \mathcal{B}_w by a binary word $w \in F_2^*$ where a superscript r indicates it is reversed.

A horizontal or vertical *stacked boundary string* for $w \in F_2$ is a union of $\{T_i^+\} := \mathcal{B}_w$ and $\{T_i^-\} := \mathcal{B}_{\mathbf{rev}(w)}^r$ both oriented in the same direction. The first tiles T_1^+ and T_1^- in each

string and the shared direction dictate the relative positions,

$$c(T_1^+) - c(T_1^-) = v_{n/d',j'} \quad (4.39)$$

where $j' \in \{1, 2\}$ is the perpendicular direction and $n/d' \in \{p, q\}$ is the type of T_1^- . See Figure 4.9.

We now observe that tile offsets between perpendicular adjacent tiles in a stacked boundary string are given by a simple formula if the binary word describing the string is an almost palindrome.

Lemma 4.5.3. *If w is an almost palindrome, then for all $1 < i \leq |w|$*

$$c(T_i^+) - c(T_i^-) = v_{n/d',j'} + (v_{a,j} - v_{b,j})$$

where $j' \in \{1, 2\}$ is the perpendicular direction, $n/d', a, b \in \{p, q\}$ is the type of T_i^- , T_1^+ and T_1^- respectively.

Proof. For concreteness and since w is an almost palindrome, take $j = 1$, $T_1^+ = T_p$ and $T_1^- = T_q$. If T_2^- and T_2^+ are both of type p , then

$$\begin{aligned} c(T_2^+) - c(T_2^-) &= (c(T_2^+) - c(T_1^+)) + (c(T_1^+) - c(T_1^-)) + (c(T_1^-) - c(T_2^-)) \\ &= v_{p,1} + v_{q,2} - (v_{q,1} + (v_{q,2} - v_{p,2})) \\ &= v_{p,2} + (v_{p,1} - v_{q,1}). \end{aligned}$$

If T_2^- and T_2^+ are both of type q , then

$$c(T_2^+) - c(T_2^-) = v_{p,1} + v_{q,2} - v_{q,1}.$$

Conclude by similar computations together with an induction on $1 < i \leq |w|$.

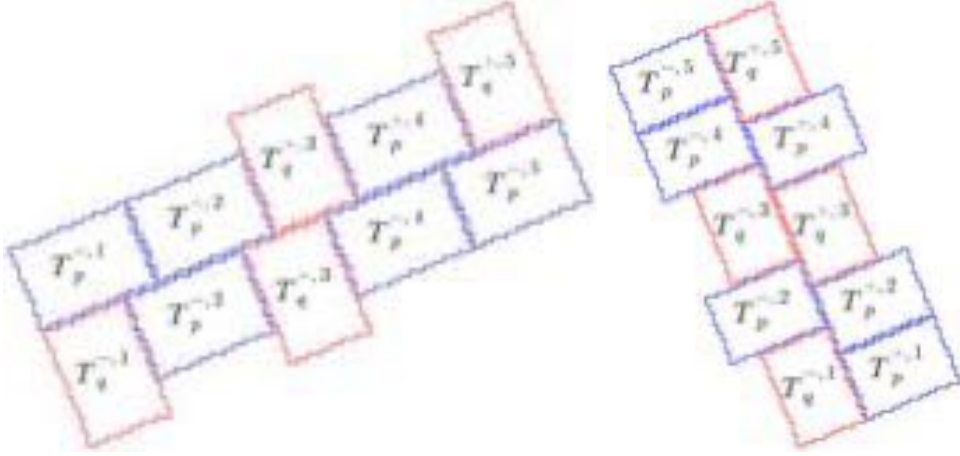


Figure 4.9: Stacked horizontal and vertical boundary strings. The superscripts $+$, $-$ denote the non-reversed and reversed strings respectively and, e.g., $T_p^{+,i}$ refers to T_i^+ and indicates that T_i^+ is type p . Here the tiles are outlined in the dual lattice.

□

4.5.4 A degenerate boundary string

We now examine a degenerate boundary string which we later show completely describes the odometer recursion. Due to the degenerate nature of the tiles in the string, the offsets in the definition of boundary string must be modified slightly. Let $p, q = 0/1, 1/1$ and the lattice vectors be as defined in Section 4.3:

$$v_{p,1} = 2 \quad v_{p,2} = -1 + \mathbf{i}$$

$$v_{q,1} = 1 + \mathbf{i} \quad v_{q,2} = 2\mathbf{i}.$$

The *zero-tile* is $T_{0/1} = \{0, \mathbf{i}, 2\mathbf{i}, 1, 1 + \mathbf{i}, 1 + 2\mathbf{i}\}$ and the *one-tile* is $T_{1/1} = \{0, \mathbf{i}, 1, 1 + \mathbf{i}\}$.

A *zero-one horizontal* boundary string is a collection of tiles $T_i \in \{T_{0/1}, T_{1/1}\}$ with offsets given by

$$c(T_i) - c(T_{i-1}) = \begin{cases} v_{q,1} & \text{if } T_{i-1} = T_q \\ v_{p,1} & \text{if } T_{i-1} = T_p, \end{cases} \quad (4.40)$$

and in the reversed case

$$c(T_i) - c(T_{i-1}) = \begin{cases} v_{q,1} + 1 & \text{if } pq \\ v_{p,1} & \text{if } pp \\ v_{p,1} - 1 & \text{if } qp \\ v_{q,1} & \text{if } qq, \end{cases} \quad (4.41)$$

where the right column denotes the tile tuple. We further impose that a (resp. reversed) horizontal zero-one boundary string begins with (resp. $T_{0/1}$) $T_{1/1}$. We also label horizontal zero-one boundary strings by binary words.

A *zero-one stacked horizontal* boundary string is a union of a horizontal zero-one boundary string $\{T_i^+\}$ and its reversal $\{T_i^-\}$ where

$$c(T^{+,1}) - c(T^{-,1}) = v_{p,2} + \mathbf{i}. \quad (4.42)$$

We again label the zero-one stacked horizontal boundary string by the non-reversed binary word. Unfortunately, in this case the stacked boundary strings may leave gaps which are too large. This occurs for exactly one particular interface qq , which we have displayed in Figure 4.10. To fix this, we fill the gap by requiring that whenever $T_{1/1}$ follows a $T_{1/1}$, the subsequent tile is replaced by an enlarged version:

$$T_{1/1}^d = T_{1/1} \cup \{\mathbf{i} - 1, 1 - \mathbf{i}\}, \quad (4.43)$$

but there are no other changes, *i.e.*, we impose $c(T_{1/1}^d) = c(T_{1/1})$. See Figure 4.11.

To define vertical strings, we simply rotate each of the above conditions by 90 degrees but exclude the doubled tiles. To be specific, a *zero-one vertical* boundary string is also a

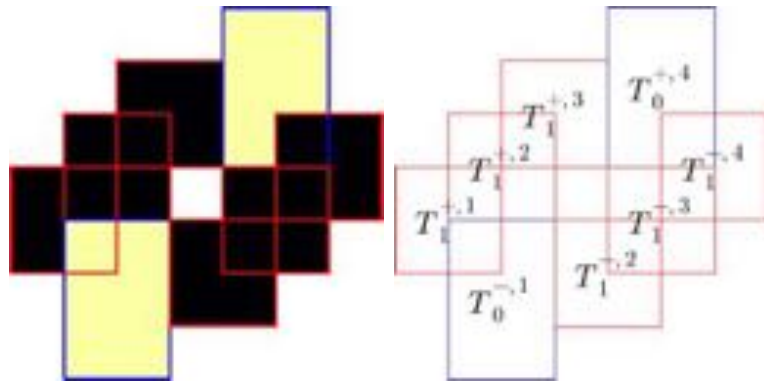


Figure 4.10: A gap inside a zero-one horizontal stacked boundary string corresponding to the word $qqqp$. Here we are outlining tiles on a square grid where each $x \in \mathbb{Z}[\mathbf{i}]$ is in the center of a square. On the left, points in the stacked string are filled in with either black ($T_{0/1}$) or yellow ($T_{1/1}$). On the right the outlines and annotations are displayed and the labeling is as in Figure 4.9. For brevity, we write 0 and 1 for 0/1 and 1/1 respectively.

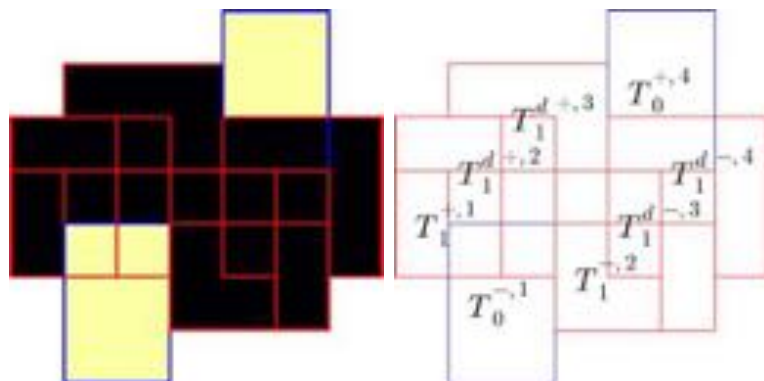


Figure 4.11: As Figure 4.10 but with gap fixed by $T_{1/1}^d$.

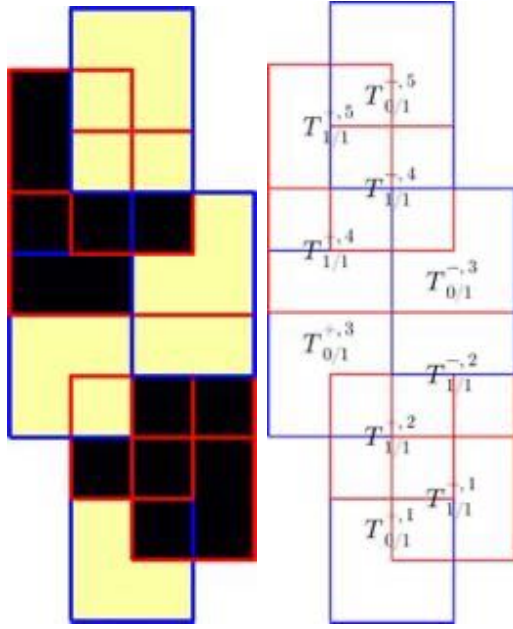


Figure 4.12: A vertical stacked zero-one boundary string corresponding to the word $pqpqq$ with the same labeling scheme as Figure 4.10.

collection of tiles $T_i \in \{T_{0/1}, T_{1/1}\}$ but with rotated offsets:

$$c(T_i) - c(T_{i-1}) = \begin{cases} v_{q,2} & \text{if } T_i = T_q \\ v_{p,2} & \text{if } T_i = T_p \end{cases} \quad (4.44)$$

and in the reversed case

$$c(T_i) - c(T_{i-1}) = \begin{cases} v_{p,2} + \mathbf{i} & \text{if } pq \\ v_{p,2} & \text{if } pp \\ v_{q,2} - \mathbf{i} & \text{if } qp \\ v_{q,2} & \text{if } qq. \end{cases} \quad (4.45)$$

A *zero-one stacked vertical boundary string* is a union of a vertical zero-one boundary string

$\{T_i^+\}$ and its reversal $\{T_i^-\}$ where

$$c(T^{+,1}) - c(T^{-,1}) = -v_{q,1}. \quad (4.46)$$

In the vertical case, we do not use doubled tiles and we further impose that every (resp. reversed) vertical zero-one boundary string begins with $T_{0/1}$ (resp. $T_{1/1}$). See an example of a stacked vertical zero-one boundary string in Figure 4.12. We again label the zero-one vertical boundary string by a binary word and the stacked string by the non-reversed word.

We conclude with a similar counterpart to Lemma 4.5.3.

Lemma 4.5.4. *If w is an almost palindrome the offsets between perpendicular tiles in the zero-one stacked string are fixed: in the horizontal case, if w starts with q and ends with p ,*

$$\begin{aligned} c(T_1^{+,1}) - c(T_1^{-,1}) &= -1 + 2\mathbf{i} = v_{p,2} + \mathbf{i} - qp \\ c(T_{1/1}^{+}) - c(T_{1/1}^{-}) &= -2 + 2\mathbf{i} = v_{p,2} + \mathbf{i} - 1 - qq \\ c(T_{0/1}^{+}) - c(T_{0/1}^{-}) &= -1 + 2\mathbf{i} = v_{p,2} + \mathbf{i} - pp \\ c(T_{|w|}^{+}) - c(T_{|w|}^{-}) &= -1 + \mathbf{i} = (v_{p,1} - v_{q,1}) + (v_{p,2} + \mathbf{i} - 1) - pq \end{aligned}$$

and in the vertical case, if w starts with p and ends with q ,

$$\begin{aligned} c(T_1^{+,1}) - c(T_1^{-,1}) &= -1 - \mathbf{i} = -v_{q,1} - pq \\ c(T_{1/1}^{+}) - c(T_{1/1}^{-}) &= -1 - \mathbf{i} = -v_{q,1} - qq \\ c(T_{0/1}^{+}) - c(T_{0/1}^{-}) &= -2 - \mathbf{i} = v_{p,2} - v_{q,1} - (v_{q,2} - \mathbf{i}) - pp \\ c(T_{|w|}^{+}) - c(T_{|w|}^{-}) &= -1 = -v_{q,1} + \mathbf{i} - qp, \end{aligned}$$

where the right column denotes the tile tuple.

In particular, there are finitely many types of pairwise intersecting tiles in such stacked

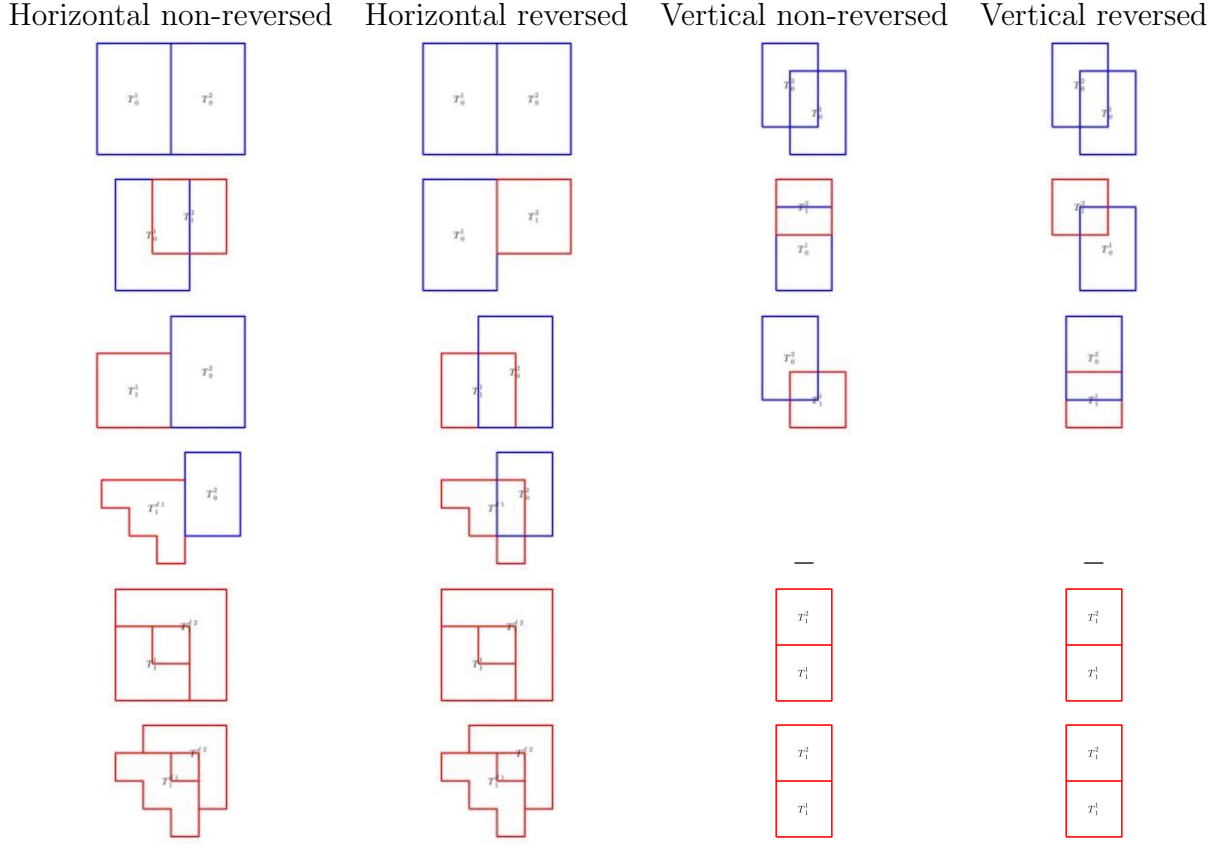


Table 4.1: Possible pairwise overlaps in a zero-one boundary string with labeling as Figure 4.10.

strings. See Figures 4.13 and 4.14 respectively. This finite check implies every stacked zero-one boundary string is simply connected.

□

4.5.5 Function data

We now associate function data to zero-one boundary strings. Recall the affine offsets associated to the hyperbola bases,

$$a_{p,1} = 0 \quad a_{p,2} = -\mathbf{i}$$

$$a_{q,1} = 0 \quad a_{q,2} = 1 - \mathbf{i},$$

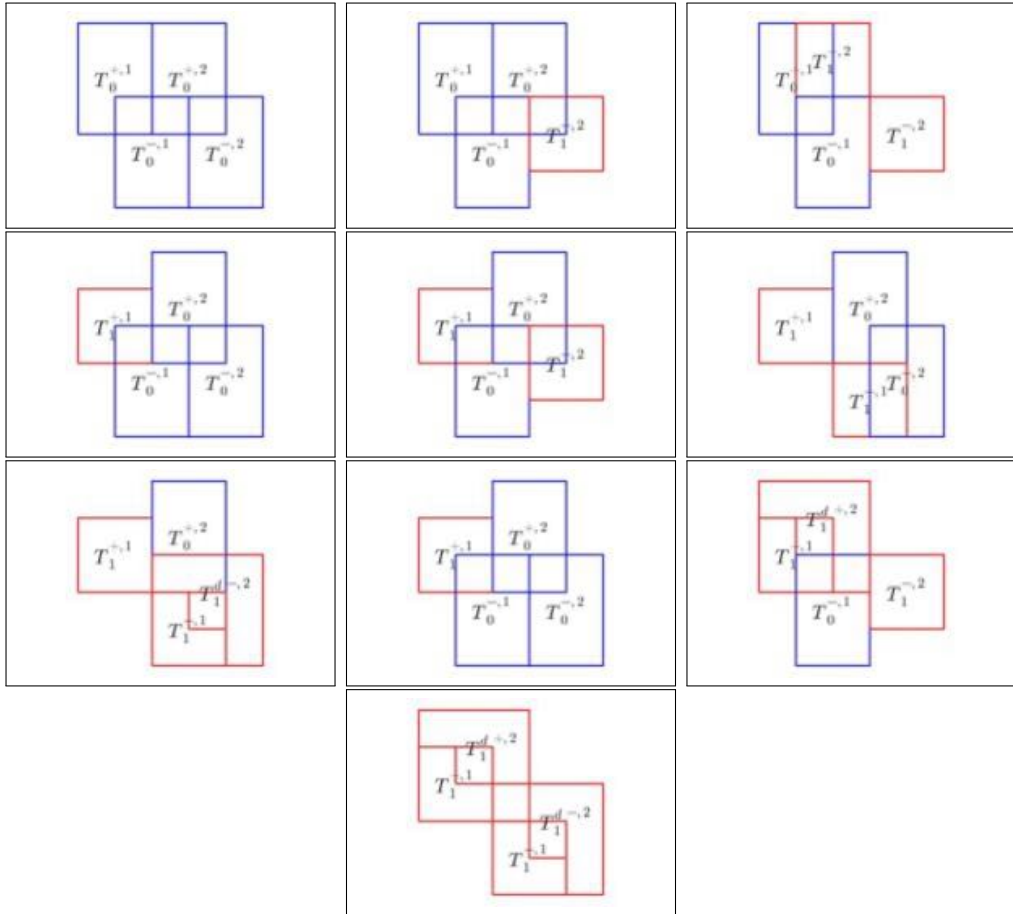


Figure 4.13: Possible overlaps in a stacked almost palindrome zero-one horizontal boundary string with labeling as Figure 4.10. Note that the first $T_{1/1}$ tile may be a $T_{1/1}^d$ tile.

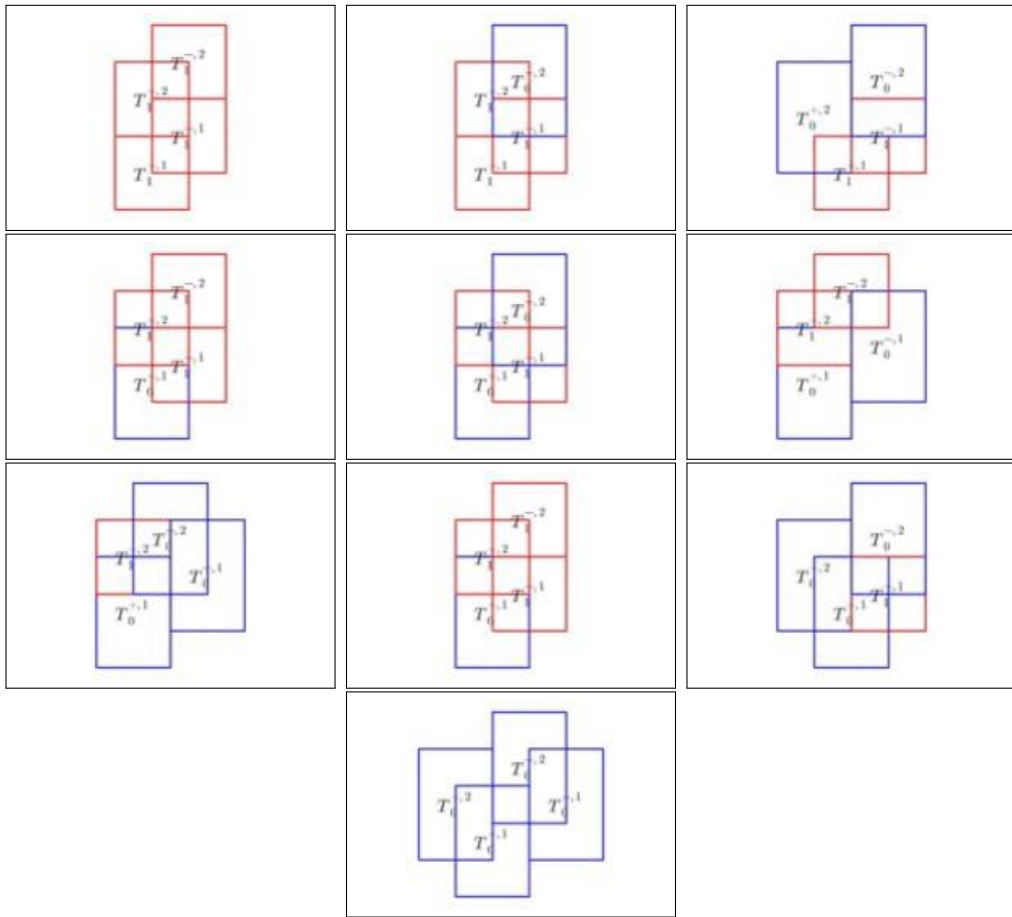


Figure 4.14: Possible overlaps in a stacked almost palindrome zero-one vertical boundary string with labeling as Figure 4.10.

for $p, q = 0/1, 1/1$.

The *zero-odometer* is any translation of $o_{0/1} : T_{0/1} \rightarrow \mathbb{Z}$, defined by $o_{0/1}(0) = o_{0/1}(1) = o_{0/1}(i) = o_{0/1}(1 + \mathbf{i}) = 0$ and $o_{0/1}(2i) = o_{0/1}(1 + 2\mathbf{i}) = -1$. The *one-odometer* is any translation of $o_{1/1} : T_{1/1} \rightarrow \mathbb{Z}$, defined by $o_{1/1}(0) = o_{1/1}(1) = o_{1/1}(1 + \mathbf{i}) = 0$ and $o_{1/1}(\mathbf{i}) = -1$. The *enlarged one-odometer* is any translation of $o_{1/1}^d : T_{1/1}^d \rightarrow \mathbb{Z}$ defined by $o_{1/1}^d = o_{1/1}$ on T_1 and $o_{1/1}^d(\mathbf{i} - 1) = -2$, $o_{1/1}^d(1 - \mathbf{i}) = 0$.

A sequence of zero/one-odometers $\{o_i\}$ respects a zero-one boundary string $\{T_i\}$ if each successive tile T_i is the domain of o_i and

$$\begin{aligned} s(o_{i+1}) - s(o_i) &= a_{i,j} && \text{non-reversed case} \\ s(o_{i+1}) - s(o_i) &= a_{i,j} + (a_{i,j'} - a_{i+1,j'}) && \text{reversed case,} \end{aligned} \tag{4.47}$$

where $(j, j') \in \{1, 2\}$ are the direction and its perpendicular respectively.

From Table 4.1, one can see some consecutive pairs of tiles do not overlap. This means odometers corresponding to such tiles may blow up across the boundary. We fix this by requiring a further compatibility relation between pairs of non-overlapping tiles. We assume that if T_1, T_2 are a consecutive sequence of horizontal tiles that do not overlap then, after a shared translation, o_i and o_{i+1} are constant across the shared boundary. That is, after the translation, $o_i(x) = o_{i+1}(y)$ for all $|y - x| = 1$. In the vertical case, if T_i and T_{i+1} do not overlap, then they must both be type 1/1; we assume that after a shared translation, $o_{i+1}(y) - o_i(x) = -1$ for $|y - x| = 1$.

We now check existence, using Lemma 4.5.4.

Lemma 4.5.5. *Given any word w , a sequence of zero-one odometers with a common extension which respects its boundary string or its reversal exists. Moreover, if w is an almost palindrome, then there exists a sequence of odometers $\{o_i^+\}$, and $\{o_i^-\}$ respecting $\mathcal{B}_w = \{T_i^+\}$ and a sequence $\{o_i^-\}$ respecting the reversed string $\mathcal{B}_{\text{rev}(w)}^r$ which have a common extension to the stacked string where $s(o_{1/1}^+) - s(o_{1/1}^-) = 0$ in the vertical case and $s(o_{1/1}^+) - s(o_{1/1}^-) = a_{p,2}$*

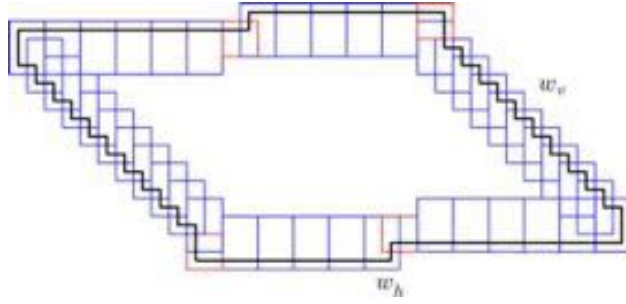


Figure 4.15: The boundary of a (w_h, w_v) -pseudo-square tile where w_h is the horizontal word qp^kqp^{k+1} and w_v is the vertical word $p^{2k+1}q$ for $k = 5$. The boundary word is outlined in the dual lattice in black.

in the horizontal case.

Proof. From the definitions, one can see that no three consecutive pairs of tiles in a boundary string can overlap - only two consecutive pairs can. Therefore, existence of a sequence of zero/one odometers respecting a boundary string reduces to checking compatibility between partial odometers for pairwise consecutive tiles. Since compatibility is an affine invariant relationship, we can translate so that the first odometer is exactly $o_{1/1}$ or $o_{0/1}$. This then reduces the compatibility check to a finite one, see Table 4.1.

The existence problem for a stacked string is similar - by Lemma 4.5.4, there are only ten possible cases for overlaps between tiles in a stacked string. We have enumerated these cases in Figures 4.13 and 4.14.

□

4.5.6 Pseudo-square tiles and boundary strings

We now associate horizontal and vertical boundary strings to tiles and partial odometers. Let (w_h, w_v) denote almost palindromes which define zero-one horizontal and vertical boundary strings respectively.

Definition 1. A (w_h, w_v) -pseudo-square is a tile, T , which can be decomposed along its

boundary into a sequence of subtiles

$$\mathcal{T}_{h,v} := \{T_{i,h}^+\} \cup \{T_{i,h}^-\} \cup \{T_{i,v}^+\} \cup \{T_{i,v}^-\}$$

each of which respectively form a w_h , $\text{rev}(w_h)$, w_v , and $\text{rev}(w_v)$ zero-one horizontal, reversed horizontal, vertical, and reversed vertical boundary string. That is, $\mathcal{T}_{h,v} \subset T$, $c(T_{1,h}^+) = c(T_{1,v}^-) = c(T)$ and $\partial T \cap \mathcal{T}_{h,v} = \partial T$.

A partial odometer $o : T \rightarrow \mathbb{Z}$ respects (w_h, w_v) if its restrictions to $\mathcal{T}_{h,v}$ respect w_h -horizontal, w_v -vertical, and $\text{rev}(w_h)$ -reversed-horizontal and $\text{rev}(w_v)$ -reversed-vertical zero-one boundary strings respectively.

We sometimes overload notation and also refer to the word describing the boundary string as a set of tiles.

We now extend the rotation operator to pseudo-square tiles. For a binary word w , let $\mathcal{F}(w)$ denote the *flipping operator* which flips every p to a q and vice versa. Then,

$$\mathcal{R}(w_h, w_v) = (\mathcal{F}(w_v), \mathcal{F}(w_h)) \quad (4.48)$$

sends a pair of horizontal/vertical strings to a rotated pair. We now extend this to tiles. If T is a (w_h, w_v) -pseudo-square then

$$\mathcal{R}(T) = T_r, \quad (4.49)$$

where T_r is a $\mathcal{R}(w_h, w_v)$ -pseudo-square with $c(T_r) = c(T)$.

We now define a map $G(w_h, w_v) \in F_2^*$ to $(w_1, w_2) \in F_2$. We start by defining it for pairs

of horizontal zero-one tiles (strings),

$$\left\{ \begin{array}{ll} g(p * q) & \rightarrow 1 * \mathbf{i} \\ g(q * p) & \rightarrow 1 * 1 \\ g(q_d * p) & \rightarrow \mathbf{i} * 1 \\ g(p * p) & \rightarrow 1 * 1 \\ g(q * q) & \rightarrow \mathbf{i} * 1 \\ g(q_d * q) & \rightarrow \mathbf{i} * 1, \end{array} \right. \quad (4.50)$$

where q_d indicates a $T_{1/1}^d$ tile. Next extend the map to w_h by,

$$G(w_h) = g(w_h[1 : 2]) * g(w_h[2 : 3]) * \cdots * g(w_h[|w_h| - 1, |w_h|]) * 1 \quad (4.51)$$

and extend this to w_v by

$$G(w_v) = \mathbf{i} \cdot G(\mathcal{F}(w_h)), \quad (4.52)$$

where $\mathbf{i} \cdot w_1$ denotes component multiplication in $\mathbb{Z}[\mathbf{i}]$ (for example, $\mathbf{i} \cdot (\mathbf{i} * 1) = -1 * \mathbf{i}$). And finally, extend the map pairwise $G(w_h, w_v) = (G(w_h), G(w_v))$.

Our next lemma uses this to express (w_h, w_v) pseudo-squares using the boundary words from Section 4.4. See Figures 4.16 and 4.15 for an illustration of this.

Lemma 4.5.6. *The boundary word of (w_h, w_v) -pseudo-square T can be written as $w_1 * w_2 * \widehat{\text{rev}}(w_1) * \widehat{\text{rev}}(w_2)$ where $(w_1, w_2) = G(w_h, w_v)$. In particular, T is 180-degree symmetric and $\mathcal{R}(T)$ is a 90-degree rotation of T .*

Proof. We first check that $G(w_h)$ traces out the lower boundary of w_1 . By checking Table 4.1, we see that the (4.50) does traces out the lower boundary for each pair of tiles. Indeed, if neither tile in the pair (T^1, T^2) is $T_{1/1}^d$, the path starts at $c(T^1)$ and ends at $c(T^2)$. Otherwise,

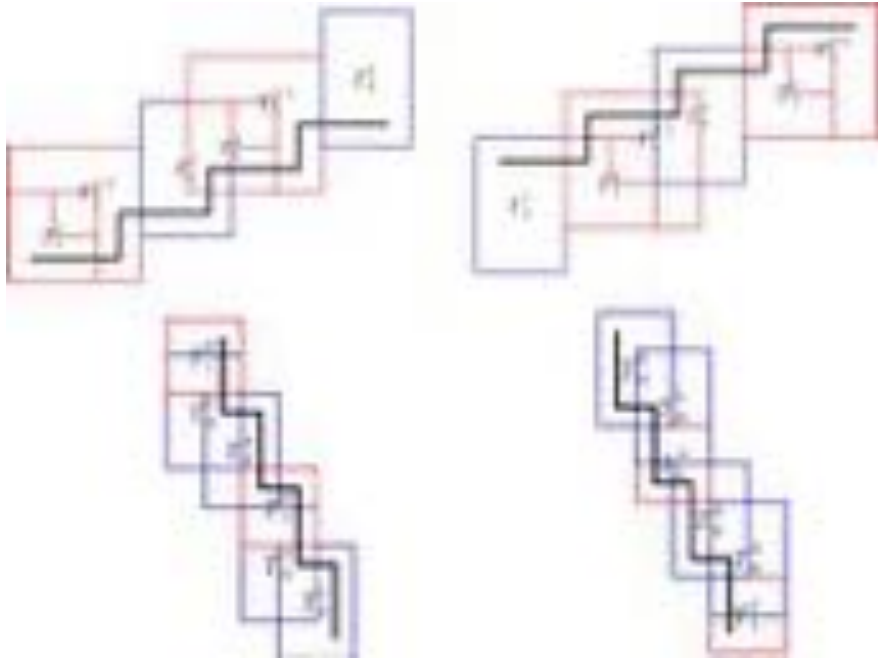


Figure 4.16: From top left to bottom right, $w_h = q^2pq^2p$, reversed $\text{rev}(w_h)$, $w_v = \mathcal{F}(w_h)$, reversed $\text{rev}(w_v)$. The boundary words, $G(w_h, w_v)$ are drawn in black.

the path starts or ends at $c(T_{1/1}^d) + (1 - \mathbf{i})$. The extra $*1$ in (4.51) ensures the path ends at the lower right corner of $T_{0/1}$. The lower right corner of $T_{0/1}$, after a 90-degree clockwise rotation maps to the lower-left corner of $T_{1/1}$. In general, the lower boundary of every pair of horizontal tiles in Table 4.1 maps to the right boundary of the flipped pair of vertical tiles. We can also use the table to check that the reversed string $\text{rev}(w_h)$ is a 180-degree rotation of w_h , thus $\text{rev}(w_1)$ traces the top boundary of $\text{rev}(w_h)$.

□

This next lemma shows that if a partial odometer respects a pseudo-square, then it has a common extension to the plane.

Lemma 4.5.7. *Let T be a (w_h, w_v) -pseudo-square, $(w_1, w_2) = G(w_h, w_v)$, and suppose $o : T \rightarrow \mathbb{Z}$ respects (w_h, w_v) . If the conditions in Lemma 4.4.1 on (w_1, w_2) are met, T generates a $(v_1, v_2) := (\sum w_1 + \mathbf{i}, \sum w_2 - 1)$ regular almost-tiling.*

Further suppose $(v_1, v_2) = v_{n/d, 1}, v_{n/d, 2}$ for some reduced fraction $0 < n/d < 1$. Then,

the surrounding of T with respect to $(v_{n/d,1}, v_{n/d,2})$ consists of two stacked zero-one horizontal and two vertical boundary strings and the translation condition,

$$o(x \pm v_{n/d,i}) = o(x) \pm a_{n/d,i}^T x + k_{n/d,\pm i} \quad \text{for } x \in \mathbb{Z}^2, \quad (4.53)$$

where $k_{n/d,\pm i}$ are constants and $i \in \{1, 2\}$ selects the lattice vector, uniquely extends $o : T \rightarrow \mathbb{Z}$ to the plane.

Proof. The first claim follows from Lemmas 4.5.6 and 4.4.1. We next check that the interfaces $(T, T \pm v_{n/d,2})$ and $(T, T \pm v_{n/d,1})$ are stacked horizontal or vertical zero-one boundary strings respectively.

Let A be the horizontal string for T and B the reversed horizontal string for $T - v_{n/d,2}$. By Lemma 4.5.6, the first tile in B is located at $c(T) - v_{n/d,2} + v_{n/d,2} - (2\mathbf{i} - 1)$. Thus, the offset between the first tile in B and the first tile in A is $2\mathbf{i} - 1 = v_{0/1,2} + \mathbf{i}$, the correct initial offset for a stacked string.

Similarly if C is the vertical string for T and D the reversed vertical string for $T + v_{n/d,1}$, then the offset between the respective first tiles in C and D is $(\mathbf{i} + 1) = -v_{1/1,1}$. The other two interfaces are stacked strings by the above arguments for $T - v_{n/d,1}$ and $T + v_{n/d,2}$.

Let $\mathcal{T} = \{T + iv_{n/d,1} + jv_{n/d,2}\}$ denote the almost tiling of T and for $T_{i,j} \in \mathcal{T}$, let $o_{i,j} : T_{i,j} \rightarrow \mathbb{Z}$ denote the translations of o by $(iv_{n/d,1} + jv_{n/d,2}, ia_{n/d,1} + ja_{n/d,2})$. By definition, each $o_{i,j}$ respects (w_h, w_v) on $T_{i,j}$. Restrict the $o_{i,j}$ to the stacked boundary strings and check, by repeating the above argument, that the slope difference between the first two perpendicular tiles in the stacked horizontal strings are $-a_{p,2}$. Similarly, the slope difference for the stacked vertical strings is $a_{q,1} = 0$. Therefore, by Lemma 4.5.5, each pair of odometers is compatible. This together with Lemma 4.5.2 implies there is a common extension of $o_{i,j}$ tp the plane. \square

We also require the notion of a tile odometer respecting only a horizontal boundary or

vertical boundary string.

Definition 2. A w_h or w_v -pseudo-square is a tile T , whose boundary contains (but may not be equal to)

$$\mathcal{T}_{h,*} = \{T_{i,h}^+\} \cup \{T_{i,h}^-\}$$

or

$$\mathcal{T}_{*,v} = \{T_{i,v}^+\} \cup \{T_{i,v}^-\},$$

where T are as in Definition 1 and either $c(T) = c(T_{1,h}^+)$ or $c(T) = c(T_{1,v}^-)$

A partial odometer $o : T \rightarrow \mathbb{Z}$ respects w_h or w_v if its restriction to $\mathcal{T}_{h,*}$ are w_h -horizontal and $\text{rev}(w_h)$ -reversed-horizontal strings or its restriction to $\mathcal{T}_{*,v}$ are w_v and and $\text{rev}(w_v)$ -reversed-vertical zero-one boundary strings respectively.

4.5.7 Explicit formulae for zero-one boundary strings

We collect in this section some explicit formulae for zero-one boundary strings which are straightforward consequences of the definitions. In particular, these will correspond to the degenerate base cases in (4.32).

The formulae are only used to verify the explicit odometers in Section 4.6 and may be skipped on a first read.

Horizontal boundary strings

We first note the form of the odometers after a translation. The zero-odometer translated by $-a_{p,2}$, $\hat{o}_{0/1} : T_{0/1} \rightarrow \mathbb{Z}$ is given by $\hat{o}_{0/1}(0) = \hat{o}_{0/1}(1) = -1$ and $\hat{o}_{0/1}(\mathbf{i}) = \hat{o}_{0/1}(1 + \mathbf{i}) = 0 = \hat{o}_{0/1}(2\mathbf{i}) = \hat{o}_{0/1}(1 + 2\mathbf{i}) = 0$. The one-odometer translated by $-a_{q,2}$, $\hat{o}_{1/1} : T_{1/1} \rightarrow \mathbb{Z}$ is given by $\hat{o}_{1/1}(0) = \hat{o}_{1/1}(\mathbf{i}) = \hat{o}_{1/1}(1 + \mathbf{i}) = 0$ and $\hat{o}_{1/1}(1) = -1$. Similarly, the enlarged one-odometer translated by $-a_{q,2}$, $\hat{o}_{1/1}^d : T_{1/1}^d \rightarrow \mathbb{Z}$ is given by $\hat{o}_{1/1}^d = \hat{o}_{1/1}$ on $T_{1/1}$ and $\hat{o}_{1/1}(1 - \mathbf{i}) = -2$, $\hat{o}_{1/1}(\mathbf{i} - 1) = 0$.

Now, let $\{o_i^+\}$ (resp. $\{o_i^-\}$) respect an arbitrary (resp. reversed) horizontal boundary string. If $o_1^+ \in \{o_{0/1}, o_{1/1}\}$, then, $o_i^+ \in \{o_{0/1}, o_{1/1}\}$ depending on the respective letter. Similarly, if $o_1^- \in \{\hat{o}_{0/1}, \hat{o}_{1/1}\}$ then $o_i^- \in \{\hat{o}_{0/1}, \hat{o}_{1/1}\}$.

Vertical boundary strings

The vertical boundary string case involves more computations since the translations involve non-zero affine factors. Fix $k \geq 1$. The following functions, corresponding to the quadratic growth of the hyperbola bases, will be used:

$$t(j) = -j(j+1)/2 \quad q(j) = -\lfloor \frac{j^2}{4} \rfloor \quad (4.54)$$

In each case, let $\{o_i^+\}$ (resp. $\{o_i^-\}$) respect the indicated (resp. reversed) vertical boundary string.

Case 1: $p^k q$ and its reversal

Suppose $o_1^+ = o_{0/1}$ on $T_{1/1}$, the first tile in $p^k q$. Then, for $1 \leq j \leq k$

$$o_j^+ = \begin{bmatrix} t(j) & t(j) \\ t(j-1) & t(j-1) \\ t(j-2) & t(j-2) \end{bmatrix} \quad (4.55)$$

and

$$o_{k+1}^+ = \begin{bmatrix} t(k+1) & t(k+1)+1 \\ t(k) & t(k) \end{bmatrix}. \quad (4.56)$$

If $o_1^- = o_{0/1}$ on $T_{0/1}$, the first tile in $\text{rev}(p^k q)$, then

$$o_j^- = \begin{bmatrix} t(j+1)+2 & t(j+1)+3 \\ t(j)+1 & t(j)+2 \\ t(j-1) & t(j-1)+1 \end{bmatrix} \quad (4.57)$$

for $2 \leq j \leq k+1$.

Case 2: pq^k and its reversal

Suppose $o_1^+ = o_{0/1}$ on $T_{0/1}$, the first tile in pq^k . Then for $2 \leq j \leq k+1$, $j' = 2(j-1)$

$$o_j^+ = \begin{bmatrix} q(j'+2)+1 & q(j'+1) \\ q(j'+1)+1 & q(j') \end{bmatrix}. \quad (4.58)$$

If $o_{1/1}^- = o_{1/1}$ on $T_{1/1}$, the first tile in $\text{rev}(pq^k)$ then for $1 \leq j \leq k$

$$o_j^- = \begin{bmatrix} q(2j) & q(2j-1) \\ q(2j-1) & q(2j-2) \end{bmatrix} \quad (4.59)$$

and

$$o_{k+1}^- = \begin{bmatrix} q(2k+2) & q(2k+1)-1 \\ q(2k+1) & q(2k) \\ q(2k) & q(2k-1) \end{bmatrix}. \quad (4.60)$$

Draft Mar 13

Case 3: $pq^k pq^{k+1}$ and its reversal

Suppose $o_{1/1}^+ = o_{0/1}$ on $T_{0/1}$, the first tile in $pq^k pq^{k+1}$. Then o_j^+ for $1 \leq j \leq (k+1)$ are as

Case 2 above. Then

$$o_{k+2} = \begin{bmatrix} q(2(k+1)+3) + 3 & q(2(k+1)+2) + 1 \\ q(2(k+1)+2) + 3 & q(2(k+1)+1) + 1 \\ q(2(k+1)+1) & q(2(k+1)) + 1 \end{bmatrix} \quad (4.61)$$

and for $k+3 \leq j \leq 2k+3$, $j'' = 2(j-2)$

$$o_j = \begin{bmatrix} q(j''+4) + 3 & q(j''+3) + 1 \\ q(j''+3) + 3 & q(j''+2) + 1 \end{bmatrix}. \quad (4.62)$$

If $o_{1/1}^- = o_{1/1}$ on $T_{1/1}$, the first tile in $\text{rev}(pq^k pq^{k+1})$ then o_j^- for $1 \leq j \leq (k+2)$ the first $(k+2)$ are as Case 2 above. Then, for $(k+3) \leq j \leq 2k+2$,

$$o_j^- = \begin{bmatrix} q(2(j-1)+2) + 1 & q(2(j-1)+1) \\ q(2(j-1)+1) + 1 & q(2(j-1)) \end{bmatrix} \quad (4.63)$$

and for $w = 2(k+1)$

$$o_{2k+3}^- = \begin{bmatrix} q(2w+2) + 1 & q(2w+1) \\ q(2w+1) + 1 & q(2w) \\ q(2w) + 1 & q(2w-1) \end{bmatrix}. \quad (4.64)$$

4.6 Base cases

Before we extend the hyperbola recursion to all odometers and tiles, we study a degenerate family and in fact prove Theorem 4.1.3 for this family. The reader is encouraged to skim or skip this section and come back to it only after reading Section 4.7.

Draft Mar 13

The reduced fractions which we analyze here are those in a Farey quadruple where at least one of the two parents is $(0/1)$ or $(1/1)$. Specifically, we prove the following.

Proposition 4.6.1. *For each Farey quadruple of the form $\mathbf{q}_{(w)} = (p_1, q_1, p_2, q_2)$ where $w = 3^k$ or 2^k for $k \geq 0$ there is a quadruple of standard and alternate tile odometers*

$$(o_{p_1}, o_{q_1}, o_{p_2}, o_{q_2}) \quad \text{and} \quad (\hat{o}_{p_1}, \hat{o}_{q_1}, \hat{o}_{p_2}, \hat{o}_{q_2})$$

with finite domains, $T(o_{n/d}) = T_{n/d}$ and $T(\hat{o}_{n/d}) = \hat{T}_{n/d}$. The tile odometers of each such child Farey pair satisfy the following properties.

- (a) *Under the lattice $L'(n/d)$, $T(n/d)$ generates an almost pseudo-square tiling.*
- (b) *$\hat{T}(n/d)$ covers \mathbb{Z}^2 under $L'(n/d)$.*
- (c) *There exist unique, distinct recurrent extensions $o_{n/d} : \mathbb{Z}^2 \rightarrow \mathbb{Z}$ and $\hat{o}_{n/d} : \mathbb{Z}^2 \rightarrow \mathbb{Z}$ satisfying the correct growth dictated by (4.9).*
- (d) *$T(n/d)$ is a (w_h, w_v) -pseudo-square which $o_{n/d}$ respects.*

Standard case		w_h	w_v
3^k odd, $k \geq 1$	$1/d$, $d \geq 4$ even	$qp^k qp^{k+1}$	$p^{2k+1} q$
3^k even, $k \geq 0$	$1/d$, $d \geq 3$ even	qp^{k+1}	$p^{2(k+1)} q$
2^k odd, $k \geq 0$	$\mathcal{R}(1/d)$, $d \geq 3$ even	$q^{2(k+1)} p$	$p q^{k+1}$
2^k even, $k \geq 1$	$\mathcal{R}(1/d)$, $d \geq 4$ even	$q^{2k+1} p$	$p q^k p q^{k+1}$

The first column denotes a word which selects a degenerate Farey quadruple and the parity of the reduced fraction displayed in the second column.

- (e) *$\hat{T}(n/d)$ is a $w_{h/v}$ -pseudo-square which $\hat{o}_{n/d}$ respects*

Draft Mar 13

Alternate case		w_h	w_v
3^k odd, $k \geq 1$	$1/d, d \geq 4$ even	-	$p^{2k+1}q$
3^k even, $k \geq 0$	$1/d, d \geq 3$ even	qp^{k+1}	-
2^k odd, $k \geq 0$	$\mathcal{R}(1/d), d \geq 3$ even	-	pq^{k+1}
2^k even, $k \geq 1$	$\mathcal{R}(1/d), d \geq 4$ even	$q^{2k+1}p$	-

In particular, the alternates coincide with the standards on one set of boundaries.

(f) Some later odometers contain exact translations of earlier odometers. To state this succinctly, write $w(p, q)$ for the even and odd reduced fraction in the child Farey pair of \mathbf{q}_w and let $T(n/d)(v) = T(n/d) \cup (T(n/d) + v)$ for $v \in \mathbb{Z}[\mathbf{i}]$ and $n/d \in \{p, q\}$. The following holds for all $k \geq 1$:

$$\begin{aligned} T(3^k(p)) &\supset T(q, v_{q,1} + v_{p,1} + v_{p,2}) & \text{offset} = 0 \\ \hat{T}(3^k(p)) &\supset T(q, v_{q,1} + v_{p,1} + 2v_{p,2}) & \text{offset} = 0 \\ \hat{T}(3^k(q)) &\supset T(q, -v_{q,1} - v_{p,1}) & \text{offset} = v_{p,2} + v_{p,1} \end{aligned} \tag{4.65}$$

where $(p, q) = 3^{k-1}(p, q)$ and

$$\begin{aligned} T(2^k(q)) &\supset T(p, v_{p,2} + v_{q,2} - v_{q,1}) & \text{offset} = v_{q,1} \\ \hat{T}(2^k(q)) &\supset T(p, v_{p,2} + v_{q,2} - 2v_{q,1}) & \text{offset} = v_{q,1} \\ \hat{T}(2^k(p)) &\supset T(p, v_{p,2} + v_{q,2}) & \text{offset} = v_{q,1} \end{aligned} \tag{4.66}$$

where $(p, q) = 2^{k-1}(p, q)$. The third column records $c(T_1) - c(T_2)$ where T_1 is the tile in the second column and T_2 is the tile in the first column.

The tile odometers for $k \geq 1$ have an analogous decomposition with affine factors and translations dictated by (4.65) and (4.66). For example, the restriction of $o_{3^k(p)}$ to $T(q, v_{q,1} + v_{p,1} + v_{p,2})$ is exactly equal to translated earlier tile odometers, $o_q^1 \cup o_q^2$ where

$c(T(o_q^1)) - c(T_{o_{3^k(p)}}) = 0$, $T(o_q^1) \cup T(o_q^2) = T(q, v_{q,1} + v_{p,1} + v_{p,2})$, $s(o_q^1) - s(o_q^2) = a_{p,2}$,
and $s(o_q^2) - s(o_{3^k(p)}) = 0$.

(g) Some later odometers contain partial translations of earlier odometers. The following holds for all $k \geq 1$ (using the same notation as the previous item):

$$T(3^k(q)) \supset T(q, v_{p,1} + 2v_{p,2}) \quad \text{offset} = 0 \quad (4.67)$$

where $(p, q) = 3^{k-1}(p, q)$ and

$$T(2^k(p)) \supset T(p, -2v_{q,1} + v_{q,2}) \quad \text{offset} = 2v_{q,1} \quad (4.68)$$

where $(p, q) = 2^{k-1}(p, q)$. The tile odometers for $k \geq 1$ have an analogous decomposition (as in the previous item) but only after removing two corner cells from each of the subtiles on the right-hand-side:

$$T^{sm}(q) = T(q) \setminus \{c_1 \cup c_2\} \quad \text{where } (p, q) = 3^{k-1}(p, q) \quad (4.69)$$

where $c_1 = c(T(q))$ and $c_2 = c_1 + (v_{q,1} + v_{q,2} - v_{p,2})$ and

$$T^{sm}(p) = T(p) \setminus \{c'_1 \cup c'_2\} \quad \text{where } (p, q) = 2^{k-1}(p, q) \quad (4.70)$$

where $c'_1 = c(T(p)) + v_{p,1} - \mathbf{i}$ and $c'_2 = c(T(p)) + v_{p,2} + 1$.

This family will form the base cases for the general recursion in the subsequent section. As noted above, there is a recursive structure here but with some ‘errors’ in the full decomposition. If the tile sizes are reduced to avoid these errors, then later tiles will be too small to cover \mathbb{Z}^2 .

Since these errors are limited to the degenerate family and the odometers for this family

are so simple, we take the cumbersome but elementary approach and provide the exact formulae. One could avoid this by adding additional cases to the general recursion.

4.6.1 Base points

We first check that the base points of the hyperbola $0/1$ and $1/1$, are on $\partial\Gamma_F$ via an explicit construction. We recall a criteria for checking recurrence from the sandpile literature. Let $s : \mathbb{Z}^2 \rightarrow \mathbb{Z}$ and let H be a finite induced subgraph of the F -lattice. H is *allowed* for s if there is a vertex v of H where $s(v)$ is at least the in-degree of v in H and otherwise is *forbidden*.

Proposition 4.6.2. *Holroyd et al. [2008] An integer superharmonic function g is recurrent if and only if every nonempty induced subgraph of the F -lattice is allowed for $s := \Delta g + 1$.*

In particular, Proposition 4.6.2 reduces verifying recurrence of a function to checking a condition on its Laplacian (which is no surprise given the function s in the statement is usually referred to as a recurrent sandpile Levine and Propp [2010]).

Lemma 4.6.1. *The functions*

$$g_{0/1}(x) = -\frac{x_2(x_2+1)}{2} \quad g_{1/1}(x) = -\lfloor \frac{(x_2-x_1)^2}{4} \rfloor$$

are odometers for $0/1$ and $1/1$ respectively.

Proof. The growth condition can be checked using the definition (4.2). Moreover, $\Delta g_{0/1}(x) = \Delta g_{1/1}(x) = -1\{(x_1+x_2)\text{ is even}\}$. By Proposition 4.6.2 it remains to check that every nonempty induced subgraph H of the F -lattice is allowed for $s = 1\{(x_1+x_2)\text{ is odd}\}$. Let x denote the lower left vertex of H . That is x has minimal x_2 coordinate and of all other $y \in H$ with $y_2 = x_2$, x_1 is minimal. This implies the only possible neighbors of x in H are $x + e_1$ or $x + e_2$. If (x_1+x_2) is odd, then $s(x) = 1$ so we may suppose otherwise. If

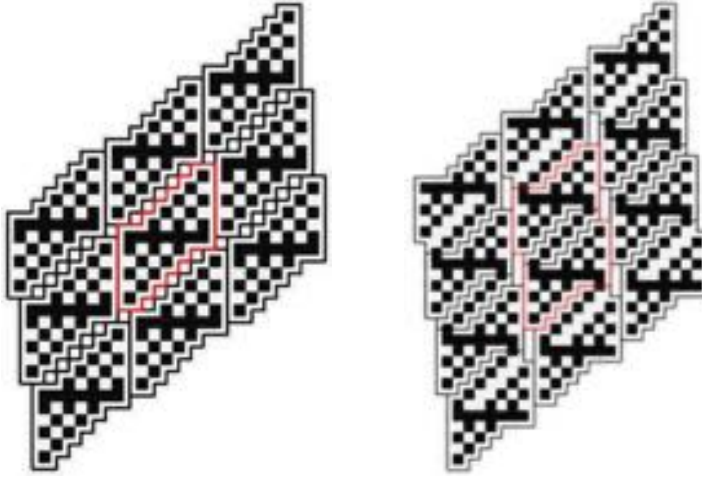


Figure 4.17: A period of the Laplacian of a staircase odometer on the left and its alternate. The string is 22 and the fraction is $3/4$. Each tile is outlined in the dual lattice.

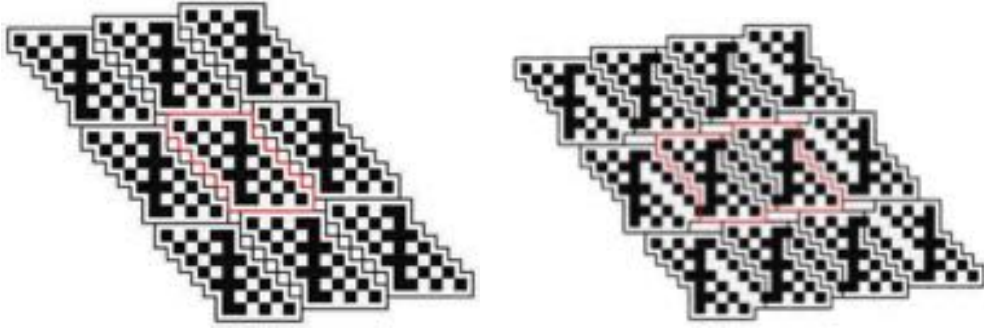


Figure 4.18: The rotated standard and alternate staircase odometers of Figure 4.17. The string is 33 and the fraction is $1/7$.

$(x + e_1) \in H$, then $s(x + e_1) = 1$ and by our choice of x , $(x + e_1 - e_2) \notin H$, thus $s(x + e_1)$ is larger than its in-degree in H , completing the proof. \square

4.6.2 Staircases

The *staircase* fractions are the reduced fractions of the form $\frac{1}{d}$ for d odd and their rotations, $\mathcal{R}(1, d) = (\frac{d-1}{2}, \frac{d+1}{2})$. These fractions are the even or odd child in Farey quadruples \mathbf{q}_3^k or \mathbf{q}_2^k for $k \geq 0$ respectively. The constructed tiles and Laplacians will respect the rotational invariance inherited from Lemma 4.3.6.

We start with the standard even child of \mathbf{q}_{3^k} for $k \geq 0$.

Lemma 4.6.2. *For each $d \geq 3$ odd,*

$$T_{1/d} := \{(x_1, x_2) \in [2-d, d] \times [0, d+1] : 1 \leq (x_1 + x_2) \leq (d+2)\} \cup \{(0, 0), (2, d+1)\}$$

is a $(qp^{k+1}, p^{2(k+1)}q)$ -pseudo-square which $g_{1/d} : T_{1/d} \rightarrow \mathbb{Z}$, given by,

$$g_{1/d}(x) = -\frac{1}{2}x_2(x_2 + 1) + (x_2 + \min(x_1 - 1, 0)) + 1\{(x_1, x_2) \in \{(0, 0), (2, d+1)\}\}$$

respects.

Proof. We start by observing that the bottom boundary of $T_{1/d}$ is qp^{k+1} zero-one horizontal boundary string. Indeed,

$$T_{1/d} \supset A_1 \cup A_2 := \{[0, 1] \times [0, 1]\} \cup \{[2, d] \times [0, 2]\}$$

is a qp^{k+1} horizontal boundary string:

$$A_1 = T_{1/1} \quad A_2 = v_{p,1} + \cup_{j=1}^{k+1} (T_{0/1} + jv_{p,1})$$

Moreover an inspection of the formula shows that $g_{1/d} = o_{1/1}$ on A_1 and $g_{1/d} = o_{0/1}$ on the translations of $T_{0/1}$ which form A_2 .

The top boundary of $T_{1/d}$ is a $\text{rev}(p^{k+1}q)$ zero-one horizontal reversed boundary string. Indeed,

$$T_{1/d} \supset A_2^r \cup A_1^r := \{[2-d, 0] \times [d-1, d+1]\} \cup \{[1, 2] \times [d, d+1]\}$$

is a $p^{k+1}q$ zero-one reversed horizontal boundary string:

$$A_2^r = \cup_{j=0}^k \{T_{0/1} + jv_{p,1}\} \quad A_1^r = T_{1/1} + kv_{p,1} + v_{q,1} + 1.$$

To check that $g_{1/d}$ respects the string, it is convenient to consider the translation

$$g_{1/d}^r = g_{1/d} - (1, -d)^T x - \frac{1}{2}d(d+1) + 1$$

and recall the translated versions of the zero-one odometers, $\hat{o}_{1/1}$ and $\hat{o}_{0/1}$ defined in Section 4.5.7. Once we make this translation, we can use the formula to compute

$$g_{1/d}^r([1, 2] \times [d, d+1]) = \hat{o}_{1/1} = \begin{bmatrix} 0 & 0 \\ 0 & -1 \end{bmatrix}$$

and $g_{1/d}^r([2-d, 0] \times [d-1, d+1]) = 0$ and $g_{1/d}^r([2-d, 0], d-1) = -1$ which coincides with copies of $\hat{o}_{0/1}$.

The check for the right and left boundaries proceeds by comparing to the explicit formulae for the degenerate zero-one strings given in Section 4.5.7. We use the notation defined there. We first check that the right-boundary is a $p^{2(k+1)}q$ string by observing

$$T_{1/d} - (d-1, 0) \supset A_1 \cup A_2 := \bigcup_{j=0}^{2(k+1)-1} (T_{1/1} + jv_{p,2}) \cup (T_{0/1} + (2(k+1)-1)v_{p,2} + v_{q,2}).$$

Indeed, the upper right corner of each $v_{p,2}$ translation of $T_{1/1}$ satisfies the equality $x_1+x_2 = 3$ and the upper right corner of $T_{0/1} + (2(k+1)-1)v_{p,2} + v_{q,2}$ is $(3-d, d+1)$. To check the formula matches (4.55) observe that on $A_1 \cup A_2 + (d-1, 0)$, $g_{1/d} = -\frac{1}{2}x_2(x_2+1) + x_2$. And so, on each $T_j := T_{1/1} + (j-1)v_{p,2} + (d-1, 0)$,

$$g_{1/d} \upharpoonright_{T_j} = \begin{bmatrix} t(j+1) & t(j+1) \\ t(j) & t(j) \\ t(j-1) & t(j-1) \end{bmatrix} + \begin{bmatrix} j+1 & j+1 \\ j & j \\ j-1 & j-1 \end{bmatrix} = \begin{bmatrix} t(j) & t(j) \\ t(j-1) & t(j-1) \\ t(j-2) & t(j-2) \end{bmatrix}.$$

The formula also implies it coincides with (4.56) on A_2 .

The argument for the left boundary is symmetric. Start by observing

$$T_{1/d} \supset A_1 \cup A_2 := T_{0/1} \cup \bigcup_{j=0}^{2(k+1)-1} (T_{1/1} + jv_{p,2} + \mathbf{i}).$$

Since, on the left boundary $g_{1/d} = -\frac{1}{2}x_2(x_2 + 1) + (x_1 + x_2 - 1)$, $g_{1/d} \upharpoonright_{A_1} = o_{0/1}$. The lower left corner of each $T_j := T_{1/1} + \mathbf{i} + (j - 2)v_{p,2}$ for $2 \leq j \leq 2(k + 1) + 1$ lies on the left boundary, $(x_1 + x_2) = 1$. Hence,

$$g_{1/d} \upharpoonright_{T_j} = \begin{bmatrix} t(j+1) & t(j+1) \\ t(j) & t(j) \\ t(j-1) & t(j-1) \end{bmatrix} + \begin{bmatrix} 2 & 3 \\ 1 & 2 \\ 0 & 1 \end{bmatrix}$$

which is exactly (4.57).

□

Next is the standard odd child of \mathbf{q}_{2k} .

Lemma 4.6.3. *For each $p_1 = \frac{\frac{d-1}{2}}{\frac{d+1}{2}}$, $d \geq 3$ odd,*

$$T_{p_1} := \{(x_1, x_2) \in [0, d+1] \times [1, 2d-1] : -1 \leq (x_2 - x_1) \leq d\} \cup \{(0, d+1), (d+1, d-1)\}$$

is a $(q^{2(k+1)}p, pq^{(k+1)})$ -pseudo-square which $g_{p_1} : T_{p_1} \rightarrow \mathbb{Z}$, given by,

$$g_{p_1}(x) = -\lfloor \frac{(x_2 - x_1)^2}{4} \rfloor + \min(d - x_2, 0) + 1\{x \in \{(0, d+1), (d+1, d-1)\}\}$$

respects.

Proof. The computations are identical to that of previous Lemma. In this case, the vertical strings match the formula given by (4.58), (4.59), (4.60).

□

We next construct the alternate staircase odometers. By Lemma 4.5.6, each of the tile odometers defined in the previous two lemmas extend to \mathbb{Z}^2 under $L'(n/d)$ with the correct growth (4.104). However, in the next two cases, we require a different argument as the tiling of alternate tiles will result in overlaps. We start with the alternate even child of \mathbf{q}_{3^k}

Lemma 4.6.4. *For each $d \geq 3$ odd, there is a unique function $\hat{g}_{1/d} : \mathbb{Z}^2 \rightarrow \mathbb{Z}$ with*

$$\begin{aligned}\hat{g}_{1/d}(x) = & -\frac{1}{2}x_2(x_2+1) + \min(0, 2-x_1) + \min(0, d-2+x_1) \quad \text{for } x \in \hat{T}_d \\ & + \max(x_1+x_2-2, 0) + 1_{A \cup B}\end{aligned}$$

where

$$A = \{-(d-1) \times [-1, 0]\} \cup \{3 \times [d, d+1]\}$$

$$B = \{(x_1, x_2) : (x_1 + x_2) = 2 \text{ and } 0 < x_2 < d\}$$

$$C = \{-1 \times [1-d, 0]\} \cup \{(d+1) \times [4-d, 3]\}$$

$$D = \{(x_1, x_2) \in [4-2d, d] \times [0, d] : -d+2 \leq x_1 + x_2 \leq d+2\}$$

$$\hat{T}_{1/d} = A \cup B \cup C \cup D$$

and

$$\hat{g}_{1/d}(x \pm v_{1/d,i}) = \hat{g}_{1/d}(x) \pm a_{1/d,i}^T x + k_{1/d,i} \quad \text{for } x \in \mathbb{Z}^2,$$

where $k_{p,\pm i} \in \mathbb{Z}$ is a constant and $i \in \{1, 2\}$ selects the lattice vector. Moreover, $\hat{T}_{1/d}$ is a $w_h = qp^{k+1}$ pseudo-square which $\hat{g}_{1/d}$ respects.

Proof. Consistency of the first condition and translation by $(v_{1/d,1}, a_{1/d,1})$ comes after checking that $\hat{g}_{1/d}(x) = \hat{g}_{1/d}(x + v_{1/d,1})$ for $x, (x + v_{1/d,1}) \in \hat{T}_{1/d}$. In particular, this shows the constant $k_{1/d,i} = 0$ for $i = 1$. Write $\hat{g}_{1/d} : \mathbf{T}_h \rightarrow \mathbb{Z}$ for the common extension of $\hat{g}_{1/d} : T \rightarrow \mathbb{Z}$ to $\mathbf{T}_h := \cup_{i \in \mathbb{Z}} (T + \mathbf{i}v_{1/d,1})$. Note that since there are no gaps between T and $T \pm v_{1/d,1}$, \mathbf{T}_h is simply connected.

From the formula and Section 4.5.7 we may check there is a w_h horizontal boundary string starting at $(0, 0)$ and a $\text{rev}(w_h)$ reversed horizontal boundary string starting at $(4 - 2d, d - 2)$ which $\hat{g}_{1/d}$ respects on $T_{1/d}$. In fact, the top boundary of \mathbf{T}_h is a repeating sequence of $\text{rev}(w_h)$ and the bottom boundary is a repeating sequence of w_h and $\hat{g}_{1/d}$ respects both infinite strings. This implies $(\pm v_{1/d, 2}, \pm a_{1/d, 2})$ translations of $\hat{g}_{1/d}$ form stacked boundary strings and thus have a common extension to $\cup_{j \in \mathbb{Z}} (\mathbf{T}_h + jv_{1/d, 2})$.

Vertical translations of \mathbf{T}_h cover the plane since \mathbf{T}_h is simply connected and each $\pm v_{1/d, 2}$ interface is a stacked zero-one boundary string which is simply connected by Lemma 4.5.4.

□

Next is the alternate odd child of \mathbf{q}_{2^k} .

Lemma 4.6.5. *For each $p_1 = \frac{\frac{d-1}{2}}{\frac{d+1}{2}}$, $d \geq 3$ odd, there is a unique function $\hat{g}_{p_1} : \mathbb{Z}^2 \rightarrow \mathbb{Z}$ with*

$$\begin{aligned} \hat{g}_{p_1}(x) = & -\lfloor \frac{(x_2 - x_1)^2}{4} \rfloor + \min(d - x_2 - 1, 0) + \min((2d - 1) - x_2, 0) \quad \text{for } x \in \hat{T}_{p_1} \\ & + \max((x_2 - x_1) - d + 1, 0) + 1_{A \cup B} \end{aligned}$$

where

$$A = \{[-1, 0] \times 2d\} \cup \{[d, d + 1] \times d - 2\}$$

$$B = \{(x_1, x_2) : (x_2 - x_1) = d - 1 \text{ and } 0 < x_1 < d\}$$

$$C = \{-1 \times [d + 1, 2d]\} \cup \{(d + 1) \times [d - 2, 2d - 3]\}$$

$$D = \{(x_1, x_2) \in [0, d] \times [1, 3d - 3] : -1 \leq x_2 - x_1 \leq 2d - 1\}$$

$$\hat{T}_{p_1} = A \cup B \cup C \cup D$$

and

$$\hat{g}_{p_1}(x \pm v_{p,i}) = \hat{g}_{p_1}(x) \pm a_{p_1,i}^T x + k_{p_1,i} \quad \text{for } x \in \mathbb{Z}^2,$$

where $k_{p_1,\pm i} \in \mathbb{Z}$ is a constant and $i \in \{1, 2\}$ selects the lattice vector. Moreover, \hat{T}_{p_1} is a $w_v = pq^{k+1}$ pseudo-square which \hat{g}_{p_1} respects.

Proof. Consistency of the first condition and translation by $(v_{p_1,2}, a_{p_1,2})$ comes after checking that

$$\hat{g}_{p_1}(x) = \hat{g}_{p_1}(x + v_{p_1,2}) + a_{p_1,2}^T x - \left(\frac{d-3}{2}\right)^2$$

for $x, (x + v_{p_1,2}) \in \hat{T}_{p_1}$ and

$$\hat{g}_{p_1}(x) = \hat{g}_{p_1}(x - v_{p_1,2}) - a_{p_1,2}^T x - \left(\frac{d-3}{2}\right)^2 + 1$$

for $x, (x - v_{p_1,2}) \in \hat{T}_{p_1}$. Write $\hat{g}_{p_1} : \mathbf{T}_v$ for the common extension of $\hat{g}_{p_1} : T \rightarrow \mathbb{Z}$ to $\mathbf{T}_v := \cup_{i \in \mathbb{Z}} (T + \mathbf{i}v_{p_1,2})$. As \mathbf{T}_v is a rotation of \mathbf{T}_h from the previous lemma, it is also simply connected.

By checking the formula for \hat{g}_{p_1} against (4.58), (4.59), (4.60), we see that there is a $\mathbf{rev}(w_v)$ boundary string starting at $(0, 1)$ in \hat{T}_{p_1} which \hat{g}_{p_1} respects. There is also a $(a_{p_1,2} - a_{1/1,2})$ translated w_v boundary string starting at $(d-1, 2d-3)$. Actually, a stronger statement holds: \hat{g}_{p_1} on \mathbf{T}_v respects infinite repeating pq^{k+1} strings on both sides. Thus, we may combine the strips to extend \hat{g}_{p_1} to the plane. The tiling by \mathbf{T}_v leaves no gaps by the same argument as the previous lemma.

□

We next record the formula for the Laplacians. Recall that $\partial T = \{x \in \mathbb{Z}^2 : \exists y \notin T \text{ such that } |y - x| = 1\}$. For $x \in T$, write $\mathcal{R}(x)$ for the image of x under $\mathcal{R}(T)$, defined in (4.49). If T generates a tiling, this definition extends $\mathcal{R}(x)$ to $x \in \mathbb{Z}^2$.

Lemma 4.6.6. For $d \geq 3$ odd, let $T_{1/d}$, $\hat{T}_{1/d}$ be the tiles and $g_{1/d}$, $\hat{g}_{1/d}$ the plane extensions of the objects given in Lemmas 4.6.2 and 4.6.4. The Laplacian, $\Delta g_{1/d}$, satisfies

$$\begin{aligned} \Delta g_{1/d}(x) &= \Delta g_{1/d}(x \pm v_{1/d,*}) \text{ for all } x \in \mathbb{Z}^2 \\ \Delta g_{1/d}(x) &= -1\{(x_1 + x_2) \text{ is odd}\} \\ &\quad - 1\{(x_1 + x_2) \text{ is even and } x_1 = 1\} \quad \text{on } T_d \setminus \partial T_{1/d} \\ \Delta g_{1/d}(x) &= 0 \quad \text{on } \partial T_{1/d} \end{aligned} \tag{4.71}$$

The Laplacian of the alternate, $\Delta \hat{g}_{1/d}$ satisfies

$$\begin{aligned} \Delta \hat{g}_{1/d}(x) &= \Delta \hat{g}_{1/d}(x \pm v_{1/d,*}) \text{ for all } x \in \mathbb{Z}^2 \\ \Delta \hat{g}_{1/d}(x) &= -1\{(x_1 + x_2) \text{ is odd}\} \\ &\quad - 1\{(x_1 + x_2) \text{ is even and } x \in \{-(d-2) \times [0, d-1]\} \cup \{2 \times [1, d]\}\} \\ &\quad - 1\{(x_1 + x_2) = 2 \text{ and } 1 \leq x_2 \leq d-1\} \\ &\quad + 1\{(x_1 + x_2) = 1 \text{ and } 1 \leq x_2 \leq d-2\} \\ &\quad + 1\{(x_1 + x_2) = 3 \text{ and } 2 \leq x_2 \leq d-1\} \quad \text{on } T_d \setminus \partial T_{1/d} \\ \Delta \hat{g}_{1/d}(x) &= -1_{(1-d,0) \cup (3,d)} \quad \text{on } \partial T_{1/d}. \end{aligned} \tag{4.72}$$

In both cases, the Laplacians are 180-degree symmetric and

$$\Delta g_{\mathcal{R}(1/d)}(x) = \Delta g_{1/d}(\mathcal{R}(x))$$

$$\Delta \hat{g}_{\mathcal{R}(1/d)}(x) = \Delta \hat{g}_{1/d}(\mathcal{R}(x)).$$

4.6.3 Doubled staircases

The *doubled staircases* are the reduced fractions of the form $\frac{1}{d}$ for $d \geq 4$ even and their rotations $\mathcal{R}(1, d) = (d-1, d+1)$. These are respectively the odd and even child in Farey

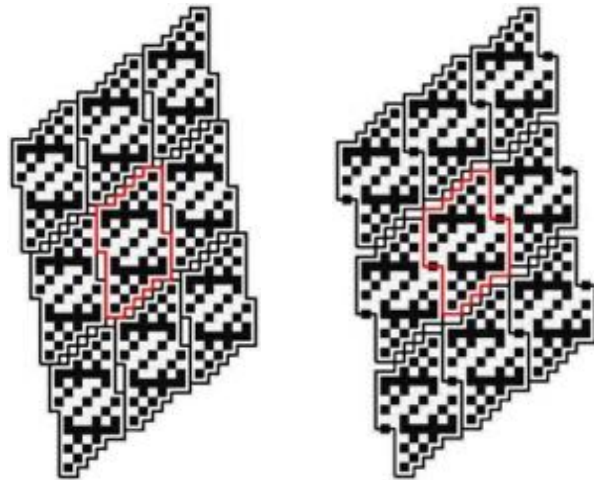


Figure 4.19: A period of the Laplacian of a doubled staircase odometer on the left and its alternate. The string is 22 and the reduced fraction is $5/7$. Each tile is outlined in the dual lattice.

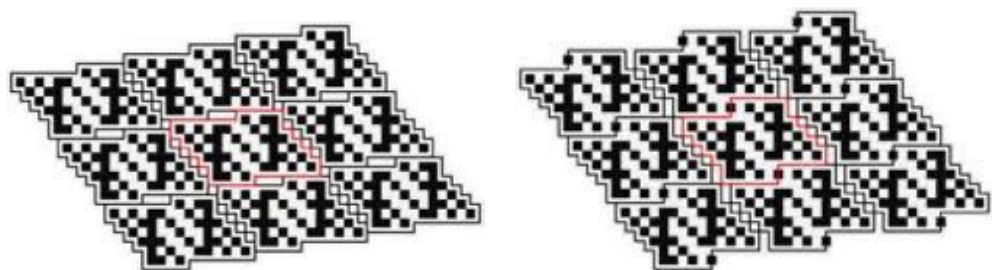


Figure 4.20: The rotated standard and alternate doubled staircase odometers of Figure 4.19. The string is 33 and the reduced fraction is $1/6$.

quadruples \mathbf{q}_{3^k} and \mathbf{q}_{2^k} for $k \geq 1$. In particular, doubled staircases are siblings of the staircases.

We start with the odd standard child of \mathbf{q}_{3^k} .

Lemma 4.6.7. *For each $d \geq 4$ even,*

$$A = (0, 0) \cup (d+2, d+2)$$

$$B = \{(x_1, x_2) : (x_1 + x_2) = (d+2) \text{ and } 1 < x_2 < d+1\}$$

$$C = \{(x_1, x_2) \in [-d+2, 2d] \times [0, d+2] : 1 \leq (x_1 + x_2) \leq 2d+3\}$$

$$D = \{(x_1, x_2) : x_1 \geq d \text{ and } x_2 = 0 \text{ or } x_1 \leq 2 \text{ and } x_2 = d+2\}$$

$$T_{1/d} := \{A \cup B \cup C\} \setminus D$$

is a $(qp^k qp^{k+1}, p^{(2k+1)}q)$ pseudo-square which $g_{1/d} : T_{1/d} \rightarrow \mathbb{Z}$, given by,

$$\begin{aligned} g_{1/d}(x) = & -\frac{1}{2}x_2(x_2+1) + (x_2 + \min(0, x_1 - 1)) + \min(0, d+1 - x_1) \quad \text{for } x \in T_{1/d} \\ & + \max((x_2 + x_1) - d - 2, 0) + 1_{A \cup B} \end{aligned}$$

respects.

Proof. The computation in Lemma 4.6.2 also shows that the bottom and top boundaries of $T_{1/d}$ are given by $qp^k qp^{k+1}$ and $\text{rev}(qp^k qp^{k+1})$ zero-one horizontal boundary strings which $g_{1/d}$ respects. Also, the explicit formulae for $p^{(2k+1)}q$ given in (4.58), (4.59), (4.60) also shows that the left and right boundaries of $T_{1/d}$ are reversed and non-reversed vertical $p^{(2k+1)}q$ zero-one boundary strings which $g_{1/d}$ respects. \square

Next is the even standard child of \mathbf{q}_{2^k} .

Lemma 4.6.8. For each $q_1 = \frac{d-1}{d+1}$ $d \geq 4$ even,

$$A = (-1, 2d+1) \cup (d+1, d-1)$$

$$B = \{(x_1, x_2) : (x_2 - x_1) = d \text{ and } 0 < x_1 < d\}$$

$$C = \{(x_1, x_2) \in [-1, d+1] \times [1, 3d-1] : -1 \leq (x_2 - x_1) \leq 2d+1\}$$

$$D = \{(x_1, x_2) : x_1 = -1 \text{ and } x_2 \leq d+1 \text{ or } x_1 = d+1 \text{ and } x_2 \geq 2d-1\}$$

$$T_{q_1} := \{A \cup B \cup C\} \setminus D$$

is a $(q^{(2k+1)}p, pq^k pq^{(k+1)})$ -pseudo-square which $g_{q_1} : T_{q_1} \rightarrow \mathbb{Z}$, given by,

$$\begin{aligned} g_{q_1}(x) = & -\lfloor \frac{(x_2 - x_1)^2}{4} \rfloor + \min(0, d - x_2) + \min(0, 2d - x_2) \quad \text{for } x \in T_{q_1} \\ & + \max((x_2 - x_1) - d, 0) + 1_{A \cup B} \end{aligned}$$

respects.

Proof. As in Lemma 4.6.7, the computations are identical to Lemma 4.6.2. For the vertical strings in this case, we check against the formulae (4.61), (4.62), (4.63). \square

As for the standard staircases, by Lemma 4.5.6, each of the doubled staircase tile odometers defined in the previous two lemmas extend to \mathbb{Z}^2 under $L'(n/d)$ with the correct growth (4.104). Again, however, for the alternates the argument is different.

We start with the alternate odd child of \mathbf{q}_{3^k} .

Lemma 4.6.9. For each $d \geq 4$ even, there is a unique function $\hat{g}_{1/d} : \mathbb{Z}^2 \rightarrow \mathbb{Z}$ with

$$\begin{aligned} \hat{g}_{1/d}(x) = & -\frac{1}{2}x_2(x_2 + 1) + \min(0, x_1) + \min(0, d - x_1 - 1) \quad \text{for } x \in \hat{T}_{1/d} \\ & + \max((x_2 + x_1) - d, 0) + 1_{A \cup B} \end{aligned}$$

where

$$A = (-1, -1) \cup (d, d+2)$$

$$B = \{(x_1, x_2) : (x_1 + x_2) = d \text{ and } 0 < x_1 < d-1\}$$

$$C = \{(x_1, x_2) \in [-d+1, 2d-2] \times [-1, d+2] : -1 \leq (x_1 + x_2) \leq 2d+1\}$$

$$D = \{(x_1, x_2) : x_1 \geq d \text{ and } x_2 \in [-1, 0] \text{ or } x_1 \leq -1 \text{ and } x_2 \in [d+1, d+2]\}$$

$$\hat{T}_{1/d} := \{A \cup B \cup C\} \setminus D$$

and

$$\hat{g}_{1/d}(x \pm v_{1/d,i}) = \hat{g}_{1/d}(x) \pm a_{1/d,i}^T x + k_{1/d,\pm i} \quad \text{for } x \in \mathbb{Z}^2,$$

where $k_{1/d,\pm i}$ is a constant and $i \in \{1, 2\}$ selects the lattice vectors. Moreover, $\hat{T}_{1/d}$ is a $w_v = p^{(2k+1)}q$ pseudo-square which $\hat{g}_{1/d}$ respects.

Proof. By comparing against (4.57), one sees there is a reversed $\mathbf{rev}(p^{(2k+1)}q)$ -vertical boundary string starting at $(-1, -1)$ in $\hat{T}_{1/d}$ which $\hat{g}_{1/d}$ respects. Also, after a slope $a_{0/1,2}$ translation, the $p^{(2k+1)}q$ string given by (4.55) and (4.56) coincides with $\hat{g}_{1/d}$ starting at $(2d-3, 1)$. Thus, $\hat{g}_{1/d}$ is compatible with its horizontal translates and there are no gaps in $\cup_{i \in \mathbb{Z}} (\hat{T}_{1/d} + \mathbf{i}v_{1/d,1})$.

Also, after translation by $v_{1/d,2} = (-(d-1), d+1)$, the bottom boundary of $\hat{T}_{1/d}$, given by,

$$L := \{x_2 = -1, -1 \leq x_1 \leq d-1\} \cup (d-1, 0) \cup \{x_2 = 1, d-1 \leq x_1 \leq 2(d-1)\}$$

maps to

$$U_p := \{x_2 = d, -d \leq x_1 \leq 0\} \cup (0, d+1) \cup \{x_2 = d+2, 0 \leq x_1 \leq d-1\}$$

and $U := U_p \cup (d, d+2) \setminus (-d, d)$ is the top boundary. In particular,

$$\hat{g}_{1/d}(x + v_{1/d,2}) = \hat{g}_{1/d}(x) + a_{1/d,2}^T x - \left(\frac{d(d+5)}{2} - 1\right)$$

for $x \in L$. Similarly,

$$\hat{g}_{1/d}(x - v_{1/d,2}) = \hat{g}_{1/d}(x) - a_{1/d,2}^T x - \frac{d(d-1)}{2}$$

for $x \in U$. This shows compatibility of $\hat{g}_{1/d}$ with its vertical translates and that $\cup_{j \in \mathbb{Z}} (\hat{T}_{1/d} + jv_{1/d,2})$ has no gaps. \square

Finally, we give the alternate even child of \mathbf{q}_{2k} .

Lemma 4.6.10. *For each $q_1 = \frac{d-1}{d+1}$, $d \geq 4$ even, there is a unique function $\hat{g}_{q_1} : \mathbb{Z}^2 \rightarrow \mathbb{Z}$ with*

$$\begin{aligned} \hat{g}_{q_1}(x) = & -\lfloor \frac{(x_2 - x_1)^2}{4} \rfloor + \min(0, d - x_2) + \min(0, 2d - 1 - x_2) \quad \text{for } x \in T_{q_1} \\ & + \max(0, x_2 - x_1 - d) + 1_{A \cup B} \end{aligned}$$

where

$$A = (-2, 2d) \cup (d+1, d-1)$$

$$B = \{(x_1, x_2) : (x_2 - x_1) = d \text{ and } 0 < x_1 < d\}$$

$$C = \{(x_1, x_2) \in [-2, d+1] \times [1, 3d-2] : -1 \leq (x_2 - x_1) \leq 2d+1\}$$

$$D = \{(x_1, x_2) : x_1 \leq -1 \text{ and } x_2 \leq d+1 \text{ or } x_1 \geq d \text{ and } x_2 \geq 2d\}$$

$$T_{q_1} := \{A \cup B \cup C\} \setminus D$$

and

$$\hat{g}_{q_1}(x \pm v_{q_1,i}) = g_{q_1}(x) \pm a_{q_1,i}^T x + k_{q_1,\pm i} \quad \text{for } x \in \mathbb{Z}^2,$$

where $\hat{k}_{d,\pm i}$ is a constant and $i \in \{1, 2\}$ selects the lattice vectors. Moreover, $\hat{T}_{1/d}$ is a $w_h = q^{(2k+1)}p$ pseudo-square which \hat{g}_{q_1} respects.

Proof. The proof is similar to Lemma 4.6.10. First, we check that there is a $q^{(2k+1)}p$ horizontal boundary string starting $(0, 1)$ which \hat{g}_{q_1} respects. As in Lemma 4.6.2, there is a $\text{rev}(q^{(2k+1)}p)$ reversed horizontal boundary string starting at $(-2, 2(d-1))$ which \hat{g}_{q_1} respects. This implies compatibility and no gaps in the vertical direction.

For the other direction, after translation by $v_{q_1,1} = (d+1, d-1)$, the left boundary of \hat{T}_{q_1} , given by,

$$L := \{x_1 = 0, 1 \leq x_2 \leq d\} \cup (-1, d) \cup \{x_1 = -2, d \leq x_2 \leq 2d\}$$

maps to

$$R_p := \{x_1 = d+1, d \leq x_2 \leq 2d-1\} \cup (d, 2d-1) \cup \{x_1 = d-1, 2d-1 \leq x_2 \leq 3d-1\}$$

and $R := R_p \cup (d+1, d-1) \setminus (d-1, 3d-1)$ is the top boundary. In particular,

$$\hat{g}_{q_1}(x + v_{q_1,1}) = \hat{g}_{q_1}(x)$$

for $x \in L$. Similarly,

$$\hat{g}_{q_1}(x - v_{q_1,2}) = \hat{g}_{q_1}(x)$$

for $x \in R$. This shows compatibility of \hat{g}_{q_1} with its horizontal translates and that $\cup_{j \in \mathbb{Z}} (\hat{T}_{q_1} + jv_{q_1,1})$ has no gaps.

□

Lemma 4.6.11. *For $d \geq 4$ even, let $T_{1/d}, \hat{T}_{1/d}$ be the tiles and $g_{1/d}, \hat{g}_{1/d}$ the plane exten-*

sions of the objects given in Lemmas 4.6.7 and 4.6.9. The Laplacian, $\Delta g_{1/d}$, satisfies

$$\begin{aligned}
 \Delta g_{1/d}(x) &= \Delta g_{1/d}(x \pm v_{1/d,*}) \text{ for all } x \in \mathbb{Z}^2 \\
 \Delta g_{1/d}(x) &= -1\{(x_1 + x_2) \text{ is odd}\} \\
 &\quad - 1\{(x_1 + x_2) \text{ is even and } x \in \{1 \times [1, d]\} \cup \{d+1 \times [2, d+1]\}\} \\
 &\quad - 1\{(x_1 + x_2) = d+2 \text{ and } 2 \leq x_2 \leq d\} \\
 &\quad + 1\{(x_1 + x_2) = d+3 \text{ and } 3 \leq x_2 \leq d\} \\
 &\quad + 1\{(x_1 + x_2) = d+1 \text{ and } 2 \leq x_2 \leq d-1\} \quad \text{on } T_d \setminus \partial T_{1/d} \\
 \Delta g_{1/d}(x) &= 0 \quad \text{on } \partial T_{1/d}
 \end{aligned} \tag{4.73}$$

The Laplacian of the alternate, $\Delta \hat{g}_{1/d}$ satisfies

$$\begin{aligned}
 \Delta \hat{g}_{1/d}(x) &= \Delta \hat{g}_{1/d}(x \pm v_{1/d,*}) \text{ for all } x \in \mathbb{Z}^2 \\
 \Delta \hat{g}_{1/d}(x) &= -1\{(x_1 + x_2) \text{ is odd}\} \\
 &\quad - 1\{(x_1 + x_2) \text{ is even and } x \in \{0 \times [-1, d-1]\} \cup \{d-1 \times [2, d+2]\}\} \\
 &\quad - 1\{(x_1 + x_2) = d \text{ and } 2 \leq x_2 \leq d-1\} \\
 &\quad + 1\{(x_1 + x_2) = d+1 \text{ and } 3 \leq x_2 \leq d\} \\
 &\quad + 1\{(x_1 + x_2) = d-1 \text{ and } 1 \leq x_2 \leq d-2\} \quad \text{on } T_d \setminus \partial T_{1/d} \\
 \Delta \hat{g}_{1/d}(x) &= -1_{(d-1,0) \cup (0,d+1)} \quad \text{on } \partial T_{1/d}
 \end{aligned} \tag{4.74}$$

In both cases, the Laplacians are 180-degree symmetric and

$$\begin{aligned}
 \Delta g_{\mathcal{R}(1/d)}(x) &= \Delta g_{1/d}(\mathcal{R}(x)) \\
 \Delta \hat{g}_{\mathcal{R}(1/d)}(x) &= \Delta \hat{g}_{1/d}(\mathcal{R}(x)).
 \end{aligned}$$

4.6.4 One-sided recurrence

In this section we prove that the constructed functions are recurrent. In fact, we prove a sufficient property which we later use to prove recurrence in the general construction. First, we observe that recurrence is preserved under rotations which flip parity.

Lemma 4.6.12. *Suppose $v : \mathbb{Z}^2 \rightarrow \mathbb{Z}$ is integer superharmonic and recurrent and*

$$\Delta v = \Delta(v \circ \mathcal{R})$$

for a 90-degree rotation and translation $\mathcal{R}(\mathbb{Z}^2) = \mathbb{Z}^2$ which flips parity: if $(x_1 + x_2)$ is even and $y = \mathcal{R}(x)$ then $(y_1 + y_2)$ is odd. Then $v \circ \mathcal{R}$ is integer superharmonic and recurrent.

Proof. This is an immediate consequence of the definition. Indeed, let $s_1 = \Delta v + 1$ and $s_2 = \Delta(v \circ \mathcal{R}) + 1$. Since \mathcal{R} is a bijection, every finite induced subgraph of the rotated F -lattice can be written as $\mathcal{R} \circ H$, for H a finite induced subgraph of the F -lattice. Since v is recurrent, there is a vertex $x \in H$ with $s_1(x)$ larger than its in-degree in H . Let $y = \mathcal{R}(x)$. By assumption, $s_2(y) = s_1(x)$ and as \mathcal{R} is a rotation and flips the parity of x , the horizontal/vertical neighbors of x become the vertical/horizontal neighbors of y and the edges between either pair of neighbors are preserved. \square

In light of Lemma 4.6.4 and the observed rotational invariance of the Laplacians, we need only prove recurrence for \mathbf{q}_{3k} , $k \geq 0$.

We start with the standard even child. Figure 4.18 will be a useful reference in the next two proofs.

Lemma 4.6.13. *For each $d \geq 3$ odd, the extension of $g_{1/d} : \mathbb{Z}^2 \rightarrow \mathbb{Z}$ defined in Lemma 4.6.2 is integer superharmonic and recurrent.*

Proof. By the explicit formula of the Laplacian, Lemma 4.6.6, it suffices to check recurrence.

Let $s = \Delta g_{1/d} + 1$ and suppose, for sake of contradiction, that there is an induced subgraph of the F -lattice, H , which is forbidden for s . Let $c^0 = -\infty$ and for $j \geq 1$, let

$$\begin{aligned} c^j &= \min\{x_1 > c^{j-1} : x \in H\} \\ V^j &= \{x \in H : x_1 = c^j\}. \end{aligned} \tag{4.75}$$

In words, sets of possibly disjoint vertical lines enumerated from left to right. Since H is forbidden, it is nonempty, hence V^1 exists.

Write $\partial^h T(1/d) := \partial T(1/d) \cap \{x_2 \in \{0, d+1\}\}$. We prove the following by induction on $j \geq 1$ for all $L'(1/d)$ translations of $T(1/d)$:

1. If $\bigcup_{j' < j} V^{j'} \cap T(1/d) = \emptyset$ but $V^j \cap T(1/d) \neq \emptyset$ then $c_j = 1$, otherwise $c_j > 1$.
2. If $V^j \cap T(1/d) \neq \emptyset$, then $V^j \cap \partial^h T(1/d) = \emptyset$.
3. If $V^j \cap T(1/d) \neq \emptyset$ then $V^{j+1} \cap T(1/d) \neq \emptyset$.

The third condition will result in a contradiction as $T(1/d)$ is finite. The idea is to continually use the fact that H is forbidden.

Proof of (1)

Suppose $V^j \cap T(1/d) \neq \emptyset$ but $c_j \neq 1$. If $y \in V^j$ and is even, then, since $c_j \neq 1$, $s(y) = 1$ and therefore $y - e_1 \in H$, since H is forbidden. This contradicts either the assumption $\bigcup_{j' < j} V^{j'} \cap T(1/d) = \emptyset$ or $y - e_1 \notin T(1/d)$. In the latter case, there are two subcases, (i) $y = (2-d, d)$ or (ii) $y = (0, 0)$. In case (i), $s(y - e_1) = 1$ and so $y - e_1 - e_2 \in H$, contradicting inductive (2). In case (ii), $s(y - e_1) = 0$ and either $y - e_1 - e_2 \in H$, contradicting inductive (2) or $y - e_1 + e_2 \in H$. In the latter case, $s(y - e_1 + e_2) = 1$ and there is an even-odd chain of points all with $s(x_i) = 1$ ending at $x_k \in \partial^h T(1/d) - v_{1/d, 1}$, contradicting inductive (1). (In other words, the vertical boundaries of $T(1/d)$ are F -lattice connected).

Otherwise if y is odd and $s(y) = 1$, then $y \pm e_2 \in H$ and at least one such neighbor is in $T(1/d)$, a contradiction by the above. If y is odd and $s(y) = 0$, then both $y \pm e_2$ are in

$T(1/d)$ and at least one neighbor is in V^j as H is forbidden.

Proof of (2)

Suppose there is $y \in \partial^h T(1/d) \cap V^j$. By the explicit formula, $s(y) = 1$. If $c_j = 1$, then $y \in \{(1, 0), (1, d+1)\}$. If $y = (1, 0)$, then $y' \in \{y - e_2, y - e_2 - e_1\}$ satisfies $s(y') = 1$ and $y' \in H$, contradicting the inductive hypothesis as $y - e_2 - e_1$ is on $\partial^h(T(1/d) - v_{1/d,1})$. If $y = (1, d+1)$, then $y + e_2$ and $y + e_2 - e_1 \in H$ and $s(y + e_2) = 1$ and $s(y + e_2 - e_1) = 0$. Since H is forbidden at least one of $(y + e_2 - e_1 \pm e_2)$ must be in H , contradicting inductive (2) as in the Proof of (1).

If $y = (2, d+1)$, then $s(y) = 1$ and $y - e_1 \in H \cap \partial^h T(1/d)$, contradicting inductive 2. Otherwise, by inductive (1), $c_j > 1$ and so $x_2 = 0$. If x is even, then $x - e_1 \in H$, contradicting inductive (2). Otherwise if x is odd, then $x \pm e_2 \in H$ and $x - e_2 \in T'^{1/d} := T(1/d) - v_{1/d,2}$. Since $x - e_2 + v_{1/d,2} \leq 1$, by inductive (1) applied to $T'^{1/d}$, $x - e_2 + v_{1/d,2} = 1$ and $x = (d, 0)$. In this case, $s(x + e_2) = 1$ and so $x + e_2 - e_1 \in H$. However, $s(x + e_2 - e_1) = 0$ and since x is odd, this means $x + e_2 - e_1 \pm e_2 \in H$, however, by the same argument as the Proof of (1) this contradicts inductive (2).

Proof of (3)

We may suppose by the above arguments that $x \in V^j \cap \{T(1/d) \setminus \partial T(1/d)\}$ and $x_1 \geq 1$.

If $c^j = 1$, then there are no $y \in H \cap T(1/d)$ with $y_1 < 1$. Therefore if x is even, $x + e_1 \in H$.

If x is odd, at least one neighbor $x \pm e_2 \in H$ and that neighbor is even.

Otherwise, suppose $c^j > 1$. By the same argument, there must be an even $x \in H \cap T(1/d)$.

However, since $c^j > 1$, $s(x) = 1$, meaning $x \pm e_1 \in H$.

□

Next is the alternate even child.

Lemma 4.6.14. *For each $d \geq 3$ odd, the extension of $\hat{g}_{1/d} : \mathbb{Z}^2 \rightarrow \mathbb{Z}$ defined in Lemma 4.6.9 is integer superharmonic and recurrent.*

Proof. Let $\hat{s} = \Delta\hat{g}_{1/d} + 1$ and begin the proof as in Lemma 4.6.13 except modify the induction hypotheses as follows.

Write $\partial^h \hat{T}(1/d) := \partial \hat{T}(1/d) \cap \{x_2 \in \{-1, 0, d, d+1\}\}$. We claim following holds for all $L'(1/d)$ -translations of $\hat{T}(1/d)$ and all $j \geq 1$:

1. If $\bigcup_{j' < j} V^{j'} \cap \hat{T}(1/d) = \emptyset$ but $V^j \cap \hat{T}(1/d) \neq \emptyset$ then $c^j \in \{2-d, 2\}$ or V^j is a singleton, $\{(1-d, 0), (1, 1)\}$. Moreover, if $c_j \in \{2-d, 2\}$, then $V^{j'} \cap \hat{T}(1/d) = \emptyset$ for $j' < j$.
2. If $V^j \cap \hat{T}(1/d) \neq \emptyset$, then $V^j \cap \partial^h \hat{T}(1/d) = \emptyset$.
3. If $V^j \cap \hat{T}(1/d) \neq \emptyset$ then $V^{j+1} \cap \hat{T}(1/d) \neq \emptyset$.

Proof of (1)

Suppose $\bigcup_{j' < j} V^{j'} \cap \hat{T}(1/d) = \emptyset$ and $V^j \cap \hat{T}(1/d) \neq \emptyset$ but $c^j \notin \{2-d, 2\}$ and take $x \in V^j$ for $x \notin \{(1-d, 0), (1, 1)\}$.

If $x = (3, d)$, then since x is even and there are no points before it (by the case we're in), $x + e_1 \in H$. However, $x + e_1$ is odd and $\hat{s}(x + e_1) = 1$, so we can build an odd-even chain all with $\hat{s}(x') = 1$ and in H : $\{x + e_1, x + e_1 + e_2, x + e_2, x + 2e_2, x + 2e_2 - e_1\}$, contradicting inductive (2) as $(x + 2e_2 - e_1) \in (\partial^h \hat{T}(1/d) + v_{1/d, 2}) \cap V^{j-1}$.

Next, if $(x_1 + x_2) = 2$ and $1 \leq x_2 \leq d-1$, then $\hat{s}(x) = 0$ and $x + e_1 \in H$. By our assumption, in this case, $x_2 \geq 2$, so $\hat{s}(x + e_1) = 1$ and hence $x + e_1, x + e_1 + e_2, x + e_2, x + 2e_2 \in H$. However, $\hat{s}(x + 2e_2) = 1$ and even, a contradiction if $(x + 2e_2 - e_1) \in \hat{T}(1/d)$ as its in-degree is at most one by the case we are in. Otherwise $x + 2e_2 - e_1 \in \partial^h \hat{T}(1/d) + v_{n/d, 2}$, contradicting inductive (2).

Otherwise, if x is odd, either $\hat{s}(x) = 1$ and one of $s(x \pm e_2) = 1$ or $\hat{s}(x) = 0$ and both $\hat{s}(x \pm e_2) = 1$. If x is even, then $\hat{s}(x) = 1$. Both cases lead to a contradiction as we cannot have even $x \in V^j$ with $\hat{s}(x) = 1$.

Now, suppose $c_j = 2$ but $\bigcup_{j' < j} V^{j'} \cap \hat{T}(1/d) \neq \emptyset$. By inductive (3), there is some $y \in V^{j'}$, $j' < j$ with $(y_1 + y_2) = 1$. If $y = (2-d, d-1)$, then by inductive (1), $y - e_2, y - e_2 + e_1 \in H$

so we may assume $y_2 \leq d - 2$. In fact, iterating this shows that $(1, 0) \in H$, contradicting inductive (2) as $(1, 0) \in V^{j-1} \cap \partial^h \hat{T}(1/d)$.

Proof of (2)

Suppose not and take $y \in V^j \cap \{\partial^h \hat{T}(1/d)\}$ so that $\hat{s}(y) = 1$. We divide into subcases (i) $y_2 \in \{-1, 0\}$ and (ii) $y_2 \in \{d, d+1\}$.

In case (i), if y is even, then $y - e_1 \in H \cap \partial^h \hat{T}(1/d) \cap V^{j-1}$, a contradiction. Otherwise, y is odd and there are three subcases. In the first subcase $y - e_2 \in \hat{T}(1/d) - v_{1/d,2}$ and $y - e_2 + v_{1/d,2} < 2$, contradicting (1). In the second subcase $y - e_2 \in \hat{T}(1/d) - v_{1/d,2} + v_{1/d,1}$ and $y - e_2 + v_{1/d,2} - v_{1/d,1} < 2$ contradicting (1). In the third subcase, $\hat{s}(y) = \hat{s}(y - e_2) = \hat{s}(y - e_2 - e_1) = 1$, so $y - e_1 \in H$, contradicting inductive (2) for V^{j-1} .

In case (ii), we may similarly assume y is odd, in which case by (1) applied to all of $\hat{T}(1/d) + \mathbf{i}_1 v_{1/d,1} + \mathbf{i}_2 v_{1/d,2}$ for $|i_j| \leq 1$, $y \in \{(3-d, d), (3, d+1)\}$ and $\hat{s}(y) = \hat{s}(y + e_2) = \hat{s}(y + e_2 - e_1) = 1$ and all points are in H , contradicting inductive (2) for V^{j-1} .

Proof of (3)

Take $y \in V^j \cap \hat{T}(1/d) \setminus \partial^h \hat{T}(1/d)$ and argue, as in the proof of (3) in Lemma 4.6.13, that either $y + e_1 \in H$ or one of $y \pm e_2 + e_1 \in H$. If $c_j \in \{2-d, 2\}$, since $V^{j-1} \cap \hat{T}(1/d) = \emptyset$, then there must be even $y' \in V^{j-1} \cap \hat{T}(1/d)$ with $y' + e_1 \in V^j \cap \hat{T}(1/d)$. Similarly, if $y \in \{(1-d, 0), (1, 1)\}$ then y is even and so $y + e_1 \in V^j$.

Otherwise, if y is odd and $\hat{s}(y) = 0$, then $s(y \pm e_2) = 1$ and so at least one of $(y \pm e_2 + e_1) \in H$. If y is odd and $\hat{s}(y) = 1$ then both $y' \in \{y \pm e_2\} \in H$ and at least one $\hat{s}(y') = 1$ with $y' \in \hat{T}(1/d)$ or $y' \in \partial^H \hat{T}(1/d) \pm v_{1/d,2}$, the latter case contradicting (1).

If y is even and $\hat{s}(y) = 0$ but $y + e_1 \notin H$, then $y - e_1 \in H$. If $y = (3-d, d)$, then by inductive (1) and the formula of \hat{s} , $\{y - e_1, y - e_1 - e_2, y - e_2, y - 2e_2, y - 2e_2 + e_1, y - e_2 + e_1\} \subset H$. Otherwise, $\hat{s}(y - e_1) = 1$ and similarly $\{y - e_1 - e_2, y - e_2, y - 2e_2, y - 2e_2 + e_1, y - e_2 + e_1\} \subset H$. \square

Next is the standard odd child. Figure 4.20 will be a reference in the next two proofs.

Lemma 4.6.15. *For each $d \geq 4$ even, the extension of $g_{1/d}$ defined in Lemma 4.6.2 is integer superharmonic and recurrent.*

Proof. Let $s = \Delta g_{1/d} + 1$ and begin the proof as Lemma 4.6.14 modifying the inductive hypotheses as follows.

Write $\partial^h T(1/d) := \partial T(1/d) \cap \{x_2 \in \{0, 1, d+1, d+2\}\}$ and T^1, T^2 for the two copies of $T(1/(d-1))$ contained within $T(1/d)$: $T^1 = T(1/(d-1))$ and $T^2 = T(1/(d-1)) + v_{1/(d-1),1} + 1 + \mathbf{i}$

We claim following holds for all $L'(1/d)$ translations of $T(1/d)$ and all $j \geq 1$:

1. If $\bigcup_{j' < j} V^{j'} \cap T(1/d) = \emptyset$ but $V^j \cap T(1/d) \neq \emptyset$ then $c^j \in \{1, d+1\}$ or $V^j = (d, 2)$. Moreover, $c_j \in \{1, d+1\}$, then $V^{j'} \cap T(1/d) = \emptyset$ for $j' < j$. If $V^j \cap T^1 \neq \emptyset$, then $V^{j'} \cap T(1/d) = \emptyset$ for $c_{j'} < 1$. If $V^j \cap T^2 \neq \emptyset$, then $V^{j'} \cap \{T(1/d) \setminus (d, 2)\} = \emptyset$ for $c_{j'} < d+1$.
2. If $V^j \cap T(1/d) \neq \emptyset$, then $V^j \cap \partial^h T(1/d) = \emptyset$.
3. If $V^j \cap T(1/d) \neq \emptyset$ then $V^{j+1} \cap T(1/d) \neq \emptyset$.

Proof of (1)

Suppose $\bigcup_{j' < j} V^{j'} \cap T(1/d) = \emptyset$ and $V^j \cap T(1/d) \neq \emptyset$ but $c^j \notin \{1, d+1\}$ and take $x \in V^j$ for $x \notin \{(1-d, 0), (1, 1)\}$.

If $(x_1 + x_2) = (d+2)$ and $2 \leq x_2 \leq d$, then $s(x) = 0$ and $x + e_1 \in H$. By assumption, in this case, $x_2 \geq 3$, so $s(x + e_1) = 1$ and $x + e_1, x + e_1 + e_2, x + e_2, x + 2e_2 \in H$. However, $s(x + e_2) = 1$ and even, a contradiction.

The rest of the proof proceeds along the same lines as the corresponding proof of (1) in Lemma 4.6.14. Indeed, if $V^j \cap T^2 \neq \emptyset$, but $V^{j'} \cap T(1/d) \neq \emptyset$ for $c_{j'} < d+1$, then $V^{j-1} \cap T(1/d) \neq \emptyset$, in which case by inductive (3) there is some $y \in V^{j'}, j' < j$ with $(y_1 + y_2) = d+1$.

Proof of (2)

The proof is similar to the corresponding proof of (2) in Lemma 4.6.14 except here instead of comparing to just the translations of $T(1/d)$, compare to the embedded subtiles T^1 and T^2 also.

Suppose not and take $y \in V^j \cap \{\partial^h T(1/d)\}$ so that $s(y) = 1$. We divide into subcases

- (i) $y_2 \in \{0, 1\}$ and (ii) $y_2 \in \{d + 1, d + 2\}$.

In case (i), if y is even, then $y - e_1 \in H \cap \partial^h T(1/d) \cap V^{j-1}$, a contradiction. Otherwise, y is odd and there are three subcases. In the first subcase $y - e_2 \in T(1/d) - v_{1/d,2}$ and $y - e_2 + v_{1/d,2} < 1$, contradicting (1). In the second subcase $y - e_2 \in T^2$ and $y - e_2 + v_{1/d,2} - v_{1/d,1} < d + 1$ contradicting (1). In the third subcase, $s(y) = s(y - e_2) = s(y - e_2 - e_1) = 1$, so $y - e_1 \in H$, contradicting inductive (2) for V^{j-1} .

In case (ii), we may similarly assume y is odd, in which case we apply (1) to all of $T' + v_{1/d,2}$ for $T' \in \{T(1/d), T^1, T^2\}$, $y \in \{(2, d + 1), (d + 1, d + 2)\}$. In the first subcase, $s(y) = s(y + e_2) = s(y + e_2 - e_1) = 1$ and all are in H , contradicting inductive (2) for V^{j-1} . In the second subcase, $s(y) = s(y + e_2) = 1$ and $s(y + e_2 - e_1) = 0$. By inductive (2), $y + 2e_2 - e_1 \in H$. However, by iterating, this means we can build a chain of points y_i with $s(y_i) = 1$ and $y_i \in H$ that eventually intersects $\partial^h T(1/d) + v_{1/d,2}$, contradicting inductive (2).

Proof of (3)

The argument repeats the proof of (3) in Lemma 4.6.14.

□

We conclude with the alternate odd child. The key difference/simplification here is that the vertical boundaries in the $L'(n/s)$ tiling of $\hat{T}(1/d)$ are connected with respect to the F -lattice.

Lemma 4.6.16. *For each $d \geq 4$ even, the extension of $\hat{g}_{1/d}$ defined in Lemma 4.6.4 is integer superharmonic and recurrent.*

Proof. Let $\hat{s} = \Delta\hat{g}_{1/d} + 1$ and begin the proof as Lemma 4.6.14 modifying the inductive hypotheses as follows.

Write $\partial^h \hat{T}(1/d) := \partial \hat{T}(1/d) \cap (T^1 \cup T^2) \cap \{x_2 \in \{-1, 1, d, d+2\}\}$ where T^1, T^2 are the two copies of $T(1/(d-1))$ contained within $\hat{T}(1/d)$: $T^1 = T(1/(d-1))$ and $T^2 = T(1/(d-1)) + v_{1/(d-1),1} + 2\mathbf{i}$

We claim the following holds for all $L'(1/d)$ translations of $\hat{T}(1/d)$ and all $j \geq 1$:

1. If $\bigcup_{j' < j} V^{j'} \cap \hat{T}(1/d) = \emptyset$ but $V^j \cap \hat{T}(1/d) \neq \emptyset$ then $c^j \in \{0, d-1\}$ or $V^j = (d-3, 1)$. Moreover, if $c_j = (d-1)$, then $V^{j'} \cap \hat{T}(1/d) \cap T^2 \cap \{x_2 > 3\} = \emptyset$ for $j' < j$.
2. If $V^j \cap \hat{T}(1/d) \neq \emptyset$, then $V^j \cap \partial^h \hat{T}(1/d) = \emptyset$
3. If $V^j \cap \hat{T}(1/d) \neq \emptyset$ then $V^{j+1} \cap \hat{T}(1/d) \neq \emptyset$.

Proof of (1)

Suppose $\bigcup_{j' < j} V^{j'} \cap \hat{T}(1/d) = \emptyset$ and $V^j \cap \hat{T}(1/d) \neq \emptyset$ but $c^j \notin \{0, d-1\}$ and take $x \in V^j$ for $x \neq (d-2, 1)$. By a similar argument as in Lemma 4.6.15 this contradicts either the assumption or inductive (2). In this case since ∂^h is smaller, there's an extra step which uses the connected path of 1s on the left boundary.

Now, suppose $c_j = (d-1)$ but $y \in V^{j'} \cap \hat{T}(1/d) \cap T_2 \cap \{x_2 > 3\} \neq \emptyset$. If $\hat{s}(y) = 1$, then $y - e_1 \in H$. If $\hat{s}(y) = 0$ then both $\hat{s}(y \pm e_2) = 1$ and at least one such neighbor $y \pm e_2$ is in H . Iterating, this means there is $y \in H$ on ∂T^2 . This either immediately contradicts inductive (2) or there is an F -lattice path of $\hat{s}(y_i) = 1$ from y to $(0, d+1)$. This implies either $(0, d) \in H$ and $(-1, d) \in H$, contradicting inductive (1) or $(0, d+2) \in H$ and $(1, d+2) \in H$ which contradicts inductive (2).

Proof of (2)

Suppose not and take $y \in V^j \cap \partial^h \hat{T}(1/d)$. We divide into subcases (i) $y_2 = -1$ and (ii) $y_2 = d+2$.

Case (i) is identical to the previous proof. In case (ii), by (1), $y \in \{(d-1, d+2), (d, d+2)\}$.

Since $(d, d+2) \in H$ implies $(d-1, d+2)$ in H , we may take $y = (d-1, d+2)$. In this case, $y \in H$ implies the existence of a chain of points $\{y_i\} \subset H$ with $\hat{s}(y_i) = 1$ ending at $y + v_{1/d,2}$, contradicting inductive (2) for $T(1/d) + v_{1/d,2}$.

Proof of (3)

The argument is almost identical to the proof of (3) in Lemma 4.6.14 in which we argue case by case. The only new cases are case (i) $y \in \{(1-d, 0), (3, d)\}$ and case (ii) $y = (d-3, 1)$.

In case (i), both $\hat{s}(y \pm e_2) = 1$ hence one of $y \pm e_2 + e_1$ is in H .

In case (ii), if $y + e_1 \notin H$, then $\{y - e_1, y - e_1 - e_2, y - e_2, y - 2e_2, y - 2e_2 + e_1\} \subset H$.

□

4.7 Odometers and tiles

This section extends the hyperbola recursion of Section 4.3 to odometers and tiles. That is, we associate to each rational in a Farey quadruple a pair of tiles and odometers. For continuity of the literature, the formality which we use to define the recursion is similar to Levine et al. [2017].

4.7.1 Standard tiles

Let $(p_0, q_0) = \mathcal{C}(p_1, q_1)$ form a Farey quadruple labeled by a recursion word $w \in F_3^*$. Let \mathcal{W}_1 count the number of 1s in w .

Definition 3. A pair of tiles $(T(p_0), T(q_0)) \subset \mathbb{Z}^2$ are standard tiles for (p_0, q_0) if they appear in Proposition 4.6.1, are $(T_{0/1}, T_{1/1})$ from Section 4.5.4, or have the standard tile decomposition:

$$\begin{aligned} T(p_0) &= T(p_1)^+ \cup T(p_1)^- \cup T^d(q_1)^+ \cup T^d(q_1)^- \\ T(q_0) &= T^d(p_1)^+ \cup T^d(p_1)^- \cup T(q_1)^+ \cup T(q_1)^- \end{aligned} \tag{4.76}$$

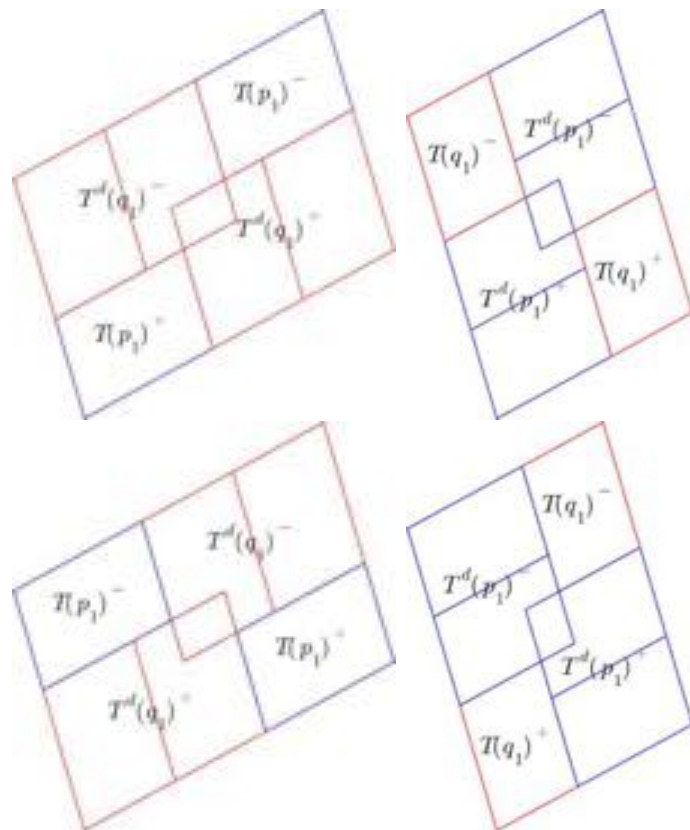


Figure 4.21: The two possible orientations for a standard tile pair from Definition 3. The left column is the odd child and the right column is the even child. The first row is the odd-first orientation and the second is the even-first orientation. Only one type of overlap between parents (corresponding to Type 1 children) is displayed - see Figure 4.22 for the other types of overlaps.

where $T^d(n/d)^\pm$ denote doubled tiles,

$$\begin{aligned} T^d(p)^\pm &= T(p)^{\pm,1} \cup T(p)^{\pm,2} := T(p) \cup (T(p) + v_{p,2}) \\ T^d(q)^\pm &= T(q)^{\pm,1} \cup T(q)^{\pm,2} := T(q) \cup (T(q) + v_{q,1}) \end{aligned} \quad (4.77)$$

and $(T(p_1), T(q_1))$, with or without superscripts, are standard tiles for (p_1, q_1) . The tile positions in (4.76) depend on the parity of \mathcal{W}_1 : if \mathcal{W}_1 is odd

$$\begin{aligned} c(T) - c(T(p_0)) &= \begin{cases} 0 & \text{if } T = T(p_1)^+ \\ 2v_{q_1,1} + v_{q_1,2} & \text{if } T = T(p_1)^- \\ v_{p_1,1} & \text{if } T = T^d(q_1)^+ \\ v_{p_1,2} & \text{if } T = T^d(q_1)^- \end{cases} \\ c(T) - c(T(q_0)) &= \begin{cases} 0 & \text{if } T = T^d(p_1)^+ \\ v_{q_1,1} + v_{q_1,2} & \text{if } T = T^d(p_1)^- \\ v_{p_1,1} & \text{if } T = T(q_1)^+ \\ 2v_{p_1,2} & \text{if } T = T(q_1)^- \end{cases} \end{aligned} \quad (4.78)$$

otherwise

$$c(T) - c(T(p_0)) = \begin{cases} 0 & \text{if } T = T^d(q_1)^+ \\ v_{p_1,1} + v_{p_1,2} & \text{if } T = T^d(q_1)^- \\ 2v_{q_1,1} & \text{if } T = T(p_1)^+ \\ v_{q_1,2} & \text{if } T = T(p_1)^- \end{cases} \quad (4.79)$$

$$c(T) - c(T(q_0)) = \begin{cases} 0 & \text{if } T = T(q_1)^+ \\ v_{p_1,1} + v_{p_1,2} & \text{if } T = T(q_1)^- \\ v_{q_1,1} & \text{if } T = T^d(p_1)^+ \\ v_{q_1,2} & \text{if } T = T^d(p_1)^-, \end{cases}$$

see Figure 4.21.

The tiles in the standard tile decomposition of $T(n/d)$ will be called subtiles of $T(n/d)$. The tile orientations in (4.78) and (4.79) will be referred to as the odd-first and even-first orientations respectively. A single tile in a pair of standard tiles is a standard tile.

Before proving general existence of standard tiles, we derive an extension of rotation invariance Lemma 4.3.6, to tiles and a tiling property, assuming existence up to a certain depth.

Lemma 4.7.1. Suppose standard tiles exist for all $n/d \in \mathcal{T}_m$, for $m \leq m_0$, some $m_0 \geq 1$. Then, the following properties are satisfied for each such $0 < n/d < 1$.

1. *Rotation invariance:* $\mathcal{R}(T(n/d)) = T(\mathcal{R}(n/d))$

2. *Boundary tiling:* starting at $c(T(n/d))$ the boundary word of $T(n/d)$ can be written as

$w = w_1 * w_2 * \widehat{\mathbf{rev}(w_1)} * \widehat{\mathbf{rev}(w_2)}$ where w_1, w_2 satisfy the hypotheses in Lemma 4.4.1

and $\sum w_1 + \mathbf{i} = v_{n/d,1}$ and $\sum w_2 - 1 = v_{n/d,2}$.

Proof. Both properties are true by Proposition 4.6.1 if $T(n/d)$ does not have a standard tile

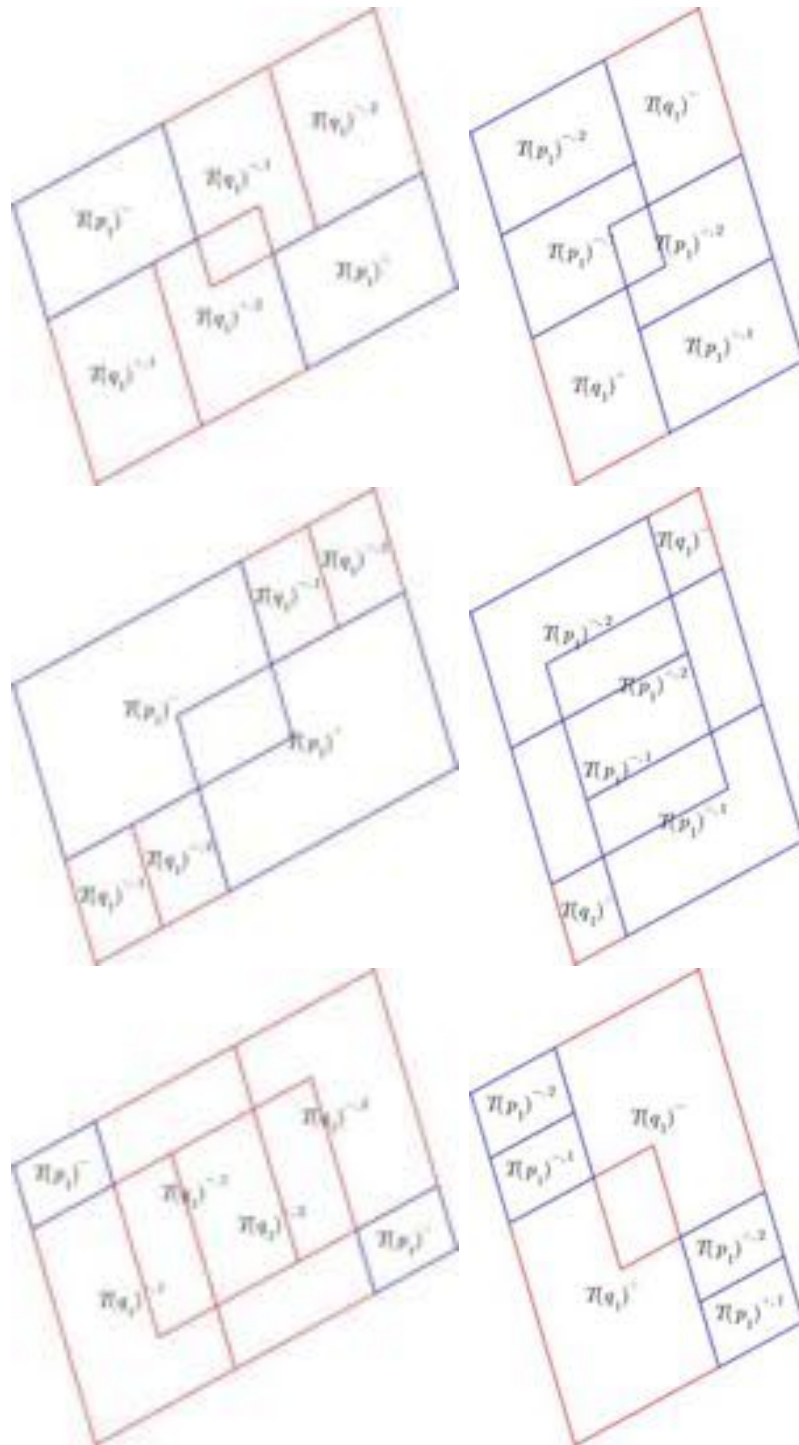


Figure 4.22: All possible overlaps between parents in a standard tile. The left column denotes the odd child and the right column is the even child. The rows from top to bottom correspond to Type 1, 2, then 3 children. The parent tiles are labeled in their centers with notation from Definition 3. The orientation is the even-first orientation.

decomposition. Thus, we may assume $T(n/d)$ has a standard tile decomposition and that both properties are satisfied for the parent tiles of $T(n/d)$.

Step 1: Rotation invariance

If (n/d) is even, then its parent tiles are $T^d(p_1)^\pm$ and $T(q_1)$. By Lemma 4.3.7 and the inductive hypothesis, $\mathcal{R}(T^d(p_1)^\pm) = T^d(\mathcal{R}(p_1))$ and $\mathcal{R}(T(q_1)) = T(\mathcal{R}(q_1))$. By Lemma 4.3.6, these are the parent tiles of $T(\mathcal{R}(n/d))$. This together with the standard decomposition and Lemma 4.3.7 again implies $T(\mathcal{R}(n/d)) = \mathcal{R}(T(n/d))$. The proof applies to (n/d) odd after observing \mathcal{R} on the parent tiles is an involution. Indeed, the second hypothesis implies 180-degree symmetry.

Step 2: Boundary tiling

Every base case tile, $T(n/d)$ has a (w_1, w_2) -boundary word of the form

$$w_1 * w_2 * \widehat{\mathbf{rev}(w_1)} \widehat{\mathbf{rev}(w_2)}$$

and $T(\mathcal{R}(n/d))$ has a $(-\mathbf{i}w_2, -\mathbf{i}w_1)$ boundary word both of which start at $c(T)$. Moreover, each such w_1 and w_2 satisfy the desired properties. By induction and the standard decomposition every subsequent standard tile has a boundary word decomposition. Thus, by Step 1, it suffices to show that the *bottom edges*, the w_1 in the boundary word decompositions satisfy the conditions in Lemma 4.4.1.

We start by rewriting the standard tile recursion to produce just the two bottom edges for each odd-even tile pair for each child Farey pair in a Farey quadruple: $(w_t, v_t) \in F_2 \times F_2$. The base cases are quadruples \mathbf{q}_{2^k} for $k \geq 0$ and \mathbf{q}_{3^k} for $k > 0$ for which we have explicit

formulae from Section 4.6 for the odd-even pair of edges (w_0, v_0) :

$$\begin{pmatrix} w_0 \\ v_0 \end{pmatrix} = \begin{cases} \begin{pmatrix} 1 * (1 * \mathbf{i})^{2k+1} * (1 * 1) \\ 1 * (1 * \mathbf{i})^{2k} (1 * 1) \end{pmatrix} & \mathbf{q}_{2^k} \text{ for } k \geq 0 \\ \begin{pmatrix} (1 * 1)^k (1 * \mathbf{i}) * (1 * 1)^{k+1} * 1 \\ 1 * (1 * 1)^{k+1} \end{pmatrix} & \mathbf{q}_{3^k} \text{ for } k > 0. \end{cases}$$

Now, given a recursion word $str \in F_3^*$ describing a quadruple \mathbf{q}_{str} the standard tile decomposition implies

$$\begin{pmatrix} w_{t+1} \\ v_{t+1} \end{pmatrix} = \begin{cases} \begin{pmatrix} w_t * \mathbf{i} * v_t * \mathbf{i} * v_t \\ w_t * \mathbf{i} * v_t \end{pmatrix} & \text{if } \sum(str[i] = 1) \text{ is odd} \\ \begin{pmatrix} v_t * \mathbf{i} * v_t * w_t \\ v_t * \mathbf{i} * w_t \end{pmatrix} & \text{if } \sum(str[i] = 1) \text{ is even,} \end{cases} \quad (4.80)$$

where w_t, v_t are the edges of the odd-even parent Farey pair in \mathbf{q}_{str} .

It will be convenient to augment the recursion so that it generates the bottom edge

Draft Mar 13

concatenated with an extra \mathbf{i} . The augmented recursion has as base cases

$$\begin{pmatrix} \tilde{w}_0 \\ \tilde{v}_0 \end{pmatrix} = \begin{cases} \begin{pmatrix} 1 * (1 * \mathbf{i})^{2k+1} * (1 * 1 * \mathbf{i}) \\ 1 * (1 * \mathbf{i})^{2k} (1 * 1 * \mathbf{i}) \end{pmatrix} & \text{if } str = 2^k \text{ for } k \geq 0 \\ \begin{pmatrix} (1 * 1)^k (1 * \mathbf{i}) * (1 * 1)^{k+1} * (1 * \mathbf{i}) \\ (1 * 1)^{k+1} * (1 * \mathbf{i}) \end{pmatrix} & \text{if } str = 3^k \text{ for } k > 0 \end{cases}$$

and the recursive step is

$$\begin{pmatrix} \tilde{w}_{t+1} \\ \tilde{v}_{t+1} \end{pmatrix} = \begin{cases} \begin{pmatrix} \tilde{w}_t * \tilde{v}_t * \tilde{v}_t \\ \tilde{w}_t * \tilde{v}_t \end{pmatrix} & \text{if } \sum(str[i] = 1) \text{ is odd} \\ \begin{pmatrix} \tilde{v}_t * \tilde{v}_t * \tilde{w}_t \\ \tilde{v}_t * \tilde{w}_t \end{pmatrix} & \text{if } \sum(str[i] = 1) \text{ is even,} \end{cases} \quad (4.81)$$

where similarly \tilde{w}_t, \tilde{v}_t are the augmented edges of the odd-even parents of str . Use induction and compute using (4.81) to show that the augmented words sum to the desired lattice vectors. It remains to verify the rest of the hypotheses for which we use (4.81) and the forms of the base cases. We split into cases based on the structure of the recursion word \mathbf{q}_{str} .

Case 1: $str = 2^k * s * str'$ for $k \geq 0$, $s \in \{1, 3\}$ and $|str'| \geq 0$

If $k = 0$ and $s = 3$ then proceed to Case 2. Otherwise, write

$$\begin{pmatrix} p_k \\ q_k \end{pmatrix} = \begin{pmatrix} 1 * (1 * \mathbf{i})^{2k+1} * (1 * 1 * \mathbf{i}) \\ 1 * (1 * \mathbf{i})^{2k} (1 * 1 * \mathbf{i}) \end{pmatrix}.$$

By Lemma 4.5.1 both w_t and v_t are of the form $p * \tilde{w} * q$ where \tilde{w} is a palindrome in the

letters p, q where

$$(p, q) = \begin{cases} (p_k, q_k) & \text{if } s = 1 \\ (q_k, p_{k-1}) & \text{if } s = 3. \end{cases}$$

An inspection of the formula shows that

$$\mathbf{rev}(b) * \mathbf{i} = \mathbf{i} * b \quad \text{for } b \in \{p, q\} \quad (4.82)$$

as words in the letters $\{1, i\}$. We claim this implies that case (b) of Lemma 4.4.1 holds.

First take $s = 1$ and write in the letters $\{1, i\}$,

$$\begin{aligned} p_k \tilde{w} q_k &= (1 * 1 * \mathbf{i}) * (1 * \mathbf{i})^{2k} * (1 * 1 * \mathbf{i}) * \tilde{w} * 1 * (1 * \mathbf{i})^{2k} * (1 * 1 * \mathbf{i}) \\ &= (1 * 1 * \mathbf{i}) * \left((1 * \mathbf{i})^{2k} * (1 * 1 * \mathbf{i}) * \tilde{w} * 1 * (1 * \mathbf{i})^{2k} * 1 \right) * 1 * \mathbf{i} \\ &=: (1 * 1 * \mathbf{i}) * \tilde{v} * 1 * \mathbf{i}. \end{aligned}$$

As we have augmented a trailing i , it suffices to show \tilde{v} is a palindrome in the letters $\{1, i\}$:

$$\begin{aligned} \mathbf{rev}(\tilde{v}) &= 1 * (\mathbf{i} * 1)^{2k} * 1 * \mathbf{rev} \tilde{w} * (\mathbf{i} * 1 * 1) * (\mathbf{i} * 1)^{2k} \\ &= (1 * \mathbf{i})^{2k} * 1 * 1 * (\mathbf{rev} \tilde{w} * \mathbf{i}) * 1 * (1 * \mathbf{i})^{2k} * 1 \\ &= (1 * \mathbf{i})^{2k} * (1 * 1 * \mathbf{i}) * \tilde{w} * 1 * (1 * \mathbf{i})^{2k} * 1 \\ &= \tilde{v}, \end{aligned}$$

where in the second to last step we used (4.82). The argument when $s = 3$ and $k \geq 1$ proceeds in the same fashion using (4.82).

Case 2: $str = 3^k * s * str'$ for $k > 0$, $s \in \{1, 2\}$ and $|str'| \geq 0$

The argument is similar to Case 1, however, the letters in this case are:

$$\begin{pmatrix} p_k \\ q_k \end{pmatrix} = \begin{pmatrix} h_k * h_{k+1} \\ h_{k+1} \end{pmatrix} := \begin{pmatrix} (1 * 1)^k * (1 * \mathbf{i}) * (1 * 1)^{k+1} * (1 * \mathbf{i}) \\ (1 * 1)^{k+1} (1 * \mathbf{i}) \end{pmatrix}.$$

By Lemma 4.5.1 both w_t and v_t are of the form $p * \tilde{w} * q$ where \tilde{w} is a palindrome in the letters p, q where

$$(p, q) = \begin{cases} (p_k, q_k) & \text{if } s = 1 \\ (q_{k-1}, p_k) & \text{if } s = 2. \end{cases}$$

Compute to see that

$$\begin{aligned} \mathbf{rev}(b) * \mathbf{rev}(h_{k+1}) * \mathbf{i} &= (\mathbf{rev}(h_{k+1}) * \mathbf{i}) * b \\ &= \mathbf{i} * h_{k+1} * b \quad \text{for } b \in \{p_k, q_k\}. \end{aligned} \tag{4.83}$$

and

$$1 * (1 * 1)^k * \mathbf{rev}(b) = b * 1 * (1 * 1)^k \quad \text{for } b \in \{p_k, q_{k-1}\}. \tag{4.84}$$

The rest of the argument is similar to Case 1: when $s = 1$ use (4.83) and when $s = 2$ use (4.84).

□

The next lemma uses the abstract recursion on binary words in (4.31) as well as the pseudo-square boundary decomposition. For notational convenience, write $w_h(n/d)$ for the binary word associated to the reduced fraction in (4.31) with initial seed $w_0 = \{\}$ and $\mathbf{Q}_{\{\}} = (qqp, qp, p, q)$. Also write $w_v(n/d) = \mathcal{F}(w_h(\mathcal{R}(n/d)))$.

Lemma 4.7.2. *A standard tile, $T(n/d)$ exists for every reduced rational $0 \leq n/d \leq 1$. Moreover, when $0 < n/d < 1$, the tile has the following properties.*

- (a) $T(n/d)$ generates a $(v_{n/d,1}, v_{n/d,2})$ -regular almost pseudo-square tiling.

- (b) Each $T(n/d)$ is a $(w_h(n/d), w_v(n/d))$ -pseudo-square with offsets respecting the tiling:
- (a) $c(T) - c(T(n/d)) = v_{n/d,1} - (\mathbf{i} + 1)$ where T is the last tile of $w_h(n/d)$
 - (b) $c(T') - c(T(n/d)) = v_{n/d,2} - (2\mathbf{i} - 1)$ where T' is the last tile of $\text{rev}(w_v(n/d))$
 - (c) The surrounding of $T(n/d)$ with respect to $(v_{n/d,1}, v_{n/d,2})$ consists of two stacked zero-one horizontal and two vertical boundary strings.
 - (d) When $T(n/d)$ has a standard decomposition, the shared boundary between neighboring subtiles is part of or is a stacked horizontal or vertical zero-one boundary string.

Proof. In light of Proposition 4.6.1, we may assume $T(n/d)$ has a standard decomposition and the statements are true for its parents, $T(p_1)$ and $T(q_1)$. Also, by Lemma 4.7.1 to prove part (a) it suffices to show that $T(n/d)$ is a topological disk, *i.e.*, does not have any internal holes. This however follows from part (c) and Lemma 4.5.4, hence it remains to prove (b), (c), and (d). We assume that the decomposition given is in the even-first orientation, otherwise flip the subsequent statements.

Step 1: (b)

By the inductive hypothesis, $T(p_1)$ and $T(q_1)$ are $(w_h(p_1), w_v(p_1))$ and $(w_h(q_1), w_v(q_1))$ pseudo-squares. By rotation, we may assume $T(n/d)$ is odd. Let T be the last tile in $T(q_1)^{+,1}$ and T' the first tile in $T(q_1)^{+,2}$. By definition T is a translation of $T_{0/1}$ and T' a translation of $T_{1/1}$. Moreover, by the definition of the standard decomposition and the inductive hypothesis on the offsets, $c(T') - c(T) = (1 + \mathbf{i})$, in particular, we can glue the two boundary strings together. A similar argument applies to the interface between $T(q_1)^{+,2}$ and $T(p_1)$. This shows if (n/d) is odd, then $T(n/d)$ respects $w_h(q_1) * w_h(q_1) * w_h(p_1)$ otherwise it respects $w_h(q_1) * w_h(p_1)$. A symmetric argument applies to the vertical boundary strings and a computation shows that the offsets respect the tiling.

Step 2: (c)

Let A be the horizontal string for $T(n/d)$ and B the reversed horizontal string for $T(n/d) -$

$v_{n/d,2}$. Set $c(T(n/d)) = 0$. By part (b), the first tile in B is located at $c(T(n/d)) - v_{n/d,2} + v_{n/d,2} - (2\mathbf{i} - 1)$. Thus, the offset between the first tile in B and the first tile in A is $2\mathbf{i} - 1 = v_{0/1,2} + \mathbf{i}$, the correct initial offset for a stacked string.

Similarly if C is the vertical string for $T(n/d)$ and D the reversed vertical string for $T(n/d) + v_{n/d,1}$, then the offsets between the first tiles is $(\mathbf{i} + 1) = -v_{1/1,1}$. The other two sides are stacked strings by the above arguments for $T(n/d) - v_{n/d,1}$ and $T(n/d) + v_{n/d,2}$.

Step 3: (d)

We state the arguments with the aid of Figure 4.22. First consider the three possible boundaries between $T(q_1)^{+,1/2}$ and $T(p_1)^-$ when $T(n/d)$ is odd. By the inductive hypothesis, the offset between the first tile in the reversed zero-one horizontal boundary string for $T(q_1)^{+,1}$ and the first tile for the zero-one horizontal string in $T(p_1)^-$ is $v_{0/1,2} + \mathbf{i}$. Since the initial offset is correct, the rest of the interface forms part of a stacked horizontal zero-one boundary string by part (3) of Lemma 4.5.1. Indeed, every letter other than the first matches across the interface. Reversing p_1 and q_1 above shows the three possible interfaces between $T(p_1)^+$ and $T(q_1)^{-,1/2}$ also form part of a stacked horizontal boundary string. When $T(n/d)$ is even, the interface between $T(p_1)^{+,1}$ and $T(p_1)^{+,2}$ is exactly a stacked horizontal boundary string by the inductive hypothesis part (c). By rotation, the above arguments apply to the vertical interfaces. \square

4.7.2 Weak standard odometers

Our current goal is to extend the standard tile decomposition to odometers. In order to do so, we must define the operation of doubling a partial odometer. However, in the course of the recursion, doubled odometers may need to be corrected in the interior of the tile so we need a notion of tile that only depends on the boundary in the pseudo-square decomposition.

Draft Mar 13

Definition 4. Let $T(n/d)$ be a $(w_h(n/d), w_v(n/d))$ pseudo-square. A partial tile

$$T^{h^\pm/v^\pm}(n/d)$$

is a tile which coincides with $T(n/d)$ on one of the four sides:

$$T^{h^\pm/v^\pm}(n/d) \cap T(n/d) \supset \begin{cases} w_h(n/d) & \text{case } h^+ \\ \mathbf{rev}(w_h(n/d)) & \text{case } h^- \\ w_v(n/d) & \text{case } v^+ \\ \mathbf{rev}(w_v(n/d)) & \text{case } v^- . \end{cases} \quad (4.85)$$

A boundary tile

$$T^b(n/d)$$

coincides with $T(n/d)$ on every side:

$$T^b(n/d) \cap T(n/d) \supset w_h(n/d) \cup \mathbf{rev}(w_h(n/d)) \cup w_v(n/d) \cup \mathbf{rev}(w_v(n/d)). \quad (4.86)$$

We now define the notion of a doubled odometer using partial tiles. But before we do so, we define an operation, for convenience, which will allow us to quickly pass from a tile decomposition to an odometer decomposition. Say $T(n/d)$ and $T(n'/d')$ are two tiles with $c(T(n'/d')) - c(T(n/d)) = v_{n/d,i}$. Then, two partial odometers $o(n/d)$ and $o(n'/d')$ respect the tile translations if $s(o(n'/d')) - s(o(n/d)) = a_{n/d,i}$ and the domains of $o(n/d)$ and $o(n'/d')$ are $T(n/d)$ and $T(n'/d')$ respectively.

Definition 5. For $(n/d) \in \{p_0, q_0\}$ let $T(n/d)$ be a standard tile and $T^{h^\pm/v^\pm}(n/d)$ a partial tile. Denote by

$$T^{d,p,\pm}(n/d) = T^b(n/d)^1 \cup T^{h^\pm/v^\pm}(n/d)^2 := T^b(n/d) \cup (T^{h^\pm/v^\pm}(n/d) + v_{n/d}) \quad (4.87)$$

a partial doubled tile where $v_{n/d} = v_{p_0,2}$ or $v_{n/d} = v_{q_0,1}$ for $n/d = p_0$ odd or $n/d = q_0$ even respectively.

The weak doubling of a partial odometer $o_{n/d}$ with domain $T^b(n/d)$ is a partial odometer $d(o)_{n/d}^\pm : T^{d,p}(n/d) \rightarrow \mathbb{Z}$ with the decomposition

$$d(o)_{n/d}^\pm = o_{n/d} \cup o_{n/d}^* \quad (4.88)$$

where $T(o_{n/d}) = T^b(n/d)^1$ and $T(o_{n/d}^*) = T^{h^\pm/v^\pm}(n/d)^2$ and, after being restricted to the relevant zero-one boundary strings from Definition 4, $o_{n/d}^*$ and $o_{n/d}$ respect the tile translations.

We now use these to partially define the standard recursion. The full recursion requires alternate tiles odometers which are defined in the next two subsections.

Definition 6. A pair of partial odometers $o_{p_0} : T^b(p_0) \rightarrow \mathbb{Z}$ and $o_{q_0} : T^b(q_0) \rightarrow \mathbb{Z}$ are weak standard tile odometers for (p_0, q_0) if they appear in Proposition 4.6.1, are $(o_{0/1}, o_{1/1})$ from Section 4.5.4 or if $(T(p_0), T(q_0))$ are standard tiles with standard decompositions for (p_0, q_0) and the partial odometers have the standard decompositions:

$$\begin{aligned} o_{p_0} &= o_{p_1}^+ \cup o_{p_1}^- \cup d(o)_{q_1}^+ \cup d(o)_{q_1}^- \\ o_{q_0} &= d(o)_{p_1}^+ \cup d(o)_{p_1}^- \cup o_{q_1}^+ \cup o_{q_1}^- \end{aligned} \quad (4.89)$$

where each $o_{n/d}$ is a weak standard tile odometer for (n/d) and the offsets are specified by requiring the odometers respect the tile translations in Definition 3. The weak standard tile odometers on the right-hand-side of (4.89) will be called weak subodometers of o_{p_0} or o_{q_0} respectively.

We say weak standard tile odometers $o_{n/d}$ and $o'_{n/d}$ are *lattice adjacent* if

$$\begin{aligned} c(T(o_{n/d})) - c(T(o_{n/d})') &= v_{n/d,i} \\ s(o_{n/d}) - s(o'_{n/d}) &= \pm a_{n/d,i}, \end{aligned}$$

for $i \in \{1, 2\}$. We now prove an analogue of Lemma 4.7.2 for weak standard odometers.

Lemma 4.7.3. *A weak standard odometer, $o(n/d)$ exists for every reduced rational $0 \leq n/d \leq 1$. Moreover, when $0 < n/d < 1$, the odometer has the following properties.*

- (a) $o(n/d)$ respects $(w_h(n/d), w_v(n/d))$
- (b) Let A, B, C, D denote the first and last tiles of $w_h(n/d)$ and the last and first tiles of $\text{rev}(w_h)(n/d)$ respectively (geometrically a counter-clockwise walk around the tile). Let o_Z be the restriction of $o(n/d)$ to $Z \in \{A, B, C, D\}$. Then, $s(o_B) - s(o_A) = 0$, $s(o_C) - s(o_D) = a_{0/1,2} - a_{1/1,2}$ and $s(o_C) - s(o_B) = a_{n/d,2} - a_{1/1,2}$.
- (c) Lattice adjacent $o'_{n/d}$ and $o_{n/d}$ are compatible.

Proof. By Proposition 4.6.1, we may assume the tile $T(n/d)$ has a standard decomposition and hence the subodometers of $o(n/d)$ exist and satisfy the inductive hypotheses.

Step 1: Existence

Since subodometers exist, it suffices to show that the odometer decomposition is well-defined *i.e.*, the subodometers have a common extension on their overlaps. By possibly deleting parts of the subodometers, we may assume that the only overlaps are on the internal zero-one stacked boundary strings. By an inductive application of (a) and (b) the subodometers respect the corresponding stacked boundary strings and therefore by Lemma 4.5.5 have a common extension to $T^b(n/d)$.

Step 2. Inductive hypotheses

We copy the proof of parts (b) and (c) of Lemma 4.7.2. To check that the affine offsets are

the ones required in Lemma 4.5.5, we use the fact that the subodometers respect the tiling together with an inductive application of (b).

□

4.7.3 Alternate tiles

We now construct alternate tiles. In this case, the decomposition depends on the last letter of the recursion word, in particular, the parents of the parents. If the last letter of the recursion word is s , we say that we are in the Type s case. (Note that the initial quadruple is one of the base cases.)

Definition 7. A pair of tiles $(\hat{T}(p_0), \hat{T}(q_0)) \subset \mathbb{Z}^2$ are alternate tiles for (p_0, q_0) if they appear in Proposition 4.6.1, are $(T_{0/1}, T_{1/1})$ from Section 4.5.4 or if they have the alternate tile decomposition

$$\begin{aligned}\hat{T}(p_0) &= T^{ds}(p_1)^+ \cup T^{ds}(p_1)^- \cup T(q_1)^+ \cup T(q_1)^- \cup \hat{T}(q_1) \\ \hat{T}(q_0) &= T(p_1)^+ \cup T(p_1)^- \cup T^{ds}(q_1)^+ \cup T^{ds}(q_1)^- \cup \hat{T}(p_1)\end{aligned}\tag{4.90}$$

where $T^{ds}(n/d)^\pm$ denote doubled tiles where the doubling is different depending on the orientation:

$$\begin{aligned}T^{ds}(p)^\pm &= T(p)^{\pm,1} \cup T(p)^{\pm,2} := T(p) \cup (T(p) + S_p) \\ T^{ds}(q)^\pm &= T(q)^{\pm,1} \cup T(q)^{\pm,2} := T(q) \cup (T(q) + S_q),\end{aligned}\tag{4.91}$$

where

$$(S_p, S_q) = \begin{cases} (v_{q,1} + v_{p,2}, -v_{q,1} + v_{p,2}) & \text{if } \mathcal{W}_1 \text{ is even} \\ (-v_{q,1} + v_{p,2}, v_{q,1} + v_{p,2}) & \text{otherwise} \end{cases}\tag{4.92}$$

and $(T(p_1), T(q_1))$ with or without superscripts are standard tiles for (p_1, q_1) and $\hat{T}(n/d)$ is an alternate tile for n/d .

The standard tile positions in (4.90) depend on the parity of \mathcal{W}_1 : if \mathcal{W}_1 is odd

$$c(T) - c(\hat{T}(p_0)) = \begin{cases} v_{p_1,1} & \text{if } T = T(q_1)^+ \\ 2v_{p_1,2} - v_{q_1,1} & \text{if } T = T(q_1)^- \\ 0 & \text{if } T = T^{ds}(p_1)^+ \\ v_{q_1,1} + v_{q_1,2} & \text{if } T = T^{ds}(p_1)^- \end{cases} \quad (4.93)$$

$$c(T) - c(\hat{T}(q_0)) = \begin{cases} v_{p_1,1} & \text{if } T = T^{ds}(q_1)^+ \\ v_{p_1,2} & \text{if } T = T^{ds}(q_1)^- \\ 0 & \text{if } T = T(p_1)^+ \\ v_{p_1,2} + v_{q_1,2} + 2v_{q_1,1} & \text{if } T = T(p_1)^- \end{cases}$$

otherwise

$$c(T) - c(\hat{T}(p_0)) = \begin{cases} 0 & \text{if } T = T(q_1)^+ \\ v_{p_1,1} + 2v_{p_1,2} + v_{q_1,1} & \text{if } T = T(q_1)^- \\ v_{q_1,1} & \text{if } T = T^{ds}(p_1)^+ \\ v_{q_1,2} & \text{if } T = T^{ds}(p_1)^- \end{cases} \quad (4.94)$$

$$c(T) - c(\hat{T}(q_0)) = \begin{cases} 0 & \text{if } T = T^{ds}(q_1)^+ \\ v_{p_1,1} + v_{p_1,2} & \text{if } T = T^{ds}(q_1)^- \\ v_{q_1,1} & \text{if } T = T(p_1)^+ \\ v_{p_1,2} + v_{q_1,2} - v_{q_1,1} & \text{if } T = T(p_1)^- \end{cases}$$

The alternate tile positions in (4.90) may depend on both the parity of \mathcal{W}_1 , (even-

first/odd-first) and the type of the child:

$$c(\hat{T}(q_1)) - c(\hat{T}(p_0)) = \begin{cases} v_{p_1,2} + v_{p_1,1} - v_{q_1,1} & \text{odd-first and Type 1 or 3} \\ - & \text{odd-first and Type 2} \\ v_{q_1,1} + v_{p_1,2} & \text{even-first and Type 1 or 3} \\ - & \text{even-first and Type 2} \end{cases} \quad (4.95)$$

$$c(\hat{T}(p_1)) - c(\hat{T}(q_0)) = \begin{cases} v_{p_1,2} + v_{q_1,1} & \text{odd-first and Type 1} \\ 2v_{q_1,1} + v_{q_1,2} & \text{odd-first and Type 2} \\ - & \text{odd-first and Type 3} \\ v_{p_1,2} + v_{p_1,1} - v_{q_1,1} & \text{even-first and Type 1} \\ v_{q_1,2} & \text{even-first and Type 2} \\ - & \text{even-first and Type 3} \end{cases} \quad (4.96)$$

where in the cases indicated by $-$ the alternate tile is omitted.

We now make an important exception in the definition of $c(\cdot)$ for alternate tiles. If $\hat{T}(n/d)$ has an alternate decomposition, then

$$c(\hat{T}(n/d)) = \begin{cases} c(T(q_1)^{+,1}) & \text{even-first and } n/d \text{ even} \\ c(T(q_1)^+) & \text{even-first and } n/d \text{ odd} \\ c(T(p_1)^+) & \text{odd-first and } n/d \text{ even} \\ c(T(p_1)^{+,1}) & \text{odd-first and } n/d \text{ odd.} \end{cases} \quad (4.97)$$

Next is the analogue of Lemma 4.7.2 for alternate tiles.

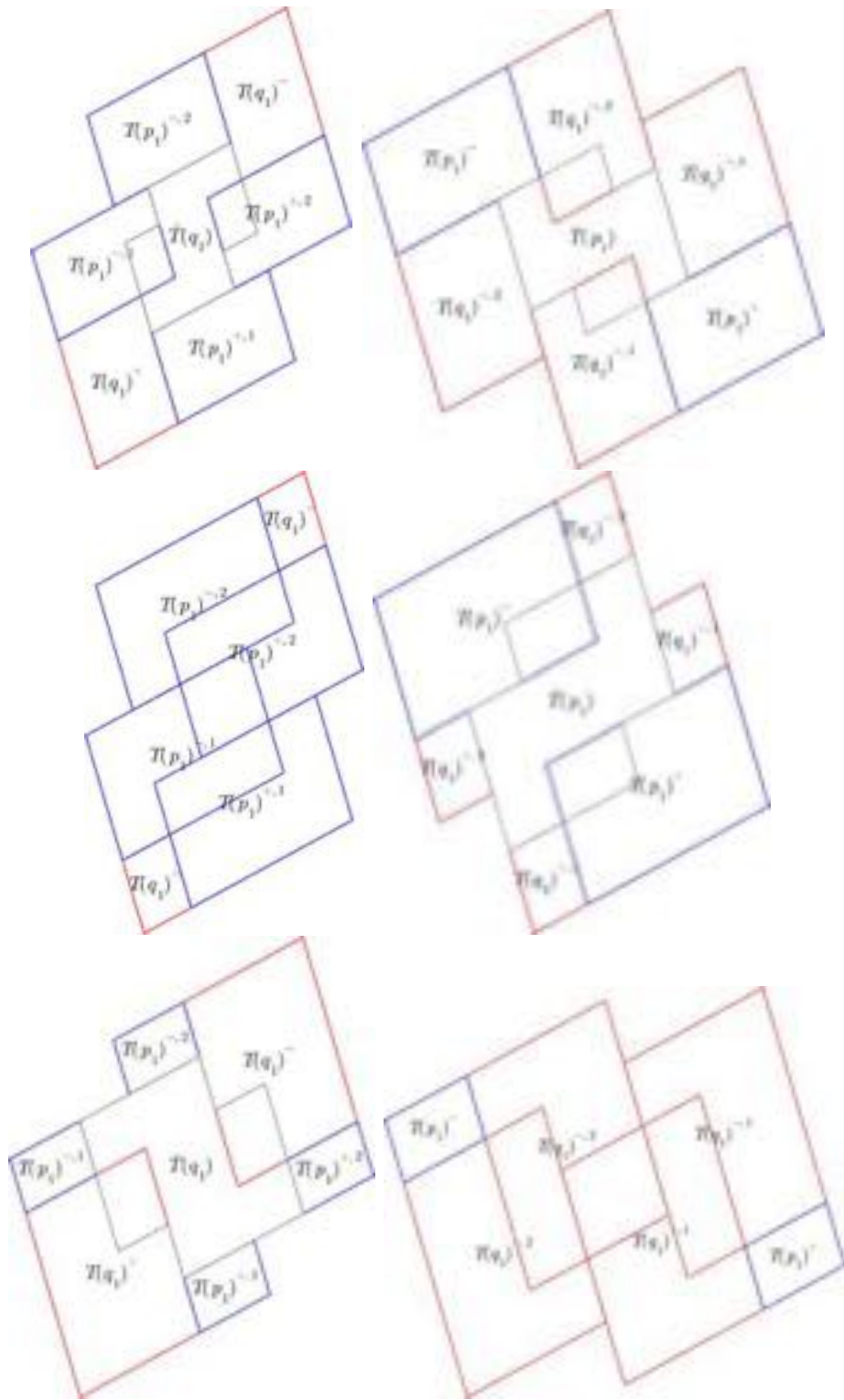


Figure 4.23: As Figure 4.22 (even-first) but for alternate tiles with labels from Definition 7.

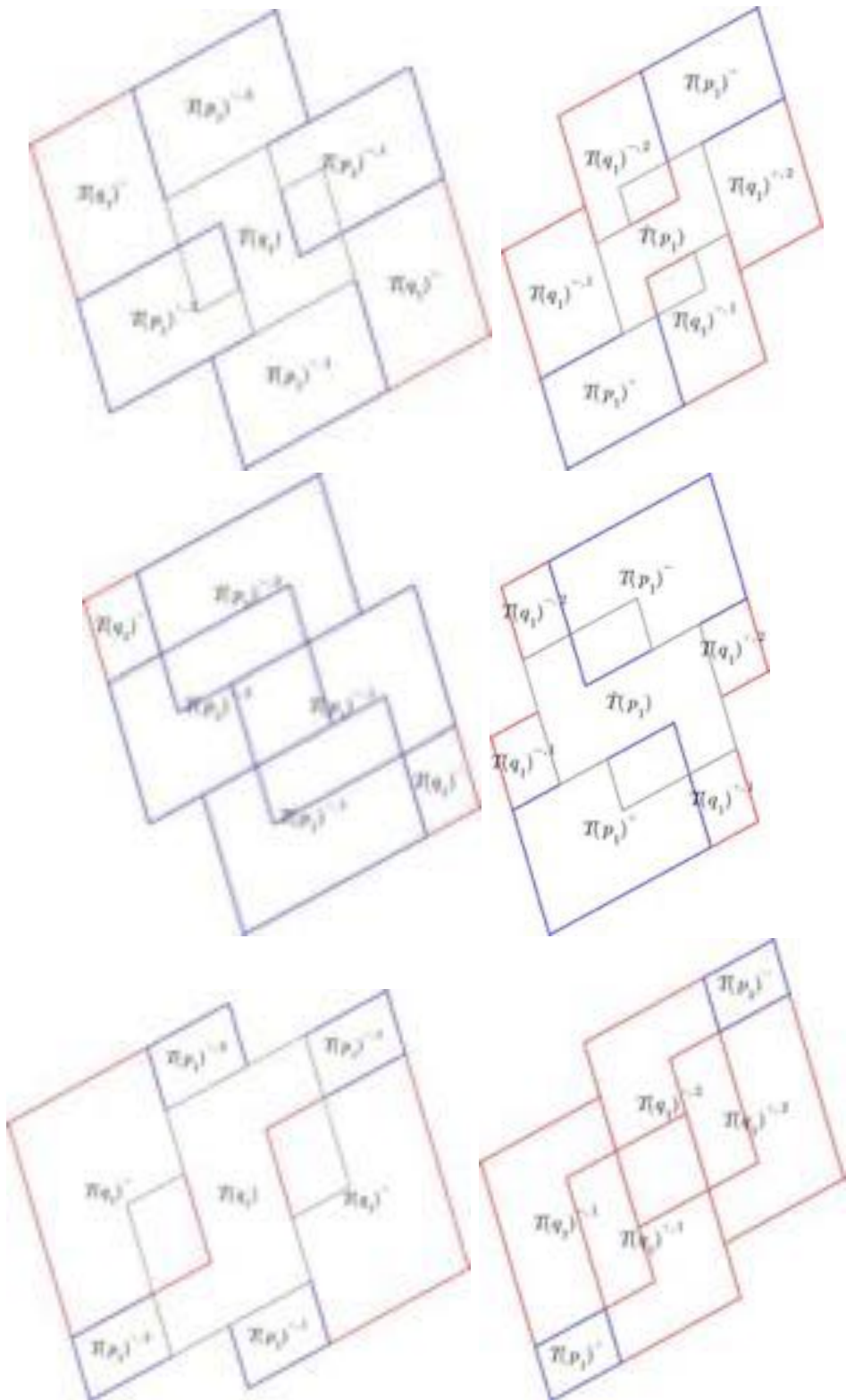


Figure 4.24: As Figure 4.23 but in the odd-first orientation

Lemma 4.7.4. *An alternate tile, $\hat{T}(n/d)$ exists for every reduced rational $0 \leq \frac{n}{d} \leq 1$.*

Moreover, when $0 < n/d < 1$, the alternate tile has the following properties.

1. *Symmetry and rotation invariance: $\hat{T}(n/d)$ is 180-degree symmetric and*

$$\mathcal{R}(\hat{T}(n/d)) = \hat{T}(\mathcal{R}(n/d)).$$

2. *$\hat{T}(n/d)$ covers space under the lattice $L'(n/d)$*
3. *If n/d is even $\hat{T}(n/d)$ is a $w_h(n/d)$ -pseudo-square, otherwise a $w_v(n/d)$ pseudo-square with offsets respecting the tiling:*
 - (a) *Even case: $c(T_1) = c(\hat{T}(n/d))$ where T_1 is first tile of $w_h(n/d)$*
 - (b) *Odd case: $c(T'_1) = c(\hat{T}(n/d)) + s$ where T'_1 is the first tile of $\text{rev}(w_v(n/d))$ where $s = 0$ in the even-first orientation, otherwise $s = -v_{q1,1} + v_{p1,2}$.*
4. *The surrounding of $\hat{T}(n/d)$ with respect to $(v_{n/d,1}, v_{n/d,2})$ consists of either part of a stacked zero-one boundary string or a complete overlap on a subtile.*
5. *When $\hat{T}(n/d)$ has an alternate decomposition, the shared boundary between neighboring subtiles is part of or is a stacked horizontal or vertical zero-one boundary string.*

Proof. We may assume by Proposition 4.6.1 that $\hat{T}(n/d)$ has an alternate decomposition.

The proof of (1) is identical to that of Lemma 4.7.1.

Step 1: (2)

By (1), we may assume $\hat{T}(n/d)$ is even. We also suppose $\hat{T}(n/d)$ is in the even-first orientation, as the odd-first argument is repetitive. Let $w_{n'/d',i}$ denote the boundary words of the standard subtiles as specified by Lemma 4.7.1. Consider the enlarged tile, $T^e(n/d)$ with boundary word $w_1 = w_{q1,1} * w_{q1,1} * w_{p1,1}$ and $w_2 = w_{p1,2} * w_{q1,2} * w_{p1,2}$. Translate the enlarged tile so that $c(T^e(n/d)) - c(\hat{T}(n/d)) = -v_{q1,1}$.

By Lemma 4.4.1, $T^e(n/d)$ generates a regular $(\sum v_{n/d,1} + v_{q,1}, \sum v_{n/d,2})$ almost pseudo-square tiling. We use this to show there are no gaps in the $(\sum v_{n/d,1} + v_{q,1}, \sum v_{n/d,2})$ -regular tiling of $\hat{T}(n/d)$ and the only subtiles which overlap are $T(q_1)^{-,1}$ and $T(q_1)^{+,2}$. The proof proceeds along the lines of Figure 4.25.

By 180-degree symmetry, it suffices to analyze the lower-right corner of a surrounding. Take the shifted tiling of $\hat{T}(n/d)$ with respect to $(\sum v_{n/d,1} + v_{q,1}, \sum v_{n/d,2})$ and compare the lower-right surrounding:

$$S^s := \hat{T}(n/d) \cup (\hat{T}(n/d) + v_{n/d,1} + v_{q_1,1}) \cup (\hat{T}(n/d) - v_{n/d,2}) \cup (\hat{T}(n/d) + v_{n/d,1} + v_{q_1,1})$$

to the corresponding corner of the non-shifted tiling

$$S := \hat{T}(n/d) \cup (\hat{T}(n/d) + v_{n/d,1}) \cup (\hat{T}(n/d) - v_{n/d,2}) \cup (\hat{T}(n/d) - v_{n/d,2} + v_{n/d,1}).$$

Since $T^e(n/d)$ generates a $(v_{n/d,1} + v_{q,1}, v_{n/d,2})$ almost pseudo-square tiling, each pair of tiles in S^s can only overlap on their boundaries and by definition of $T^e(n/d)$, there are only two gaps in S^s both of which are squares with a $(w_{q_1,1}, w_{p_1,2})$ boundary word. Using the alternate decomposition, these two gaps are filled in the non-shifted tiling and $T(q_1)^{-,1}$ and $T(q_1)^{+,2}$ overlap completely, concluding the proof of this step.

Step 2: (3) (4) and (5)

Given Step 1, the proof is similar to that of Lemma 4.7.2. Indeed, we can use the alternate decomposition to concatenate boundary strings of the standard subtiles which make up the boundary of $\hat{T}(n/d)$. See Figures 4.23, 4.24, and the bottom of Figure 4.25.

□

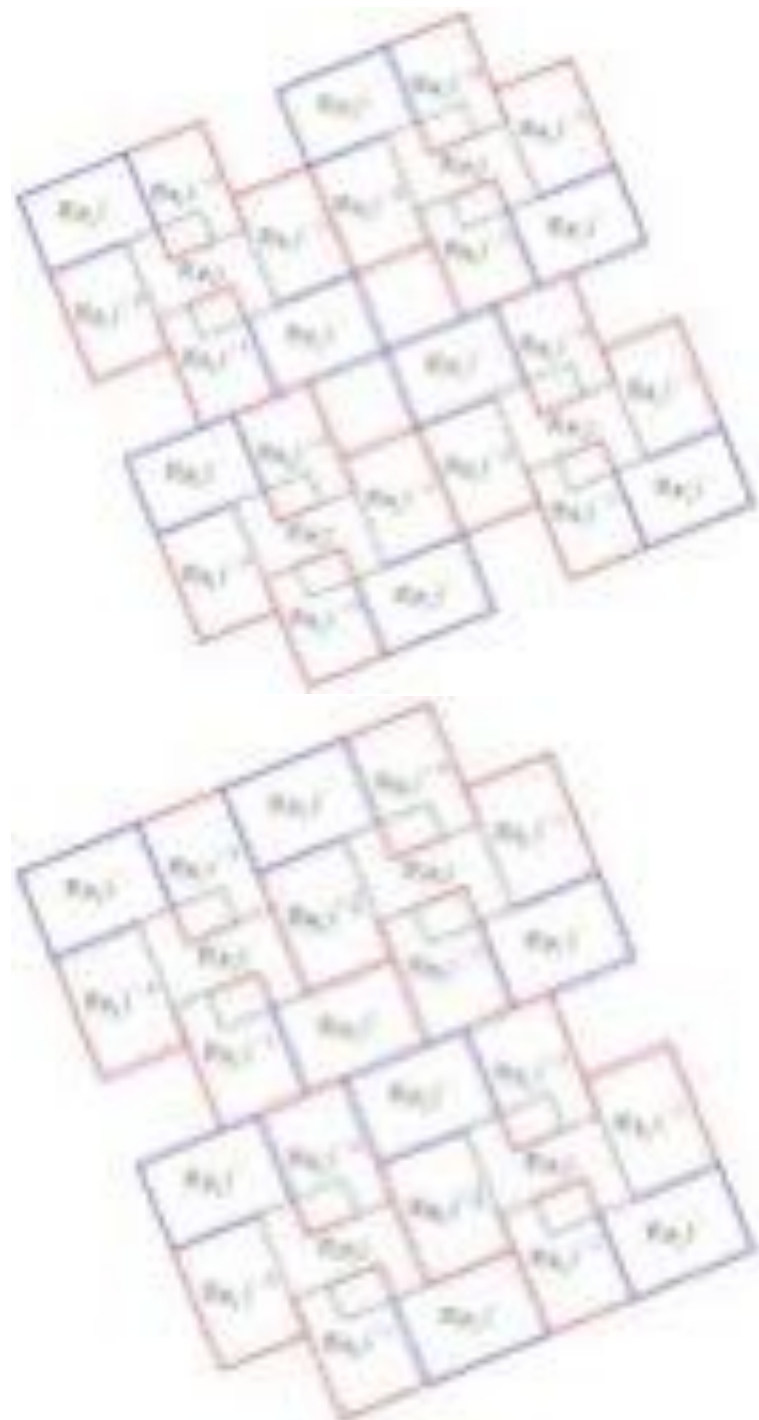


Figure 4.25: A visual explanation of the proof of Lemma 4.7.4. On the top is a lower-right surrounding of the shifted tiling and on the bottom is a lower-right surrounding of the non-shifted tiling.

4.7.4 Weak alternate odometers

The recursion for alternate odometers given the subtle placement is similar to the standard ones. To that end, we first extend the notion of boundary tile and doubled odometers to this shifted case.

Definition 8. When $\hat{T}(n/d)$ has an alternate decomposition, an alternate boundary tile, $\hat{T}^b(n/d)$ coincides with the standard boundary subtiles in its decomposition

$$\hat{T}^b(n/d) \cap \hat{T}(n/d) = \bigcup T^b(n'/d') \quad \text{where } T(n'/d') \text{ ranges over the standard subtiles} \quad (4.98)$$

Let $T^{ds,h/v,\pm}(n/d) = T^b(n/d) \cup (T^{h/v,\pm}(n/d) + S_{n/d})$ denote the shifted doubling of $T(n/d)$ where $S_{n/d}$ is from (4.91). As in Definition 5 extend the weak doubled odometer $ds(o)_{n/d} : T^{ds,h/v,\pm}(n/d) \rightarrow \mathbb{Z}$ to this case.

We are now ready to state a weak version of the alternate odometer recursion, analogous to the standard one from before.

Definition 9. A pair of partial odometers $\hat{o}_{p_0} : T(p_0) \rightarrow \mathbb{Z}$ and $\hat{o}_{q_0} : T(q_0) \rightarrow \mathbb{Z}$ are weak alternate tile odometers for (p_0, q_0) if they appear in Proposition 4.6.1, are $(o_{0/1}, o_{1/1})$ from Section 4.5.4 or $(\hat{T}(p_0), \hat{T}(q_0))$ are alternate tiles for (p_0, q_0) and the partial odometers have the alternate decompositions:

$$\begin{aligned} \hat{o}_{p_0} &= ds(o)_{p_1}^+ \cup ds(o)_{p_1}^- \cup o_{q_1}^+ \cup o_{q_1}^- \cup \hat{o}(q_1) \\ \hat{o}_{q_0} &= o_{p_1}^+ \cup o_{p_1}^- \cup ds(o)_{q_1}^+ \cup ds(o)_{q_1}^- \cup \hat{o}(p_1) \end{aligned} \quad (4.99)$$

where $ds(o)_{n/d}^\pm$ and $\hat{o}(n/d)$ are the respective weak shifted doublings and weak alternate parent odometers respecting the tile translations in Definition 7. In the indicated cases in Definition 7, we omit the alternate parent odometers.

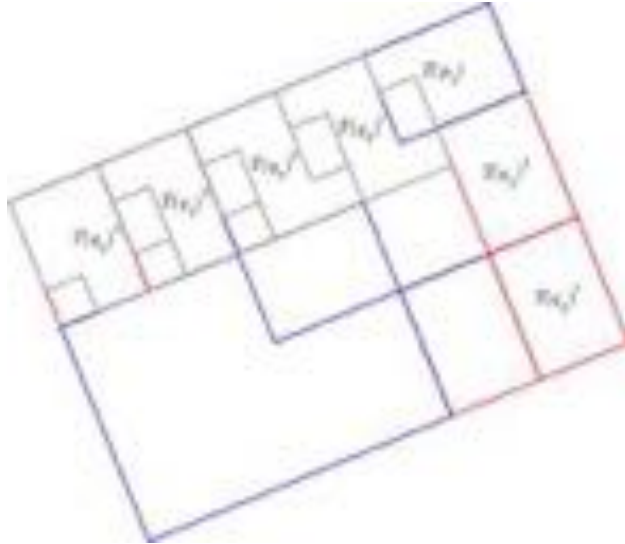


Figure 4.26: An odd L -correction with labels as in Definition 10 overlaid on its standard tile.

(a) $\hat{o}(n/d)$ respects $w_h(n/d)$ or $w_v(n/d)$ if (n/d) is even or odd respectively.

(b) Lattice adjacent $\hat{o}'_{n/d}$ and $\hat{o}_{n/d}$ are compatible.

Proof. Given Lemma 4.7.4 the proof is identical to the proof of Lemma 4.7.3. \square

4.8 Correcting the recursion

In this section we complete the weak recursion defined in the previous section. This step requires us to possibly ‘correct’ doubled odometers which overlap. This

4.8.1 Corrected partial tiles

In this section we define a partial tile, Definition 4, for every standard tile which will aid us in fully defining doubled weak odometers which don't overlap on a common ancestor. The construction of this partial tile will involve a chain of ancestor tiles. Let $(p_0, q_0) = \mathcal{C}(p_1, q_1)$ be a Farey child pair in quadruple \mathbf{q}_w with recursion word $w \in F_3^*$. Recall the standard tile decomposition from Definition 3.

Definition 10 (Odd L -correction). *Suppose $w = w_1 * s * 2^k$ where $|w_1| \geq 0$, $s \in \{1, 3\}$, and $k \geq 0$. Let (p_2, q_2) be the parent Farey pair corresponding to the string $w = w_1 * s$ and let $(T(p_2), T(q_2))$ be standard tiles for (p_2, q_2) and $\hat{T}(q_2)$ an alternate tile for q_2 .*

An L -correction for $T(p_0)$, $T^{L,\pm}(p_0)$ is a partial tile, $T^{v,\pm}(p_0)$ with the following decomposition

$$T^{L,\pm}(p_0) = \bigcup_{j=0}^k (T(q_2) + K_1 j) \cup (T(p_2) + K_2) \cup \left(K_3 + \bigcup_{i=1}^{2(k+1)-z} (\hat{T}(q_2) + K_4 i) \right) \quad (4.100)$$

where the initial offset is specified by requiring $T(q_2)$ match an outer $T(q_1)$ tile in the standard decomposition of $T(p_0)$:

$$\begin{cases} T(q_1)^{+,2} & 10 \\ T(q_1)^{-,1} & 11 \\ T(q_1)^{+,1} & 00 \\ T(q_1)^{-,2} & 01 \end{cases}$$

Draft Mar 13

and the subsequent offsets are

$$[K_1, K_2] = \begin{cases} [v_{q_2,2}, v_{q_2,2} + (v_{q_2,1} - 2v_{p_2,1})] & 10 \\ [v_{q_2,2}, -v_{p_2,2}] & 11 \\ [v_{q_2,2}, v_{q_2,2}] & 00 \\ [-v_{q_2,2}, -v_{p_2,2} - (2v_{p_2,1} - v_{q_2,1})] & 01 \end{cases}$$

and

$$[K_3, K_4] = \begin{cases} [(-v_{q_2,2} + v_{p_2,2}) + (2v_{p_2,1} - v_{q_2,1}), -v_{q_2,1}] & 10 \\ [2v_{p_2,1} - v_{q_2,1}, v_{q_2,1}] & 11 \\ [-(v_{q_2,2} + v_{p_2,2}), v_{q_2,1}] & 00 \\ [0, -v_{q_2,1}] & 01, \end{cases}$$

where the right-hand side columns denote the case:

$$\begin{aligned} 10 &= \mathcal{W}_1 \text{ is odd and } + \\ 11 &= \mathcal{W}_1 \text{ is odd and } - \\ 00 &= \mathcal{W}_1 \text{ is even and } + \\ 01 &= \mathcal{W}_1 \text{ is even and } -. \end{aligned} \tag{4.101}$$

The term z in (4.100) is either 0 or 1 and if $z = 0$, we say the L-correction is elongated.

The correction in the even-case is similar but the offsets are slightly different due to the lack of rotational symmetry in the parameterization.

Definition 11 (Even L-correction). Suppose $w = w_1 * s * 3^k$ where $|w_1| \geq 0$, $s \in \{1, 2\}$, and $k \geq 0$. Let (p_2, q_2) be the parent Farey pair corresponding to the string $w = w_1 * s$ and let $(T(p_2), T(q_2))$ be standard tiles for (p_2, q_2) and $\hat{T}(p_2)$ an alternate tile for p_2 .

An L-correction for $T(q_0)$, $T^{L,\pm}(q_0)$ is a partial tile $T^{h,\pm}(q_0)$ with the following decom-

position.

$$T^{L,\pm}(q_0) = \bigcup_{j=0}^k (T(p_2) + K_1 j) \cup (T(q_2) + K_2) \cup \left(K_3 + \bigcup_{i=1}^{2(k+1)-z} (\hat{T}(p_2) + K_4 i) \right) \quad (4.102)$$

where the initial offset is specified by requiring $T(p_2)$ match an outer $T(p_1)$ tile in the standard decomposition of $T(p_0)$:

$$\begin{cases} T(p_1)^{+,1} & \{0 \text{ or } 1\}0 \\ T(p_1)^{-,2} & \{0 \text{ or } 1\}1 \end{cases}$$

and

$$[K_1, K_2, K_4] = \begin{cases} [2v_{p_2,1}, 2v_{p_2,1}, v_{p_2,2}] & 10 \\ [-2v_{p_2,1}, -v_{q_2,1}, v_{p_2,2}] & 00 \\ [-2v_{p_2,1}, -v_{q_2,1} + v_{p_2,1} - v_{q_2,1}, -v_{p_2,2}] & 11 \\ [2v_{p_2,1}, 2v_{p_2,1} + v_{p_2,2} - v_{q_2,2}, -v_{p_2,2}] & 01 \end{cases}$$

and

$$K_3 = \begin{cases} v_{q_2,1} - 2v_{p_2,1} + (v_{q_2,2} - v_{p_2,2} + v_{q_2,1}) & 10 \text{ and } s = 2 \\ v_{q_2,1} - 2v_{p_2,1} & 10 \text{ and } s = 1 \\ v_{q_2,2} - v_{p_2,2} & 00 \text{ and } s = 2 \\ 2v_{p_2,1} - v_{q_2,1} & 00 \text{ and } s = 1 \\ v_{q_2,2} - v_{p_2,2} + v_{q_2,1} & 11 \text{ and } s = 2 \\ 0 & 11 \text{ and } s = 1 \\ v_{q_2,2} - v_{p_2,2} - 2v_{p_2,1} + v_{q_2,1} & 01 \text{ and } s = 2 \\ 0 & 01 \text{ and } s = 2, \end{cases}$$

where the cases on the right are described by (4.101). The term z in (4.102) is either 0 or 1 and if $z = 0$, we say the L -correction is elongated.

Note that the initial offset requirement assumes that $T(p_2) = T(p_1)$ in the odd case and $T(q_2) = T(q_1)$ in the even case but this follows the standard tile decomposition or Proposition 4.6.1. We assert a final exception to the definition of $c(\cdot)$

$$c(T^{L,\pm}(n/d)) = c(T(n/d)). \quad (4.103)$$

We next verify existence of L -corrections.

Lemma 4.8.1. *For every $n/d \in \{p_0, q_0\}$ from Definition 11 or 10 an L -correction exists and has the following properties.*

1. *Rotation invariance:*

$$\mathcal{R}^1(T^{L,+}(q_0)) = T^{L,-}(\mathcal{R}(q_0))$$

$$\mathcal{R}^2(T^{L,+}(q_0)) = T^{L,-}(q_0)$$

$$\mathcal{R}^3(T^{L,+}(q_0)) = T^{L,+}(\mathcal{R}(q_0))$$

$$\mathcal{R}^4(T^{L,+}(q_0)) = T^{L,+}(q_0).$$

2. *The elongated $T^{L,\pm}(q_0)$ coincides with $T(q_0)$ on two sides*

$$T^{L,\pm}(q_0) \cap T(q_0) \supset \begin{cases} w_h(q_0) \cup w_v(q_0) & 10 \\ w_h(q_0) \cup \mathbf{rev}(w_v(q_0)) & 00 \\ \mathbf{rev}(w_h(q_0)) \cup \mathbf{rev}(w_v(q_0)) & 11 \\ \mathbf{rev}(w_h(q_0)) \cup w_v(q_0) & 01 \end{cases}$$

where the cases on the right are described by (4.101).

Proof. The stated rotation invariance follows from the decomposition and rotation invariance of standard and alternate tiles. To prove the second claim, we rotate and flip to assume we

are in case ‘10’ and $w = w_1 * s * 3^k$ from Definition (11). We then proceed by induction on $k \geq 0$

If $k = 0$, the claim follows by the standard decomposition of $T(q_0)$ and the definition of the L -correction. Indeed, the elongated $T^{L,+}(q_0) \cap T(q_0) \supseteq T(p_1)^{+,1} \cup T(q_1)^+$ which shows $T^{L,\pm}(q_0) \cap T(q_0) \supseteq w_h(q_0)$. For the vertical direction, since $\hat{T}(p_1)$ is a $w_v(p_1)$ -pseudo-square, it agrees with $T(p_1)$ on the vertical boundaries.

Now, suppose $k \geq 1$ is given and let q'_0 be the even child in $\mathbf{q}_{w[1:w|-1]}$. By the inductive hypothesis, the elongated $T^{L,+}(q'_0)$ coincides with $T(q'_0)$ on the bottom and left boundaries. Also, by definition, we may write the elongated correction for q_0 as

$$\begin{aligned} T^{+,L}(q_0) &= T(p_1) \cup (T^{+,L}(q'_0) + v_{p_1,1}) \\ &\cup (\hat{T}(p_1) \cup \hat{T}(p_1) + v_{p_1,2}) + (v_{q_1,1} + v_{q_0,1} + v_{q_0,2}). \end{aligned}$$

We can then conclude using the standard decomposition for $T(q_0)$. □

4.8.2 Tile odometers

We are now ready to fully define the recursion. Roughly, the full recursion proceeds by taking the weak recursion and filling in the interior. The difficulty occurs whenever there is overlap that is not on a boundary string. Whenever the doubled odometers overlap on a common ancestor or do not overlap at all, the doubled odometers may be taken to be usual standard odometers. Otherwise, the overlap is *corrected* by a pair of complementary $\pm L$ -corrections.

Definition 12. A weak standard (resp. alternate) tile odometer is a standard (resp. alternate) tile odometer if it is one of the base cases or in the decomposition (4.89) (resp. (4.99)), weak subodometers are replaced by respective tile subodometers. Further, depending on the recursion word and parity, each weak doubled subodometer is either two standard tile subodometers or a standard tile subodometer and an odometer which respects an L -correction.



Figure 4.27: The four possible orientations for an odd L -correction as described in Definition 10. From top left to bottom right, 10, 00, 11 then 01.

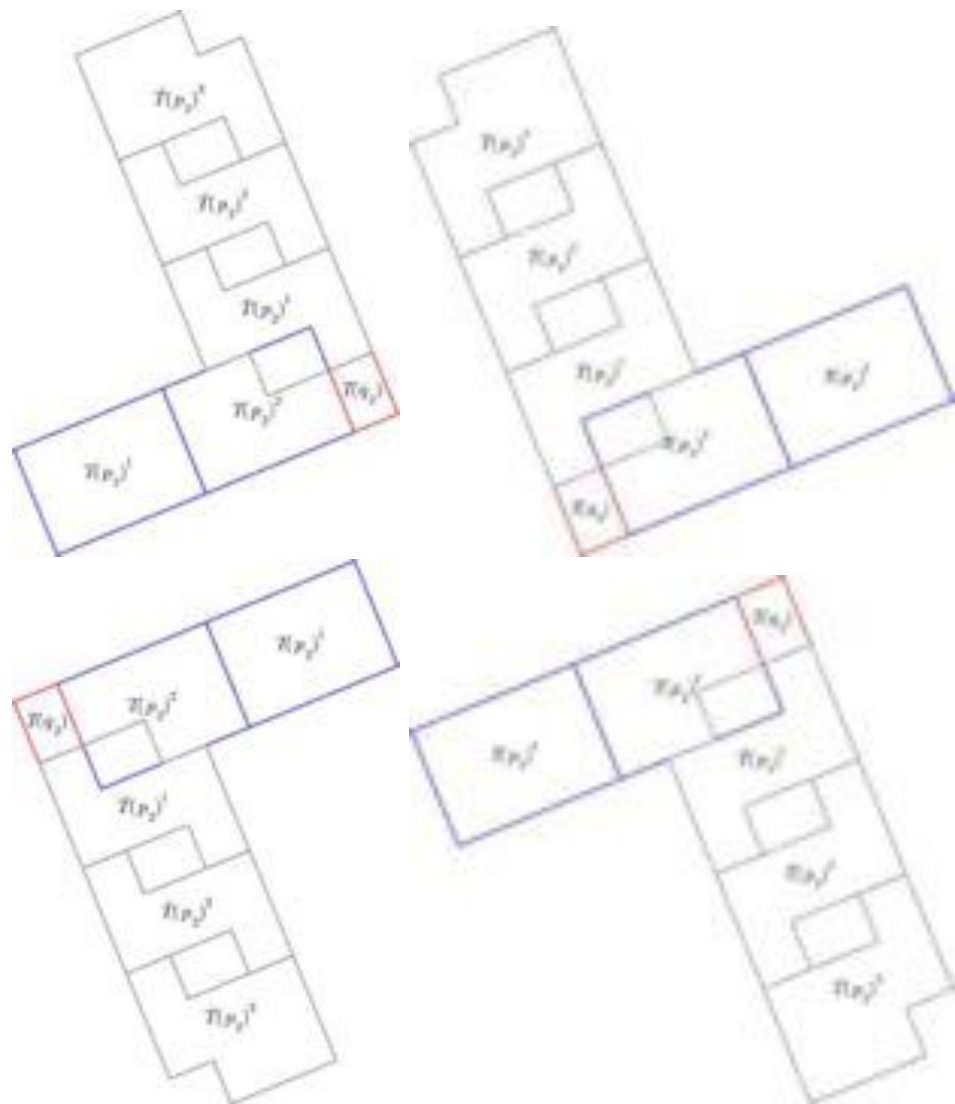


Figure 4.28: The four possible orientations for an even L -correction as described in Definition 11. From top left to bottom right, 10, 00, 11 then 01.

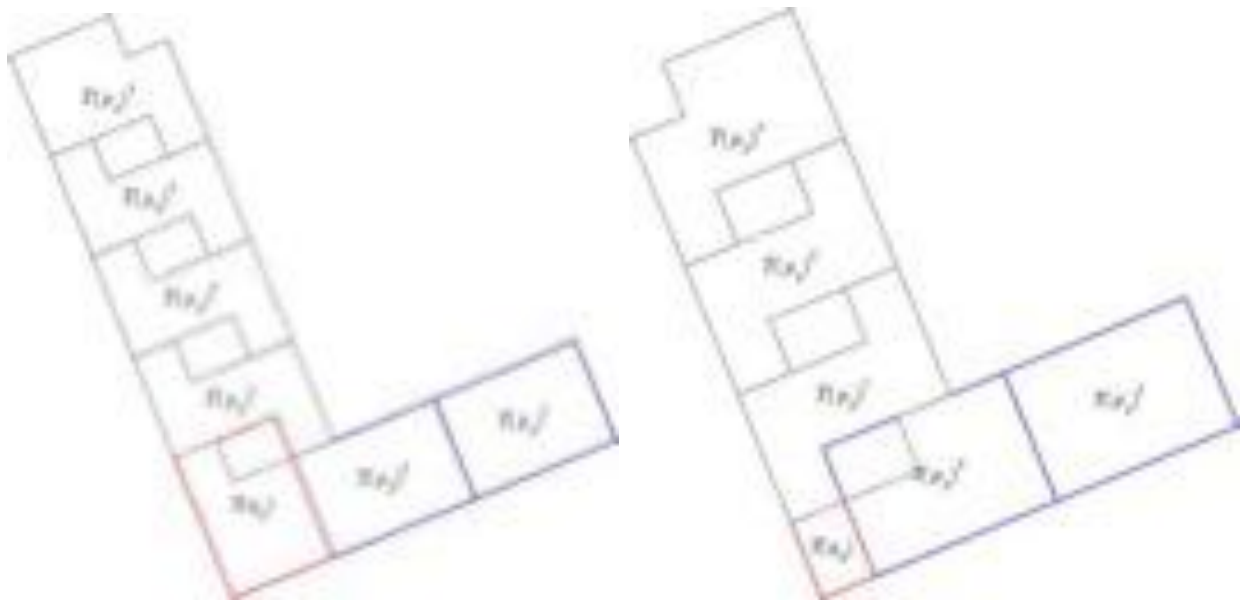


Figure 4.29: The two possible odd-even overlaps for an even L -correction as described in Definition 11: $s = 1$ on the left (elongated) and $s = 2$ on the right.

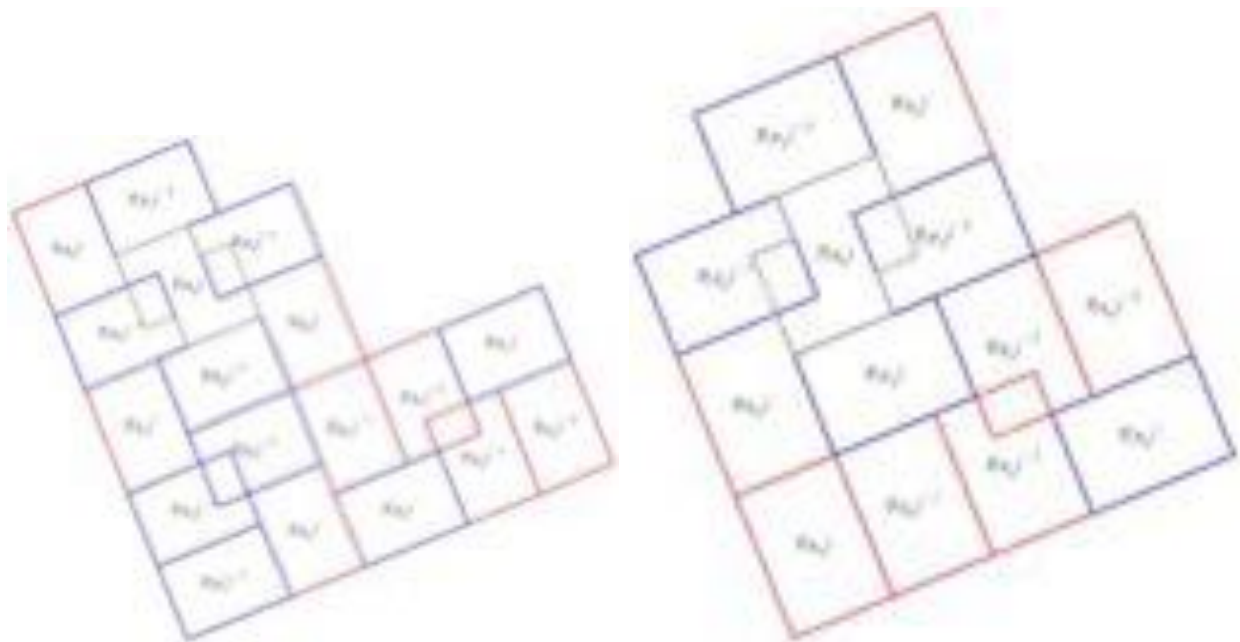


Figure 4.30: Decompositions of the triple $(\hat{T}(p_2)^1, T(q_2), \hat{T}(p_2)^2)$ in Figure 4.29: $s = 1$ on the left and $s = 2$ on the right.

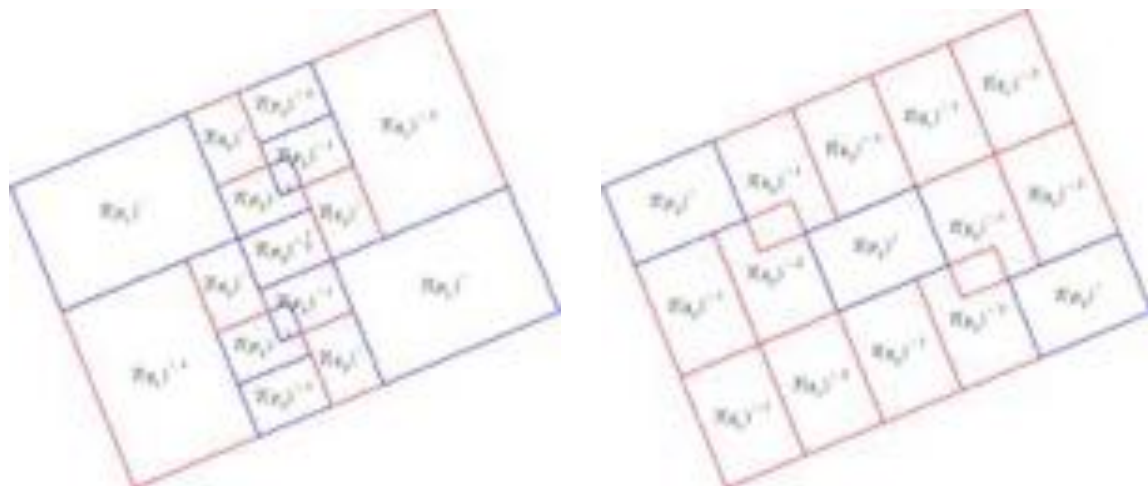


Figure 4.31: Double decomposition of $T(p_0)$ in the even-first orientation for recursion words $w = *1$ and $w = *2$ respectively.



Figure 4.32: Decomposition and then double decomposition of corrected $T(p_0)$ in the even-first orientation. The first row is $w = *13$ and the second is $w = *23$

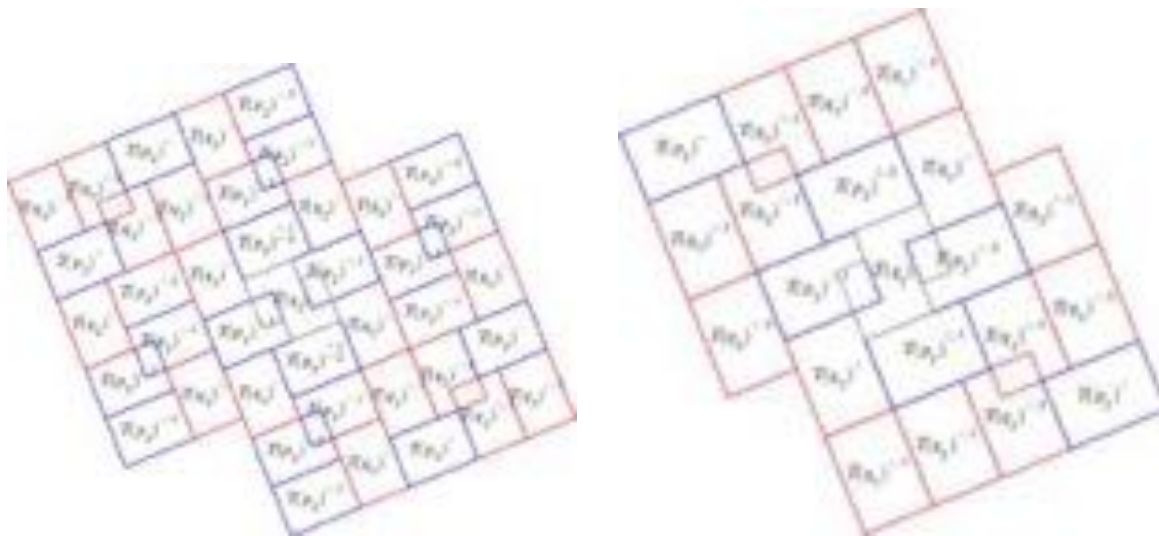


Figure 4.33: Double decomposition of $\hat{T}(q_0)$ in the even-first orientation for recursion words $w = *1$ and $w = *2$ respectively.



Figure 4.34: Decomposition and then double decomposition of corrected $\hat{T}(q_0)$ in the even-first orientation. The first row is $w = *13$ and the second is $w = *23$

Specifically, let n/d be a child in \mathbf{q}_w and let (p_1, q_1) denote the parent Farey pair. In the standard case, if n/d is odd, then in (4.89), each doubled term is replaced by

$$d(o)_{q_1}^{\pm} \rightarrow \begin{cases} o_{q_1}^{\pm,1} \cup o_{q_1}^{\pm,2} & \text{if } w = *\{1 \text{ or } 2\} \\ o_{q_1}^{\pm} \cup o_{q_1}^{L,\pm} & \text{if } w = *3 \end{cases}$$

where $o_{q_1,\pm i}$ are standard tile odometers for $T(q_1)^{\pm,i}$. In the even-first orientation, $o^{\pm}(q_1)$ is a tile odometer for $T(q_1)^{+,1}$ or $T(q_1)^{-,2}$ and $o_{q_1}^{L,\pm}$ is a partial odometer with decomposition that respects the L-corrections for $T(q_1)^{-,1}$ or $T(q_1)^{+,2}$. In the odd-first orientation, 1 and 2 are flipped. If n/d is even, the decomposition is defined by rotating the decomposition for $\mathcal{R}(n/d)$.

Similarly, in the alternate case, if n/d is even, then each weak shifted doubled term is replaced in the exact same way as the standard odd case except the L correction is taken to be the elongated L correction. Rotate to complete the definition.

Before proving existence of tile odometers, we prove that L-corrected odometers exist, assuming existence up to a certain depth. An important tool in the remaining proofs will be the *double decomposition*, a decomposition of all or select subtiles in the standard or alternate decomposition. In the figures, grandparent subtiles are indicated with a 2 subscript.

Lemma 4.8.2. *Suppose tile odometers exist for all $n/d \in \mathcal{T}_m$, for $m \leq m_0$, some $m_0 \geq 1$, then partial odometers which respect the L-correction $o_{n/d}^{L,\pm}$ exist for all $n/d \in \mathcal{T}_{m_0+1}$ and respect the appropriate zero-one boundary strings from Lemma 4.8.1.*

Proof. We show that the L-corrected odometer, $o_{n/d}^{L,\pm}$ exists by showing each pair of overlapping subodometers in the L-correction is compatible. The decomposition of $o_{n/d}^{L,\pm}$ consists of lattice adjacent tile odometers and one of two possible new types of intersection seen in Figure 4.29. Since we have shown lattice adjacent odometers to be compatible (and that there are no gaps between lattice adjacent odometers), it suffices deal with the new inter-

section. This can be dealt with by the double decomposition see Figure 4.30. In particular, in the double decomposition, every pair of interfaces between the triple are part of or are a complete stacked zero-one boundary string. In case the triple comes from the base cases, compatibility is a consequence of Proposition 4.6.1.

To see that $o_{n/d}^{L,\pm}$ coincides with the standard odometer on the appropriate zero-one boundary strings, we induct on $k \geq 0$ from Definitions (11) or (10) as in the proof of Lemma 4.8.1. \square

We finally prove existence of tile odometers. Figures 4.31, 4.32, 4.33, 4.34 will be a visual aid throughout the proof.

Lemma 4.8.3. *Tile odometers exist.*

Proof. We proceed by induction. Start by using Lemma 4.8.2 to see that tile odometers are indeed weak tile odometers. It remains to verify the internal odometer decomposition is well-defined. That is, we check that each pair of overlapping subodometers is pairwise consistent. As compatibility is affine invariant, and the decompositions are, up to affine factors, rotationally invariant, it suffices to show compatibility for either n/d or $\mathcal{R}(n/d)$. Let \mathbf{q}_w denote the quadruple for which n/d is a child. We split the remainder of proof into cases. In each case, we use the double decomposition displayed in the indicated Figure to show that the subodometers either overlap on stacked boundary strings or on grandparent tiles. Also, assume the even-first orientation, otherwise flip the subsequent arguments.

*Case 1: Odd standard odometer: $w = *1$ or $*2$; Figure 4.31*

The interfaces between every non-overlapping tile consist of stacked zero-one boundary strings therefore those odometers are compatible. If $w = *1$, the tiles $T(q_1)^{+,2}$ and $T(q_1)^{-,1}$ overlap, by the double decomposition, exactly on $T(p_2)^{+,1/2}$, and therefore those subodometers are compatible. Similarly, if $w = *2$, $T(p_1)^-$ and $T(p_1)^+$ overlap on $T(p_2)^{+,1/2}$ and so those subodometers are compatible.

*Case 2: Odd standard odometer: $w = *3$; Figure 4.32*

In this case, due to the L -correction, the only overlaps are that of lattice adjacent $\hat{T}(p_2)$ (subsubtiles). The rest of the interfaces are part of or are stacked zero-one boundary strings. By previous arguments, the $(T(q_1)^{+,1}, T(p_1)^{-})$ and $T(q_1)^{-,2}$ interfaces are parts of stacked boundary strings. The interface between $T(p_1)^{\pm}$ and $T^{L,\pm}(q_1)$ corresponds to full stacked vertical boundary strings – the interfaces are that of lattice adjacent standard tiles $T(p_1)$.

It remains to analyze the interface between $T^{L,\pm}(q_1)$ and $T(q_1)^{+,1}, T(q_1)^{-,2}$. By Lemma 4.8.2 $(T^{L,+}(q_1), T(q_1)^{+,1})$ each intersect on a $w_v(q_1)$ stacked boundary string. By induction on k in the recursion word for the L correction, similar to the proof of Lemma 4.8.2, the interface between $(T^{L,+}(q_1), T(q_1)^{-,2})$ and $(T^{L,-}(q_1), T(q_1)^{+,1})$ consists of a sequence of lattice adjacent standard odometers for $T(p_1)^{+}$ followed by a (q_2, p_2) interface which is an almost palindrome by Lemma 4.5.1.

*Case 3: Even alternate odometer: $w = *\{1 \text{ or } 2\}$; Figure 4.33*

The overlap argument is similar to Case 1. If $w = *1$, $T(q_1)^{+,1}$ and $T(q_1)^{-,2}$ overlap $\hat{T}(p_1)$ on $T(p_2)^{\pm,1/2}$. The interfaces between $(T(p_1)^{+}, T(q_1)^{-,1})$, $(T(p_1)^{-}, T(q_1)^{+,2})$, $(T(p_1)^{+}, T(q_1)^{+,1})$, $(T(p_1)^{-}, T(q_1)^{-,2})$ are part of stacked zero-one boundary strings by the same argument as given previously in the weak standard case.

The new interfaces are

$$(T(q_1)^{\pm,1}, T(q_1)^{\pm,2}, \hat{T}(p_1))$$

and

$$(T(p_1), \hat{T}(p_1)).$$

In the latter case, by the double decomposition, $(T(p_1), \hat{T}(p_1))$ intersect on the boundary of lattice adjacent standard tile odometers for $T(q_2)$. In the former case, the interface between $(T(q_1)^{+,1}, T(q_1)^{+,2}, \hat{T}(p_1))$ is part of a stacked vertical zero-one boundary string. Indeed, augment the vertical boundary string of $T(q_1)^{+,2}$ by concatenating $w_v(p_1)$ at the start. Then,

since $\hat{T}(p_1)$ is a $w_v(p_1)$ pseudo-square, the augmented interface is exactly $w_v(p_1) \cup w_v(q_1)$ and $\mathbf{rev}(w_v(q_1)) \cup \mathbf{rev}(w_v(p_1))$. This is exactly stacked boundary string for p_0 and therefore, the odometers which intersect on it are compatible. The argument for $w = *2$ is identical.

*Case 4: Even alternate odometer: $w = *3$; Figure 4.34*

This is almost identical to Case 2. The only difference is in the overlaps $(T^{L,+}(q_1), T(q_1)^{+,2})$ and $(T^{L,-}(q_1), T(q_1)^{-,1})$. In this case, we need to augment the vertical boundary strings as in Case 3 for $T(q_1)$. Once augmented, those interfaces then become exactly stacked vertical boundary string for p_0 .

□

4.9 Global odometers

We now observe that both standard and alternate tile odometers can be extended to global odometers with the correct growth.

Lemma 4.9.1. *For every reduced fraction $0 < n/d < 1$, there are two functions, $g_{n/d}, \hat{g}_{n/d}$ on \mathbb{Z}^2 whose restriction to a standard or alternate tile are alternate and standard tile odometers for which the periodicity condition (4.9) holds and for which*

$$x \rightarrow f(x) - \frac{1}{2}x^T M(n, d)x - b^T x \quad (4.104)$$

is $L'(n/d)$ -periodic for some $b \in \mathbb{R}^2$, for each $f \in \{g_{n/d}, \hat{g}_{n/d}\}$.

Proof. Given that we have proved standard and alternate tile odometers which are lattice adjacent are compatible, the proof is identical to Lemma 10.1 in Levine et al. [2017]. □

It remains to check that the functions which we have constructed are recurrent, which we do by induction. We first check that the constructed functions are indeed integer superharmonic.

Lemma 4.9.2. *For each $0 < n/d < 1$, $g_{n/d}$ and $\hat{g}_{n/d}$ are integer superharmonic.*

Proof. Let $s \in \{\Delta g_{n/d} + 1, \Delta \hat{g}_{n/d} + 1\}$ and proceed by induction. By Lemma 4.6.4 and Proposition 4.6.1 it suffices to take n/d odd and suppose $T(n/d)$ and $\hat{T}(n/d)$ have double decompositions.

Case 1: Standard odometer.

If x lies in the intersection of two neighboring tiles, $T(n/d) \cap T(n/d')$ then, by Lemma 4.7.2, it must be contained within a zero-one stacked boundary string. In this case $s(x) = 1$ by the explicit formulae in Section 4.5. Otherwise, x is in the interior of $T(n/d)$. If x is in the interior of a subtile in the double decomposition, we conclude by induction. Otherwise, by considering the cases in Figures 4.31 and 4.32 as in the proof of Lemma 4.8.3, x either lies within a zero-one stacked boundary string or in the interior of an ancestor tile. In the latter case we can use induction and in the former $s(x) = 1$.

Case 2: Alternate odometer.

If x is in the interior of $\hat{T}(n/d)$, the argument is similar to Step 1; as in Lemma 4.8.3 check the cases in Figures 4.34 and Figure 4.33 to see that x must be on a stacked zero-one boundary string or within the interior of a subtile. If $x \in \partial \hat{T}(n/d)$, then, by Lemma 4.7.4, x is within a stacked zero-one boundary string or in the interior of a subtile.

□

We conclude by checking recurrence.

Lemma 4.9.3. *For each $0 < n/d < 1$, $g_{n/d}$ and $\hat{g}_{n/d}$ are recurrent.*

Proof. Let $s \in \{\Delta g_{n/d} + 1, \Delta \hat{g}_{n/d} + 1\}$ and suppose the claim is true for all Farey quadruples $\mathbf{q}_{|w|}$ with $|w| \leq n$. By Lemma 4.6.4 and Proposition 4.6.1, it suffices to check $w = 3^k w'$, for $k \geq 0$ and $|w'| \geq 1$, where, if $k = 0$, $w'[1] = 1$.

Therefore, $T(n/d)$ and $\hat{T}(n/d)$ have double decompositions and each of the interfaces in the tiling of $T(n/d)$ consist of stacked $q - p$ boundary strings where (q, p) depend on the

first letter of w' . If $w'[1] = 1$, (q, p) is the Farey child of \mathbf{q}_{3^k} . Otherwise, p is the odd child in \mathbf{q}_{3^k} and q is the even child in $\mathbf{q}_{3^{k-1}}$. In either case, the explicit forms of the odometers and their Laplacians are given in Section 4.6.

Let $T \in \{T(n/d), \hat{T}(n/d)\}$ and write T^i, s^i for the subtiles and ancestor Laplacians in the double decomposition.

The inductive proof starts as in the proof of Lemma 4.6.13: suppose for sake of contradiction there is an induced subgraph of the F -lattice, H , which is forbidden for s . Let $c^0 = -\infty$ and for $j \geq 1$, let

$$\begin{aligned} c^j &= \min\{x_1 > c^{j-1} : x \in H\} \\ V^j &= \{x \in H : x_1 = c^j\}. \end{aligned} \tag{4.105}$$

In words, sets of possibly disjoint vertical lines enumerated from left to right. Since H is forbidden, it is nonempty, hence V^1 exists.

We prove the following inductive hypotheses by induction on $j \geq 1$ for all translations of T and all ancestor tiles $T_a := \{T(p), T(q), \hat{T}(p), \hat{T}(q)\}$.

1. The hypotheses listed in Lemmas 4.6.13, 4.6.14, 4.6.15, 4.6.16 for $T(p), \hat{T}(p), T(q)$ and $\hat{T}(q)$ respectively.
2. If for some subtile T^i , $V^j \cap T^i \neq \emptyset$ then $V^j \cap \partial T^i = \emptyset$.

In fact, we suppose, by induction, that the inductive hypotheses are satisfied for every parent. Indeed, the cases $\mathbf{q}_{\tilde{w}}$ for $\tilde{w} = 3^k * \{1 \text{ or } 2^{k'}\}$ for $k \geq 0, k' \geq 1$ may be checked directly using the explicit formulae in Section 4.6 following the outline in Lemma 4.6.13. Thus, we may suppose that the boundary of each subtile T^i , including grandparent subtiles, consists of a $q - p$ boundary string and that the inductive hypotheses hold for each subtile.

Hypothesis (2) implies the existence of a forbidden subconfiguration strictly contained in some T^i , contradicting inductive recurrence. Thus it remains to verify the hypotheses.

Proof of (1) and (2).

Suppose $y \in V^j \cap T'$ for some $T' \in \mathcal{T}_a$. By construction, $y \in T' \cap T^i$ for some subtile T^i of T in the double decomposition. If $V^j \cap \partial T^i = \emptyset$, then we may conclude by induction.

Otherwise, if there is $y \in V^j \cap \partial T^i$, then, y must be contained in a stacked $q-p$ boundary string. However, the fixed interfaces in Lemma 4.5.3 allow for the arguments of Lemmas 4.6.13 and Lemma 4.6.15 to be repeated, resulting in a contradiction.

□

CHAPTER 5

DYNAMIC DIMENSIONAL REDUCTION IN THE ABELIAN SANDPILE

This chapter is based on the article Bou-Rabee [2022] which is published in Communications in Mathematical Physics.

5.1 Introduction

5.1.1 Overview

Let $\mathcal{C}_N^{(d)}$ be a hypercube of side length N centered at the origin in the d -dimensional integer lattice \mathbb{Z}^d . Start with $2d$ chips in the hypercube, $s = s_0^{(d)} \equiv 2d$, then iterate the following rule: every site with at least $2d$ chips on it becomes *unstable* and *topples* in *parallel*, simultaneously giving one chip to each of its $2d$ neighbors. If a boundary site topples, it loses chips over the edge. Eventually every site is stable and the process stops, yielding a sequence of sandpiles over time $\{s_t^{(d)}\}_{t \geq 0}$.

Simulations suggest an exact relationship between these sandpiles across size N , time t , and dimension d — see Figures 5.1 and 5.2. Specifically, it appears that smaller sandpiles are embedded in larger sandpiles of the same dimension at certain times. Moreover, central cross sections of d -dimensional sandpiles coincide almost exactly with $(d - 1)$ -dimensional sandpiles for all time.

In this chapter, we provide a rigorous proof of these observations, *self-similarity* and *dimensional reduction*, via a simultaneous induction on all parameters: size, time, and dimension. Along the way, we develop new techniques for analyzing the parallel toppling process which may be of independent interest.

Dimensional reduction in sandpiles has been known experimentally since at least the work of Liu et al. [1990]. Later, Fey et al. [2010] formulated an approximate dimensional

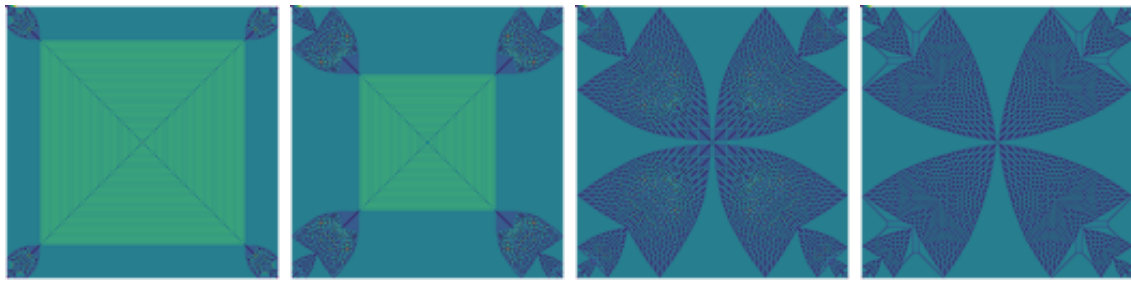


Figure 5.1: $s_t^{(2)}$ for $t = (25)^2, (50)^2, (100)^2, \infty$, where $N = 200$ and $s_0 \equiv 4$. Sites with $0, \dots, 7$ chips are represented by different colors.

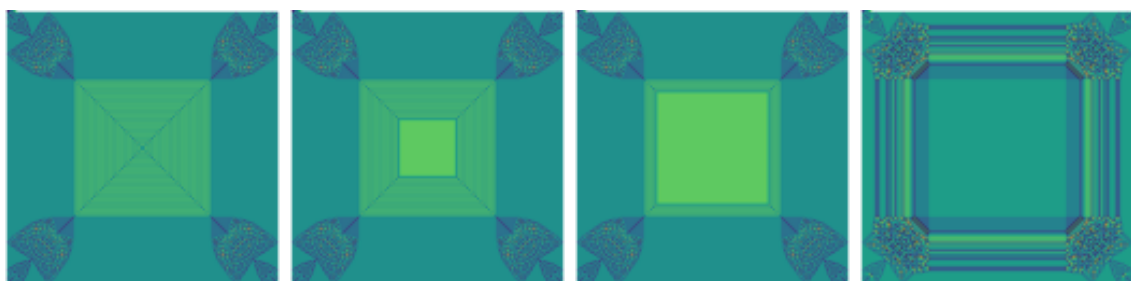


Figure 5.2: $s_t^{(3)}(\cdot, \cdot, \text{offset})$ for offset = 0, 20, 40, 60, where $t = (50)^2$, $N = 200$, and $s_0 \equiv 6$. Sites with $0, \dots, 11$ chips are represented by different colors and ‘offset’ is distance to the center of $\mathcal{C}_N^{(3)}$.

reduction conjecture in the context of the single-source sandpile — this was then highlighted in a survey Levine and Propp [2010].

The structure of the sandpile PDE on \mathbb{Z}^2 reveals that on torus-like domains one can construct limit sandpiles in \mathbb{R}^d from those in \mathbb{R}^{d-1} . This is also possible for the random sandpiles discussed in Chapter 2. However, it has remained completely open to prove (or disprove) dimensional reduction for any natural example, on either the lattice or the continuum, till now.

Our proof in this chapter leverages discrete techniques to establish dimensional reduction on the hypercube when $s_0 \equiv 2d$. The main insight is recognizing that the parallel toppling process together with strong induction can be used to control the sandpile as it stabilizes. We identify a delicate interplay between the initial condition and the symmetry of the hypercube which forces the ‘flow’ of parallel toppling to preserve dimensional reduction. In fact, we do not know how to prove dimensional reduction for only the terminal sandpile. Our proof involves no technology from viscosity solutions nor knowledge of the sandpile PDE.

A key step in the proof is the application of certain discrete derivative bounds — Corollary 5.2.2 and Lemma 5.2.5 below. The strength of these bounds deteriorates as the initial condition grows and it is only when $s_0 \equiv 2d$ that they are strong enough to ensure dimensional reduction.

This dependence on the initial condition provides some explanation for what occurs in the single-source version. Fey-Levine-Peres conjectured that when the initial condition is $(2d - 2) + n\delta_0$ dimensional reduction occurs after carving out a region near the origin. This is likely because our derivative bound (which, in the single-source version, has a flipped dependence on the constant background) does not hold near the origin, but only holds away from it. Proving this remains open, but we believe the methods in this chapter extend to this and other initial data.

In fact, the result in this chapter appears to be a special case of a more general one

which we cannot yet prove: dimensional reduction occurs for any uniform initial condition in high enough dimensions. Specifically, for integer $k \geq 0$, when $s_0 \equiv 2d+k$, above a critical dimension, $d > d_0 := k+1$, exact dimensional reduction, modulo (d_0-1) -dimensional defects, appears to persist throughout the parallel toppling process. We show that when $d = d_0$, dimensional reduction fails to occur, providing one explanation for why (d_0-1) -dimensional defects appear — see Table 5.1.

5.1.2 Main Result

Our proof begins with the *odometer* v_t , which encodes the number of topples at each site over time. Let $v_0 : \mathcal{C}_N^{(d)} \rightarrow \mathbb{Z}^+$ be the initial odometer $v_0 \equiv 0$; then, recursively,

$$v_{t+1} = v_t + 1\{s_t \geq 2d\}, \quad (5.1)$$

$$s_{t+1} = s_t + \Delta(v_{t+1} - v_t), \quad (5.2)$$

where Δ is the graph Laplacian on $\mathcal{C}_N^{(d)}$ with dissipating boundary conditions. Dependence on d and N is indicated by writing $v_t^{(d,N)}$ and $s_t^{(d,N)}$.

We prove dimensional reduction and self-similarity of sandpiles via an analysis of the parallel toppling odometers. It will be more convenient to state the result after making a symmetry reduction. Let $\text{Aut}_{\mathcal{C}_d}$ denote the group of symmetries of the d -dimensional hypercube and let it act on \mathbb{Z}^d by matrix-vector multiplication. The definitions imply that parallel toppling preserves the symmetries of the hypercube: $v_t^{(d,N)}(\mathbf{x}) = v_t^{(d,N)}(\sigma\mathbf{x})$ for all $t \geq 1$, $\mathbf{x} \in \mathcal{C}_N^{(d)}$, and $\sigma \in \text{Aut}_{\mathcal{C}_d}$ (we give a simple proof in Section 5.2.3 below). Hence the odometer and sandpile are fully determined by their restrictions to a fundamental domain of the hypercube — we choose a particular one in the statement of the theorem.

Theorem 5.1.1. *Let $N \geq 1$, $d \geq 2$, and $M = \lceil N/2 \rceil$. Denote the fundamental domain of $\mathcal{C}_N^{(d)}$ consisting of sorted coordinates in decreasing order by $\mathcal{S}_M^{(d)} := \{(x_1, \dots, x_d) : M \geq x_1 \geq$*

$\dots \geq x_d \geq 1\}.$

1. Dimensional reduction: for all $t \geq 1$ and $\mathbf{x}_{d-1} \in \mathcal{S}_M^{(d-1)}$

$$v_t^{(d,N)}(\mathbf{x}_{d-1}, 1) = v_t^{(d-1,N)}(\mathbf{x}_{d-1})$$

and for $\mathbf{x}_{d-1} \geq 2$

$$v_\infty^{(d,N)}(\mathbf{x}_{d-1}, 2) = v_\infty^{(d-1,N)}(\mathbf{x}_{d-1}).$$

2. Self-similarity: for all $j < M$, $t \leq \tau_j$, and $\mathbf{x} \in \mathcal{S}_M^{(d)}$ with $\mathbf{x} > M - j$

$$v_t^{(d,N)}(\mathbf{x}) = v_t^{(d,2j)}(\mathbf{x} - (M - j)),$$

where

$$\tau_j := \min\{t \geq 1 : v_t^{(d,2j)}(\mathbf{x}) \geq j \text{ for } \mathbf{x} \in \partial \mathcal{C}_{2j}^{(d)}\},$$

and $\partial \mathcal{C}_i^{(d)} := \{\mathbf{x} \in \mathcal{C}_i^{(d)} : \text{there is } \mathbf{y} \notin \mathcal{C}_i^{(d)} \text{ with } |\mathbf{y} - \mathbf{x}| = 1\}$ denotes the inner boundary of the cube.

Both of these results immediately translate to the sandpile.

Corollary 5.1.1. *The results in Theorem 5.1.1, using the same notation, extend to the sequence of sandpiles.*

1. Dimensional reduction: for all $\mathbf{x}_{d-1} \in \mathcal{S}_M^{(d-1)}$ with $\mathbf{x}_{d-1} \geq 2$

$$s_\infty^{(d,N)}(\mathbf{x}_{d-1}, 1) = s_\infty^{(d-1,N)}(\mathbf{x}_{d-1}) + 2.$$

2. Self-similarity: for all $j < M$, $t \leq \tau_j$, and $\mathbf{x} \in \mathcal{S}_M^{(d)}$ with $\mathbf{x} > M - j + 1$

$$s_t^{(d,N)}(\mathbf{x}) = s_t^{(d,2j)}(\mathbf{x} - (M - j)).$$

k	0	1	2	3	4
$s_\infty^{(2)}(\cdot, \cdot)$					
$s_\infty^{(3)}(\cdot, \cdot, 1)$					
$s_\infty^{(4)}(\cdot, \cdot, 1, 1)$					
$s_\infty^{(5)}(\cdot, \cdot, 1, 1, 1)$					
$s_\infty^{(6)}(\cdot, \cdot, 1, 1, 1, 1)$					

Table 5.1: Center slices of terminal sandpile configurations for $s_0 \equiv 2d + k$ and $N = 64$. Site colors are normalized by column so that in dimension d a site with z chips has the same color as a site with $(z - 2)$ chips in dimension $(d - 1)$.

The first part of Theorem 5.1.1 states that the parallel toppling odometer restricted to a center slice of a d -dimensional hypercube coincides with the $(d - 1)$ -dimensional parallel toppling odometer for all time. Dimensional reduction holds for the final odometer off the center, implying dimensional reduction on the center for the final, stable sandpile.

The second part of the theorem relates the parallel toppling odometers for different sized cubes: the odometer for the size N cube contains the size $2j$ cube odometer up until the first time a boundary site exceeds j topples. These automatically imply, after shrinking the domains by one, the same for the sequence of sandpiles.

As mentioned previously, we expect Theorem 5.1.1 to be a special case of a more general

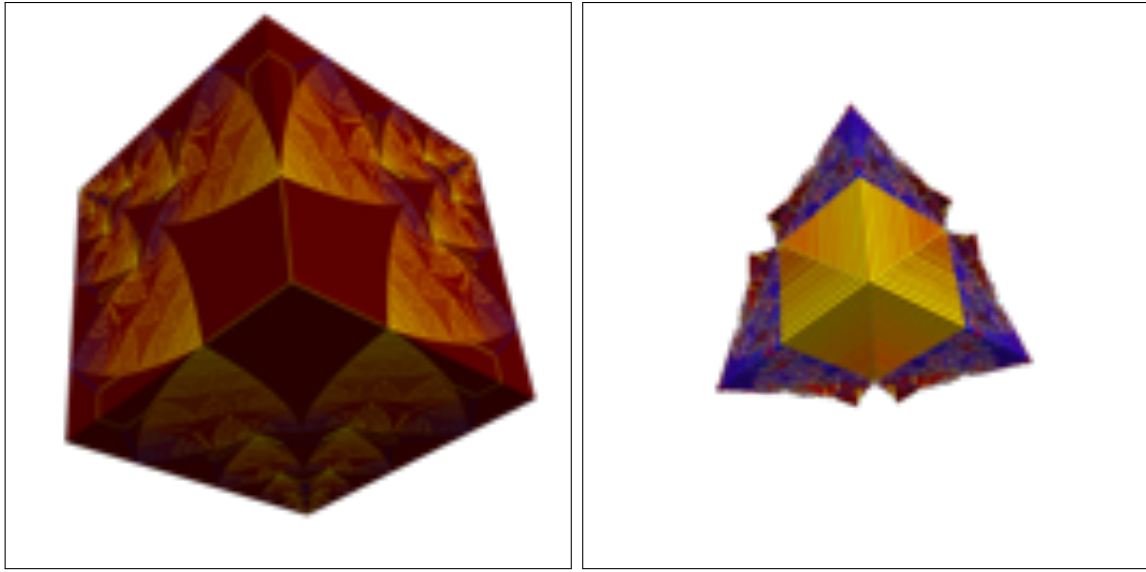


Figure 5.3: On the left, a corner cube of $s_\infty^{(N,3)}$ and on the right the same corner with all cross sections which match $s_\infty^{(N,2)}$ removed. The initial condition is $s_0 \equiv 7$ and $N = 2^{11}$. Sites with $0, \dots, 5$ chips are represented by different colors.

result. In Section 5.3 we show that dimensional reduction does not occur when $s_0 \equiv 2d + (d - 1)$ in all dimensions $d \geq 2$ when $N = 2$. We also provide an explicit description of the parallel toppling odometer when $s_0 \equiv 2d + (d - 1)$ and $N = 4$ for all $d \geq 1$. This explicit form suggests that the proof template in this chapter may help with the following.

Problem 5.1.2. *Show that Theorem 5.1.1 holds when $s_0 \equiv 2d + k$ for all $k \geq 0$ and $d > d_0 := (k + 1)$.*

We expect an even stronger result to be true, although it is likely the proof will require techniques beyond those presented here. In simulations, exact dimensional reduction appears to occur away from the central slice. For example, when $s_0 \equiv 4$, $d = 2$, and N is large, the center of the sandpile contains large curved triangles of 3s. In fact, for every dimension and size we could simulate, whenever dimensional reduction occurs along the central cross sections of the hypercube, it extends; see Figure 5.3 for an example in three dimensions.

Problem 5.1.3. *Extend dimensional reduction on the hypercube to a domain of codimension zero.*

The following is closely related.

Problem 5.1.4. *Show that the odometer for any bounded initial sandpile on the hypercube has bounded second differences. For instance, show for all $t \geq 1$ and $i = 1, 2$ that*

$$-3 \leq -2v_t(\mathbf{x}) + v_t(\mathbf{x} + e_i) + v_t(\mathbf{x} - e_i) \leq 2$$

when $d = 2$ and $s_0 \equiv 4$.

Numerical evidence indicates the hypercube is a necessary hypothesis in Problem 5.1.4. In fact, in most other domains, including the discrete circle, the odometer does not appear to have bounded second differences. On the hypercube, our proof of dimensional reduction shows that the odometer has bounded second differences along the central cross sections; however, a method to propagate those bounds to the interior remains out of reach.

5.1.3 Outline of the proof

The proof of Theorem 5.1.1 is a careful induction on hypercube dimension, side length, and time. Some parts of the argument can be simplified but we present it in this fashion to suggest a template for proving dimensional reduction with more general initial data. At a high level, we show that if the parallel toppling process for a d_0 -dimensional sandpile is sufficiently regular, then dimensional reduction is guaranteed in all dimensions $d > d_0$. We prove this regularity when $d_0 = 1$; the case $d_0 > 1$ remains open.

Our main technical tool is a technique introduced by Babai and Gorodezky to prove discrete quasiconcavity of the single-source sandpile odometer in \mathbb{Z}^2 Babai and Gorodezky [2007]. By an iteration of their technique, we gain symmetry of the odometer, a derivative comparison result, and a parabolic least action principle. These results, which appear in Section 5.2, extend beyond the hypercube and so may be of independent interest.

In Section 5.3 we explicitly determine $v_t^{(d,N)}$ when $N = 4$ in all dimensions $d \geq 1$ when

the initial sandpile is $s_0 \equiv 2d + d - 1$. This is done by mapping the hypercube to a line via a radial decomposition. The explicit form of v_t provides both a base case for our proof and progress towards Problem 5.1.2. We also show that when $N = 2$ dimensional reduction does not occur at the critical dimension d_0 .

The explicit solution when $N = 4$ establishes the base case for an odometer regularity result which is then proved in Section 5.4. Finally, in Section 5.5, we use the established regularity of the odometer in dimension $(d - 1)$ to prove dimensional reduction in dimension d .

An efficient algorithm for computing high-dimensional sandpiles

In Section 5.2.3 we show that $v_t^{(d,N)}$ can be computed via the parallel toppling procedure restricted to the simplex. In fact, the argument shows that any sandpile with a symmetric initial condition on \mathbb{Z}^d , including the single-source sandpile, retains symmetry throughout the parallel toppling process and can be computed in this way.

For d large, computing sandpiles on the simplex improves space complexity by a factor of d^d . Moreover, the reduction in size also leads to a faster algorithm when using parallelization. We wrote a program in Julia Bezanson et al. [2017], Besard et al. [2018] for computing arbitrary dimensional sandpiles which implements these improvements. The program, which may be freely used and modified, is included in the arXiv post.

5.2 Preliminaries

5.2.1 Babai-Gorodezky technique

In this subsection and the next, let $s_0 \leq 2(2d) - 1$ be an arbitrary initial sandpile on \mathcal{C} and v_t its odometer. A straightforward induction argument and the definition of the graph Laplacian yields the following lemma.

Lemma 5.2.1. *For each $x \in \mathcal{C}$ and all $t \geq 0$,*

$$v_{t+1}(x) = \lfloor \frac{s_0(x) + \sum_{y \sim x} v_t(y)}{2d} \rfloor. \quad (5.3)$$

Babai and Gorodezky used this simple lemma to prove a nontrivial discrete quasiconcavity property of the single-source sandpile in \mathbb{Z}^d Babai and Gorodezky [2007]. A more general version of their argument appears below in Lemma 5.2.4. Roughly, their technique recognizes that if a property of the odometer holds at $t = 1$, is consistent across the symmetry axes, and can be verified on the boundaries of the domain, it must hold for all $t \geq 1$.

Lemma 5.2.1 is used many other times throughout this chapter; notably we use it to prove a parabolic least action principle and symmetry of the odometer on the hypercube.

5.2.2 Parabolic least action principle

The least action principle Fey et al. [2010] shows that v_∞ is minimal among all $w : \mathcal{C} \rightarrow \mathbb{Z}^+$ which stabilize s_0 : $\Delta w + s_0 \leq 2d - 1$. We upgrade this to a parabolic least action principle by observing the parallel toppling procedure as a directed sandpile on $\mathcal{G} = \mathbb{Z}^+ \times \mathcal{C}$. The initial sandpile and odometer over time are stacked, $s(t, x) := s_0(x)$ and $v(t, x) := v_t(x)$ for all $t \geq 0$ and $x \in \mathcal{C}$. The graph Laplacian operates on functions $f : \mathcal{G} \rightarrow \mathbb{R}$ as

$$\Delta^{\mathcal{G}} f(t, x) = -2df(t, x) + \sum_{y \sim x} f(t-1, y), \quad (5.4)$$

for $t \geq 1$ and $x \in \mathcal{C}$, where the sum $y \sim x$ is over the nearest neighbors of x in \mathcal{C} .

Lemma 5.2.2 (Parabolic least action principle).

$$v(t, x) = \min\{u : \mathcal{G} \rightarrow \mathbb{Z}^+ : \Delta^{\mathcal{G}} u(t, x) + s(t, x) \leq 2d - 1 \text{ for all } x \in \mathcal{C} \text{ and } t \geq 1\} \quad (5.5)$$

Proof. Let $w(t, x)$ denote the right-hand side of (5.5). We show using Lemma 5.2.1 and

induction that $v(t, x) = w(t, x)$. Indeed, by the directed structure of \mathcal{G} , it suffices to show this equality one time slice at a time. Equality holds at $t = 0$ as $v(0, x) = w(0, x) = 0$. Assume that $v(t', \cdot) = w(t', \cdot)$ for $t' \leq t$ and let $x \in \mathcal{C}$ be given. The monotonicity of the graph Laplacian implies $\Delta^{\mathcal{G}} w + s \leq 2d - 1$, hence,

$$\Delta^{\mathcal{G}} w(t+1, x) + s(t+1, x) = -2dw(t+1, x) + s_0(x) + \sum_{y \sim x} w(t, y) < 2d,$$

and a rearrangement yields,

$$w(t+1, x) \geq \left\lfloor \frac{s_0(x) + \sum_{y \sim x} w(t, y)}{2d} \right\rfloor.$$

By Lemma 5.2.1 and the inductive hypothesis, the right-hand side of the above is exactly $v(t+1, x)$. Similarly, for the other direction,

$$\begin{aligned} \Delta^{\mathcal{G}} v(t+1, x) + s(t+1, x) &= 2d \left(\frac{s_0(x) + \sum_{y \sim x} w(t, y)}{2d} - \left\lfloor \frac{s_0(x) + \sum_{y \sim x} w(t, y)}{2d} \right\rfloor \right) \\ &< 2d, \end{aligned}$$

which concludes the proof by minimality of w . □

Our usage of the parabolic least action principle in the main argument is minimal and can be avoided. And, in some sense, it is a restatement of Lemma 5.2.1. We included it as it may be of independent interest.

5.2.3 Symmetry and fundamental domains

In this section we observe that sandpile dynamics on $\mathcal{C}_N^{(d)}$ preserve the symmetry structure of the d -dimensional hypercube. This is then used to reduce to the sandpile on a *fundamental domain* of the hypercube with reflecting boundary conditions. The main contribution of this

subsection is a coordinate-wise description of this domain along with an explicit formula for the reflecting graph Laplacian.

We briefly provide a presentation of the group of automorphisms of the hypercube and its action on \mathbb{Z}^d ; for more details see, for example, Godsil and Royle [2013]. Let $\text{Aut}_{\mathcal{C}_d}$ be the group of $(d \times d)$ matrices with exactly one ± 1 in each row and in each column and 0s elsewhere. Let $\sigma \in \text{Aut}_{\mathcal{C}_d}$ act on $x \in \mathbb{Z}^d$ by matrix-vector multiplication followed by a translation and let it act on $f : \mathbb{Z}^d \rightarrow \mathbb{R}$ by $\sigma f(x) := f(\sigma x)$. The translation is chosen to preserve $\mathcal{C}_N^{(d)}$ when N is even or odd in our choice of coordinates.

Each σ is an isometry and hence preserves nearest neighbors and $\mathcal{C}_N^{(d)}$. That is, if $y \notin \mathcal{C}_N^{(d)}$, then $\sigma y \notin \mathcal{C}_N^{(d)}$. And, if $|y - x| = 1$, then $|\sigma y - \sigma x| = 1$, so

$$\sum_{y' \sim \sigma x} f(y') = \sum_{y \sim x} f(\sigma y). \quad (5.6)$$

We say $\Omega \subseteq \mathcal{C}_N^{(d)}$ is a fundamental domain if there exists a set $\{\sigma_1, \sigma_2, \dots\} \subset \text{Aut}_{\mathcal{C}_d}$ so that $\bigcup_j \sigma_j \Omega = \mathcal{C}_N^{(d)}$. For example, a fundamental domain of an interval is half of it, while a fundamental domain of a square is a right triangle with one side along a central cross section of the square. The fundamental domains which we consider have coordinate consistency across dimensions. Let $M = \lceil N/2 \rceil$ and

$$\mathcal{S}_M^{(d)} := \{(x_1, \dots, x_d) : M \geq x_1 \geq \dots \geq x_d \geq 1\}. \quad (5.7)$$

Observe that $\{\mathbf{x}_{d-1} : (\mathbf{x}_{d-1}, 1) \in \mathcal{S}_M^{(d)}\} = \mathcal{S}_M^{(d-1)}$; this is the first step towards proving dimensional reduction on the hypercube.

Let v_t be the odometer function for an initial sandpile, s_0 , on $\mathcal{C}_N^{(d)}$ which is *symmetric*, $\sigma s_0 = s_0$ for all $\sigma \in \text{Aut}_{\mathcal{C}_d}$. We show that the parallel toppling odometer coincides with the *symmetrized* odometer v_t^S on $\mathcal{S}_M^{(d)}$ with appropriate reflecting boundary conditions. That is, for each $x \in \mathcal{S}_M^{(d)}$ and $y \sim x$ there exists a unique rotation or reflection, $\sigma_y \in \text{Aut}_{\mathcal{C}_d}$, so

that $\sigma_y y \in \mathcal{S}_M^{(d)}$. Let $y \stackrel{\mathcal{S}}{\sim} x$ denote iteration over the set $\{\sigma_y y : y \sim x\}$. For all $t \geq 0$ and $x \in \mathcal{S}_M^{(d)}$, let

$$v_{t+1}^{\mathcal{S}}(x) = \lfloor \frac{s_0(x) + \sum_{y \stackrel{\mathcal{S}}{\sim} x} v_t^{\mathcal{S}}(y)}{2d} \rfloor, \quad (5.8)$$

where $v_0^{\mathcal{S}} := 0$.

We provide an algorithmic construction of this which we use to prove Lemma 5.2.4 below.

Suppose $M \geq 2$, let $x \in \mathcal{S}_M^{(d)}$ be given and define $x_0 = M$ and $x_{d+1} = 1$. The following algorithm produces a sequence of indices describing the symmetrized nearest neighbors of x . Start with $l_0 = 0$ and pick the largest $(d+1) \geq r_0 \geq l_0$ with $x_{l_0} = x_{r_0}$. If $r_0 = (d+1)$, stop, otherwise, set $l_1 = (r_0 + 1)$ and repeat, generating

$$\mathbf{I}^{(M,d)}(x) := \{(l_0, r_0), \dots, (l_n, r_n)\}, \quad (5.9)$$

where $n \leq (d+1)$. Observe that

$$M = x_{l_0} = x_{r_0} < \dots < x_{l_k} = x_{r_k} < \dots < x_{l_n} = x_{r_n} = 1$$

so that

$$\begin{aligned} \sum_{y \stackrel{\mathcal{S}}{\sim} x} v_t(y) &= \sum_{k=1}^{n-1} (1 + r_k - l_k) (v_t(x - e_{r_k}) + v_t(x + e_{l_k})) \\ &\quad + (r_0 - l_0)v_t(x - e_{r_0}) \\ &\quad + (r_n - l_n)(v_t(x - e_{r_n}) + v_t(x + e_{l_n})) \end{aligned} \quad (5.10)$$

where $v_t(x - e_0) = v_t(x + e_{d+1}) := 0$ and

$$v_t(x - e_{r_n}) = \begin{cases} v_t(x) & \text{if } N \text{ is even} \\ v_t(x + e_{l_n}) & \text{if } N \text{ is odd.} \end{cases} \quad (5.11)$$

Lemma 5.2.3 (Symmetry). *For each $t \geq 0$ and each $\sigma \in \text{Aut}_{\mathcal{C}_d}$, $\sigma v_t = v_t$. Hence, $v_t = v_t^{\mathcal{S}}$ on $\mathcal{S}_M^{(d)}$.*

Proof. We prove symmetry of v_t by induction and Lemma 5.2.1. At $t = 0$, $v_t \equiv 0$, so suppose symmetry holds at time t . Let $\sigma \in \text{Aut}_{\mathcal{C}_d}$, $x \in \mathcal{C}_N^{(d)}$ be given. By Lemma 5.2.1, (5.6), and the inductive hypothesis,

$$\begin{aligned} v_{t+1}(\sigma x) &= \lfloor \frac{s_0(\sigma x) + \sum_{y' \sim \sigma x} v_t(y')}{2d} \rfloor \\ &= \lfloor \frac{s_0(\sigma x) + \sum_{y \sim x} v_t(\sigma y)}{2d} \rfloor \\ &= \lfloor \frac{s_0(x) + \sum_{y \sim x} v_t(y)}{2d} \rfloor \\ &= v_{t+1}(x). \end{aligned}$$

□

Note that the proof indicates that Lemma 5.2.3 can be extended in a natural way to other graphs and domains which are preserved under the automorphism group of the graph.

Henceforth, we consider $v_t^{\mathcal{S}}$ in $\mathcal{S}_M^{(d)}$ and drop all \mathcal{S} superscripts. To reduce the number of cases with similar arguments, we only consider $N = 2M$. Indeed, when N is odd, the proofs are identical except for slight changes to the boundary arguments. Also, we will use $\mathcal{S}_M^{(d)}$ to refer exclusively to the sorted fundamental domain of $\mathcal{C}_{2M}^{(d)}$. The expressions $v_t^{(d,M)}$ and $s_t^{(d,M)}$ will refer to the parallel toppling odometers and sandpiles on $\mathcal{S}_M^{(d)}$.

5.2.4 Derivative comparison

In this section we provide a general parabolic comparison result for first order differences of v_t on \mathcal{S}_M when the initial sandpile, s_0 , is constant. For $w \in \mathbb{Z}^d$, let D_w denote a first order difference operator of the form $D_w v_t(\cdot) = v_t(\cdot) - v_t(\cdot + w)$. Pad v_t by $v_t(x) := 0$ for

all $x \notin \mathcal{C}_N$. Denote the interior with respect to w as

$$\text{Int}_w(\mathcal{S}_M) = \{x \in \mathcal{S}_M : y' \in \mathcal{S}_M \text{ for all } |y' - (x + w)| = 1\} \quad (5.12)$$

and the boundary as

$$\partial_w \mathcal{S}_M = \mathcal{S}_M \setminus \text{Int}_w(\mathcal{S}_M). \quad (5.13)$$

Observe that every symmetrized $y \sim x \in \mathcal{S}_M$ is of the form $y = (x \pm e_i) \mp d_i$, where d_i is either a reflection, $d_i = e_i$ or a rotation $d_i = e_i - e_j$. We will show that if one can control $D_w v_t$ over the reflecting, rotating, and dissipating boundaries of \mathcal{S}_M , then that control persists over time. The dissipating boundary on \mathcal{S}_M is

$$\mathcal{B}_w^{(disp)} \mathcal{S}_M = \{x \in \mathcal{S}_M : (x + w)_i \geq M \text{ for some } 1 \leq i \leq d\} \quad (5.14)$$

while the reflecting and rotating boundaries are

$$\mathcal{B}_w^{(ref)} \mathcal{S}_M = \{x \in \mathcal{S}_M : (x + w)_i \leq 1 \text{ for some } 1 \leq i \leq d\} \quad (5.15)$$

and

$$\mathcal{B}_w^{(rot)} \mathcal{S}_M = \{x \in \mathcal{S}_M : (x + w)_i \leq (x + w)_j \text{ for some } 1 \leq i < j \leq d\}. \quad (5.16)$$

For notational convenience write

$$\mathcal{B}_w = \{\mathcal{B}_w^{(disp)} \cup \mathcal{B}_w^{(ref)} \cup \mathcal{B}_w^{(rot)}\} \quad (5.17)$$

and $\mathcal{B}_{w_1, \dots, w_n} = \cup_{i=1}^n \mathcal{B}_{w_i}$ for points $w_i \in \mathbb{Z}^d$. Note that in next lemma, we employ our convention to sometimes omit distinguishing sub/superscripts.

Lemma 5.2.4. *Let $\mathbf{w} := \{w_1, \dots, w_n\}$ be a set of points in \mathbb{Z}^d each equipped with a function*

$g_j : \mathcal{S} \rightarrow \mathbb{Z}$ which is superharmonic in the interior of \mathcal{S} . If

$$\sup_j (D_{w_j} v_{t_0}(x) - g_j(x)) \leq 0 \quad \text{for all } x \in \mathcal{S} \quad (5.18)$$

and for all $t \geq t_0$ and $x \in \{\mathcal{B}_0 \cup \mathcal{B}_w\} \mathcal{S}$,

$$\sup_j (\sum_{y \sim x} v_t(y) - \sum_{y' \sim (x+w_j)} v_t(y') - 2d g_j(x)) \leq 0 \quad (5.19)$$

or

$$\sup_j (D_{w_j} v_{t+1}(x) - g_j(x)) \leq 0$$

then

$$\sup_j (D_{w_j} v_{t+1}(x) - g_j(x)) \leq 0 \quad (5.20)$$

for all $t \geq t_0$ and $x \in \mathcal{S}$.

Proof. We prove this by induction on t , starting at t_0 , the base case guaranteed by (5.18).

Suppose (5.20) holds at t and let $w_j, x \in \mathcal{S}$ be given. First suppose $x \in \{\text{Int}_{w_j} \cap \text{Int}_0\}(\mathcal{S})$.

By Lemma 5.2.1

$$\begin{aligned} D_{w_j} v_{t+1}(x) - g_j(x) &\leq \lfloor \frac{(2d-1) + \sum_{y \sim x} v_t(y) - \sum_{y' \sim (x+w_j)} v_t(y')}{2d} \rfloor - g_j(x) \\ &= \lfloor \frac{(2d-1) + \sum_{y \sim x} D_{w_j} v_t(y)}{2d} \rfloor - g_j(x) \\ &= \lfloor \frac{(2d-1) + \sum_{y \sim x} (D_{w_j} v_t(y) - g_j(y)) + \sum_{y \sim x} (g_j(y) - g_j(x))}{2d} \rfloor \\ &\leq 0 \end{aligned}$$

as g_j is superharmonic and integer-valued. If $x \in \{\mathcal{B}_0 \cup \mathcal{B}_w\}$, then we either use the same argument or conclude depending on the case in (5.19).

□

As a corollary, we deduce the following discrete quasiconcavity property of v_t on a hypercube, which was proved in Babai and Gorodezky [2007] for axis monotonic initial sandpiles on \mathbb{Z}^2 . (Note that Aleksanyan and Shahgholian, using a discrete analogue of the method of moving planes, proved axis monotonicity of v_∞ in Aleksanyan and Shahgholian [2019].)

Corollary 5.2.1 (Axis monotonicity Babai and Gorodezky [2007]). *For all $t \geq 1$, $x \in \mathcal{S}$, and all sets of indices*

$$\mathcal{I} = \{i_1, \dots, i_n : 1 \leq i_1 < \dots < i_n \leq d\}$$

and

$$\mathcal{J} = \{j_1, \dots, j_m : i_n < j_1 < \dots < j_m \leq d\}$$

where $n \geq 1$ and $m \geq 0$ we have

$$v_t(x) \geq v_t(x + e_{\mathcal{I}} - e_{\mathcal{J}}) \quad \text{for } (x + e_{\mathcal{I}} - e_{\mathcal{J}}) \in \mathcal{S}$$

where $e_{\mathcal{I}} = \sum_{i \in \mathcal{I}} e_i$ denotes a sum over standard basis vectors indexed by \mathcal{I} .

We also have control on the derivative given an odometer upper bound on the dissipating boundary.

Corollary 5.2.2 (Derivative bound). *Suppose $v_\infty(M, \mathbf{1}_{d-1}) \leq kM$ for integer $k \geq 1$. Then, for all $1 \leq j \leq d$ and $t \geq 0$*

$$v_t(x) - v_t(x + e_j) \leq kx_j. \tag{5.21}$$

Proof. The claim is immediate if $M = 1$, so suppose $M \geq 2$. Let e_j and x be given and let

$$\mathbf{I}^{(M,d)}(x) := \{(l_0, r_0), \dots, (l_n, r_n)\}, \tag{5.22}$$

be the indices describing the nearest neighbors of x as defined in Section 5.2.3 above.

Pick the largest index J so that

$$l_J \leq j \leq r_J,$$

$v_t(x + e_j) = v_t(x + e_{l_J})$, and (recalling $l_J = r_{J-1} + 1$)

$$\mathbf{I}^{(M,d)}(x+e_{l_J}) = \begin{cases} \{\dots, (l_{J-1}, r_{J-1} + 1), (l_J + 1, r_J), \dots\} & \text{if } x_{r_{J-1}} = x_{l_J} + 1 \\ \{\dots, (l_{J-1}, r_{J-1}), (l_J, l_J), (l_J + 1, r_J), \dots\} & \text{if } x_{r_{J-1}} > x_{l_J} + 1. \end{cases} \quad (5.23)$$

As $g_j(x) := kx_j$ is harmonic in the interior of \mathcal{S} , it remains to check (5.19) in Lemma 5.2.4. For later reference, we label the expression we bound,

$$\sum_{y \sim x} v_t(y) - \sum_{y' \sim (x+e_{l_J})} v_t(y'). \quad (5.24)$$

The computations are similar in other cases, so we assume $x_{r_{J-1}} = x_{l_J} + 1$ and $l_J + 1 \leq r_J$.

Case 1: $J = 0$

As we are on the dissipating boundary, $v_{t+1}(x + e_{l_J}) = 0$ and $x_{l_J} = \dots = x_j = M$, hence

$$v_{t+1}(x) - v_{t+1}(x + e_{l_J}) = v_{t+1}(x) \leq v_\infty(M, \mathbf{1}_{d-1}) \leq kM$$

by axis monotonicity and our assumption on the odometer.

Case 2: $1 < J < n$

We compute (5.24), observing that all differences except for those near r_J are unaffected by

the symmetrization;

$$\begin{aligned}
(5.24) = & \sum_{k=1, k \notin [J-1, J]}^{n-1} (1 + r_k - l_k)(v_t(x - e_{r_k}) - v_t(x - e_{r_k} + e_{l_J})) \\
& + \sum_{k=1, k \notin [J-1, J]}^{n-1} (1 + r_k - l_k)(v_t(x + e_{l_k}) - v_t(x + e_{l_k} + e_{l_J})) \\
& + (r_0 - l_0)(v_t(x - e_{r_0}) - v_t(x - e_{r_0} + e_{l_J})) \\
& + (r_n - l_n)(v_t(x) - v_t(x + e_{l_J}) + v_t(x + e_{l_n}) - v_t(x + e_{l_n} + e_{l_J})) \\
& + \star_{\{J-1, J\}} \\
\leq & (2d - 2(1 + r_J - l_{J-1}))kx_j + \star_{\{J-1, J\}}
\end{aligned}$$

where $\star_{\{J-1, J\}}$ is defined as the sum of terms in the difference with indices $\{J-1, J\}$. This can then be computed,

$$\begin{aligned}
\star_{\{J-1, J\}} = & (1 + r_J - l_J)(v_t(x - e_{r_J}) + v_t(x + e_{l_J})) \\
& - (r_J - l_J)(v_t(x + e_{l_J} - e_{r_J}) + v_t(x + e_{l_J} + e_{l_J+1})) \\
& + (1 + r_{J-1} - l_{J-1})(v_t(x - e_{r_{J-1}}) + v_t(x + e_{l_{J-1}})) \\
& - (2 + r_{J-1} - l_{J-1})(v_t(x + e_{l_J} - e_{l_J}) + v_t(x + e_{l_J} + e_{l_{J-1}})) \\
\leq & (r_J - l_J)2kx_j + (1 + r_{J-1} - l_{J-1})(k(x_j + 1 - 1) + kx_j) \\
& + k(x_j - 1) + k(x_j + 1) \\
= & 2(1 + r_J - l_{J-1})kx_j.
\end{aligned}$$

Case 3: $J = 1 < n$

We bound differences with indices $\{0, 1\}$ in (5.24),

$$\begin{aligned}
 *_{\{0,1\}} &\leq (r_0 - l_0)kx_{l_1} \\
 &+ (r_1 - l_1)2kx_{l_1} \\
 &+ (v_t(x - e_{r_1}) - v_t(x)) + (v_t(x + e_{l_1}) - 0) \\
 &\leq (r_0 - l_0)kx_{l_1} + (r_1 - l_1)2kx_{l_1} + k(x_{l_1} - 1) + k(x_{l_1} + 1) \\
 &\leq 2(r_1 - l_0)kx_{l_1}.
 \end{aligned}$$

Case 4: $J = n > 1$

We bound differences with indices $\{n - 1, n\}$ in (5.24),

$$\begin{aligned}
 *_{\{n-1,n\}} &\leq (1 + r_{n-1} - l_{n-1})(k(x_{r_{n-1}} - 1) + kx_{l_n}) \\
 &+ (r_n - l_n - 1)(kx_{l_n} + kx_{l_n+1}) \\
 &+ (v_t(x) - v_t(x)) + (v_t(x + e_{l_n}) - v_t(x + e_{l_n} + e_{l_{n-1}})) \\
 &\leq (1 + r_{n-1} - l_{n-1})2kx_{l_n} + (r_n - l_n - 1)2kx_{l_n} \\
 &+ k(x_{l_{n-1}}) \\
 &\leq 2(r_n - l_{n-1})kx_{l_n}.
 \end{aligned}$$

In the last step we used $x_{l_{n-1}} = x_{l_n} + 1 = 2x_{l_n}$.

Case 5: $J = n = 1$

We bound differences with indices $\{0, n\}$ in (5.24),

$$\begin{aligned}
 *_{\{0,n\}} &\leq (r_0 - l_0)(k(x_{r_0} - 1)) \\
 &+ (r_n - l_n - 1)(kx_{l_n} + kx_{l_n+1}) \\
 &+ (v_t(x + e_{l_n}) - 0) + (v_t(x) - v_t(x)) \\
 &\leq (r_0 - l_0)2kx_{l_n} + (r_n - l_n - 1)2kx_{l_n} \\
 &+ kx_{l_n} \\
 &\leq 2(r_n - l_0 - 1)kx_{l_n}.
 \end{aligned}$$

□

5.2.5 Weak topple control

We provide a difference-in-time analogue of Lemma 5.2.4

Lemma 5.2.5. *For all $t \geq t_0$ and $j \geq 0$,*

$$\max_{z \in \mathcal{S}} (v_{t+j}(z) - v_t(z)) \leq \max_{z \in \mathcal{S}} (v_{t_0+j}(z) - v_{t_0}(z))$$

Proof. We induct on t starting at t_0 . Suppose the result holds for $(t-1)$ and let $x \in \mathcal{S}$ be given. Lemma 5.2.1 implies

$$v_{t+j}(x) - v_t(x) \leq \lfloor \frac{(2d-1) + \sum_{y \sim x} (v_{t+j-1}(y) - v_{t-1}(y))}{2d} \rfloor,$$

hence, by induction

$$v_{t+j}(x) - v_t(x) \leq \lfloor \frac{(2d-1) + 2d (\max_{z \in \mathcal{S}} (v_{t_0+j}(z) - v_{t_0}(z)))}{2d} \rfloor = \max_{z \in \mathcal{S}} (v_{t_0+j}(z) - v_{t_0}(z)).$$

□

5.3 Explicit solutions for small cubes

In this section, we compute $v_t^{(d)}$ when $s_0^{(d)} \equiv 2d + (d - 1)$ for all $d \geq 1$ when $M = 2$. We also show that dimensional reduction does not occur at dimension $d = d_0$ when $s_0^{(d)} \equiv 2d + (d_0 - 1)$ and $M = 1$.

5.3.1 Side length two

We first consider the case $M = 1$. As we do not know how to define a 0-dimensional sandpile, suppose $d_0 \geq 2$.

Proposition 5.3.1. *When $s_0^{(d)} \equiv 2d + (d_0 - 1)$, $v_\infty^{(d_0)} \equiv 1$ but $v_\infty^{(d_0-1)} \equiv 2$.*

Proof. In dimension d , a corner site of the hypercube has d internal neighbors so $\Delta^{(d)}(\mathbf{1}) = -2d + d = -d$. Hence, in dimension d_0 ,

$$s_1^{(d_0)}(\mathbf{1}) = (2d_0 + (d_0 - 1)) - d_0 = 2d_0 - 1$$

however, in dimension $(d_0 - 1)$,

$$s_1^{(d_0-1)}(\mathbf{1}) = (2(d_0 - 1) + (d_0 - 1)) - (d_0 - 1) = 2(d_0 - 1).$$

□

5.3.2 Side length four

Now, suppose $d \geq 1$ and take $M = 2$. After a radial reparameterization of \mathcal{S}_2 , arbitrary dimensional sandpiles become one-dimensional with a simple nearest-neighbor toppling rule. Indeed, every $\mathbf{x} \in \mathcal{S}_2$ is of the form $\mathbf{x} = (\mathbf{2}_x, \mathbf{1}_{d-x})$, for $x = 0, \dots, d$. Overload notation and consider s_t and v_t as functions on $\{0, \dots, d\}$. The Laplacian on the one-dimensional graph can then be computed using symmetry.

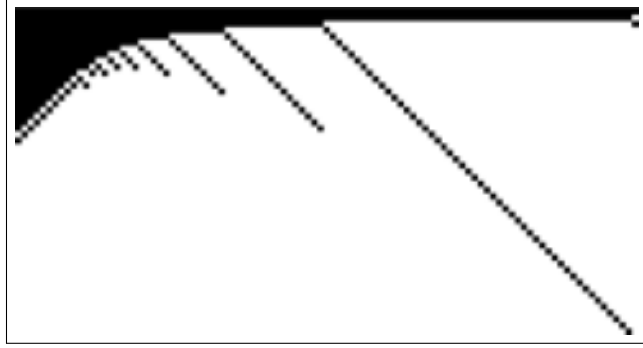


Figure 5.4: The parallel toppling odometer for $s_0 \equiv 2d + (d - 1)$ when $d = 100$ and $M = 2$. A black pixel in row t and column x indicates that $v_t(x) = v_{t-1}(x) + 1$. The top row is $t = 0$ and t increases from top to bottom. The left column is $x = 1$ and x increases from left to right.

Lemma 5.3.1. *If we define $0 = v_t(d + 1) = v_t(-1)$, then*

$$\Delta v_t(x) = (-d - x)v_t(x) + (d - x)v_t(x + 1) + xv_t(x - 1).$$

Proof. Let $\mathbf{x} = (\mathbf{2}_x, \mathbf{1}_{d-x})$ so that $\mathbf{I}^{(2,d)}(\mathbf{x}) = \{(0, x), (x + 1, d + 1)\}$. Hence, by definition of the symmetric Laplacian,

$$\begin{aligned} \Delta v_t(\mathbf{x}) &= -2dv_t(\mathbf{x}) + xv_t(\mathbf{x} - e_x) + (d - x)(v_t(\mathbf{x}) + v_t(\mathbf{x} + e_{x+1})) \\ &= -2dv_t(x) + (d - x)v_t(x) + (d - x)v_t(x + 1) + xv_t(x - 1). \end{aligned}$$

□

See Figure 5.4 for a display of the odometer throughout the parallel toppling process when $s_0^{(d)} \equiv 2d + (d - 1)$ in dimension $d = 100$. Visually, a contiguous block of decreasing size fires at each step, followed by a ripple of outwards firings. For $t > t_d := (\lceil \sqrt{d-1} \rceil + 1)$, the firing block appears to decrease by one every step. In particular, if a_t indexes the right

Draft Mar 13

edge of the block at time t , then $a_1 = d$ and

$$a_t = \begin{cases} \lfloor \frac{d-1}{t-1} \rfloor & \text{for } t \leq t_d \\ a_{t-1} - 1 & \text{for } t > t_d. \end{cases}$$

This leads to a simple formula for v_t .

Proposition 5.3.2. *For all $d \geq 1$, when $s_0^{(d)} = 2d + (d - 1)$, the radially reparameterized parallel toppling odometer has the following form. For all $t \geq 1$,*

$$v_t(x) = \begin{cases} v_{t-1}(x) + 1 & \text{for } x \leq a_t \\ v_{t-1}(x) & \text{for } a_t < x \leq a_{t-1}. \end{cases} \quad (5.25)$$

And for each $t' < t$ and $a_{t'-1} \geq x > a_{t'}$

$$v_t(x) = v_{t-1}(x - 1). \quad (5.26)$$

Proof. We induct on t . Since $s_0 \geq 2d$, $v_1 \equiv 1$. Suppose (5.25) and (5.26) hold for all $t' \leq t$.

Step 1: (5.25)

By strong induction for $t' \leq t$, (5.25) implies $v_t(x) = t$ for $x \leq a_t$. Thus,

$$s_t(x) = \begin{cases} 2d + (d - 1) - tx & \text{for } x < a_t \\ 2d + (d - 1) - tx - (d - x) & \text{for } x = a_t. \end{cases}$$

Let $g(x) := (d - 1) - tx$. If $g(x) \geq 0$, $v_{t+1}(x) = v_t(x) + 1$, otherwise $v_{t+1}(x) = v_t(x)$. When $a_{t+1} < x \leq a_t$, $g(x) < 0$. Indeed, $g(a_{t+1}) \leq (t - 1)$ and $g(x + 1) - g(x) = -t$.

As g is increasing in x , it remains to check $g(a_{t+1}) \geq 0$ for all t . If $x \leq \frac{d-1}{t}$ then $g(x) \geq 0$.

If $(t + 1) > t_d$, then

$$\frac{d-1}{t-1} - \frac{d-1}{t} \leq \frac{d-1}{\sqrt{d-1}(\sqrt{d-1}+1)} \leq 1,$$

thus

$$\begin{aligned} a_{t+1} &= a_t - 1 \\ &\leq \frac{d-1}{t-1} - 1 \\ &\leq \frac{d-1}{t}. \end{aligned}$$

Step 2: (5.26)

Now, take $a_{t'-1} \geq x > a_{t'}$ for $1 \leq t' \leq (t - 1)$. If $v_t(x - 1) = v_t(x) + 1$, then by strong induction for $t' \leq t$, (5.26) and (5.25) imply that $v_t(x - 2) = v_t(x - 1) = t'$ and $v_t(x) = t' - 1 = v_t(x + 1)$. Thus,

$$\begin{aligned} s_t(x) &\geq 2d + (d - 1) - (t' - 2)x \\ &\geq 2d + (d - 1) - (t' - 2)a_{t'-1} \\ &\geq 2d + (d - 1) - (d - 1) \\ &= 2d. \end{aligned}$$

However,

$$\begin{aligned} s_t(x - 1) &= 2d + (d - 1) - t'x - d + x \\ &= 2d - 1 - (t' - 1)x \\ &\leq 2d - 1, \end{aligned}$$

as $t' \geq 1$. If $v_t(x-1) = v_t(x) = v_t(x+1) = (t'-1)$, then

$$\begin{aligned} s_t(x) &\leq 2d + (d-1) - (t'-1)x \\ &< 2d + (d-1) - (t'-1)(a_{t'}) \\ &\leq 2d. \end{aligned}$$

□

5.4 Odometer regularity in dimension one

From here onward, suppose $s_0 \equiv 2d$. We start the inductive proof of Theorem 5.1.1 by establishing some regularity of the odometer in the critical dimension $d = d_0 = 1$. In the next section, we inductively use dimensional reduction to show that $d \geq 2$ sandpiles inherit this regularity. This regularity ensures that the dynamics of lower-dimensional sandpiles agree with their higher-dimensional embeddings.

When reading Section 5.5 below, the reader should observe that whenever Proposition 5.4.1 (or something close to it) holds, dimensional reduction follows. For example, if a version of this result is established in every critical dimension $d_0 \geq 1$, then dimensional reduction follows for all sandpiles of the form $2d + (d_0 - 1)$ in dimensions $d > d_0$. Proposition 5.3.2 should be understood as a step in this direction.

Proposition 5.4.1. *Recall the definition of τ_j from Theorem 5.1.1. For all $M \geq 2$ and $d \geq 1$, the odometer maintains the following properties throughout the parallel toppling process.*

Self-similarity *For each $1 \leq j \leq M$ and $t \leq \tau_j$*

$$v_t^{(M)}(\mathbf{x}) = v_t^{(j)}(\mathbf{x} - (M-j)) \text{ for } \mathbf{x} > M-j. \quad (5.27)$$

Weak facet compatibility For all $\mathbf{x}_i \geq 2$, $t \geq 1$, $i \geq 0$, $j \geq 0$ and $i + j + 1 = d$

$$\begin{aligned} v_t^{(M)}(\mathbf{x}_i, 1, \mathbf{1}_j) &= v_t^{(M)}(\mathbf{x}_i, 2, \mathbf{1}_j) + 1 \\ \implies v_{t+1}^{(M)}(\mathbf{x}_i, 1, \mathbf{1}_j) &= v_{t+1}^{(M)}(\mathbf{x}_i, 1, \mathbf{1}_j). \end{aligned} \tag{5.28}$$

Strong facet compatibility For all $\mathbf{x}_i \geq 2$, $j \geq 0$, $i < d$, ($t < \tau_M$ and $i \geq 0$) or ($i \geq 1$ and $t \geq \tau_M$)

$$v_t^{(M)}(\mathbf{x}) - v_t^{(M)}(\mathbf{x} + 2e_{i+1}) \leq 2 \tag{5.29}$$

and

$$\begin{aligned} v_t^{(M)}(\mathbf{x}_i, 1, \mathbf{1}_j) &= v_t^{(M)}(\mathbf{x}_i, 2, \mathbf{1}) + 1 \\ \implies v_{t+1}^{(M)}(\mathbf{x}_i, 1, \mathbf{1}_j) &= v_t^{(M)}(\mathbf{x}_i, 1, \mathbf{1}_j) \\ v_{t+1}^{(M)}(\mathbf{x}_i, 2, \mathbf{1}_j) &= v_t^{(M)}(\mathbf{x}_i, 2, \mathbf{1}_j) + 1. \end{aligned} \tag{5.30}$$

Strong topple control For all $t \geq \tau_{M-1}$,

$$\sup_{\mathbf{x} \in \mathcal{S}_M} (v_{t+2}(\mathbf{x}) - v_t(\mathbf{x})) \leq 1. \tag{5.31}$$

Proof of Proposition 5.4.1 for $d = d_0 = 1$. The proof proceeds by induction on M and then on t . When $M = 2$,

	$v_t^{(M)}(1)$	$v_t^{(M)}(2)$
$t = 1$	1	1
$t = 2$	2	1
$t = 3$	2	2
$t = 4$	3	2

and $v_1^{(M-1)}(1) = v_2^{(M-1)}(1) = 1$ which verifies the base case. Now, let M be given and note

that $v_1^{(M)}(x) = 1$ for all $1 \leq x \leq M$ and $v_2^{(M)}(x) = 2$ for $1 \leq x < M$ and $v_2^{(M)}(M) = 1$.

Hence, suppose (5.27),(5.28),(5.29),(5.30), hold for $(M - 1)$ for all $t \geq 1$ and suppose they hold for M for all $t' \leq (t - 1)$. We verify each inductive step.

Self-similarity: (5.27)

By strong induction, it suffices to show $v_t^{(M)}(x) = v_t^{(M-1)}(x - 1)$ for $x \geq 2$. By Lemma 5.2.1,

$$v_t^{(M)}(x) = 1 + \lfloor \frac{v_{t-1}^{(M)}(x+1) + v_{t-1}^{(M)}(x-1)}{2} \rfloor$$

for $x > 1$. Hence, by (5.27) at $(t - 1)$, for $x > 2$,

$$v_t^{(M)}(x) = 1 + \lfloor \frac{v_{t-1}^{(M-1)}(x) + v_{t-1}^{(M-1)}(x-2)}{2} \rfloor = v_t^{(M-1)}(x-1).$$

For $x = 1$, we have reflection at the origin,

$$v_t^{(M-1)}(1) = 1 + \lfloor \frac{v_{t-1}^{(M-1)}(2) + v_{t-1}^{(M-1)}(1)}{2} \rfloor = 1 + \lfloor \frac{v_{t-1}^{(M)}(3) + v_{t-1}^{(M)}(2)}{2} \rfloor.$$

Hence, if $v_{t-1}^{(M)}(1) = v_{t-1}^{(M)}(2)$, then $v_t^{(M-1)}(1) = v_t^{(M)}(2)$.

When $v_{t-1}^{(M)}(1) = v_{t-1}^{(M)}(2) + 1$, we instead use strong facet compatibility in both layers. If $v_{t-1}^{(M-1)}(1) = v_{t-1}^{(M-1)}(2)$, then $v_t^{(M-1)}(1) = v_{t-1}^{(M-1)}(1) + 1$ and we are done, so suppose not. Since sites topple at most once per time step by Lemma 5.2.5, the odometer must then be, for some $v \geq 2$:

	$v_{\cdot}^{(M)}(1)$	$v_{\cdot}^{(M)}(2)$	$v_{\cdot}^{(M)}(3)$
$t - 2$	v	v	$v - 1$
$t - 1$	$v + 1$	v	$v - 1$
t	$v + 1$	$v + 1$	$\geq (v - 1)$

This contradicts strong facet compatibility for $v_t^{(M-1)}(1)$ from $(t - 2) \rightarrow (t - 1)$, which we

can use as $t \leq \tau_{M-1}$ and hence $(t-1) < \tau_{M-1}$.

Weak facet compatibility: (5.28)

If $v_t(1) = v_t(2) + 1$, then $\Delta v_t(1) = -1$ and so $v_{t+1}(1) = v_t(1)$.

Strong facet compatibility: (5.29) and (5.30)

We use Lemma 5.2.4 to show (5.29). The function $g(x) = 2x$ is harmonic in the interior of the interval so it suffices to check the dissipating and reflecting boundaries. We control the dissipating boundary using $t < \tau_M$ and the reflecting boundary with (5.28).

As $t < \tau_M$, $v_t(M) \leq (M-1)$ and hence by Corollary 5.2.2,

$$v_t(M-1) \leq v_t(M) + (M-1) \leq 2(M-1).$$

For the reflecting boundary, *i.e.*, $x = 1$, we check

$$\begin{aligned} & \sum_{y \sim x} v_t(y) - \sum_{y' \sim (x+2)} v_t(y) \\ &= (v_t(1) - v_t(2)) + (v_t(2) - v_t(4)) \leq (v_t(1) - v_t(2)) + 4. \end{aligned}$$

If $v_t(1) - v_t(2) = 1$, then $v_{t+1}(1) = v_t(1)$ by weak facet compatibility. Otherwise,

$$\sum_{y \sim x} v_t(y) - \sum_{y' \sim (x+2)} v_t(y) \leq 4$$

and we conclude that

$$v_t(x) - v_t(x+2) \leq 2x.$$

Taking $x = 1$, this implies

$$\Delta v_t(2) \geq -2v_t(2) + v_t(1) + v_t(1) - 2 \geq 0,$$

which shows (5.30).

Strong topple control: (5.31)

By Lemma 5.2.5, it suffices to show

$$\sup_{x \in \mathcal{S}_M} (v_{\tau_{M-1}+2}(x) - v_{\tau_{M-1}}(x)) \leq 1$$

First observe that (5.27) for $v_t^{(M)}$ and (5.31) for $v_t^{(M-1)}$ imply that

$$\tau_{M-1} \geq \tau_{M-2} + 2. \tag{5.32}$$

Suppose for sake of contradiction that

$$(v_{\tau_{M-1}+2}(x) - v_{\tau_{M-1}}(x)) = 2$$

for some $1 \leq x \leq M$. Lemma 5.2.5 then implies that some neighbor $y \sim x$ must have toppled twice previously. Pick the maximal such y . We consider three cases for y .

Case 1: $y \geq 3$

We first note that $v_{\tau_{M-1}+1}^{(M)}(y) = v_{\tau_{M-1}+1}^{(M-1)}(y-1)$. Indeed, by (5.27), as $(y-1) \geq 2$,

$$\begin{aligned} v_{\tau_{M-1}+1}^{(M)}(y) &= 1 + \left\lfloor \frac{v_{\tau_{M-1}}^{(M)}(y+1) + v_{\tau_{M-1}}^{(M)}(y-1)}{2} \right\rfloor \\ &= 1 + \left\lfloor \frac{v_{\tau_{M-1}}^{(M-1)}(y) + v_{\tau_{M-1}}^{(M-1)}(y-2)}{2} \right\rfloor \\ &= v_{\tau_{M-1}+1}^{(M-1)}(y-1) \end{aligned}$$

Hence,

$$2 = v_{\tau_{M-1}+1}^{(M)}(y) - v_{\tau_{M-1}-1}^{(M)}(y) = v_{\tau_{M-1}+1}^{(M-1)}(y-1) - v_{\tau_{M-1}-1}^{(M-1)}(y-1),$$

which contradicts (5.31) for $v_t^{(M-1)}$.

Case 2: $y = 2$

We claim that $v_{\tau_{M-1}+1}^{(M)}(2) = v_{\tau_{M-1}+1}^{(M-1)}(1)$, in which case we can use the argument of Case 1.

If not, then $v_{\tau_{M-1}}^{(M)}(2) = v_{\tau_{M-1}}^{(M)}(3) + 1$ but $v_{\tau_{M-1}}^{(M)}(1) = v_{\tau_{M-1}}^{(M)}(2) + 1$. This implies that either

$$v_{\tau_{M-1}-1}^{(M)}(1) = v_{\tau_{M-1}-1}^{(M)}(2) + 2$$

or

$$v_{\tau_{M-1}-1}^{(M)}(1) = v_{\tau_{M-1}-1}^{(M)}(2) + 1$$

and

$$v_{\tau_{M-1}}^{(M)}(1) = v_{\tau_{M-1}-1}^{(M)}(1) + 1$$

both which contradict weak facet compatibility.

Case 3: $y = 1$

In this case, the odometer near the center must be, for some $v \geq 1$,

	$v_{\cdot}^{(M)}(1)$	$v_{\cdot}^{(M)}(2)$	$v_{\cdot}^{(M)}(3)$
$\tau_{M-1} - 1$	v	v	v
τ_{M-1}	$v + 1$	$v + 1$	v
$\tau_{M-1} + 1$	$v + 2$	$v + 1$	$\geq (v)$

This shows $v_{\tau_{M-1}-2}^{(M)}(2) = v - 1$. Indeed, if $v_{\tau_{M-1}-2}^{(M)}(1) = v - 1$, then as $\Delta v_{\tau_{M-1}-2}^{(M)}(1) \geq 0$ $v_{\tau_{M-1}-2}^{(M)}(2) = v - 1$. If $v_{\tau_{M-1}-2}^{(M)}(1) = v$, then $\Delta v_{\tau_{M-1}-2}^{(M)}(1) \leq -1$ and $v_{\tau_{M-1}-2}^{(M)}(2) = v - 1$.

Hence,

$$v_{\tau_{M-1}}^{(M-1)}(1) = v_{\tau_{M-1}}^{(M)}(2) = v_{\tau_{M-1}-2}^{(M)}(2) + 2 = v_{\tau_{M-1}-2}^{(M-1)}(2) + 2,$$

which contradicts (5.31) for $v_t^{(M-1)}$ using (5.32). □

Note that the comparison principle for sandpiles (see, for example, Proposition 3.3 in Bou-Rabee [2021a]) shows

$$v_\infty(x) = \frac{1}{2} (M(M+1) - x(x-1)),$$

and so $v_\infty(x) - v_\infty(x+1) = x$. Hence we must use an assumption like $t < \tau_M$ for strong facet compatibility.

5.5 Odometer regularity and dimensional reduction

We now prove Proposition 5.4.1 for $d \geq 2$ together with dimensional reduction,

$$v_t^{(d,M)}(\mathbf{x}_{d-1}, 1) = v_t^{(d-1,M)}(\mathbf{x}_{d-1}), \quad (5.33)$$

by strong induction on M , d , and t . Specifically, given M , d , and t , suppose

$$(5.27), (5.28), (5.29), (5.30), (5.31)$$

hold for

$$\begin{aligned} v_{t'}^{(d', M')} &\quad \text{for all } M' \geq 1, t' \geq 1, d' < d, \\ v_{t'}^{(d, M')} &\quad \text{for all } M' < M, t' \geq 1, \\ v_{t'}^{(d, M)} &\quad \text{for all } t' < t. \end{aligned}$$

We also suppose (5.33) holds for $v_{t-1}^{(d', M')}$ for all $d' \geq 2$ and $M' \leq M$. Indeed, $v_1^{(d, M)} \equiv 1$ for all $d \geq 1$ and $M \geq 1$.

5.5.1 Dimensional reduction

We start the induction in time by proving dimensional reduction given odometer regularity at $(t-1)$. Let \mathbf{x}_{d-1} be given and pick the smallest $d > i \geq 0$ so that $(\mathbf{x}_i, \mathbf{1}_{d-i}) = (\mathbf{x}_{d-1}, 1)$. By symmetry,

$$\begin{aligned} \Delta^{(d)} v_{t-1}^{(d)}(\mathbf{x}_i, \mathbf{1}_{d-i}) &= -2d v_{t-1}^{(d)}(\mathbf{x}_i, \mathbf{1}_{d-i}) \\ &\quad + \sum_{\mathbf{y}_i \sim \mathbf{x}_i} v_{t-1}^{(d)}(\mathbf{y}_i, \mathbf{1}_{d-i}) \\ &\quad + (d-i) \left(v_{t-1}^{(d)}(\mathbf{x}_i, \mathbf{1}_{d-i}) + v_{t-1}^{(d)}(\mathbf{x}_i, 2, \mathbf{1}_{d-i-1}) \right). \end{aligned}$$

We consider two cases at time $(t-1)$.

Case 1: $v_{t-1}^{(d)}(\mathbf{x}_i, \mathbf{1}_{d-i}) = v_{t-1}^{(d)}(\mathbf{x}_i, 2, \mathbf{1}_{d-i-1})$

By (5.33) at $(t-1)$, $v_{t-1}^{(d)}(\mathbf{x}_i, \mathbf{1}_{d-i}) = v_{t-1}^{(i+1)}(\mathbf{x}_i, 1)$. Thus,

$$\begin{aligned} \Delta^{(d)} v_{t-1}^{(d, M)}(\mathbf{x}_i, \mathbf{1}_{d-i}) &= -2i v_{t-1}^{(i+1)}(\mathbf{x}_i, 1) + \sum_{\mathbf{y}_i \sim \mathbf{x}_i} v_{t-1}^{(i+1)}(\mathbf{y}_i, 1) \\ &= \Delta^{(i+1)} v_{t-1}^{(i+1, M)}(\mathbf{x}_i, 1) \end{aligned}$$

which concludes this case as $v_t^{(d)} = v_{t-1}^{(d)} + 1(\Delta^{(d)} v_{t-1}^{(d)} \geq 0)$.

Case 2: $v_{t-1}^{(d)}(\mathbf{x}_i, \mathbf{1}_{d-i}) = v_{t-1}^{(d)}(\mathbf{x}_i, 2, \mathbf{1}_{d-i-1}) + 1$

If $i \leq (d-2)$, then (5.28) for $(t-1) \rightarrow t$ for both $v_{t-1}^{(i+1)}$ and $v_{t-1}^{(d)}$ imply that

$$v_{t-1}^{(i+1)}(\mathbf{x}_i, 1) = v_{t-1}^{(d)}(\mathbf{x}_i, \mathbf{1}_{d-i}) = v_t^{(d)}(\mathbf{x}_i, \mathbf{1}_{d-i}) = v_t^{(i+1)}(\mathbf{x}_i, 1).$$

If $i = (d-1)$, then (5.30) and (5.33) at $(t-1)$ and $(t-2)$ imply that

$$v_{t-1}^{(d-1)}(\mathbf{x}_{d-1}) = v_{t-1}^{(d)}(\mathbf{x}_{d-1}, 1) = v_{t-2}^{(d)}(\mathbf{x}_{d-1}, 1) + 1 = v_{t-2}^{(d-1)}(\mathbf{x}_{d-1}) + 1.$$

If $(t-2) \geq \tau_{M-1}$, (5.31) for $v_t^{(i)}$ and $v_t^{(d)}$ imply that

$$v_t^{(d-1)}(\mathbf{x}_{d-1}) = v_{t-1}^{(d-1)}(\mathbf{x}_{d-1}) = v_{t-1}^{(d)}(\mathbf{x}_{d-1}, 1) = v_t^{(d)}(\mathbf{x}_{d-1}, 1).$$

If $(t-2) < \tau_{M-1}$, then (5.27) and (5.33) for $v_{t-1}^{(M-1)}$ show

$$v_{t-1}^{(d,M)}(\mathbf{x}_{d-1}, 2) = v_{t-1}^{(d,M-1)}(\mathbf{x}_{d-1} - 1, 1) = v_{t-1}^{(d-1,M-1)}(\mathbf{x}_{d-1} - 1).$$

Similarly,

$$v_{t-1}^{(d,M)}(\mathbf{x}_{d-1}, 1) = v_{t-1}^{(d-1,M)}(\mathbf{x}_{d-1}) = v_{t-1}^{(d-1,M-1)}(\mathbf{x}_{d-1} - 1).$$

Therefore, for all $t' \leq \tau_{M-1}$,

$$v_{t'}^{(d,M)}(\mathbf{x}_{d-1}, 2) = v_{t'}^{(d,M)}(\mathbf{x}_{d-1}, 1), \quad (5.34)$$

this however contradicts the case we are in.

5.5.2 Odometer regularity in dimensions larger than one

We verify each inductive step.

Self-similarity: (5.27)

As (5.27) holds for $(M - 1)$ at t , it suffices to show that if $t \leq \tau_{M-1}$ and $\mathbf{x} > 1$,

$$v_t^{(M)}(\mathbf{x}) = v_t^{(M-1)}(\mathbf{x} - 1). \quad (5.35)$$

We split verification of this into cases.

Case 1: $\mathbf{x} > 2$

As (5.35) holds for $(t - 1)$, by Lemma 5.2.1,

$$\begin{aligned} v_t^{(M)}(\mathbf{x}) &= \lfloor \frac{s_0(\mathbf{x}) + \sum_{\mathbf{y} \sim \mathbf{x}} v_{t-1}^{(M)}(\mathbf{y})}{2d} \rfloor \\ &= \lfloor \frac{s_0(\mathbf{x} - 1) + \sum_{\mathbf{y} \sim (\mathbf{x} - 1)} v_{t-1}^{(M-1)}(\mathbf{y})}{2d} \rfloor \\ &= v_t^{(M-1)}(\mathbf{x} - 1). \end{aligned}$$

Case 2: $\mathbf{x} = (\mathbf{x}_j, 2)$ for $\mathbf{x}_j > 2$ and $0 \leq j < d$

We show that if $\Delta v_{t-1}^{(M)}(\mathbf{x}) \geq 0$, then $\Delta v_{t-1}^{(M-1)}(\mathbf{x} - 1) \geq 0$. First, decompose the Laplacian into a sum of discrete second differences,

$$\Delta v_{t-1}^{(M)}(\mathbf{x}) = \sum_{i=1}^d \Delta_{(i)} v_{t-1}^{(M)}(\mathbf{x}),$$

where

$$\Delta_{(i)} v_{t-1}^{(M)}(\mathbf{x}) = -2v_{t-1}^{(M)}(\mathbf{x}) + v_{t-1}^{(M)}(\mathbf{x} + e_i) + v_{t-1}^{(M)}(\mathbf{x} - e_i).$$

Observe that (5.27) at $(t - 1)$ implies, $\Delta_{(i)} v_{t-1}^{(M)}(\mathbf{x}) = \Delta_{(i)} v_{t-1}^{(M-1)}(\mathbf{x} - 1)$ for all $i \leq j$ and for $i > j$,

$$\Delta_{(i)}(v_{t-1}^{(M-1)}(\mathbf{x} - 1) - v_{t-1}^{(M)}(\mathbf{x})) = v_{t-1}^{(M-1)}(\mathbf{x} - e_i - 1) - v_{t-1}^{(M)}(\mathbf{x} - e_i).$$

Draft Mar 13

By reflectional symmetry, for each $i > j$,

$$v_{t-1}^{(M-1)}(\mathbf{x} - e_i - 1) = v_{t-1}^{(M-1)}(\mathbf{x} - 1) = v_{t-1}^{(M)}(\mathbf{x}),$$

thus

$$\Delta_{(i)}(v_{t-1}^{(M-1)}(\mathbf{x} - 1) - v_{t-1}^{(M)}(\mathbf{x})) = v_{t-1}^{(M)}(\mathbf{x}) - v_{t-1}^{(M)}(\mathbf{x} - e_i). \quad (5.36)$$

If $v_{t-1}^{(M)}(\mathbf{x}) = v_{t-1}^{(M)}(\mathbf{x} - e_i)$ for all $i > j$, we are done, so suppose otherwise.

Take $i > j$ where (5.36) $\neq 0$. By (5.30),

$$v_{t-2}^{(M)}(\mathbf{x}) = v_{t-1}^{(M)}(\mathbf{x}) = v_{t-1}^{(M)}(\mathbf{x} - e_i) - 1 = v_{t-2}^{(M)}(\mathbf{x} - e_i). \quad (5.37)$$

By (5.27) and (5.30) for $v_{t-2}^{(M-1)}$, if

$$v_{t-1}^{(M-1)}(\mathbf{x} - 1) = v_{t-1}^{(M-1)}(\mathbf{x} - 1 + e_i) + 1$$

then

$$v_{t-1}^{(M)}(\mathbf{x}) = v_{t-1}^{(M-1)}(\mathbf{x} - 1) = v_{t-2}^{(M-1)}(\mathbf{x} - 1) + 1 = v_{t-2}^{(M)}(\mathbf{x}) + 1$$

which contradicts (5.37). Moreover, by (5.30) we must have for each neighbor $(\mathbf{y} - e_i) \sim (\mathbf{x} - e_i)$, $v_{t-1}^{(M)}(\mathbf{y}) \geq v_{t-2}^{(M)}(\mathbf{y} - e_i)$. Thus,

$$\Delta v_{t-1}^{(M-1)}(\mathbf{x} - 1) \geq \Delta v_{t-2}^{(M)}(\mathbf{x} - e_i) \geq 0. \quad (5.38)$$

Strong facet compatibility: (5.29) and (5.30)

We first use

$$v_t(\mathbf{x}_{i-1}, 1, \mathbf{1}_j) - v_t(\mathbf{x}_{i-1}, 3, \mathbf{1}_j) \leq 2 \quad (5.39)$$

together with the inductive hypotheses to show (5.30), then we verify (5.29) below.

Draft Mar 13

Suppose $v_t(\mathbf{x}_{i-1}, 1, \mathbf{1}_j) = v_t(\mathbf{x}_{i-1}, 2, \mathbf{1}_j) + 1$. By (5.30) at $(\mathbf{x}_i, 1, \mathbf{1}_j)$ from $(t-1) \rightarrow t$, $\Delta v_{t-1}(\mathbf{x}_i, 1, \mathbf{1}_j) \geq 0$. Hence, it suffices to show

$$\Delta v_t(\mathbf{x}_i, 2, \mathbf{1}_j) \geq \Delta v_{t-1}(\mathbf{x}_i, 1, \mathbf{1}_j).$$

We use symmetry to decompose each Laplacian;

$$\begin{aligned} \Delta v_t(\mathbf{x}_{i-1}, 2, \mathbf{1}_j) &= -2d v_t(\mathbf{x}_{i-1}, 2, \mathbf{1}_j) \\ &\quad + \sum_{j'=1}^{(i-1)} (v_t(\mathbf{x}_i + e_{j'}, 2, \mathbf{1}_j) + v_t(\mathbf{x}_i - e_{j'}, 2, \mathbf{1}_j)) \end{aligned} \quad (5.40)$$

$$+ v_t(\mathbf{x}_i, 1, \mathbf{1}_j) + v_t(\mathbf{x}_i, 3, \mathbf{1}_j) \quad (5.41)$$

$$+ j(v_t(\mathbf{x}_i, 2, \mathbf{1}_j) + v_t(\mathbf{x}_i, 2, 2, \mathbf{1}_{j-1})) \quad (5.42)$$

while

$$\begin{aligned} \Delta v_{t-1}(\mathbf{x}_{i-1}, 1, \mathbf{1}_j) &= -2d v_{t-1}(\mathbf{x}_{i-1}, 1, \mathbf{1}_j) \\ &\quad + \sum_{j'=1}^{(i-1)} (v_{t-1}(\mathbf{x}_i + e_{j'}, 1, \mathbf{1}_j) + v_{t-1}(\mathbf{x}_i - e_{j'}, 1, \mathbf{1}_j)) \end{aligned} \quad (5.43)$$

$$+ v_{t-1}(\mathbf{x}_i, 1, \mathbf{1}_j) + v_{t-1}(\mathbf{x}_i, 2, \mathbf{1}_j) \quad (5.44)$$

$$+ j(v_{t-1}(\mathbf{x}_i, 1, \mathbf{1}_j) + v_{t-1}(\mathbf{x}_i, 2, \mathbf{1}_j)). \quad (5.45)$$

By (5.30) from $(t-1) \rightarrow t$, $v_{t-1}(\mathbf{x}_{i-1}, 1, \mathbf{1}_j) = v_t(\mathbf{x}_{i-1}, 2, \mathbf{1}_j)$. Also (5.30) shows that each $\mathbf{y}_i \sim \mathbf{x}_i$ with $\mathbf{y}_i \geq 2$, $v_t(\mathbf{y}_i, 2, \mathbf{1}_j) \geq v_{t-1}(\mathbf{y}_i, 1, \mathbf{1}_j)$. If $\mathbf{x}_i - e_{j'} \not\geq 2$, $v_t(\mathbf{x}_i - e_{j'}, 2, \mathbf{1}_j) = v_t(\mathbf{x}_i, 1, \mathbf{1}_j) \geq v_{t-1}(\mathbf{x}_i, 1, \mathbf{1}_j)$. This shows that (5.40) \geq (5.43). Next, (5.39) implies

$$(5.41) \geq 2v_t(x_i, 1, \mathbf{1}_j) - 2,$$

while (5.30) from $(t-1) \rightarrow t$ implies

$$(5.44) \leq 2v_{t-1}(x_i, 1, \mathbf{1}_j),$$

hence (5.41) \geq (5.44). Finally, by (5.30) from $(t-1) \rightarrow t$,

$$v_t(x_i, 2, 2, \mathbf{1}_{j-1}) \geq v_{t-1}(x_i, 2, \mathbf{1}_j)$$

which implies (5.42) \geq (5.45).

We now verify (5.29) for different regimes of t .

Case 1: $t < \tau_M$, $i \geq 1$

We use Lemma 5.2.4 as in the proof for $d = 1$ to show that

$$v_t(\mathbf{x}) - v_t(\mathbf{x} + 2e_i) \leq 2x_i$$

for all $d \leq i \leq 1$ and $\mathbf{x} \in \mathcal{S}_M$. Indeed as $t < \tau_M$

$$v_t(\mathbf{x}) - v_t(\mathbf{x} + e_j) \leq x_j \tag{5.46}$$

for all $\mathbf{x} \in \mathcal{S}_M$ and $1 \leq j \leq d$. Hence, $v_t(\mathbf{x}) - v_t(\mathbf{x} + 2e_j) \leq 2(M-1)$ on $\partial_{2e_j} \mathcal{S}_M$ for all $1 \leq j \leq d$. The reflecting boundary is checked in the same way as $d = 1$, using weak facet compatibility in higher dimensions.

Case 2: $t \geq \tau_M$, $i \geq 2$

Here we show that

$$v_t(\mathbf{x}) - v_t(\mathbf{x} + 2e_i) \leq 2x_i$$

for all $d \geq i \geq 2$ and $x_1 \geq 2$. We again use Lemma 5.2.4 except the region in which we have the derivative bound shrinks and therefore our boundaries change. The dissipating

boundary gets smaller, $\mathcal{B}^{(disp)} := \{x \in \mathcal{S}_M : x_j = M - 1 \text{ for some } 2 \leq j \leq d\}$ and the reflecting boundary remains the same except for the removal of a single point, $\mathbf{1}$. By axis monotonicity, $\sup_{x \in \mathcal{B}^{(disp)}} v_t(x) \leq v_t(M, \mathbf{1}) \leq M$. Checking the reflective boundary is as in $d = 1$ except for the point $(2, \mathbf{1}_{d-1})$. We show directly that

$$v_t(2, \mathbf{1}_{d-1}) \leq v_t(3, 2, \mathbf{1}_{d-2}) + 2. \quad (5.47)$$

Suppose for sake of contradiction that $v_t(2, \mathbf{1}_{d-1}) = v_t(3, 2, \mathbf{1}_{d-2}) + 2$ and $\Delta v_t(2, \mathbf{1}_{d-1}) \geq 0$ but $\Delta v_t(3, 2, \mathbf{1}_{d-1}) < 0$. As (5.29) has been verified for all $x \in \mathcal{S}_M$ other than $(2, \mathbf{1}_{d-1})$, (5.30) holds for $(3, 2, \mathbf{1}_{d-1})$ and so $v_t(3, 2, \mathbf{1}_{d-2}) = v_t(3, \mathbf{1}_{d-1})$. Then, by definition of the symmetric Laplacian, weak facet compatibility, and axis monotonicity,

$$\begin{aligned} \Delta v_t(2, \mathbf{1}_{d-1}) &= -2dv_t(2, \mathbf{1}_{d-1}) \\ &\quad + v_t(3, \mathbf{1}_{d-1}) + v_t(1, \mathbf{1}_{d-1}) \\ &\quad + (d-1)(v_t(2, \mathbf{1}_{d-1}) + v_t(2, 2, \mathbf{1}_{d-2})) \\ &\leq -2v_t(2, \mathbf{1}_{d-1}) + v_t(3, \mathbf{1}_{d-1}) + v_t(1, \mathbf{1}_{d-1}) \\ &\leq -1, \end{aligned}$$

which is a contradiction.

Weak facet compatibility: (5.28)

The only remaining case is

$$v_t^{(d)}(1, \mathbf{1}_j) = v_t^{(d)}(2, \mathbf{1}_j) + 1.$$

By symmetry,

$$\Delta v_t^{(d)}(1, \mathbf{1}_j) = d(v_t^{(d)}(2, \mathbf{1}_j) - v_t^{(d)}(1, \mathbf{1}_j)) = -d.$$

Strong topple control: (5.31)

We use strong topple control established in dimension $(d - 1)$. Suppose for sake of contradiction there exists $\mathbf{x} \in \mathcal{S}_M^{(d)}$ with $v_{\tau_{M-1}+2}(\mathbf{x}) - v_{\tau_{M-1}}(\mathbf{x}) = 2$. Pick $\mathbf{x} = (\mathbf{x}_{d-1}, x)$ so that $x \geq 1$ is minimal.

Case 1: $x = 1$

By dimensional reduction at time τ_{M-1} , $v_{\tau_{M-1}}^{(M,d)}(\mathbf{x}_{d-1}, 1) = v_{\tau_{M-1}}^{(M,d-1)}(\mathbf{x}_{d-1})$. By the parabolic least action principle,

$$v_{\tau_{M-1}+2}^{(M,d-1)}(\mathbf{x}_{d-1}) \geq v_{\tau_{M-1}+2}^{(M,d)}(\mathbf{x}_{d-1}, 1),$$

which contradicts (5.31) for $v_t^{(M,d-1)}$.

Case 2: $x = 2$

By (5.34),

$$v_{\tau_{M-1}}^{(M,d)}(\mathbf{x}_{d-1}, 1) = v_{\tau_{M-1}}^{(M,d)}(\mathbf{x}_{d-1}, 2),$$

which in turn, by axis monotonicity, implies $v_{\tau_{M-1}+2}^{(M,d)}(\mathbf{x}_{d-1}, 1) = v_{\tau_{M-1}}^{(M,d)}(\mathbf{x}_{d-1}, 1) + 2$, which contradicts the minimality of x .

Case 3: $x \geq 3$

Some neighbor $\mathbf{y} \sim \mathbf{x}$ must have toppled twice previously. As $x \geq 3$, $\mathbf{y} = (\mathbf{y}_{d-1}, y)$ for $y \geq 2$. The same argument for $d = 1$ when $y \geq 2$ then implies, $v_{\tau_{M-1}+1}^{(M,d)}(\mathbf{y}) = v_{\tau_{M-1}+1}^{(M-1,d)}(\mathbf{y})$ which contradicts (5.31) for $v_t^{(M-1,d)}$.

REFERENCES

- Mustafa A Akcoglu and Ulrich Krengel. Ergodic theorems for superadditive processes. *Journal für die reine und angewandte Mathematik*, 1981(323):53–67, 1981.
- Hayk Aleksanyan and Henrik Shahgholian. Discrete balayage and boundary sandpile. *Journal d'Analyse Mathématique*, 138(1):361–403, 2019.
- Ian Alevy and Sevak Mkrtchyan. The limit shape of the leaky Abelian sandpile model. *arXiv preprint arXiv:2010.01946*, 2020.
- Oswaldo SM Alves, Fabio P Machado, and S Yu Popov. The shape theorem for the frog model. *The Annals of Applied Probability*, 12(2):533–546, 2002.
- Peter Antal and Agoston Pisztora. On the chemical distance for supercritical Bernoulli percolation. *The Annals of Probability*, pages 1036–1048, 1996.
- Scott Armstrong and Pierre Cardaliaguet. Stochastic homogenization of quasilinear Hamilton–Jacobi equations and geometric motions. *Journal of the European Mathematical Society*, 20(4):797–864, 2018.
- Scott N. Armstrong and Paul Dario. Elliptic regularity and quantitative homogenization on percolation clusters. *Communications on Pure and Applied Mathematics*, 71(9):1717–1849, 2018.
- Scott N. Armstrong and Charles K. Smart. Quantitative stochastic homogenization of elliptic equations in nondivergence form. *Archive for Rational Mechanics and Analysis*, 214(3):867–911, 2014a.
- Scott N Armstrong and Charles K Smart. Regularity and stochastic homogenization of fully nonlinear equations without uniform ellipticity. *The Annals of Probability*, 42(6):2558–2594, 2014b.
- Scott N Armstrong and Charles K Smart. Stochastic homogenization of fully nonlinear uniformly elliptic equations revisited. *Calculus of Variations and Partial Differential Equations*, 50(3-4):967–980, 2014c.
- Scott N Armstrong and Panagiotis E Souganidis. Stochastic homogenization of Hamilton–Jacobi and degenerate Bellman equations in unbounded environments. *Journal de mathématiques pures et appliquées*, 97(5):460–504, 2012.
- Scott N Armstrong and Panagiotis E Souganidis. Stochastic homogenization of level-set convex Hamilton–Jacobi equations. *International Mathematics Research Notices*, 2013(15):3420–3449, 2013.
- Antonio Auffinger, Michael Damron, and Jack Hanson. *50 years of first-passage percolation*, volume 68. American Mathematical Society, 2017.

- László Babai and Igor Gorodezky. Sandpile transience on the grid is polynomially bounded. In *Proceedings of the eighteenth annual ACM-SIAM symposium on Discrete algorithms*, pages 627–636, 2007.
- Per Bak, Chao Tang, and Kurt Wiesenfeld. Self-organized criticality: An explanation of the 1/f noise. *Physical review letters*, 59(4):381, 1987.
- Guy Barles and Panagiotis E Souganidis. A new approach to front propagation problems: theory and applications. *Archive for Rational Mechanics and Analysis*, 141(3):237–296, 1998.
- Daniele Beauquier and Maurice Nivat. On translating one polyomino to tile the plane. *Discrete & Computational Geometry*, 6(4):575–592, 1991.
- Tim Besard, Christophe Foket, and Bjorn De Sutter. Effective extensible programming: unleashing julia on gpus. *IEEE Transactions on Parallel and Distributed Systems*, 30(4):827–841, 2018.
- Jeff Bezanson, Alan Edelman, Stefan Karpinski, and Viral B. Shah. Julia: A fresh approach to numerical computing. *SIAM review*, 59(1):65–98, 2017.
- Norman Biggs. Algebraic potential theory on graphs. *Bulletin of the London Mathematical Society*, 29(6):641–682, 1997.
- Norman L. Biggs. Chip-firing and the critical group of a graph. *Journal of Algebraic Combinatorics*, 9(1):25–45, 1999.
- Anders Björner and László Lovász. Chip-firing games on directed graphs. *Journal of algebraic combinatorics*, 1(4):305–328, 1992.
- Anders Björner, László Lovász, and Peter W Shor. Chip-firing games on graphs. *European Journal of Combinatorics*, 12(4):283–291, 1991.
- Béla Bollobás and Peter Winkler. The longest chain among random points in euclidean space. *Proceedings of the American Mathematical Society*, 103(2):347–353, 1988.
- Benjamin Bond and Lionel Levine. Abelian networks I. Foundations and examples. *SIAM Journal on Discrete Mathematics*, 30(2):856–874, 2016.
- Ahmed Bou-Rabee. Code for computing arbitrary dimensional sandpiles. https://github.com/nitromannitol/arbitrarydim_sandpiles.
- Ahmed Bou-Rabee. Convergence of the random abelian sandpile. *The Annals of Probability*, 49(6):3168–3196, 2021a.
- Ahmed Bou-Rabee. A shape theorem for exploding sandpiles. *arXiv preprint arXiv:2102.04422*, 2021b.

- Ahmed Bou-Rabee. Integer superharmonic matrices on the F -lattice. *arXiv preprint arXiv:2102.04422*, 2021c.
- Ahmed Bou-Rabee. Dynamic dimensional reduction in the abelian sandpile. *Communications in Mathematical Physics*, 390(2):933–958, 2022.
- LA Caffarelli and R Monneau. Counter-example in three dimension and homogenization of geometric motions in two dimension. *Archive for Rational Mechanics and Analysis*, 212(2):503–574, 2014.
- Luis A Caffarelli. A note on nonlinear homogenization. *Communications on Pure and Applied Mathematics: A Journal Issued by the Courant Institute of Mathematical Sciences*, 52(7):829–838, 1999.
- Luis A Caffarelli, Panagiotis E Souganidis, and Lihe Wang. Homogenization of fully nonlinear, uniformly elliptic and parabolic partial differential equations in stationary ergodic media. *Communications on Pure and Applied Mathematics: A Journal Issued by the Courant Institute of Mathematical Sciences*, 58(3):319–361, 2005.
- Sergio Caracciolo, Guglielmo Paoletti, and Andrea Sportiello. Explicit characterization of the identity configuration in an abelian sandpile model. *Journal of physics A: mathematical and theoretical*, 41(49):495003, 2008.
- Sergio Caracciolo, Guglielmo Paoletti, and Andrea Sportiello. Conservation laws for strings in the Abelian sandpile model. *EPL (europhysics letters)*, 90(6):60003, 2010.
- Joe Chen and Jonah Kudler-Flam. Laplacian growth and sandpiles on the sierpiński gasket: limit shape universality and exact solutions. *Annales de l'Institut Henri Poincaré D*, 7(4), 2020.
- Scott Corry and David Perkinson. *Divisors and Sandpiles: An Introduction to Chip-Firing*, volume 114. American Mathematical Soc., 2018.
- J Theodore Cox and Richard Durrett. Some limit theorems for percolation processes with necessary and sufficient conditions. *The Annals of Probability*, pages 583–603, 1981.
- Michael G Crandall. Viscosity solutions: a primer. In *Viscosity solutions and applications*, pages 1–43. Springer, 1997.
- Michael Creutz. Abelian sandpiles. *Computers in Physics*, 5(2):198–203, 1991.
- Gianni Dal Maso and Luciano Modica. *Nonlinear stochastic homogenization and ergodic theory*. Università di Pisa. Dipartimento di Matematica, 1985.
- Michael Damron, Jack Hanson, and Philippe Sosoe. Subdiffusive concentration in first passage percolation. *Electronic Journal of Probability*, 19:1–27, 2014.

- Deepak Dhar. Self-organized critical state of sandpile automaton models. *Physical Review Letters*, 64(14):1613–1616, 1990.
- Deepak Dhar. The Abelian sandpile and related models. *Physica A: Statistical Mechanics and its Applications*, 263(1-4):4–25, 1999.
- Deepak Dhar and Tridib Sadhu. Pattern formation in growing sandpiles with multiple sources or sinks. *Journal of Statistical Physics*, 138(4-5):815–837, 2010.
- Deepak Dhar and Tridib Sadhu. A sandpile model for proportionate growth. *Journal of Statistical Mechanics: Theory and Experiment*, 2013(11):P11006, 2013.
- Deepak Dhar, Philippe Ruelle, Siddhartha Sen, and D-N Verma. Algebraic aspects of abelian sandpile models. *Journal of physics A: mathematical and general*, 28(4):805, 1995.
- Deepak Dhar, Tridib Sadhu, and Samarth Chandra. Pattern formation in growing sandpiles. *EPL (Europhysics Letters)*, 85(4):48002, 2009.
- Persi Diaconis and William Fulton. A growth model, a game, an algebra, Lagrange inversion, and characteristic classes. *Rend. Sem. Mat. Univ. Pol. Torino*, 49(1):95–119, 1991.
- Richard Durrett and Thomas M. Liggett. The shape of the limit set in richardson’s growth model. *Annals of Probability*, pages 186–193, 1981.
- Arthur Engel. The probabilistic abacus. *Educational studies in mathematics*, pages 1–22, 1975.
- Matthew Farrell and Lionel Levine. Coeulerian graphs. *Proceedings of the American Mathematical Society*, 144(7):2847–2860, 2016.
- William M Feldman. Mean curvature flow with positive random forcing in 2-d. *arXiv preprint arXiv:1911.00488*, 2019.
- Anne Fey and Haiyan Liu. Limiting shapes for a non-abelian sandpile growth model and related cellular automata. *Journal of Cellular Automata*, 6, 2011.
- Anne Fey and Frank Redig. Organized versus self-organized criticality in the Abelian sandpile model. *Markov Processes Relat. Fields*, 11:425–442, 2005.
- Anne Fey, Ronald Meester, Frank Redig, et al. Stabilizability and percolation in the infinite volume sandpile model. *The Annals of Probability*, 37(2):654–675, 2009.
- Anne Fey, Lionel Levine, and Yuval Peres. Growth rates and explosions in sandpiles. *Journal of statistical physics*, 138(1):143–159, 2010.
- Anna Cathérine Fey-den Boer and FHJ Redig. *Organized versus self-organized criticality in the abelian sandpile model*. Technische Universiteit Eindhoven, Department of Mathematics and Computing Science, 2004.

- Anne Fey-den Boer and Frank Redig. Limiting shapes for deterministic centrally seeded growth models. *Journal of Statistical Physics*, 130(3):579, 2008.
- Tobias Friedrich and Lionel Levine. Fast simulation of large-scale growth models. In *Approximation, Randomization, and Combinatorial Optimization. Algorithms and Techniques*, pages 555–566. Springer, 2011.
- Olivier Garet and Régine Marchand. Asymptotic shape for the chemical distance and first-passage percolation on the infinite bernoulli cluster. *ESAIM: Probability and Statistics*, 8: 169–199, 2004.
- Olivier Garet and Régine Marchand. Large deviations for the chemical distance in supercritical Bernoulli percolation. *The Annals of Probability*, 35(3):833–866, 2007.
- Olivier Garet and Régine Marchand. Asymptotic shape for the contact process in random environment. *The Annals of Applied Probability*, 22(4):1362–1410, 2012.
- David Gilbarg, Neil S Trudinger, David Gilbarg, and NS Trudinger. *Elliptic partial differential equations of second order*, volume 224. Springer, 1977.
- Chris Godsil and Gordon F. Royle. *Algebraic graph theory*, volume 207. Springer Science & Business Media, 2013.
- Eric Goles, Pedro Montealegre, and Kévin Perrot. Freezing sandpiles and Boolean threshold networks: Equivalence and complexity. *Advances in Applied Mathematics*, 125:102161, 2021.
- Ronald L. Graham, Jeffrey C. Lagarias, Colin L. Mallows, Allan R. Wilks, and Catherine H Yan. Apollonian circle packings: geometry and group theory i. the apollonian group. *Discrete & Computational Geometry*, 34(4):547–585, 2005.
- Janko Gravner and David Griffeath. Threshold growth dynamics. *Transactions of the American Mathematical society*, pages 837–870, 1993.
- Janko Gravner and David Griffeath. First passage times for threshold growth dynamics on \mathbb{Z}^2 . *The Annals of Probability*, pages 1752–1778, 1996.
- Janko Gravner and David Griffeath. Cellular automaton growth on \mathbb{Z}^2 : theorems, examples, and problems. *Advances in Applied Mathematics*, 21(2):241–304, 1998.
- Janko Gravner and David Griffeath. Random growth models with polygonal shapes. *The Annals of Probability*, pages 181–218, 2006.
- Geoffrey R Grimmett. *Percolation*, volume 321. Springer Science & Business Media, 2013.
- Cristian E Gutiérrez. *The Monge-Ampère Equation*, volume 89. Birkhäuser, 2016.
- John M. Hammersley. A few seedlings of research. In *Theory of Statistics*, pages 345–394. University of California Press, 1972.

- Alexander E. Holroyd, Lionel Levine, Karola Mészáros, Yuyal Peres, James Propp, and David B. Wilson. Chip-firing and rotor-routing on directed graphs. In *In and out of equilibrium 2*, pages 331–364. Springer, 2008.
- Robert Hough and Hyojeong Son. Cut-off for sandpiles on tiling graphs. *arXiv preprint arXiv:1902.04174*, 2019.
- Robert D. Hough, Daniel C. Jerison, and Lionel Levine. Sandpiles on the square lattice. *Communications in Mathematical Physics*, 367(1):33–87, 2019.
- Neil S. Trudinger Hung-Ju Kuo. *Local Estimates for Parabolic Difference Operators*. Journal of Differential Equations, 1995.
- Cyril Imbert and Luis Silvestre. An introduction to fully nonlinear parabolic equations. In *An introduction to the Kähler-Ricci flow*, pages 7–88. Springer, 2013.
- Hitoshi Ishii, Gabriel E Pires, and Panagiotis E Souganidis. Threshold dynamics type approximation schemes for propagating fronts. *Journal of the Mathematical Society of Japan*, 51(2):267–308, 1999.
- Antal A Járai. Sandpile models. *Probability Surveys*, 15:243–306, 2018.
- Antal A. Járai and Frank Redig. Infinite volume limit of the abelian sandpile model in dimensions $d \geq 3$. *Probability theory and related fields*, 141(1):181–212, 2008.
- Tian-Yi Jiang. On the period lengths of the parallel chip-firing game. *arXiv preprint arXiv:1003.0943*, 2010.
- Wenjia Jing, Panagiotis E Souganidis, and Hung V Tran. Large time average of reachable sets and applications to homogenization of interfaces moving with oscillatory spatio-temporal velocity. *Discrete & Continuous Dynamical Systems-S*, 11(5):915, 2018.
- Nikita Kalinin and Mikhail Shkolnikov. Sandpile solitons via smoothing of superharmonic functions. *Communications in Mathematical Physics*, 378(3):1649–1675, 2020.
- Michael Kapovich and Alex Kontorovich. On superintegral kleinian sphere packings, bugs, and arithmetic groups. *arXiv preprint arXiv:2104.13838*, 2021.
- Mehran Kardar, Giorgio Parisi, and Yi-Cheng Zhang. Dynamic scaling of growing interfaces. *Physical Review Letters*, 56(9):889, 1986.
- Harry Kesten and Vladas Sidoravicius. A shape theorem for the spread of an infection. *Annals of mathematics*, pages 701–766, 2008.
- Caroline J. Klivans. *The mathematics of chip-firing*. CRC Press, 2018.
- Robert Kohn and Sylvia Serfaty. A deterministic-control-based approach motion by curvature. *Communications on Pure and Applied Mathematics: A Journal Issued by the Courant Institute of Mathematical Sciences*, 59(3):344–407, 2006.

- Janos Komlos and MT Shing. Probabilistic partitioning algorithms for the rectilinear steiner problem. *Networks*, 15(4):413–423, 1985.
- Hung-Ju Kuo and Neil S Trudinger. Estimates for solutions of fully nonlinear discrete schemes. In *Trends in partial differential equations of mathematical physics*, pages 275–282. Springer, 2005.
- Itamar Landau and Lionel Levine. The rotor-router model on regular trees. *Journal of Combinatorial Theory, Series A*, 116(2):421–433, 2009.
- Moritz Lang and Mikhail Shkolnikov. Harmonic dynamics of the Abelian sandpile. *Proceedings of the National Academy of Sciences*, 116(8):2821–2830, 2019.
- Gregory F Lawler and Vlada Limic. *Random walk: a modern introduction*, volume 123. Cambridge University Press, 2010.
- Gregory F. Lawler, Maury Bramson, and David Griffeath. Internal diffusion limited aggregation. *Annals of Probability*, pages 2117–2140, 1992.
- Yvan Le Borgne and Dominique Rossin. On the identity of the sandpile group. *Discrete mathematics*, 256(3):775–790, 2002.
- Lionel Levine and Yuval Peres. Strong spherical asymptotics for rotor-router aggregation and the divisible sandpile. *Potential Analysis*, 30(1):1–27, 2009.
- Lionel Levine and Yuval Peres. Scaling limits for internal aggregation models with multiple sources. *Journal d’Analyse Mathématique*, 111(1):151–219, 2010.
- Lionel Levine and Yuval Peres. Laplacian growth, sandpiles, and scaling limits. *Bulletin of the American Mathematical Society*, 54(3):355–382, 2017.
- Lionel Levine and James Propp. What is... a sandpile. In *Notices Amer. Math. Soc.*, 2010.
- Lionel Levine, Mathav Murugan, Yuval Peres, and Baris Evren Ugurcan. The divisible sandpile at critical density. *Annales Henri Poincaré*, 17(7):1677–1711, 2016a. doi: 10.1007/s00023-015-0433-x. URL <https://doi.org/10.1007/s00023-015-0433-x>.
- Lionel Levine, Wesley Pegden, and Charles K Smart. Apollonian structure in the abelian sandpile. *Geometric and functional analysis*, 26(1):306–336, 2016b.
- Lionel Levine, Wesley Pegden, and Charles K. Smart. The Apollonian structure of integer superharmonic matrices. *Annals of Mathematics*, pages 1–67, 2017.
- Thomas M Liggett, Roberto H Schonmann, and Alan M Stacey. Domination by product measures. *The Annals of Probability*, 25(1):71–95, 1997.
- Jessica Lin. On the stochastic homogenization of fully nonlinear uniformly parabolic equations in stationary ergodic spatio-temporal media. *Journal of Differential Equations*, 258(3):796–845, 2015.

- Jessica Lin and Charles Smart. Algebraic error estimates for the stochastic homogenization of uniformly parabolic equations. *Analysis & PDE*, 8(6):1497–1539, 2015.
- Jessica Lin and Andrej Zlatoš. Stochastic homogenization for reaction–diffusion equations. *Archive for Rational Mechanics and Analysis*, 232(2):813–871, 2019.
- S.H. Liu, Theodore Kaplan, and L.J. Gray. Geometry and dynamics of deterministic sand piles. *Physical Review A*, 42(6):3207, 1990.
- Dino J Lorenzini. Arithmetical graphs. *Mathematische Annalen*, 285(3):481–501, 1989.
- Cyrille Lucas. The limiting shape for drifted internal diffusion limited aggregation is a true heat ball. *Probability Theory and Related Fields*, 159(1-2):197–235, 2014.
- Satya N Majumdar and Deepak Dhar. Equivalence between the abelian sandpile model and the $q \rightarrow 0$ limit of the potts model. *Physica A: Statistical Mechanics and its Applications*, 185(1-4):129–145, 1992.
- Régine Marchand. Strict inequalities for the time constant in first passage percolation. *The Annals of Applied Probability*, 12(3):1001–1038, 2002.
- P Mathieu. Quenched invariance principles for random walks with random conductances. *Journal of Statistical Physics*, 130(5):1025–1046, 2008.
- Andrew Melchionna. The sandpile identity element on an ellipse. *arXiv preprint arXiv:2007.05792*, 2020.
- Cristopher Moore and Martin Nilsson. The computational complexity of sandpiles. *Journal of statistical physics*, 96(1):205–224, 1999.
- Adam M Oberman, Ryo Takei, and Alexander Vladimirsly. Homogenization of metric Hamilton–Jacobi equations. *Multiscale Modeling & Simulation*, 8(1):269–295, 2009.
- Srdjan Ostojic. Patterns formed by addition of grains to only one site of an abelian sandpile. *Physica A: Statistical Mechanics and its Applications*, 318(1-2):187–199, 2003.
- Norman H Packard and Stephen Wolfram. Two-dimensional cellular automata. *Journal of Statistical physics*, 38(5-6):901–946, 1985.
- Guglielmo Paoletti. *Deterministic abelian sandpile models and patterns*. Springer Science & Business Media, 2013.
- Wesley Pegden. Sandpile galleries, 2017. <http://www.math.cmu.edu/~wes/sandgallery.html>.
- Wesley Pegden and Charles K. Smart. Convergence of the abelian sandpile. *Duke mathematical journal*, 162(4):627–642, 2013.

Wesley Pegden and Charles K. Smart. Stability of patterns in the abelian sandpile. *Annales Henri Poincaré*, 21(4):1383–1399, 2020. doi: 10.1007/s00023-020-00898-1. URL <https://doi.org/10.1007/s00023-020-00898-1>.

James Propp. Prof. engel’s marvelously improbable machines. <http://web.ahthttps://mathenchant.wordpress.com/2017/08/16/prof-engels-marvelously-improbable-machines/>, 2017.

Frank Redig. Mathematical aspects of the Abelian sandpile model. *Les Houches lecture notes*, 83:657–659, 2005.

Luis A Roberts, Luis A Caffarelli, and Xavier Cabré. *Fully nonlinear elliptic equations*, volume 43. American Mathematical Soc., 1995.

Dominique Rossin. *Propriétés combinatoires de certaines familles d’automates cellulaires*. PhD thesis, École Polytechnique, 2000.

Tridib Sadhu and Deepak Dhar. The effect of noise on patterns formed by growing sandpiles. *Journal of Statistical Mechanics: Theory and Experiment*, 2011(03):P03001, 2011.

Tridib Sadhu and Deepak Dhar. Modelling proportionate growth. *Current Science*, pages 512–517, 2012a.

Tridib Sadhu and Deepak Dhar. Pattern formation in fast-growing sandpiles. *Physical Review E*, 85(2):021107, 2012b.

Klaus Schmidt and Evgeny Verbitskiy. Abelian sandpiles and the harmonic model. *Communications in Mathematical Physics*, 292(3):721–759, 2009.

Roberto H. Schonmann. On the behavior of some cellular automata related to bootstrap percolation. *Annals of Probability*, pages 174–193, 1992.

Oded Schramm. Scaling limits of loop-erased random walks and uniform spanning trees. *Israel Journal of Mathematics*, 118(1):221–288, 2000.

Charles K. Smart. Aim chip firing 2013: The f -lattice. *American Institute of Mathematics*, 2013. <https://www.aimath.org/WWN/chipfiring/flattice.pdf>.

Katherine E Stange. The sensual apollonian circle packing. *Expositiones Mathematicae*, 34(4):364–395, 2016.

Lin Tan. The group of rational points on the unit circle. *Mathematics Magazine*, 69(3):163–171, 1996.

J-F Thisse, James E Ward, and Richard E Wendell. Some properties of location problems with block and round norms. *Operations Research*, 32(6):1309–1327, 1984.

Neil S Trudinger and Xu-Jia Wang. The monge-ampère equation and its geometric applications. *Handbook of geometric analysis*, 1:467–524, 2008.

- Aernout CD van Enter. Proof of straley's argument for bootstrap percolation. *Journal of Statistical Physics*, 48(3-4):943–945, 1987.
- Stephen J Willson. On convergence of configurations. *Discrete Mathematics*, 23(3):279–300, 1978.
- Melanie Wood. The distribution of sandpile groups of random graphs. *Journal of the American Mathematical Society*, 30(4):915–958, 2017.
- Jack Xin. Front propagation in heterogeneous media. *SIAM review*, 42(2):161–230, 2000.
- Jack Xin. *An introduction to fronts in random media*, volume 5. Springer Science & Business Media, 2009.
- Yuming Paul Zhang and Andrej Zlatoš. Long time dynamics for combustion in random media. *arXiv preprint arXiv:2008.02391*, 2020.